CE-QUAL-W2: A Two-Dimensional, Laterally Averaged, Hydrodynamic and Water Quality Model, Version 4.5

User Manual Part 2: Hydrodynamic and Water Quality Model Theory

Edited by
  Scott A. Wells
  Professor
  Department of Civil and Environmental Engineering
  Portland State University
  Portland, OR 97207-0751

Contents

CONTENTS

CONTENTS

CONTENTS

List of Figures

LIST OF FIGURES

LIST OF FIGURES

List of Tables

Preface

This manual documents the two-dimensional, laterally averaged, hydrodynamic and water quality model CE-QUAL-W2. As in all complex models, there have been many contributors. This re-write of the User Manual was based on prior User Manuals: Environmental and Hydraulic Laboratories (1986), Cole and Buchak (1995) Version 2, and Cole and Wells (2000) Version 3.0 through Cole and Wells (2019) Version 4.1. Hence, one can think of the primary author as merely an editor of past documents, rather than reflecting one person's sole authorship. This updated User Manual contains numerous corrections, new figures, new sections, additional documentation, and improvements in organization and presentation of information compared to Cole and Wells (2019).

This section of the User Manual Part 2 documents the theory for the hydrodynamic and water quality computations and particle transport.

The other sections of the User Manual are divided into multiple sections for ease of updating and editing:
- User Manual Part 1: Introduction to CE-QUAL-W2, Model download package, how to run the model, model versions, changes between model versions
- User Manual Part 2: Theoretical basis for CE-QUAL-W2: hydrodynamics and water quality, particle transport and numerical scheme
- User Manual Part 3: Model input and output file descriptions and input/output file examples
- User Manual Part 4: Model examples
- User Manual Part 5: Release notes, bug fixes, differences in model versions, history of bug fixes, and other user manuals such as for the GUI interface, the water balance algorithm, and other external codes.

This report should be cited as follows:

Wells, S. A. editor (2021) "CE-QUAL-W2: A two-dimensional, laterally averaged, hydrodynamic and water quality model, version 4.5, user manual part 2, hydrodynamic and water quality model theory," Department of Civil and Environmental Engineering, Portland State University, Portland, OR.

or if a specific section with a different primary author:

Berger, C. (2021) "Macrophytes" in "CE-QUAL-W2: A two-dimensional, laterally averaged, hydrodynamic and water quality model, version 4.5, user manual part 2," ed. by S. Wells, Department of Civil and Environmental Engineering, Portland State University, Portland, OR.

Zhang, Z. (2021) "Organic Carbon Constituents" in "CE-QUAL-W2: A two-dimensional, laterally averaged, hydrodynamic and water quality model, version 4.5, user manual part 2," ed. by S. Wells, Department of Civil and Environmental Engineering, Portland State University, Portland, OR.

1.   Introduction

This section of the CE-QUAL-W2 User manual outlines the governing equations for hydrodynamics and water quality that are the basis of the model. These equations include

- fluid continuity equation (the integrated form is the water surface equation),
- x and z momentum equations
- equation of state
- temperature and water quality advective diffusion equations
- source and sink term for temperature and each water quality state variable

Also, auxiliary operations of the model are discussed in this section such as wind shear stress, bottom shear stress, turbulence closure, particle transport, ice cover dynamics, and sediment resuspension.

The numerical solution of the governing equations is discussed for both hydrodynamics and the advective diffusion equation for temperature and water quality.

The manual is divided into the following sections:
(1) Hydrodynamics and Transport Modeling
(2) Particle Tracking Algorithm
(3) Temperature and Water Quality Modeling
(4) Numerical Solution
(5) References

2.   Hydrodynamics Modeling

Contributors: Scott A. Wells, Chris Berger, Tom M. Cole, Robert Annear, Sam Gould, John Edinger, Ed Buchak

CE-QUAL-W2 uses the laterally averaged equations of fluid motion derived from the three-dimensional equations, which consist of six equations and six unknowns. The development of the final set of governing equations is described below.

Coordinate System

The general coordinate system used in the development of the laterally averaged equations of fluid motion is shown in **Figure 1**.
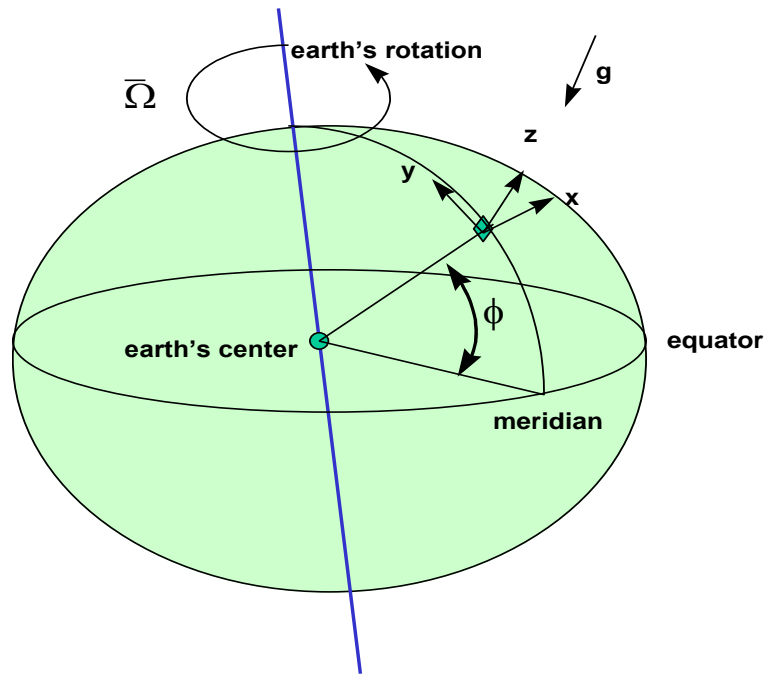
Figure 1. Definition sketch of coordinate system for governing equations where x is oriented east, y is oriented north, and z is oriented upward.

Based on this coordinate system, we then will use the following definitions:

- x and y are horizontal coordinates.
- z is a vertical coordinate assumed to be opposite the gravity force.
- Ω is a vector that represents the angular velocity of the earth spinning on its axis. The rotation of the coordinate system can result in horizontal acceleration of the fluid. This is usually restricted to large water bodies such as large lakes and ocean systems. The force that causes horizontal accelerations because of the spinning coordinate system is termed the Coriolis force.
- ϕ is the latitude of the water body.
- The meridian represents the longitude of the water body.

Turbulent Time-Averaged Equations

The governing equations are obtained by performing a mass and a momentum balance of the fluid phase about a control volume. The resulting equations are the continuity (or conservation of fluid mass) and the conservation of momentum equations for a rotating coordinate system (Batchelor, 1967; Sabersky et al., 1989; Cushman-Roisin, 1994). Using the coordinate system in **Figure 1**, we will assume:

1. Incompressible fluid (it is possible to develop compressible equations of motion for special cases, see Wells, 2009)
2. Centripetal acceleration is a minor correction to gravity
3. Boussinesq approximation where

4. All velocities (u, v, w) and pressure (p) are the sum of turbulent time averages and deviations from that average, i.e., $u = \bar{u} + u'$, where $\bar{u} = \frac{1}{T}\int_{t}^{t+T} u\,dt$ as shown in **Figure 2**, $v = \bar{v} + v'; w = \bar{w} + w'$ and $p = \bar{p} + p'$ where the overbar represents time averaged and the prime represents deviation from the temporal average.
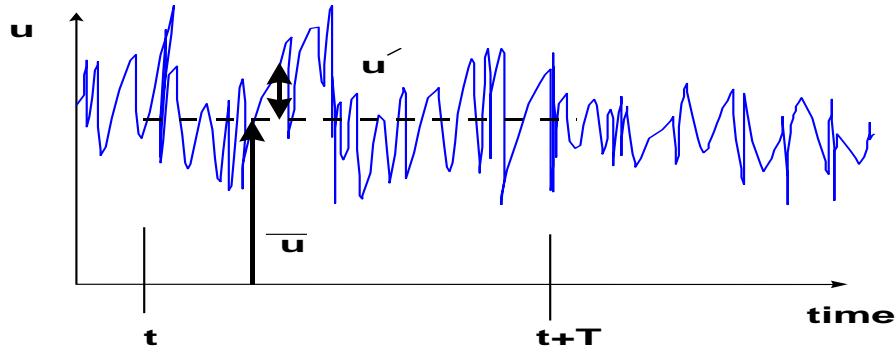
Figure 2. Definition sketch of turbulent time averaging for velocity.

The governing equations (continuity and x, y, z momentum equations) become after simplification:

Continuity

$$\frac{\partial \bar{u}}{\partial x} + \frac{\partial \bar{v}}{\partial y} + \frac{\partial \bar{w}}{\partial z} = 0 \qquad \textbf{(2-1)}$$

where:

    u = x-direction velocity
    v = y-direction velocity
    w = z-direction velocity

x-Momentum Equation

$$\underbrace{\frac{\partial \bar{u}}{\partial t}}_{\substack{\text{unsteady}\\\text{acceleration}}} + \underbrace{\bar{u}\frac{\partial \bar{u}}{\partial x} + \bar{v}\frac{\partial \bar{u}}{\partial y} + \bar{w}\frac{\partial \bar{u}}{\partial z}}_{\text{convective acceleration}} - \underbrace{2\Omega_z\bar{v} + 2\Omega_y\bar{w}}_{\text{Coriolis acceleration}} = - \underbrace{\frac{1}{\rho}\frac{\partial \bar{p}}{\partial x}}_{\substack{\text{pressure}\\\text{gradient}}} + \underbrace{\frac{\mu}{\rho}\left(\frac{\partial^2 \bar{u}}{\partial x^2} + \frac{\partial^2 \bar{u}}{\partial y^2} + \frac{\partial^2 \bar{u}}{\partial z^2}\right)}_{\text{viscous stresses}} +$$

$$\underbrace{\frac{1}{\rho}\left(\frac{\partial \tau_{xx}}{\partial x} + \frac{\partial \tau_{xy}}{\partial y} + \frac{\partial \tau_{xz}}{\partial z}\right)}_{\text{turbulent stresses}} \qquad \textbf{(2-2)}$$

where:

    τ_{xx} = turbulent shear stress acting in x direction on the x-face of control volume (Figure 3)
    τ_{xy} = turbulent shear stress acting in x direction on the y-face of control volume (Figure 3)
    τ_{xz} = turbulent shear stress acting in x direction on the z-face of control volume (Figure 3)
    μ = dynamic viscosity
    Ω = component of Coriolis acceleration where:
    Ω_z = $\Omega_E \sin\varphi$
    Ω_y = $\Omega_E \cos\varphi$
    ϕ = latitude
    Ω_E = earth's rotation rate
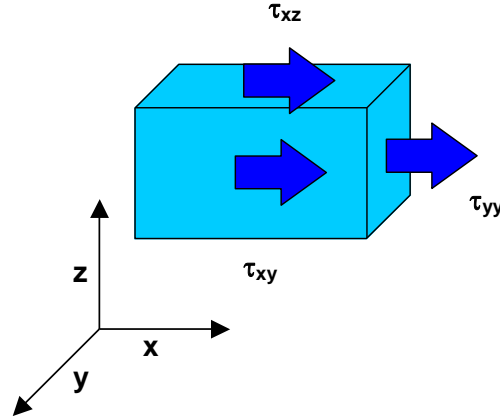
Figure 3. Definition sketch of turbulent shear stresses in x-direction.

y-Momentum Equation

$$\frac{\partial \bar{v}}{\partial t} + \bar{u}\frac{\partial \bar{v}}{\partial x} + \bar{v}\frac{\partial \bar{v}}{\partial y} + \bar{w}\frac{\partial \bar{v}}{\partial z} + 2\Omega_z\bar{u} - 2\Omega_x\bar{w} = -\frac{1}{\rho}\frac{\partial \bar{p}}{\partial y} + \frac{\mu}{\rho}\left(\frac{\partial^2 \bar{v}}{\partial x^2} + \frac{\partial^2 \bar{v}}{\partial y^2} + \frac{\partial^2 \bar{v}}{\partial z^2}\right) + \frac{1}{\rho}\left(\frac{\partial \tau_{yx}}{\partial x} + \frac{\partial \tau_{yy}}{\partial y} + \frac{\partial \tau_{yz}}{\partial z}\right)$$

(2-3)

where:

τ_{yx} = turbulent shear stress acting in y direction on the x-face of control volume (Figure 4)

τ_{yy} = turbulent shear stress acting in y direction on the y-face of control volume (Figure 4)

τ_{yz} = turbulent shear stress acting in y direction on the z-face of control volume (Figure 4)

Ω_x = 0
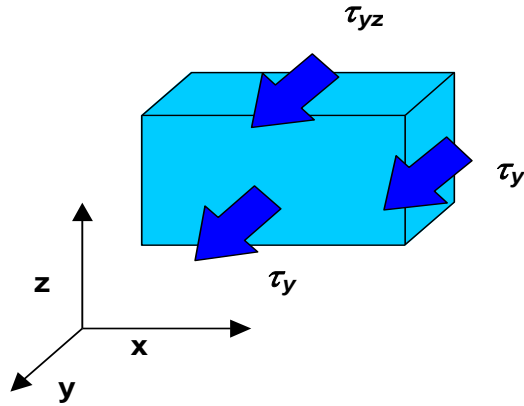
Figure 4. Sketch of turbulent shear stresses in y-direction.

z-Momentum Equation

$$\frac{\partial \bar{w}}{\partial t} + \bar{u}\frac{\partial \bar{w}}{\partial x} + \bar{v}\frac{\partial \bar{w}}{\partial y} + \bar{w}\frac{\partial \bar{w}}{\partial z} - 2\Omega_y\bar{u} + 2\Omega_x\bar{v} = -g - \frac{1}{\rho}\frac{\partial \bar{p}}{\partial z} + \frac{\mu}{\rho}\left(\frac{\partial^2 \bar{w}}{\partial x^2} + \frac{\partial^2 \bar{w}}{\partial y^2} + \frac{\partial^2 \bar{w}}{\partial z^2}\right) + \frac{1}{\rho}\left(\frac{\partial \tau_{zx}}{\partial x} + \frac{\partial \tau_{zy}}{\partial y} + \frac{\partial \tau_{zz}}{\partial z}\right)$$

(2-4)

where:

Hydrodynamics and Transport

τ_{zx} = turbulent shear stress acting in z direction on the x-face of control volume (Figure 5)
τ_{zy} = turbulent shear stress acting in z direction on the y-face of control volume (Figure 5)
τ_{zz} = turbulent shear stress acting in z direction on the z-face of control volume (Figure 5)
Ω_x = 0
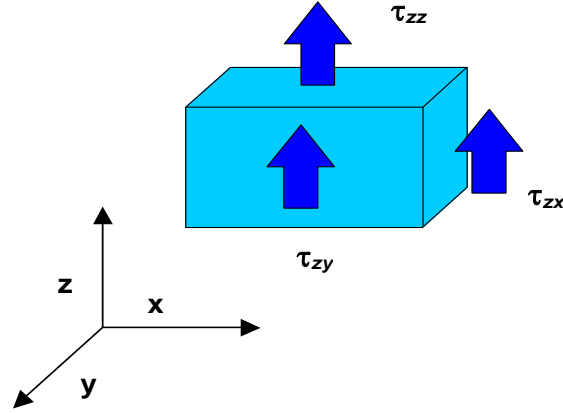
Figure 5. Sketch of turbulent shear stresses in z-direction.

Note that the turbulent shear stresses are defined as follows:

$\tau_{xx} = \rho\overline{u'u'}$

$\tau_{xy} = \rho\overline{u'v'}$ is the same as $\tau_{yx} = \rho\overline{v'u'}$

$\tau_{xz} = \rho\overline{u'w'}$ is the same as $\tau_{zx} = \rho\overline{w'u'}$

$\tau_{yy} = \rho\overline{v'v'}$

$\tau_{yz} = \rho\overline{v'w'}$ is the same as $\tau_{zy} = \rho\overline{w'v'}$

$\tau_{zz} = \rho\overline{w'w'}$

Coriolis Effect

As noted above, all the Ω_x terms are zero and can be eliminated from the y and z-momentum equations. If one integrates over the y-direction (therefore assuming the net velocity in y is zero) and assumes that the horizontal length scale is much greater than vertical length scale, it can be shown by using scaling arguments that the Coriolis acceleration forces are negligible (Cushman-Roisin, 1994). Hence, prior to lateral averaging, the Coriolis acceleration terms will be neglected.

Adjusting the Coordinate System

The coordinate system is transformed into a form compatible with the original W2 development where the vertical axis is in the direction of gravity. In addition, as shown in **Figure 6**, the coordinate system is oriented along an arbitrary slope.
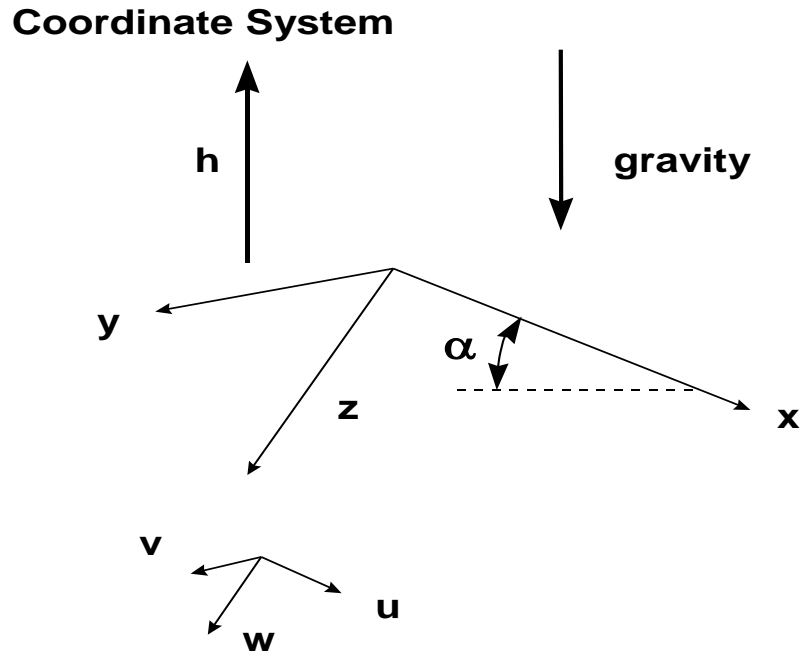
Figure 6. General coordinate system with z-axis compatible with original derivation of W2 model.

The gravity acceleration is a body force that is then represented by a vector:

$$\vec{g} = -g\vec{\nabla}h \tag{2-5}$$

where:

  h = surface normal from the earth's surface
  g = gravitational acceleration, 9.8 $m\ s^{-2}$.

This term can be written as three vector components:

$$g_x = -g\frac{\partial h}{\partial x} \tag{2-6}$$

$$g_y = -g\frac{\partial h}{\partial y} \tag{2-7}$$

$$g_z = -g\frac{\partial h}{\partial z} \tag{2-8}$$

These gravity components can be applied to an arbitrary channel slope as shown in **Figure 7**.

Hydrodynamics and Transport
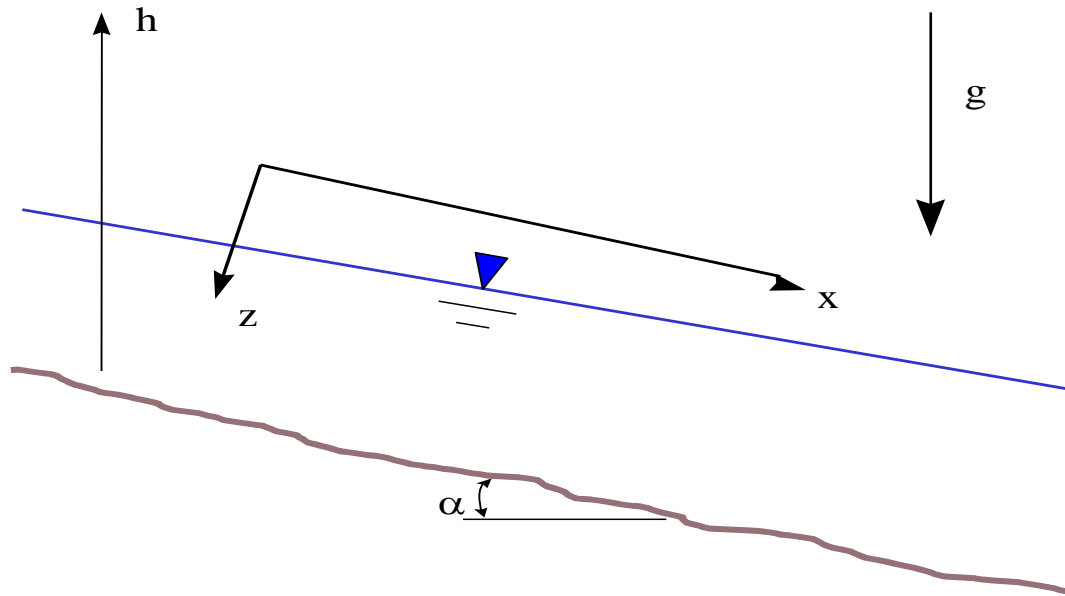
Figure 7. Sketch of channel slope and coordinate system for W2 where the x-axis is oriented along the channel slope.

The channel slope, S_o, can also be incorporated into the definition of the gravity vector if the x-axis is chosen parallel to the channel slope. The channel slope is defined as:

$$S_o = tan\ \alpha \tag{2-9}$$

and also in terms of the gravity components:

$$g_x = -g\frac{\partial h}{\partial x} = g\ sin\ \alpha \tag{2-10}$$

$$g_z = -g\frac{\partial h}{\partial z} = g\ cos\ \alpha \tag{2-11}$$

The gravity acceleration in y is assumed negligible since $\frac{\partial h}{\partial y} = 0$ in the lateral direction of the channel.

Governing Equations for General Coordinate System

After redefining the coordinate system, eliminating Coriolis effects, and neglecting viscous shear stresses the governing equations become:

Continuity

$$\frac{\partial \bar{u}}{\partial x} + \frac{\partial \bar{v}}{\partial y} + \frac{\partial \bar{w}}{\partial z} = 0 \tag{2-12}$$

x-Momentum Equation

$$\underbrace{\frac{\partial \bar{u}}{\partial t}}_{\substack{\text{unsteady} \\ \text{acceleration}}} + \underbrace{\bar{u}\frac{\partial \bar{u}}{\partial x} + \bar{v}\frac{\partial \bar{u}}{\partial y} + \bar{w}\frac{\partial \bar{u}}{\partial z}}_{\text{convective acceleration}} = \underbrace{g\sin\alpha}_{\text{gravity}} - \underbrace{\frac{1}{\rho}\frac{\partial \bar{p}}{\partial x}}_{\substack{\text{pressure} \\ \text{gradient}}} + \underbrace{\frac{1}{\rho}\left(\frac{\partial \tau_{xx}}{\partial x} + \frac{\partial \tau_{xy}}{\partial y} + \frac{\partial \tau_{xz}}{\partial z}\right)}_{\text{turbulent shear stresses}}$$

(2-13)

y-Momentum Equation

$$\underbrace{\frac{\partial \bar{v}}{\partial t}}_{\substack{\text{unsteady} \\ \text{acceleration}}} + \underbrace{\bar{u}\frac{\partial \bar{v}}{\partial x} + \bar{v}\frac{\partial \bar{v}}{\partial y} + \bar{w}\frac{\partial \bar{v}}{\partial z}}_{\text{convective acceleration}} = - \underbrace{\frac{1}{\rho}\frac{\partial \bar{p}}{\partial y}}_{\substack{\text{pressure} \\ \text{gradient}}} + \underbrace{\frac{1}{\rho}\left(\frac{\partial \tau_{yx}}{\partial x} + \frac{\partial \tau_{yy}}{\partial y} + \frac{\partial \tau_{yz}}{\partial z}\right)}_{\text{turbulent shear stresses}}$$

(2-14)

z-Momentum Equation

$$\underbrace{\frac{\partial \bar{w}}{\partial t}}_{\substack{\text{unsteady} \\ \text{acceleration}}} + \underbrace{\bar{u}\frac{\partial \bar{w}}{\partial x} + \bar{v}\frac{\partial \bar{w}}{\partial y} + \bar{w}\frac{\partial \bar{w}}{\partial z}}_{\text{convective acceleration}} = \underbrace{g\cos\alpha}_{\text{gravity}} - \underbrace{\frac{1}{\rho}\frac{\partial \bar{p}}{\partial z}}_{\substack{\text{pressure} \\ \text{gradient}}} + \underbrace{\frac{1}{\rho}\left(\frac{\partial \tau_{zx}}{\partial x} + \frac{\partial \tau_{zy}}{\partial y} + \frac{\partial \tau_{zz}}{\partial z}\right)}_{\text{turbulent shear stresses}}$$

(2-15)

Simplification of z-Momentum Equation

If the longitudinal length scale is much greater than the vertical length scale, then all vertical velocities << horizontal velocities. A result of this assumption is that vertical velocities are very small and vertical acceleration and shear stress terms in the z-momentum are negligible such that the z-momentum equation becomes the hydrostatic equation:

$$\frac{1}{\rho}\frac{\partial \bar{p}}{\partial z} = g\cos\alpha$$

(2-16)

This assumption prevents the model from accurately modeling vertical accelerations of the fluid because of convective cooling at night and other such vertical accelerations. But internal algorithms in the model mix vertical layers when there are density instabilities approximating the convective cooling process. Also, vertical accelerations in the vicinity of an outlet are approximated by using selective withdrawal theory rather than solving the full vertical momentum equation.

Lateral Averaging

The governing equations above will be laterally averaged after decomposing all velocities and pressure into a lateral average and a deviation from the lateral average. The lateral, longitudinal, and vertical velocities and pressure are defined as follows:

$$\bar{v} = \bar{\bar{v}} + v''$$

(2-17)

$$\bar{u} = \bar{\bar{u}} + u''$$

(2-18)

$$\bar{w} = \bar{\bar{w}} + w''$$

(2-19)

Hydrodynamics and Transport

$$\bar{p} = \bar{\bar{p}} + p''$$

<div align="right">(2-20)</div>

where:

$$\bar{\bar{u}} = \frac{1}{B}\int_{y_1}^{y_2}\bar{u}\,dy$$

   B = control volume width, m

   y_1 = left bank coordinate

   y_2 = right bank coordinate

The double overbars represent the spatial average of the temporal average quantity. The double prime represents the deviation from the lateral average and is a function of y. This is shown in **Figure 8**.
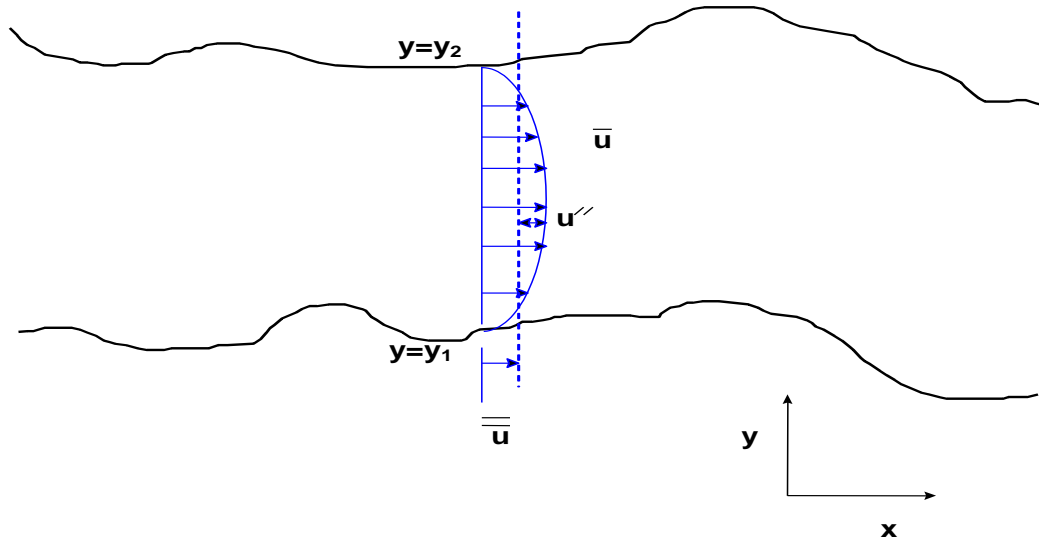
Figure 8. Lateral average and deviation from lateral average components of longitudinal velocity.

These definitions are substituted into the turbulent time-average governing equations and then laterally averaged. The y-momentum equation is neglected since the average lateral velocities are zero ($\bar{\bar{v}} = 0$) and cross shear stresses that contribute to vertical mixing will be computed from the analysis of wind stress. The equations that remain are the continuity, x-momentum, and z-momentum equations.

Continuity Equation

The continuity equation becomes after substituting the above velocity components and laterally averaging

$$\overline{\frac{\partial(\bar{u}+u'')}{\partial x}} + \overline{\frac{\partial(\bar{v}+v'')}{\partial y}} + \overline{\frac{\partial(\bar{w}+w'')}{\partial z}} = 0$$

<div align="right">(2-21)</div>

The lateral average of a double primed variable is by definition zero:

$$\overline{u''} = \frac{1}{B}\int_{y1}^{y2}u''\,dy = 0$$

<div align="right">(2-22)</div>

Also, note that:

$$\overline{\frac{\partial(\bar{v}+v'')}{\partial y}} = \frac{1}{B}\int_{y1}^{y2}\frac{\partial(\bar{v}+v'')}{\partial y}dy = \frac{(\bar{v}+v'')}{B}\Big|_{y1}^{y2} = \frac{v''}{B}\Big|_{y1}^{y2} = q \tag{2-23}$$

where q is defined as the net lateral inflow per unit volume of cell [T^{-1}], and:

$$\overline{\frac{\partial(\bar{u}+u'')}{\partial x}} = \frac{1}{B}\int_{y1}^{y2}\frac{\partial(\bar{u}+u'')}{\partial x}dy = \frac{1}{B}\int_{y1}^{y2}\frac{\partial\bar{u}}{\partial x}dy + \frac{1}{B}\int_{y1}^{y2}\frac{\partial u''}{\partial x}dy = \frac{1}{B}\frac{\partial}{\partial x}\int_{y1}^{y2}\bar{u}dy = \frac{1}{B}\frac{\partial B\bar{u}}{\partial x} \tag{2-24}$$

and:

$$\overline{\frac{\partial(\bar{w}+w'')}{\partial z}} = \frac{1}{B}\int_{y1}^{y2}\frac{\partial(\bar{w}+w'')}{\partial z}dy = \frac{1}{B}\int_{y1}^{y2}\frac{\partial\bar{w}}{\partial z}dy + \frac{1}{B}\int_{y1}^{y2}\frac{\partial w''}{\partial z}dy = \frac{1}{B}\frac{\partial}{\partial z}\int_{y1}^{y2}\bar{w}dy = \frac{1}{B}\frac{\partial B\bar{w}}{\partial z} \tag{2-25}$$

Combining terms, the continuity equation becomes:

$$\frac{\partial B\bar{u}}{\partial x} + \frac{\partial B\bar{w}}{\partial z} = qB \tag{2-26}$$

x-Momentum Equation

The laterally-averaged x-momentum equation is more easily simplified by writing it in conservative form (this can be verified by using the continuity equation with the x-momentum equation),

$$\overline{\frac{\partial(\bar{u}+u'')}{\partial t}} + \overline{\frac{\partial(\bar{u}+u'')(\bar{u}+u'')}{\partial x}} + \overline{\frac{\partial(\bar{v}+v'')(\bar{u}+u'')}{\partial y}} + \overline{\frac{\partial(\bar{w}+w'')(\bar{u}+u'')}{\partial z}} = \overline{g\sin\alpha} - \overline{\frac{1}{\rho}\frac{\partial(\bar{p}+p'')}{\partial x}} +$$
$$\overline{\frac{1}{\rho}\left(\frac{\partial\tau_{xx}}{\partial x} + \frac{\partial\tau_{xy}}{\partial y} + \frac{\partial\tau_{xz}}{\partial z}\right)} \tag{2-27}$$

Each term in this equation can be simplified as follows (note that the spatial average of any double primed variable goes to zero by definition).

The unsteady acceleration term:

$$\overline{\frac{\partial(\bar{u}+u'')}{\partial t}} = \frac{1}{B}\int_{y1}^{y2}\frac{\partial(\bar{u}+u'')}{\partial t}dy$$
$$= \frac{1}{B}\int_{y1}^{y2}\frac{\partial\bar{u}}{\partial t}dy + \frac{1}{B}\int_{y1}^{y2}\frac{\partial u''}{\partial t}dy$$
$$= \frac{1}{B}\frac{\partial}{\partial t}\int_{y1}^{y2}\bar{u}\,dy + \frac{1}{B}\frac{\partial}{\partial t}\int_{y1}^{y2}u''\,dy = \frac{1}{B}\frac{\partial B\bar{u}}{\partial t} \tag{2-28}$$

The convective acceleration terms:

$$\overline{\frac{\partial(\bar{u}+u'')(\bar{u}+u'')}{\partial x}} = \frac{1}{B}\int_{y1}^{y2}\frac{\partial(\bar{u}+u'')(\bar{u}+u'')}{\partial x}dy$$
$$= \frac{1}{B}\int_{y1}^{y2}\frac{\partial\bar{u}\bar{u}}{\partial x}dy + \frac{1}{B}\int_{y1}^{y2}\frac{2\partial\bar{u}u''}{\partial x}dy + \frac{1}{B}\int_{y1}^{y2}\frac{\partial u''u''}{\partial x}dy$$

$$= \frac{1}{B}\frac{\partial}{\partial x}\int_{y1}^{y2}\bar{\bar{u}}\bar{\bar{u}}dy + \frac{1}{B}\frac{\partial}{\partial x}\int_{y1}^{y2}u''u''dy$$

$$= \frac{1}{B}\frac{\partial B\bar{\bar{u}}\bar{\bar{u}}}{\partial x} + \underbrace{\frac{1}{B}\frac{\partial}{\partial x}\int_{y1}^{y2}u''u''dy}_{\text{dispersion term}} \tag{2-29}$$

Similarly for the other two convective acceleration terms:

$$\overline{\frac{\partial(\bar{u}+u'')(\bar{w}+w'')}{\partial z}} = \frac{1}{B}\frac{\partial B\bar{\bar{u}}\bar{\bar{w}}}{\partial z} + \underbrace{\frac{1}{B}\frac{\partial}{\partial z}\int_{y1}^{y2}u''w''dy}_{\text{dispersion term}} \tag{2-30}$$

$$\overline{\frac{\partial(\bar{u}+u'')(\bar{v}+v'')}{\partial y}} = u''v''\Big|_{y2} - u''v''\Big|_{y1} = 0 \tag{2-31}$$

The gravity term:

$$\overline{g\,sin\,\alpha} = \frac{1}{B}\int_{y1}^{y2}g\,sin\,\alpha\,dy = \frac{1}{B}(g\,sin\,\alpha)\int_{y1}^{y2}dy = g\,sin\,\alpha \tag{2-32}$$

The pressure gradient term:

$$\overline{\frac{\partial(\bar{p}+p'')}{\partial x}} = \frac{1}{B}\int_{y1}^{y2}\frac{\partial(\bar{p}+p'')}{\partial x}dy$$

$$= \frac{1}{B}\int_{y1}^{y2}\frac{\partial\bar{p}}{\partial x}dy + \frac{1}{B}\int_{y1}^{y2}\frac{\partial p''}{\partial x}dy$$

$$= \frac{1}{B}\frac{\partial}{\partial x}\int_{y1}^{y2}\bar{p}dy + \frac{1}{B}\frac{\partial}{\partial x}\int_{y1}^{y2}p''dy = \frac{1}{B}\frac{\partial B\bar{p}}{\partial x} \tag{2-33}$$

or the above equation can be written, assuming that the derivative of the lateral average pressure gradient in the x-direction is not a function of y:

$$\overline{\frac{\partial(\bar{p}+p'')}{\partial x}} = \frac{1}{B}\int_{y1}^{y2}\frac{\partial(\bar{p}+p'')}{\partial x}dy$$

$$= \frac{1}{B}\frac{\partial\bar{p}}{\partial x}\int_{y1}^{y2}dy + \frac{1}{B}\int_{y1}^{y2}\frac{\partial p''}{\partial x}dy$$

$$= \frac{1}{B}\frac{\partial\bar{p}}{\partial x}B + \frac{1}{B}\frac{\partial}{\partial x}\int_{y1}^{y2}p''dy = \frac{\partial\bar{p}}{\partial x} \tag{2-34}$$

The shear stress terms:

$$\overline{\left(\frac{\partial\tau_{xx}}{\partial x} + \frac{\partial\tau_{xy}}{\partial y} + \frac{\partial\tau_{xz}}{\partial z}\right)} = \frac{1}{B}\int_{y1}^{y2}\frac{\partial\tau_{xx}}{\partial x}dy + \frac{1}{B}\int_{y1}^{y2}\frac{\partial\tau_{xy}}{\partial y}dy + \frac{1}{B}\int_{y1}^{y2}\frac{\partial\tau_{xz}}{\partial z}dy$$

$$= \frac{1}{B}\frac{\partial}{\partial x}\int_{y1}^{y2}\tau_{xx}dy + \frac{1}{B}\frac{\partial}{\partial x}\int_{y1}^{y2}\tau_{xy}dy + \frac{1}{B}\frac{\partial}{\partial z}\int_{y1}^{y2}\tau_{xz}dy = \frac{1}{B}\left(\frac{\partial B\overline{\tau_{xx}}}{\partial x} + \frac{\partial B\overline{\tau_{xy}}}{\partial y} + \frac{\partial B\overline{\tau_{xz}}}{\partial z}\right) =$$

$$\frac{1}{B}\left(\frac{\partial B\overline{\tau_{xx}}}{\partial x} + \frac{\partial B\overline{\tau_{xz}}}{\partial z}\right) \tag{2-35}$$

Collecting all terms and neglecting all dispersion terms, the final x-momentum equation is:

$$\frac{\partial B\bar{\bar{u}}}{\partial t} + \frac{\partial B\bar{\bar{u}}\bar{\bar{u}}}{\partial x} + \frac{\partial B\bar{\bar{u}}\bar{w}}{\partial z} = Bg\,sin\,\alpha - \frac{B}{\rho}\frac{\partial \bar{\bar{p}}}{\partial x} + \frac{1}{\rho}\left(\frac{\partial B\overline{\tau_{xx}}}{\partial x} + \frac{\partial B\overline{\tau_{xz}}}{\partial z}\right) \tag{2-36}$$

Summary of Laterally Averaged Equations

In the development of CE-QUAL-W2 in Cole and Buchak (1995), the lateral average terms were represented by uppercase characters, such that $\bar{\bar{u}} = U$, $\bar{w} = W$, and $\bar{\bar{p}} = P$. The shear stress terms will be assumed lateral averages and the double overbars will be dropped for convenience. Making these simplifications, the governing equations become:

Continuity Equation

$$\frac{\partial UB}{\partial x} + \frac{\partial WB}{\partial z} = qB \tag{2-37}$$

x-Momentum Equation

$$\frac{\partial UB}{\partial t} + \frac{\partial UUB}{\partial x} + \frac{\partial WUB}{\partial z} = gB\sin\alpha - \frac{B}{\rho}\frac{\partial P}{\partial x} + \frac{1}{\rho}\frac{\partial B\tau_{xx}}{\partial x} + \frac{1}{\rho}\frac{\partial B\tau_{xz}}{\partial z} \tag{2-38}$$

z-Momentum Equation

$$\frac{1}{\rho}\frac{\partial P}{\partial z} = g\,cos\,\alpha \tag{2-39}$$

Knowing the density through the equation of state, there are now three equations and three unknowns - *U*, *W*, and *P*.

Simplification of Pressure Term

The z-momentum equation reduces to:

$$P = P_a + g\,cos\,\alpha \int_\eta^z \rho dz \tag{2-40}$$

after integration from a depth z to the water surface defined as z=η. P_a is the atmospheric pressure at the water surface (**Figure 9**).
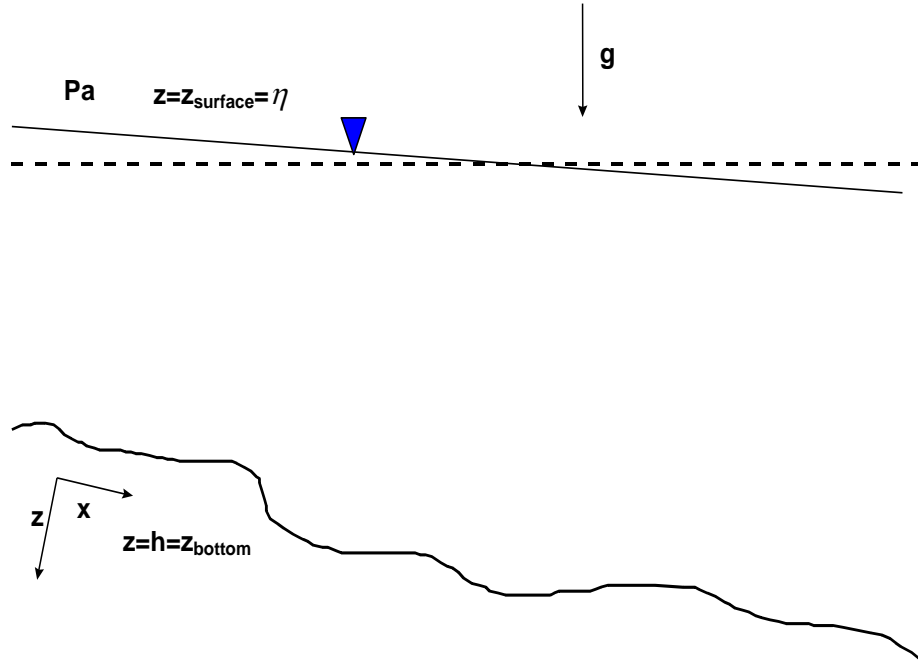
Figure 9. Schematization for simplification of pressure term.

This equation for pressure is now substituted into the x-momentum equation and simplified using Leibnitz rule. The pressure gradient term in the x-momentum equation then becomes:

$$-\frac{1}{\rho}\frac{\partial P}{\partial x} = -\frac{1}{\rho}\frac{\partial P_a}{\partial x} + g\cos\alpha\frac{\partial\eta}{\partial x} - \frac{g\cos\alpha}{\rho}\int_\eta^z \frac{\partial\rho}{\partial x}dz \tag{2-41}$$

The first term on the RHS is the atmospheric pressure term (accelerations due to atmospheric pressure changes over the water surface), the second is the barotropic pressure term (accelerations due to water surface variations), and the third is the baroclinic pressure term (accelerations due to density driven currents).

Assuming that atmospheric pressure does not vary spatially, the atmospheric pressure gradient term is neglected. This implies that for long water bodies during severe storms the model will not be able to account for accelerations because of atmospheric pressure changes in x. The pressure term then becomes:

$$-\frac{1}{\rho}\frac{\partial P}{\partial x} = g\cos\alpha\frac{\partial\eta}{\partial x} - \frac{g\cos\alpha}{\rho}\int_\eta^z \frac{\partial\rho}{\partial x}dz \tag{2-42}$$

The revised form of the x-momentum equation is then:

$$\frac{\partial UB}{\partial t} + \frac{\partial UUB}{\partial x} + \frac{\partial WUB}{\partial z} = gB\sin\alpha + g\cos\alpha B\frac{\partial\eta}{\partial x} - \frac{g\cos\alpha B}{\rho}\int_\eta^z\frac{\partial\rho}{\partial x}dz$$
$$+ \frac{1}{\rho}\frac{\partial B\tau_{xx}}{\partial x} + \frac{1}{\rho}\frac{\partial B\tau_{xz}}{\partial z} \tag{2-43}$$

Effectively, pressure has been removed from the unknowns by combining the z-momentum and x-momentum equations, but η has been added as an unknown.

Free Water Surface

This equation is a simplification of the continuity equation. The continuity equation integrated over the depth from the water surface to the bottom is called the free water surface equation. **Figure 10** and **Figure 11** are definition sketches for the computational grid without and with a channel slope, respectively.
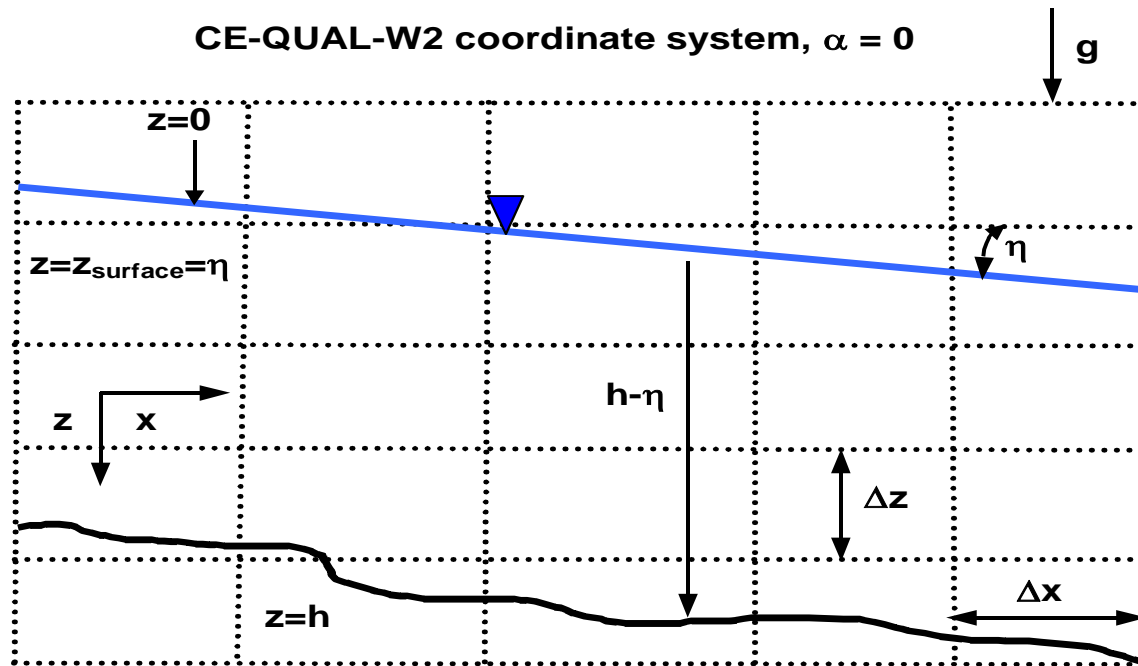
Figure 10. Coordinate system without channel slope.
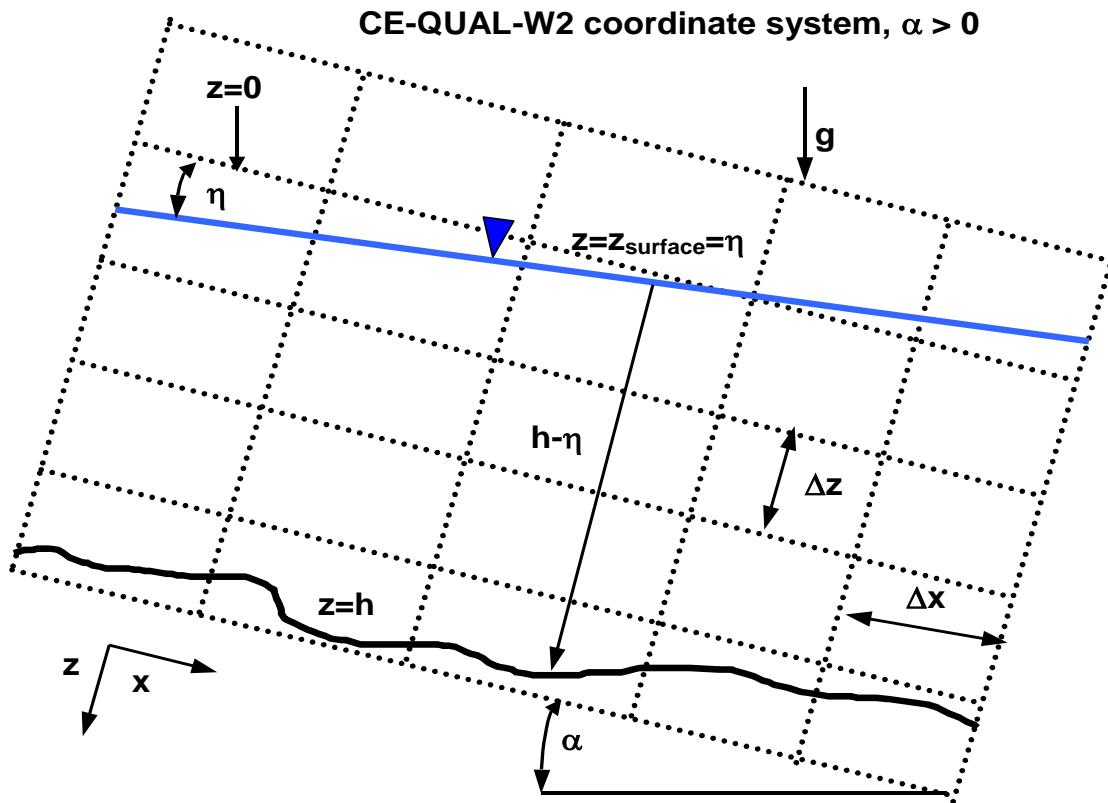
Figure 11. Coordinate system with channel slope.

The continuity equation is integrated over the depth as follows:

$$\int_{\eta}^{h} \frac{\partial UB}{\partial x} dz + \int_{\eta}^{h} \frac{\partial WB}{\partial z} dz = \int_{\eta}^{h} qB\, dz \qquad \textbf{(2-44)}$$

The first term can be expanded as follows using Leibnitz's rule:

$$\int_{\eta}^{h} \frac{\partial UB}{\partial x} dz = \frac{\partial}{\partial x} \int_{\eta}^{h} UB dz - \frac{\partial h}{\partial x} UB|_{h} + \frac{\partial \eta}{\partial x} UB|_{\eta} \qquad \textbf{(2-45)}$$

The integral of the vertical flow rate over z relates to changes in water surface elevation as shown below:

$$\int_{\eta}^{h} \frac{\partial WB}{\partial z} dz = WB|_{h} - WB|_{\eta} \qquad \textbf{(2-46)}$$

where:

$$W_h = \frac{\partial h}{\partial t} + U_h \frac{\partial h}{\partial x}$$
$$W_\eta = \frac{\partial \eta}{\partial t} + U_\eta \frac{\partial \eta}{\partial x}$$

Combining these terms together, the free surface equation becomes:

$$\int_\eta^h qB\,dz = \frac{\partial}{\partial x}\int_\eta^h UB\,dz - \frac{\partial h}{\partial x}UB|_h + \frac{\partial \eta}{\partial x}UB|_\eta + U_h B_h \frac{\partial h}{\partial t} + U_h B_h \frac{\partial h}{\partial x} - B_\eta \frac{\partial \eta}{\partial t} - B_\eta U_\eta \frac{\partial \eta}{\partial x}$$

(2-47)

Canceling out terms and applying the no-slip boundary condition that U_h is zero:

$$\frac{\partial}{\partial x}\int_\eta^h UB\,dz - B_\eta \frac{\partial \eta}{\partial t} = \int_\eta^h qB\,dz$$

(2-48)

or

$$B_\eta \frac{\partial \eta}{\partial t} = \frac{\partial}{\partial x}\int_\eta^h UB\,dz - \int_\eta^h qB\,dz$$

(2-49)

where B_η is the width at the surface.

Equation of State

The density must be known for the solution of the momentum equations. The equation of state is an equation that relates density to temperature and concentration of dissolved substances. This equation is given by:

$$\rho = f(T_w, \Phi_{TDS}, \Phi_{ISS})$$

(2-50)

where $f(T_w, \Phi_{TDS}, \Phi_{ISS})$ is a density function dependent upon water temperature (T_w), concentration of total dissolved solids or salinity (Φ_{TDS}), and concentration of inorganic suspended solids (Φ_{ISS}).

Summary of Governing Equations

Table 1 shows the governing equations after lateral averaging for a channel slope of zero and for an arbitrary channel slope. Parameters used in **Table 1** are illustrated in **Figure 12**.

Table 1. Governing equations with and without channel slope.

Equation	Governing equation assuming no channel slope and no momentum conservation at branch intersections	Governing equation assuming an arbitrary channel slope and conservation of momentum at branch intersections
x- momentum	$$\frac{\partial UB}{\partial t} + \frac{\partial UUB}{\partial x} + \frac{\partial WUB}{\partial z} =$$ $$gB\frac{\partial \eta}{\partial x} - \frac{gB}{\rho} \int_{\eta}^{z} \frac{\partial \rho}{\partial x} dz +$$ $$\frac{1}{\rho}\frac{\partial B\tau_{xx}}{\partial x} + \frac{1}{\rho}\frac{\partial B\tau_{xz}}{\partial z}$$	$$\frac{\partial UB}{\partial t} + \frac{\partial UUB}{\partial x} + \frac{\partial WUB}{\partial z} = gB\sin\alpha$$ $$+ g\cos\alpha B\frac{\partial \eta}{\partial x} - \frac{g\cos\alpha B}{\rho} \int_{\eta}^{z} \frac{\partial \rho}{\partial x} dz +$$ $$\frac{1}{\rho}\frac{\partial B\tau_{xx}}{\partial x} + \frac{1}{\rho}\frac{\partial B\tau_{xz}}{\partial z} + qBU_x$$
z-momentum	$$0 = g - \frac{1}{\rho}\frac{\partial P}{\partial z}$$	$$0 = g\cos\alpha - \frac{1}{\rho}\frac{\partial P}{\partial z}$$
continuity	$$\frac{\partial UB}{\partial x} + \frac{\partial WB}{\partial z} = qB$$	$$\frac{\partial UB}{\partial x} + \frac{\partial WB}{\partial z} = qB$$
state	$$\rho = f(T_w, \Phi_{TDS}, \Phi_{ss})$$	$$\rho = f(T_w, \Phi_{TDS}, \Phi_{ss})$$
free surface	$$B_\eta \frac{\partial \eta}{\partial t} = \frac{\partial}{\partial x} \int_{\eta}^{h} UB dz - \int_{\eta}^{h} qB dz$$	$$B_\eta \frac{\partial \eta}{\partial t} = \frac{\partial}{\partial x} \int_{\eta}^{h} UB dz - \int_{\eta}^{h} qB dz$$

U = horizontal velocity, $m\ s^{-1}$ τ_x = x-direction lateral average shear stress

W = vertical velocity, $m\ s^{-1}$ τ_y = y-direction lateral average shear stress

B = channel width ρ = density

P = pressure η = water surface

Figure 12. Definition sketch for channel slope.

Linkage of Mainstem Branches with Internal Head Boundary Conditions

Since the CE-QUAL-W2 model can represent neighboring waterbodies with different vertical grids, the vertical grids must be linked together to transfer volume, mass, and heat accurately.

In order for the volume, heat, and mass to be passed from one cell to another, the flow, temperature, and concentration from the downstream segment [ID] of the upstream branch are transferred to the upstream segment [IU] of the downstream branch. Spatial averaging to conserve flow, heat, and mass is illustrated in **Figure 13**.
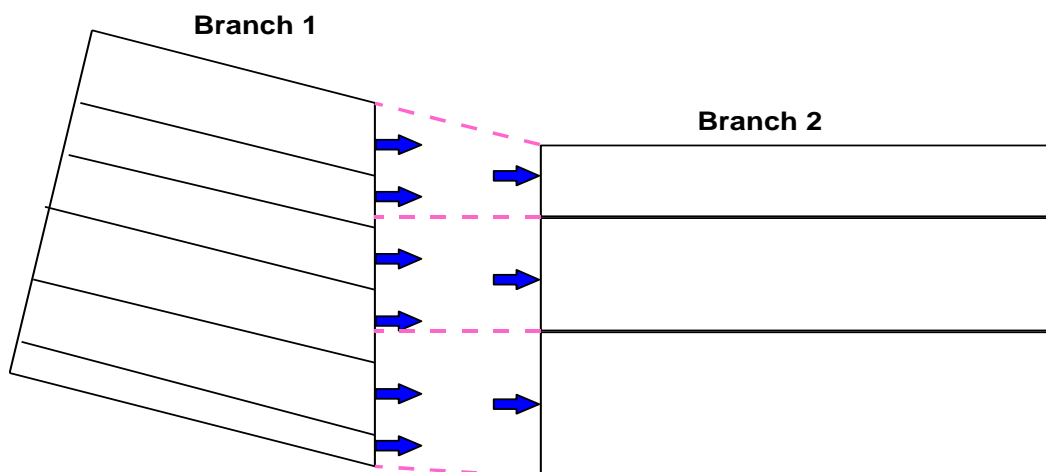
Figure 13. Transfer of mass and momentum between branches with unequal vertical grid spacing.

Linkage of Tributary or Side Branches

Tributary or side branches are not defined as "tributaries" in the model. "Tributaries" are inflows into a branch, whereas side or tributary branches are modeled as part of the model domain. Version 2 of CE-QUAL-W2 assumed all tributary branches came in at right angles to the main channel resulting in no longitudinal momentum exchange between the branches. Version 3 and later versions have included momentum transfer between the side branch and the main branch based on the segment orientation (**Figure 14**).
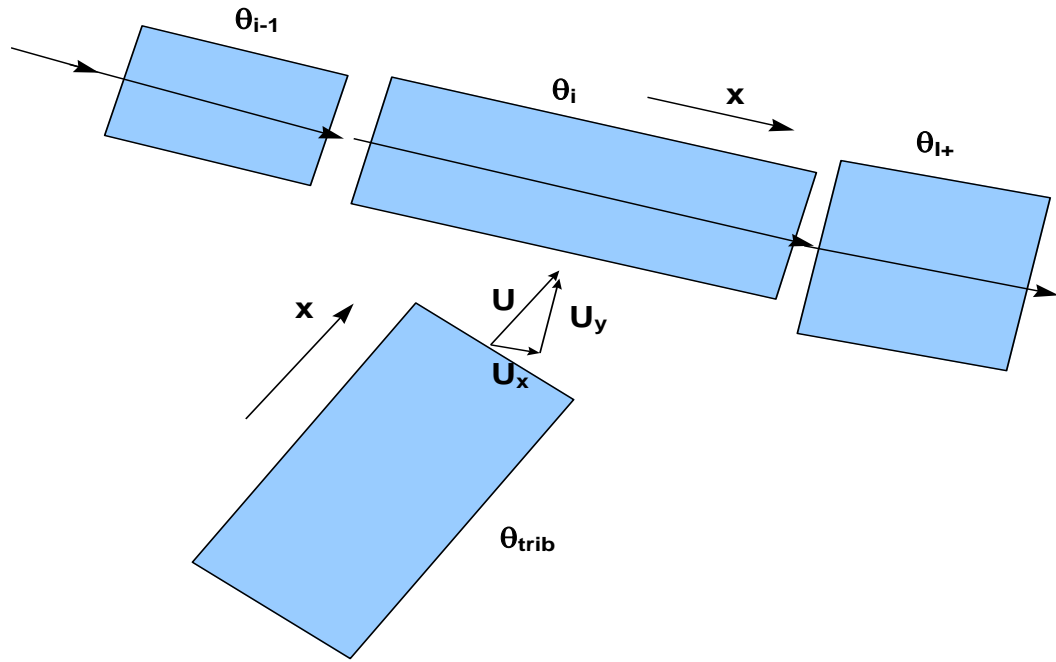
Figure 14. Linkage of tributary or side branch coming in at an angle to main branch.

The tributary branch inflow can create shear stress along both the longitudinal axis of the main stem branch and along the y-axis of the segment. The cross-shear mixing has been added to the cross-shear wind stress for the computation involving the vertical eddy viscosity and vertical diffusivity. This involves determining the y and x velocity components of the entering branch (**Figure 15**).

Longitudinal Momentum

The vector component of velocity in the x-direction of the main channel, U_x, can be computed by analysis of the channel orientations. This component in the x-direction would be:

$$U_x = U cos\beta \tag{2-51}$$

where:
  U = longitudinal velocity of the tributary at segment ID for the tributary branch
  β = difference in the angle between the main stem and tributary segments (**Figure 15**).
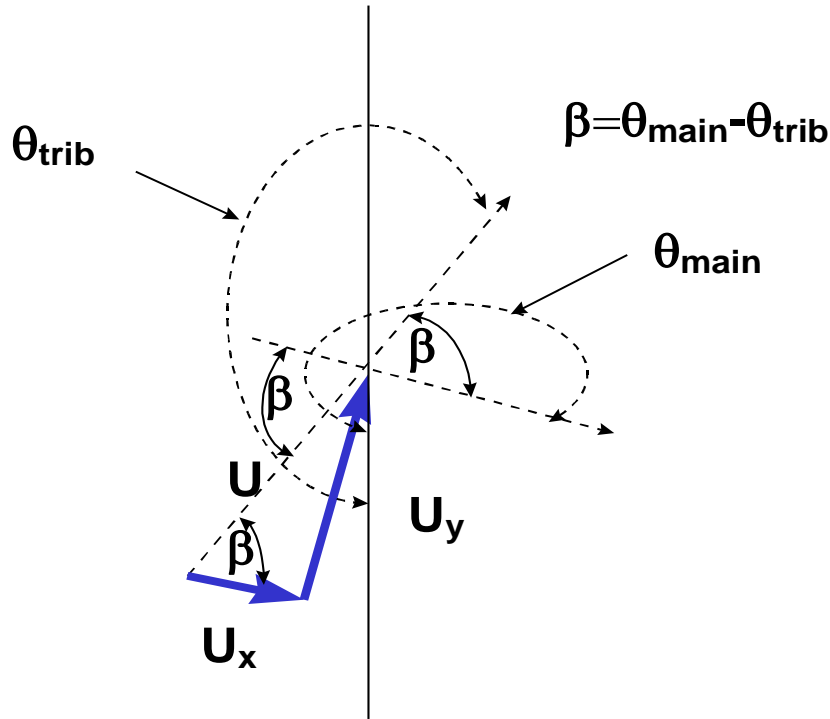
Figure 15. Schematic of x and y velocity components where Θ_{main} is the angle of the main branch segment and Θ_{trib} is the angle of the tributary segment. U_x is the x-velocity component of the tributary branch into the main segment. U_y is the y-velocity component of the tributary branch into the main segment.

The conservation of momentum about a control volume, the main stem segment, would result in an additional source of momentum. Lai (1986) shows that the correction to the x-momentum equation would be:

$$qBU_x \tag{2-52}$$

where:
$\quad q$ = lateral inflow per unit length.

This arises from re-deriving the momentum equations and assuming that all the flow entering the segment is moving at the velocity U_x. This correction to the x-momentum equation would be

$$\frac{\partial UB}{\partial t} + \frac{\partial UUB}{\partial x} + \frac{\partial WUB}{\partial z} = gB\sin\alpha + g\cos\alpha B\frac{\partial\eta}{\partial x} - \frac{g\cos\alpha B}{\rho}\int_{\eta}^{z}\frac{\partial\rho}{\partial x}dz$$

$$+ \frac{1}{\rho}\frac{\partial B\tau_{xx}}{\partial x} + \frac{1}{\rho}\frac{\partial B\tau_{xz}}{\partial z} + \underbrace{qBU_x}_{\substack{\text{momentum from} \\ \text{side tributaries}}} \tag{2-53}$$

Cross-shear of Tributary Inflow

Even though CE-QUAL-W2 assumes lateral averaging, the y-velocity coming into a reservoir may also contribute to vertical mixing. The y component of a tributary inflow is U_y = Usinβ (**Figure 15**). Since there is no y-momentum equation, this lateral shear contributes to the vertical shear stress. This is similar to how the

model also accounts for cross-shear stress from the wind given as $\tau_{wy} \cong C_D \, \rho_a \, W_h^2 \, sin(\, \Theta_1 - \Theta_2 \,)$ where this cross-shear also contributes to the vertical eddy viscosity.

For lateral inflow, the additional shear stress was parameterized as an interfacial shear:

$$\tau_{ytrib} \cong \rho \frac{f}{8} U_y^2 \qquad \qquad \textbf{(2-54)}$$

where:
    f = interfacial friction factor

For two-layer flow systems, f has been found to be of order 0.01. Therefore, the vertical eddy viscosity would be increased by a significant lateral tributary inflow.

Computation of Initial Water Surface Slope and Velocity Field for River Simulation

The initial conditions for velocity are usually set to zero, and the initial water surface elevations are set in the bathymetry input file. This is appropriate for a reservoir or lake or estuary system, but for a sloping river section setting initial water surface elevations and velocities can be computed internally in the model. The model user can turn this feature on for river systems. This feature allows for a much smoother running of the river model initially and avoids having to compute the initial water surface elevation before a model simulation. Initial water levels and horizontal velocities are computed using Manning's normal depth equation. The model bathymetry and flow files are used to determine the normal depth and horizontal velocities at the beginning of a model simulation.

The flow through each model segment is estimated first by considering all inflows and outflows such as tributaries, withdrawals, distributed tributaries, upstream branch inflows, flows associated with internal head boundaries, and dam outflows. Once the flow through each segment has been estimated, the normal depth for each segment is calculated using Manning's equation:

$$Q_i = \frac{1}{n_i} A_i R_i^{2/3} S^{1/2}$$

where:
Q_i: Flow through segment i
n_i: Manning's friction coefficient for segment i
A_i: Cross-sectional area of segment i
R_i: Hydraulic Radius of segment i
S: Branch slope

The cross-sectional area A_i and hydraulic radius R_i are a function of depth. The hydraulic radius is calculated using

$$R_i = \frac{A_i}{P_i}$$

P_i is the wetted perimeter. To calculate the normal depth, the root to the following function is found:

$$Q_i - \frac{1}{n_i} A_i R_i^{2/3} S^{1/2} = 0$$

The method of bisection (Press et al., 1992) is used to find the root, or normal depth, because the function is discontinuous (has corners).

Once the normal depth for every segment has been calculated, the water surface of each sloping branch is smoothed. If the predicted water level of a segment is less than the water level of a downstream segment, the downstream segment is considered controlling and the water level is increased to match that of the downstream segment. The effect of spillways and gates is considered by calculating the head necessary to convey the flow of the segment on the upstream side of the gate or spillway. If the normal depth predicted water level of segments upstream of a gate or spillway are less than the necessary water level at the gate or spillway, water levels of upstream segments are set to that of the segment immediately upstream of the gate or spillway.

Once water levels have been smoothed and gates or spillways have been accounted for, the average horizontal velocity U_{avg} in each segment is estimated with

$$U_{avg} = \frac{Q_i}{A_i}$$

If a branch is a "loop branch", or a branch with upstream and downstream ends that are internal head boundaries attached to segments of another, single branch, the initial velocity water level tool will set initial velocities of this branch equal to zero and estimate water levels by interpolating between the water levels in upstream and downstream boundary condition segments.

Auxiliary Functions

Auxiliary functions are relationships that describe processes independent of basic hydrodynamic and transport computational schemes in the model. Auxiliary functions include turbulent dispersion and wind shear processes, heat exchange (including ice cover), evaporation, hydraulic structures, density, and selective withdrawal.

Surface Shear Stress

Referring to **Figure 16**, the shear stress at the water surface is defined as

$$\tau_s = C_D \rho_a (W_h - u_s)^2 \cong C_D \rho_a (W_h)^2 \qquad \text{(2-55)}$$

where:
τ_s = surface shear stress at water surface, kg/m/s^2
u_s = surface velocity in water, m/s
W_h = wind velocity measured at a distance h above water surface in direction of shear, m/s
C_D = drag coefficient, [-]
ρ_a = air density, kg/m^3
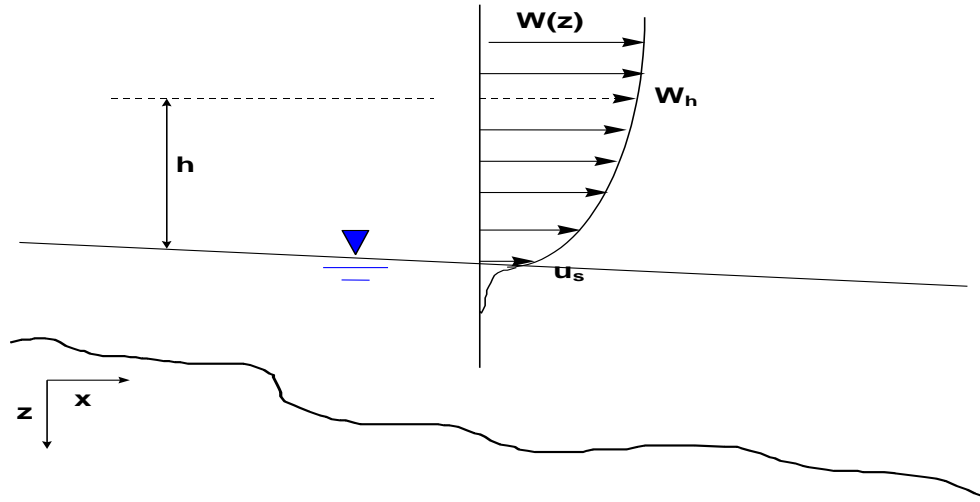
Figure 16. Shear stress at the air-water surface.

Note that this relationship leads to the "3% rule" for surface currents:

$$\tau_s = \underbrace{C_D \rho_a (W_h - u_s)^2}_{\text{air}} = \underbrace{C_D \rho_W u_s^2}_{\text{water}} \text{ if } C_{D_{\text{air}}} \sim C_{D_{\text{water}}}, \text{ then } \underbrace{u_s \sim 0.03 W_h}_{\text{3\% rule}} \qquad \textbf{(2-56)}$$

Usually the drag coefficient is a function of the measurement height, h, above the water surface. Most drag coefficient formulae have been determined based on a 10 *m* wind speed measurement height. If wind speeds are taken at other measurement heights for the shear stress calculation, these are corrected in the model to a 10 *m* height.

The wind speed is a function of measurement height. To correct the measurement height to an elevation z, the following approach is used assuming a logarithmic boundary layer:

$$\frac{W_z}{W_{z_1}} = \frac{ln(\frac{z}{z_0})}{ln(\frac{z_1}{z_0})} \qquad \textbf{(2-57)}$$

where:
   W_z = desired wind speed at elevation z
   W_{z1} = known wind speed at height z_1
   z_0 = wind roughness height (some have used 0.003 *ft* or 9.14E-4 m for wind < 5 *mph or 2.24 m/s* and 0.015 ft or 0.0046 m for wind > 5 *mph or 2.24 m/s*; the range of values are between 0.0005 to 0.03 ft or 1.5E-4 and 0.009 m; this is a user-defined coefficient in the CE-QUAL-W2 model)

This term can then be used to compute the surface stress in the direction of the x-axis and the cross-shear (the cross-shear term is used in the turbulent shear stress algorithm) as follows:

$$\tau_{wx} \cong C_D \rho_a W_h{}^2 \cos(\Theta_1 - \Theta_2) \qquad \textbf{(2-58)}$$

$$\tau_{wy} \cong C_D \rho_a W_h{}^2 \sin(\Theta_1 - \Theta_2) \qquad \textbf{(2-59)}$$

where:

τ_{wx} = surface shear stress along x-axis due to wind

τ_{wy} = surface shear stress along lateral direction due to wind

Θ_1 = wind orientation relative to North, radians

Θ_2 = segment orientation relative to North, radians

Segment and wind orientation are illustrated in **Figure 17** and **Figure 18**, respectively. The angles are measured in radians clockwise from north. A wind from the east would have an angle of $\pi/2$ radians, π radians from the south, $3\pi/2$ radians from the west, and 0 or 2π radians from the north.
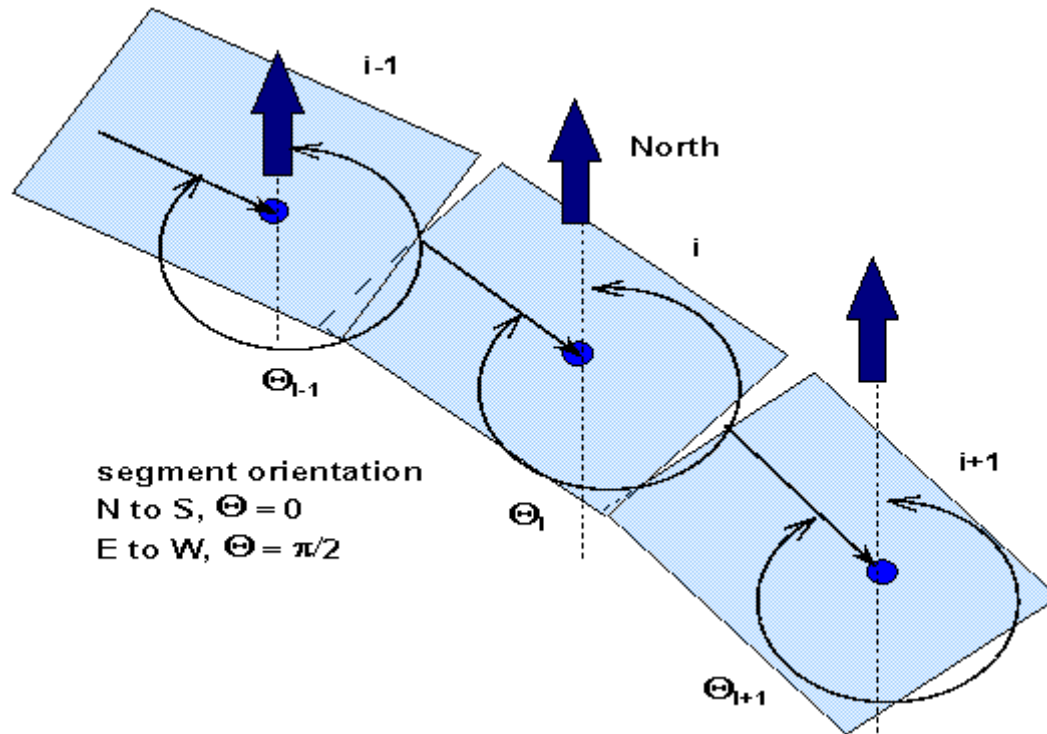
Figure 17. Segment orientation.
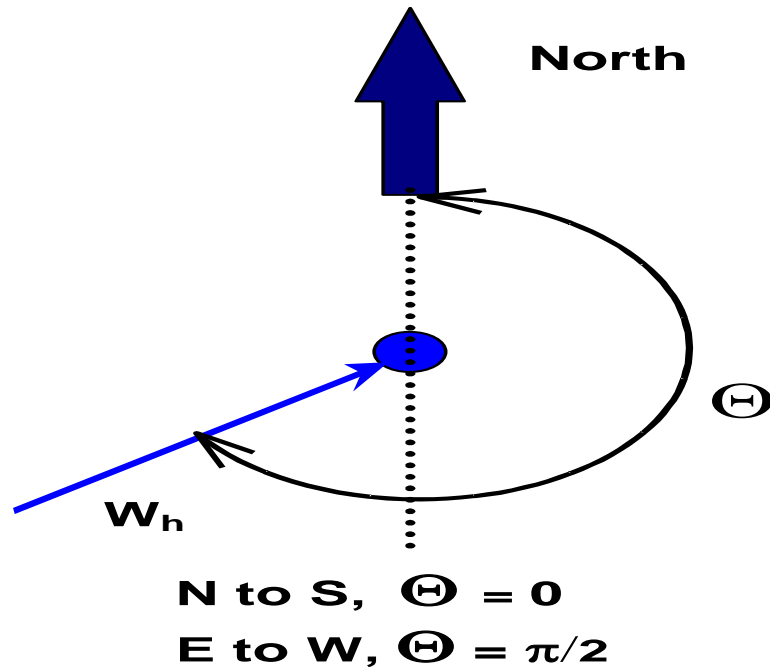
Figure 18. Wind orientation.

The CE-QUAL-W2 model Version 3.5 and earlier included a drag coefficient, C_D, that was based on the following formulae:

$$CD = 0.0 \; if \; W_{10} < 1 \; m/s$$
$$CD = 0.005W_{10}^{0.5} \; if \; 1 \; m/s \leq W_{10} < 15 \; m/s$$
$$CD = 0.0026 \; if \; W_{10} \geq 15 \; m/s$$

where W_{10} is the wind speed in m/s at 10 m.

This formulation shows that C_D decreases as wind speed decreases. It has been observed though that for wind speeds below 5 m/s, C_D increases with lowering wind speed. According to Wuest and Lorke (2003), the drag coefficient for a smooth surface (below 5 m/s) follows the following equation:

$$CD = 0.0044W_{10}^{-1.15}$$

Above a wind speed of 5 m/s, C_D can be calculated from the following implicit equation:

$$CD = \left\{ k^{-1} ln \left[\frac{10g}{CDW_{10}^2} \right] + 11.3 \right\}^{-2}$$

where k is von Karman constant (=0.41), and the '10' in the above equation has units of m. The above equation for winds greater than 5 m/s are thought to be a lower limit to the drag coefficient since the wind-wave effects at higher wind speeds probably increase the value of C_D higher than that predicted by the above implicit equation. The difference between these 2 equations is shown below in Figure 19.

Since the W2 approximation for wind speeds above 4 m/s is reasonable, for Version 3.6 and later versions the following drag coefficient formulation is used:

$$CD = 0.01 \ if \ W_{10} < 0.5 \ m/s$$
$$CD = 0.0044W_{10}^{-1.15} \ if \ W_{10} < 4 \ m/s$$
$$CD = 0.005W_{10}^{0.5} \ if \ 4 \ m/s \leq W_{10} < 15 \ m/s$$
$$CD = 0.0026 \ if \ W_{10} \geq 15 \ m/s$$

This is shown as the dotted line in Figure 19.

This will have the effect of increasing the drag coefficient at low wind speeds. The impact of this on the wind shear stress at the surface, $\tau = \rho_a CDW_{10}^2$, is shown in Figure 20.
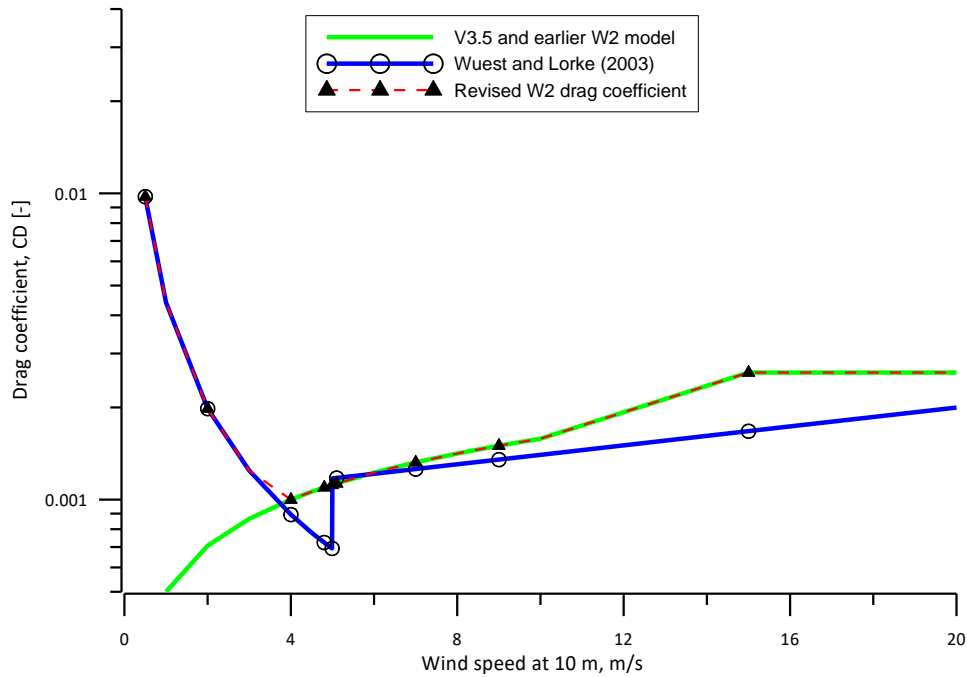
Figure 19. Comparison of current W2 model computation of C$_D$ and that recommended as a lower limit by Wuest and Lorke (2003).
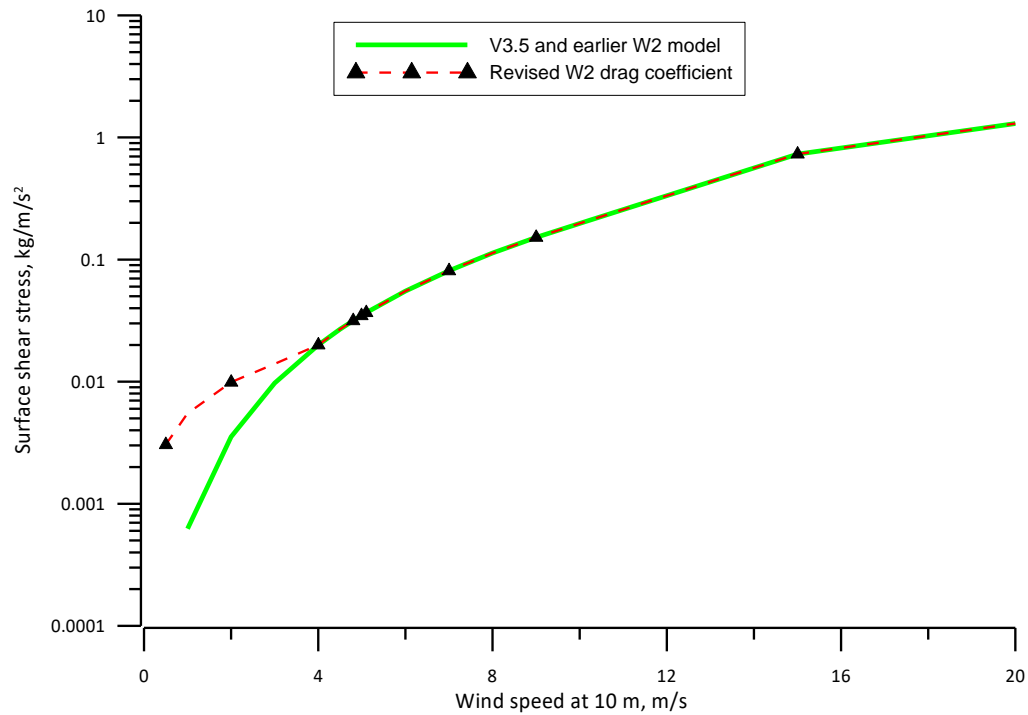
Figure 20. Surface shear stress for CE-QUAL-W2 Version 3.6 and later compared to Version 3.5 and earlier.

Wind Fetch Calculation

The wind fetch is the distance along a lake or reservoir where the wind blows unobstructed. This can contribute to enhanced wind-wave generation as the fetch distance is increased. The vertical shear stress can be enhanced as fetch increases.

The CE-QUAL-W2 model always calculates fetch distance for the vertical shear stress algorithm and for reaeration calculations. The calculation technique is a simplified one that is based on the prevailing wind direction. The fetch at a segment is the sum of the lengths of the segments either upstream or downstream based on the wind direction. For example, in Figure 21, the fetch distance of segment 5 (computed at the segment center) would be computed from the following: $Fetch = \Delta x_2 + \Delta x_3 + \Delta x_4 + \frac{\Delta x_5}{2}$. This is based on the prevailing wind direction.

A more complex fetch correction has been reviewed by Henry (2008) and will be part of an updated algorithm.

A fetch correction to the wind velocity can be used as determined by Fang and Stefan (1994). This correction is described under **Dissolved Oxygen in the lake/reservoir reaeration section**, but is not applicable to rivers.
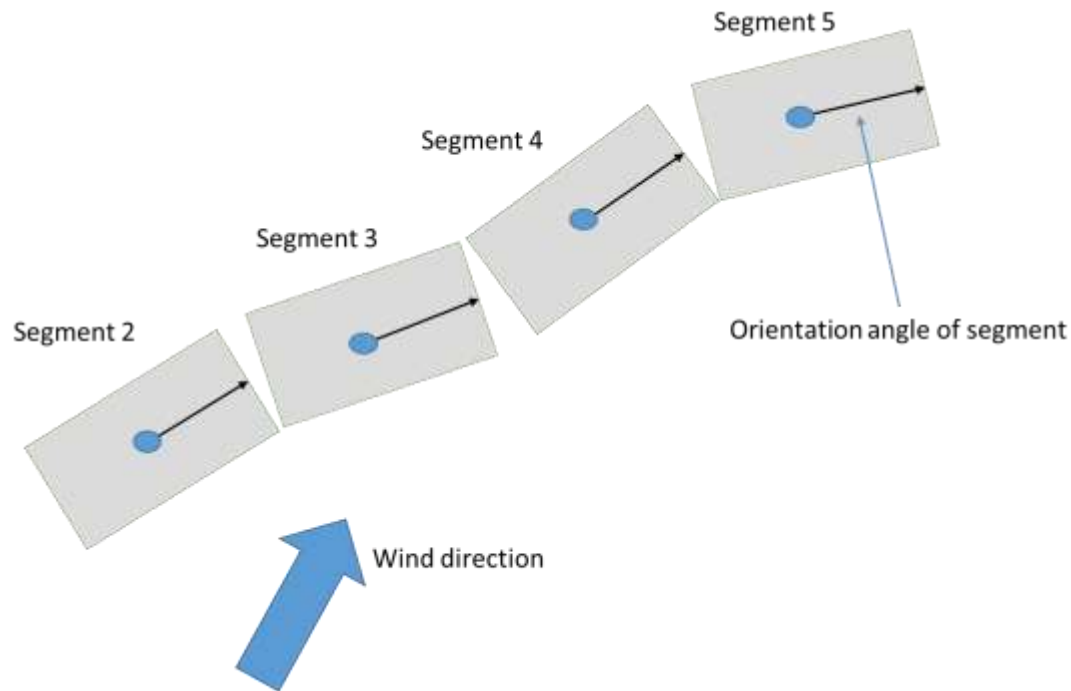
Figure 21. Illustration of fetch distance calculation.

Bottom Shear Stress

The shear stress is defined along the bottom of each cell (or for each cell in contact with side walls or channel bottom) as

$$\tau_b = \frac{\rho_w g}{C^2} U|U| \tag{2-60}$$

where:

    C = Chezy friction coefficient
    U = longitudinal velocity
    ρ_w = density of water

Also, the model user can specify a Manning's friction factor, n, where the Chezy coefficient, C, is related to the Manning's friction factor (in SI units) as

$$C = (1/n)R^{1/6} \tag{2-61}$$

where:

    n = Manning's friction factor
    R = hydraulic radius

In Version 2, the bottom shear stress was applied only to the bottom of each layer. In Version 3 and later, the sidewall friction is accounted for because of its greater importance in river systems. The user can input either the Chezy or Manning's coefficient for each model segment.

Vertical Shear Stress

The vertical shear stress is defined as

$$\frac{\tau_{xz}}{\rho} = \nu_t \frac{\partial U}{\partial z} = A_z \frac{\partial U}{\partial z} \qquad\qquad \textbf{(2-62)}$$

where:

A_z = vertical eddy viscosity, m²/s
ν_t, = vertical eddy viscosity, m²/s
U = longitudinal velocity, m/s
ρ = density of water, kg/m³
τ_{xz} = vertical shear stress, kg/m/s²

In Version 3 and later, the user must specify which formulation to use for A_z or ν_t, the vertical eddy viscosity. The formulations are shown in **Table** 2.

Table 2. Vertical eddy viscosity formulations.

Formulation	Formula	Reference
Nickuradse (NICK)	$\nu_t = \ell_m^2 \left\lvert\frac{\partial u}{\partial z}\right\rvert e^{-CRi}$ $\ell_m = H\left[0.14 - 0.08\left(1-\frac{z}{H}\right)^2 - 0.06\left(1-\frac{z}{H}\right)^4\right]$	Rodi (1993)
Parabolic (PARAB)	$\nu_t = \kappa u_* z \left(1-\frac{z}{H}\right) e^{-CRi}$	Engelund (1978)
W2 (used in Version 2)	$\nu_t = \kappa \frac{l_m^2}{2}\left[\left(\frac{\partial U}{\partial z}\right)^2 + \left(\frac{\tau_{y,wind}\, e^{-2kz} + \tau_{tributary}}{\rho \nu_t}\right)^2\right]^{1/2} e^{-CRi}$ $\ell_m = \Delta z_{max}$	Cole and Buchak (1995)
W2 with mixing length of Nickuradse (W2N)	$\nu_t = \kappa \frac{l_m^2}{2}\left[\left(\frac{\partial U}{\partial z}\right)^2 + \left(\frac{\tau_{y,wind}\, e^{-2kz} + \tau_{tributary}}{\rho \nu_t}\right)^2\right]^{1/2} e^{-CRi}$ $\ell_m = H\left[0.14 - 0.08\left(1-\frac{z}{H}\right)^2 - 0.06\left(1-\frac{z}{H}\right)^4\right]$	Cole and Buchak (1995) and Rodi (1993)
RNG (re-normaliza-tion group)	$\nu_t = \nu\left[1 + \Psi\left(3\kappa\left(\frac{zu_*}{\nu}\right)^3\left(1-\frac{z}{H}\right)^3 - C_1\right)\right]^{1/3} e^{-CRi}$	Simoes (1998)
TKE (Turbulent kinetic energy)	$\nu_t = C_\mu \frac{k^2}{\varepsilon}$ where k and ε are defined from $\frac{\partial kB}{\partial t} + \frac{\partial kBU}{\partial x} + \frac{\partial kBW}{\partial z} - \frac{\partial}{\partial z}\left(B\frac{\nu_t}{\sigma_k}\frac{\partial k}{\partial z}\right)$ $- \frac{\partial}{\partial x}\left(B\frac{\nu_t}{\sigma_k}\frac{\partial k}{\partial x}\right) = B(P + G - \varepsilon + P_k)$ $\frac{\partial \varepsilon B}{\partial t} + \frac{\partial \varepsilon BU}{\partial x} + \frac{\partial \varepsilon BW}{\partial z} - \frac{\partial}{\partial z}\left(B\frac{\nu_t}{\sigma_\varepsilon}\frac{\partial \varepsilon}{\partial z}\right)$ $- \frac{\partial}{\partial x}\left(B\frac{\nu_t}{\sigma_\varepsilon}\frac{\partial \varepsilon}{\partial x}\right) = B\left(C_{\varepsilon 1}\frac{\varepsilon}{k}P + C_{\varepsilon 2}\frac{\varepsilon^2}{k} + P_\varepsilon\right)$	Wells (2001), Gould (2006)

Formulation	Formula	Reference

where:

ℓ_m = mixing length	C = constant (assumed 0.15)	k = wave number (in W2 models)
z = vertical coordiante	u_* = shear velocity	ρ = liquid density
H = depth	κ = von Karman constant	$\Psi(x)$ = max(0,x)
u = horizontal velocity	τ_{wy} = cross-shear from wind	ν = molecular viscosity
Ri = Richardson number	Δz_{max} = maximum vertical grid spacing	C_1 = empirical constant, 100
B = width	ν_t = turbulent viscosity	k = turbulent kinetic energy (in TKE model)

ε = turbulent energy dissipation rate   P = turbulent energy production from boundary friction

U = longitudinal velocity (laterally averaged)   W = vertical velocity (laterally averaged) σ = turbulent Prandlt number

Production term: $P = \nu_t \left[\left(\frac{\partial U}{\partial z} \right)^2 \right]$ Buoyancy term: $G = -\frac{\nu_t}{\sigma_t} N^2$ Brunt–Vaisala frequency $N = \sqrt{-\frac{g}{\rho} \frac{d\rho}{dz}}$

C_ε, C_μ = constants in the TKE model τ_{ytrib} = cross-shear from lateral tributaries

The model user can also specify the maximum value of the vertical eddy viscosity **[AZMAX]**. This value is specified because the time step for numerical stability is greatly reduced when solving the momentum equations using an explicit numerical technique. In addition, the model user can choose whether to compute the vertical momentum transfer with the longitudinal momentum equation using an implicit or an explicit numerical technique. The explicit formulation was used in Version 2 with a fixed **[AZMAX]** of 1.0 x 10^{-5} $m^2 s^{-1}$. The implicit solution code was originally developed by Chapman and Cole and revised/updated.

Since the introduction of the kε turbulence closure model, this formulation works well for all waterbody types and is the suggested default model algorithm. Note that only the W2 and W2N include the effects of cross-shear from wind explicitly and from tributary or branch inflows. The kε turbulence model though accounts for total turbulent kinetic energy production from wind, not just the x-component. The W2 or W2N can be used for waterbodies with deep sections that could be stratified. The NICK, PARAB, or RNG could be used for estuary or river systems where the maximum computed **[AZMAX]** could be as high as 1 to 5 $m^2 s^{-1}$. For the river model, the model user should use the implicit solution technique. To reproduce results from Version 2 in a stratified reservoir, set **[AZMAX]** to 1.0 x 10^{-5} $m^2 s^{-1}$ and use the explicit solution.

How does one know which turbulent closure scheme to use for τ_{xz} since, according to Hamblin and Salmon (1975), "the vertical diffusion of momentum is probably the most important internal parameter" for predicting internal circulation patterns? Because of the disarray in the literature over which formulation is best, Shanahan (1980) suggested that we "use theory and literature as a guide to develop alternative viscosity functions and then test those functions in calibration runs against field data." In the absence of expensive-to-obtain current velocity data, the use of temperature profiles is often used to test the adequacy of the hydrodynamic regime against different formulations.

Typical variations of these formulations as predicted by the model are shown in **Figure 22** for Manning's fiction factor and in **Figure 23** for a Chezy friction factor. Comparison of the various turbulence closure theories to classical open channel flow theory for seven vertical layers is shown in **Figure 24**.
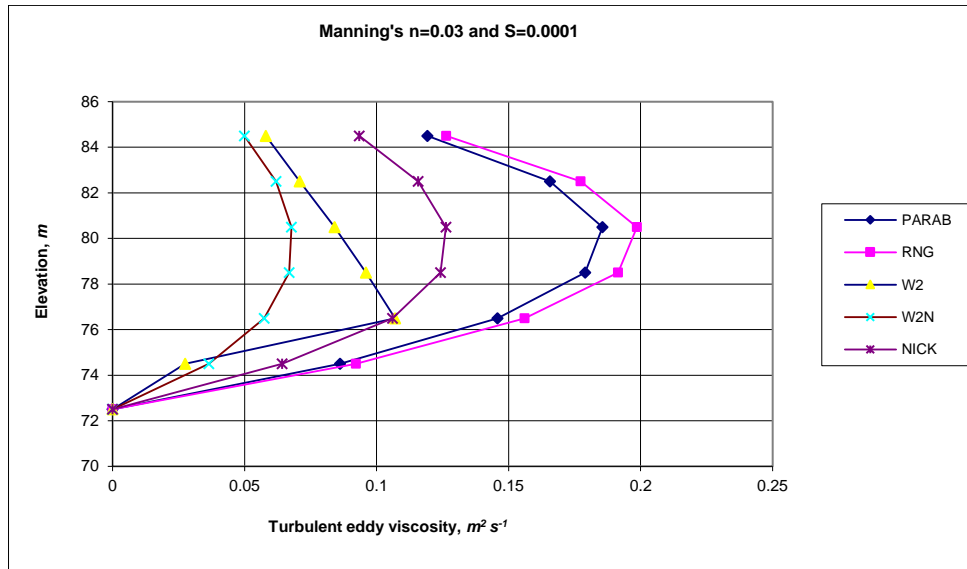
Figure 22. Variation of turbulent vertical eddy viscosity for flow of 2574 $m^3 s^{-1}$ flow down a channel of length 30 km and width of 100 m at x=15 km.
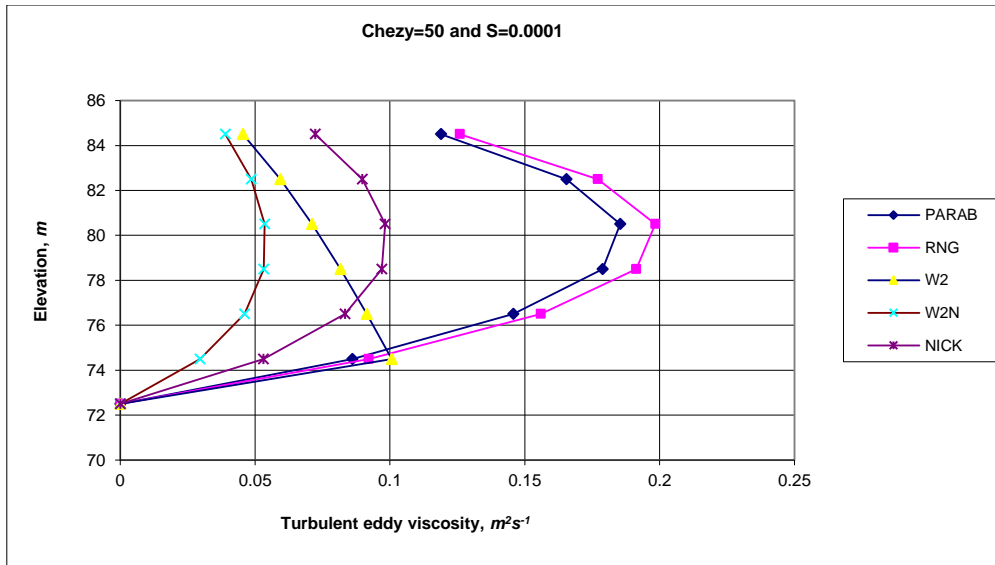
Figure 23. Variation of turbulent vertical eddy viscosity for flow of 2574 $m^3 s^{-1}$ flow down a channel of length 30 km and width of 100 m measured at x=15 km.
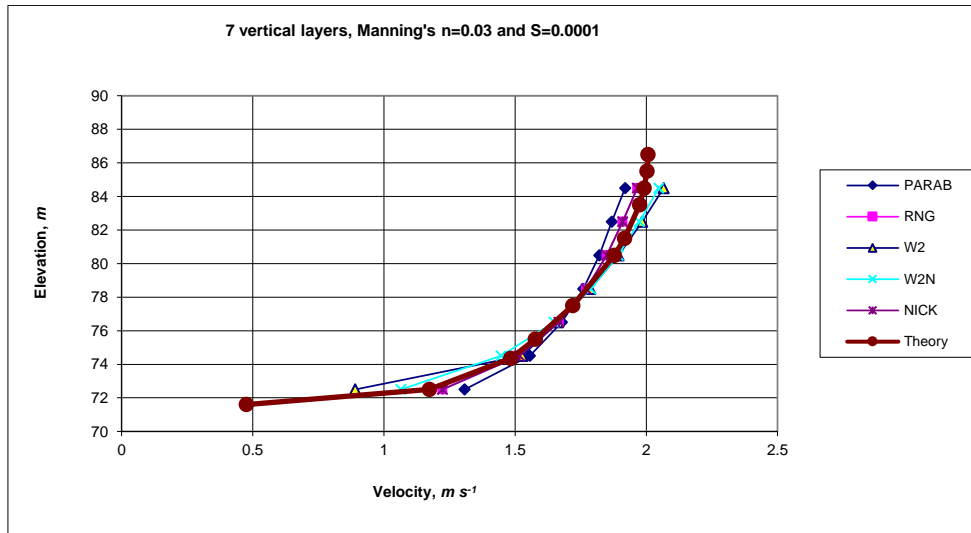
Figure 24. Comparison of vertical velocity predictions of W2 model with various eddy viscosity models compared to theory.

Formulation

In CE-QUAL-W2, the shear stress term includes the contribution to the shear stress from surface waves induced by the wind. The wind can produce waves that produce decaying motions with depth (**Figure 25**).
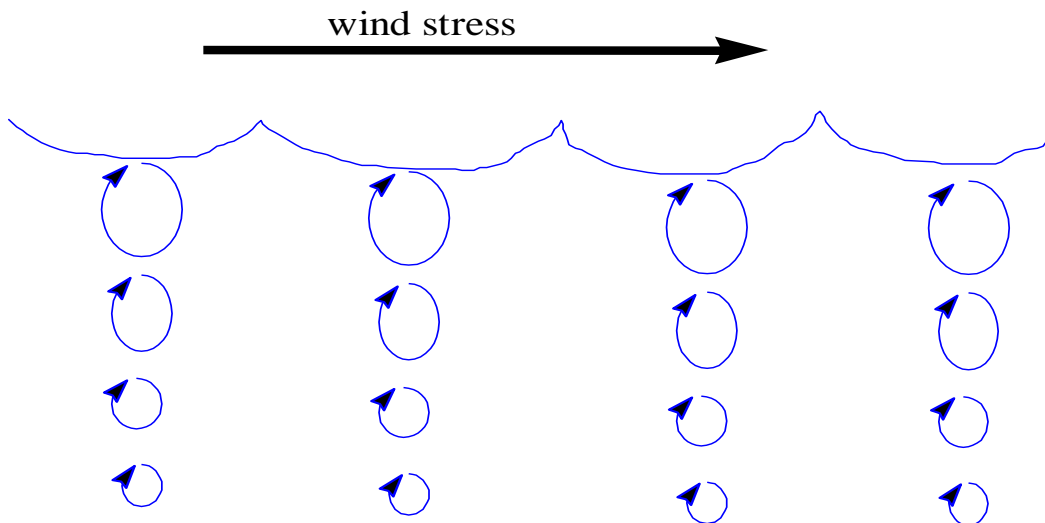
Figure 25. Conceptual diagram of wind induced motion.

The total longitudinal shear stress for a layer is defined as having contributions from interfacial velocity shear, wind wave generated shear, and friction shear along boundaries:

$$\frac{\tau_{xz}}{\rho} = A_z \frac{\partial U}{\partial z} + \frac{\tau_{wx}}{\rho} e^{-2kz} + \frac{\tau_b}{\rho} \qquad \text{(2-63)}$$

where:

τ_{wx} = longitudinal wind shear at the surface

k = wave number = $\frac{4\pi^2}{gT_w^2}$

T_w = wind wave period = $6.95E - 2 \quad F^{0.233}|W|^{0.534}$

F = wind fetch length, m

The turbulent eddy viscosity was conceptualized by Prandtl as:

$$\nu_{turbulent} = \ell^2 \left|\frac{dU}{dz}\right|$$

(2-64)

where ℓ is defined as the mixing length and can be interpreted as being proportional to the average size of large eddies or the length scale of a turbulent eddy. This length is a function of distance from a boundary or wall since the eddy sizes vary as a function of distance from a boundary. The goal in most turbulence models is the determination of the mixing length as a function of position in the fluid. Because this concept is not firmly grounded in theory, there have been many published formulations for determination of A_z in the literature (Shanahan and Harleman, 1982).

The mechanism for transporting the wind stress on the surface in the model is based on:

$$A_z = \kappa \frac{\ell^2}{2} \left[\left(\frac{\partial U}{\partial z}\right)^2 + \left(\frac{\partial V}{\partial z}\right)^2\right]^{1/2} e^{-CRi}$$

(2-65)

where:

Ri = Richardson number = $\dfrac{g\frac{\partial \rho}{\partial z}}{\rho\left(\frac{\partial U}{\partial z}\right)^2}$

κ = von Karman constant, 0.4

C = constant, 1.5

ℓ = vertical length scale chosen as cell thickness, Δz

The formulation is a typical mixing length formulation that is decreased or increased based on the Richardson number. The Richardson number accounts for the impact of density stratification on transfer of momentum between fluid parcels. In regions where there is no stratification, the Richardson number is zero and the exponential term is one. For regions where there is strong stratification, the Richardson number becomes large and the exponential term approaches zero.

In the longitudinal-vertical model, the lateral velocity, V, and its gradient, $\partial V/\partial z$, are due to the lateral component of wind wave motion and are assumed to be zero when averaged laterally, but not necessarily the square $(\partial V/\partial z)^2$. It is assumed that cross wind shear, τ_{wy}, generates lateral wave components and decays exponentially with depth such that

$$\tau_{yz} = \tau_{wy}e^{(-2kz)}$$

(2-66)

where:

τ_{wy} = lateral wind shear at the surface

Then using:

$$\frac{\tau_{yz}}{\rho} = A_z\frac{\partial V}{\partial z}$$

(2-67)

Hydrodynamics and Transport

The lateral velocity gradient squared becomes:

$$\left(\frac{\partial V}{\partial z}\right)^2 = \left[\frac{\tau_{wy}e^{(-2kz)}}{\rho A_z}\right]^2$$

(2-68)

The final equation for the vertical eddy viscosity is then:

$$A_z = \kappa \frac{l^2}{2}\left[\left(\frac{\partial U}{\partial z}\right)^2 + \left(\frac{\tau_{y,wind}e^{-2kz}}{\rho A_z}\right)^2\right]^{1/2} e^{-CRi}$$

(2-69)

The above equation is implicit. In the model, this equation is explicit since the value of A_z in the lateral wind shear term is used from the previous time step. A_z is never less than the molecular kinematic viscosity for water.

The above formulation of wind shear in horizontal momentum and evaluation of A_z leads to wind driven surface currents that are three to ten percent of the surface wind velocity with higher values appearing at higher wind speeds. This is in accordance with the attempts to relate wind speed and surface current velocity from field data appearing in the literature. With this formulation, the surface current does not reach abnormal values as it does for the case of wind shear applied only to the surface and as the surface layer thickness decreases. The depth of the wind driven surface layer increases with wind speed, and mass transport due to wind appears to be insensitive to the finite difference layer thickness.

RNG Turbulent Eddy Viscosity Formulation

The RNG model was derived from the RNG model of Yakhot and Orszag (1986) by Simoes (1998). The turbulent eddy viscosity is derived from Yakhot and Orzag (1986) as

$$\nu_t = \nu \left[1 + \Psi\left(a'\frac{\varepsilon\ell_m^4}{\nu^3} - C_1\right)\right]^{1/3}$$

(2-70)

where:
   $\Psi(x)$ = max(0,x)
   ν = molecular viscosity
   ν_t = turbulent eddy viscosity
   ℓ_m = mixing length
   ε = turbulent energy dissipation rate
   a' . 1
   C_1 . 100

Two additional equations are necessary in determining the mixing length and the turbulent energy dissipation. For the mixing length:

$$\frac{\ell_m}{H} = \kappa \frac{z}{H}\sqrt{1 - \frac{z}{H}}$$

(2-71)

and for the turbulent eddy dissipation:

$$\frac{\varepsilon H}{u_*^3} = \frac{3z}{H}\left(1 - \frac{z}{H}\right)^{3/2}$$

(2-72)

where:

$u*$ = shear velocity, $m\ s^{-1}$

H = depth of the channel, m

Z = vertical coordinate measured from the bottom of the channel, m

κ = von Karman's constant, 0.41

Substituting these into Equation 2-70:

$$v_t = v\left[1 + \Psi\left(3\kappa\left(\frac{zu_*}{v}\right)^3\left(1 - \frac{z}{H}\right)^3 - C_1\right)\right]^{1/3} \tag{2-73}$$

Simoes (1998) states that this model better represents experimental data than the more traditional parabolic eddy viscosity model of

$$v_t = \kappa z u_*\left(1 - \frac{z}{H}\right) \tag{2-74}$$

A value of v was derived as a function of temperature based on values from Batchelor (1967) using a polynomial curve fit between 0 and 30ºC.

This model was adjusted to account for stratified flow conditions by using the same Richardson number criteria as used in the original W2 model (the approach of Mamayev as quoted in French, 1985),

$$v_t = max\left(v, v_{tRNG}e^{-CRi}\right) \tag{2-75}$$

where:

Ri = Richardson number = $\dfrac{g\frac{\partial \rho}{\partial z}}{\rho\left(\frac{\partial U}{\partial z}\right)^2}$

C = empirical constant, 1.5 (French [1985] shows a value of 0.4)

The Richardson number accounts for the impact of density stratification on transfer of momentum between fluid parcels. In regions where there is no stratification, Ri=0, and the exponential term is 1. For regions where there is strong stratification (or as $\frac{d\rho}{dz} \to \infty$), the Richardson number becomes large and the exponential term approaches 0.

Nikuradse Formulation

This model, as noted in Rodi (1993), is a mixing length model where the mixing length, ℓ_m, and eddy viscosity, v_t, are determined from

$$v_t = \ell_m^2\left|\frac{\partial u}{\partial z}\right| \tag{2-76}$$

$$\ell_m = H\left[0.14 - 0.08\left(1 - \frac{z}{H}\right)^2 - 0.06\left(1 - \frac{z}{H}\right)^4\right] \tag{2-77}$$

This results in a vertical distribution for the mixing length as shown in **Figure 26**.
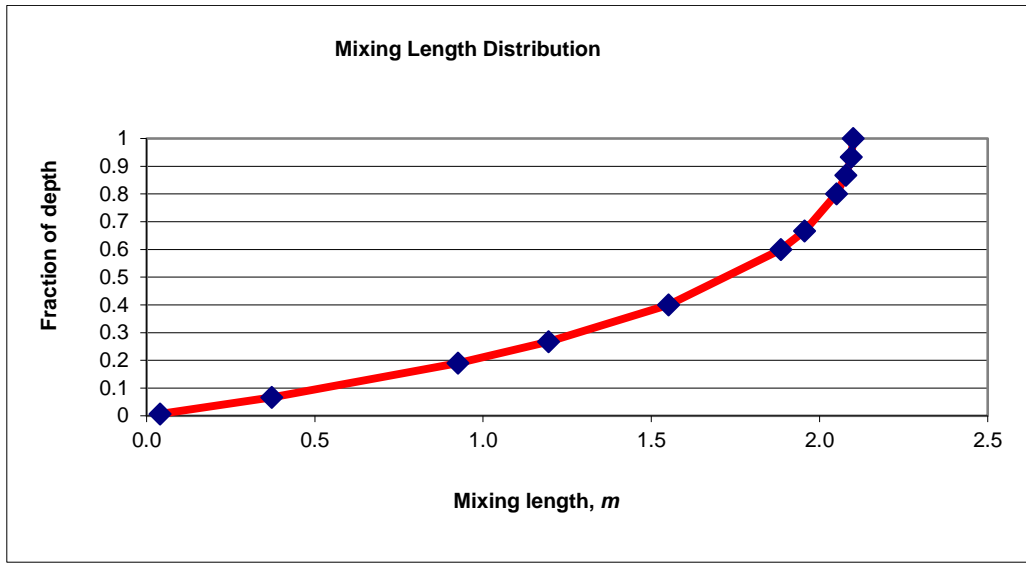
Figure 26. Mixing length as a function of depth for the Nikuradse formulation.

The stability of the water column affects the mixing length. A Richardson number criteria has been applied to correct the mixing length for stability effects such as

$$\ell_m = \ell_{mo}(1 - 7Ri) \quad if \ Ri \geq 0 \tag{2-78}$$

$$\ell_m = \ell_{mo}(1 - 14Ri)^{-0.25} \quad if \ Ri < 0 \tag{2-79}$$

This is different from the approach of Munk and Anderson (1948) where the Richardson number correction was applied to the value of A_z and not the mixing length directly.

In order to be compatible with the original formulation, the computed value of A_z is corrected using the Mamayev formulation:

$$v_t = max\left(v, v_{t_{NICK}} e^{-CRi}\right) \tag{2-80}$$

Parabolic Formulation

Another formulation is a parabolic distribution for A_z (Engelund, 1978):

$$v_t = \kappa u_* z \left(1 - \frac{z}{H}\right) \tag{2-81}$$

Figure 27 shows the spatial distribution of A_z for the parabolic model.
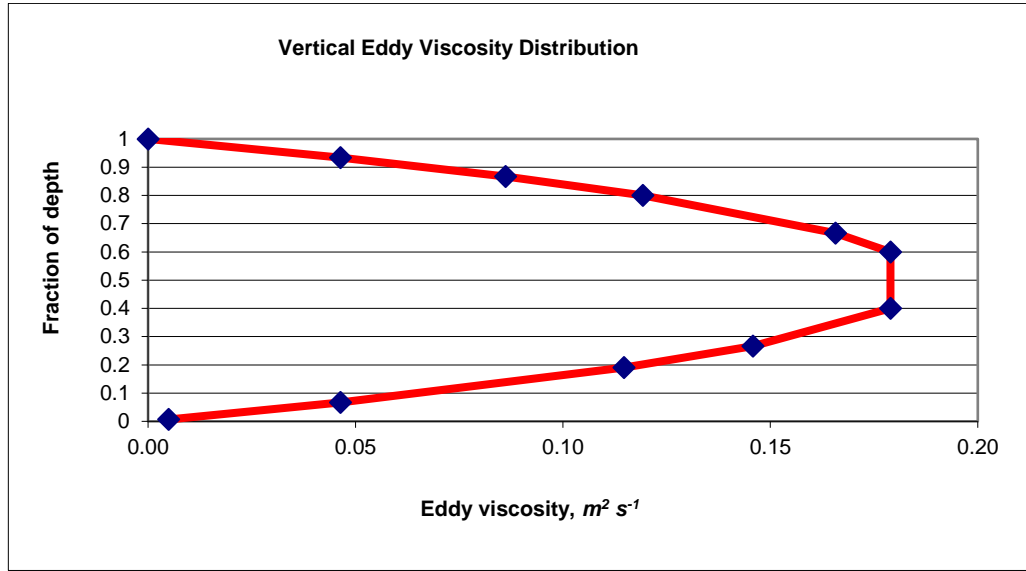
Figure 27. Variation of A_z with depth for the parabolic model of Engelund (1978).

In order to be compatible with the original formulation in the model, the computed value of A_z is corrected using the Mamayev formulation:

$$\nu_t = max\left(\nu, \nu_{t_{PARAB}}e^{-CRi}\right) \qquad \text{(2-82)}$$

W2N Formulation

The W2N formulation is the same as the W2 model except that the mixing length is no longer the layer thickness but is computed using Nickaradse's mixing length model. The equations for the W2N formulation are:

$$A_z = \kappa\left(\frac{\ell_m^2}{2}\right)\sqrt{\left(\frac{\partial U}{\partial z}\right)^2 + \left(\frac{\tau_{wy}e^{-2kz}}{\rho A_z}\right)^2}\,e^{(-CR_i)} \qquad \text{(2-83)}$$

$$\ell_m = H\left[0.14 - 0.08\left(1 - \frac{z}{H}\right)^2 - 0.06\left(1 - \frac{z}{H}\right)^4\right] \qquad \text{(2-84)}$$

TKE Formulation

The TKE formulation is a typical application of the k-ε turbulence model. This model includes both vertical transport of kinetic energy and dissipation by advection and 'diffusion' but also horizontal transport by advection. The model solves 2 partial differential equations for k and ε in order to compute the turbulent eddy viscosity:

$$\nu_t = C_\mu \frac{k^2}{\varepsilon} \qquad \text{(2-85)}$$

$$\frac{\partial \varepsilon B}{\partial t} + \frac{\partial \varepsilon BU}{\partial x} + \frac{\partial \varepsilon BW}{\partial z} - \frac{\partial}{\partial z}\left(B\frac{\nu_t}{\sigma_\varepsilon}\frac{\partial \varepsilon}{\partial z}\right) - \frac{\partial}{\partial x}\left(B\frac{\nu_t}{\sigma_\varepsilon}\frac{\partial \varepsilon}{\partial x}\right) = B\left(C_{\varepsilon 1}\frac{\varepsilon}{k}P + C_{\varepsilon 2}\frac{\varepsilon^2}{k} + P_\varepsilon\right) \qquad \text{(2-86)}$$

Hydrodynamics and Transport

$$\frac{\partial kB}{\partial t} + \frac{\partial kBU}{\partial x} + \frac{\partial kBW}{\partial z} - \frac{\partial}{\partial z}\left(B\frac{\nu_t}{\sigma_k}\frac{\partial k}{\partial z}\right) - \frac{\partial}{\partial x}\left(B\frac{\nu_t}{\sigma_k}\frac{\partial k}{\partial x}\right) = B(P + G - \varepsilon + P_k) \tag{2-87}$$

where C_μ is an empirical constant

$$P = \nu_t\left[\left(\frac{\partial U}{\partial z}\right)^2\right]$$

$$G = -\frac{\nu_t}{\sigma_t}N^2$$

$P_k = \dfrac{C_f U^3}{(0.5B)}$ Production term from boundary friction

$P_\varepsilon = \dfrac{10C_f^{1.25}U^4}{(0.5B)^2}$ Production term from boundary friction

Brunt–Vaisala frequency $N = \sqrt{-\dfrac{g}{\rho}\dfrac{d\rho}{dz}}$

B is the width, U and W are the advective velocities in x and z respectively, and other terms are empirical constants.
.
Typical values of the above model constants that have been used in other studies are:
σ_k=1.0
σ_ε=1.3
C_μ=0.09
$C_{1\varepsilon}$=1.44
$C_{2\varepsilon}$=1.92
Turbulent Prandtl/Schmidt number,σ_t, =1.0.

The solution of the above equations for k and ε used a split solution technique: explicit horizontal and source-sink term solution followed by an implicit vertical solution. A description of the solution algorithm below is based on Gould (2006).

Algorithm

The current algorithm is based on the laterally averaged k-ε turbulence model equations shown below:

$$\nu_t = C_\mu\frac{k^2}{\varepsilon} \tag{2-88}$$

$$\underbrace{\frac{\partial kB}{\partial t}}_{\text{unsteady}} + \underbrace{\frac{\partial(kUB)}{\partial x} + \frac{\partial(kWB)}{\partial z}}_{\text{convection}} - \underbrace{\frac{\partial}{\partial z}\left(B\frac{\nu_t}{\sigma_k}\frac{\partial k}{\partial z}\right)}_{\text{diffusion}} = \underbrace{B(P + G - \varepsilon + P_k)}_{\text{source/sink}} \tag{2-89}$$

$$\underbrace{\frac{\partial \varepsilon B}{\partial t}}_{\text{unsteady}} + \underbrace{\frac{\partial(\varepsilon UB)}{\partial x} + \frac{\partial(\varepsilon WB)}{\partial z}}_{\text{convection}} - \underbrace{\frac{\partial}{\partial z}\left(B\frac{\nu_t}{\sigma_\varepsilon}\frac{\partial \varepsilon}{\partial z}\right)}_{\text{diffusion}} = \underbrace{B\left(C_{\varepsilon 1}\frac{\varepsilon}{k}P - C_{\varepsilon 2}\frac{\varepsilon^2}{k} + P_e\right)}_{\text{source/sink}} \tag{2-90}$$

where ν_t, k, and ε are the eddy viscosity, turbulent kinetic energy and turbulent dissipation. P is the production term and is calculated using the following equation:

$$P = \nu_t\left(\frac{\partial U}{\partial z}\right)^2 \tag{2-91}$$

and G is the buoyancy term and is represented using

$$G = -\frac{\nu_t}{\sigma_t}N^2 \tag{2-92}$$

The production of turbulent kinetic energy and turbulent dissipation from boundary friction are represented by the terms P_k and P_ε. These terms are calculated using the following equations:

$$P_k = \frac{C_f |U^3|}{(0.5B)}$$

(2-93)

$$P_\varepsilon = \frac{10 C_f^{1.25} U^4}{(0.5B)^2}$$

(2-94)

The friction coefficient C_f is defined as

$$C_f = \frac{g}{C^2} = \frac{g n^2}{R_h^{1/3}}$$

(2-95)

Where g is gravitational acceleration, C is a Chezy friction factor, n is a Manning's friction factor, and R_h is the hydraulic radius. The remaining terms C_μ, C_ε, C_ε, σ_k, and σ_ε are empirical constants and the values used in the current model are shown in Table 3 below (Rodi, 1993).

Table 3. Constants in k-ε model (Rodi, 1993)

C_μ	$C_{\varepsilon 1}$	$C_{\varepsilon 2}$	σ_k	σ_ε
0.09	1.44	1.92	1.0	1.3

The equations above are solved using a split solution technique in a similar fashion to the horizontal momentum equation in CE-QUAL-W2. Two different methods for solving the equations were implemented. In the first method the vertical transport term was solved using an explicit finite difference along with the horizontal transport term. The second method involved integrating the vertical transport term into a fully implicit finite difference. Both methods are based on the solutions developed by Wells (2001). The computational grid used in these calculations is shown below.
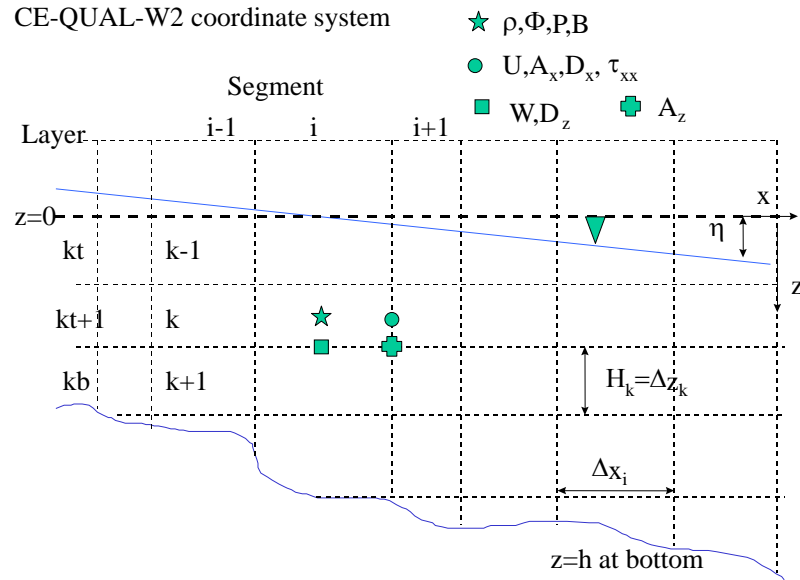
Figure 28. CE-QUAL-W2 computational grid. Width, density, pressure and water quality state variables are defined at cell centers. Horizontal velocity, longitudinal eddy viscosity and diffusivity, and longitudinal shear stress are defined at the right-hand side of the cell. Vertical velocity and vertical diffusivity are defined at the bottom of the cell, and the vertical eddy viscosity is defined at the lower right corner of the cell.

Explicit Vertical Convection

The first method developed for implementing the convective terms involved using an explicit finite difference for the vertical convection term. The first step in this method is to split the turbulent kinetic energy transport equation, equation 2-89, into the two equations shown below

$$\frac{\partial kB}{\partial t} + \frac{\partial (kUB)}{\partial x} + \frac{\partial (kWB)}{\partial z} = B(P + G - \varepsilon + P_k) \tag{2-96}$$

$$\frac{\partial kB}{\partial t} = \frac{\partial}{\partial z}\left(B\frac{\nu_t}{\sigma_k}\frac{\partial k}{\partial z}\right) \tag{2-97}$$

Next each equation is averaged over a layer:

$$\underbrace{\frac{1}{\Delta z}\frac{\partial}{\partial t}(kB\Delta z)}_{\text{unsteady}} + \underbrace{\frac{1}{\Delta z}\frac{\partial}{\partial x}(kUB\Delta z)}_{\text{convection}} + \underbrace{\frac{1}{\Delta z}\frac{\partial}{\partial z}(kWB\Delta z)}_{\text{convection}} = \underbrace{\frac{1}{\Delta z}B\Delta z(P + G - \varepsilon + P_k)}_{\text{source/sink}} \tag{2-98}$$

$$\underbrace{\frac{1}{\Delta z}\frac{\partial}{\partial t}(kB\Delta z)}_{\text{unsteady}} = \underbrace{\frac{1}{\Delta z}\left[B\frac{\nu_t}{\sigma_k}\frac{\partial k}{\partial z}\Big|^{z+\Delta z} - B\frac{\nu_t}{\sigma_k}\frac{\partial k}{\partial z}\Big|^{z}\right]}_{\text{diffusion}} \tag{2-99}$$

The partial derivatives in equation 2-98 can be replaced by the finite difference schemes below. The unsteady term is represented as an explicit finite difference, where k^* is the kinetic turbulent energy at the next time step before the application of equation 2-99.

$$\frac{\partial}{\partial t}(kB\Delta z)\Big|_{i,k} = \frac{k_{i,k}^* B_{i,k}^{n+1}\Delta z_{i,k}^{n+1} - k_{i,k}^n B_{i,k}^n \Delta z_{i,k}^n}{\Delta t} \tag{2-100}$$

The horizontal convective term is represented by an upwind difference scheme. The order of differencing depends on the direction of the horizontal component of the velocity. The difference shown below is for U>0.

$$\frac{\partial}{\partial x}(kUB\Delta z)\Big|_{i,k} = \frac{k_{i,k}^n U_{i,k}^n B_{i,k}^n \Delta z_{i,k}^n - k_{i-1,k}^n U_{i-1,k}^n B_{i-1,k}^n \Delta z_{i-1,k}^n}{\Delta x_{i,k}^n} \tag{2-101}$$

The vertical convective term is also represented by an upwind difference scheme. The order of differencing depends on the direction of the vertical component of the velocity.
The difference shown below is for W>0.

$$\frac{\partial}{\partial z}(kWB\Delta z)\Big|_{i,k} = \frac{k_{i,k}^n W_{i,k}^n B_{i,k}^n \Delta z_{i,k}^n - k_{i-1,k}^n W_{i-1,k}^n B_{i-1,k}^n \Delta z_{i-1,k}^n}{\Delta z_{i,k}^n} \tag{2-102}$$

These differences can be inserted into equation 2-96 and rearranged to give the following explicit solution for k^*.

$$k* = \frac{k_{i,k}^n B_{i,k}^n \Delta z_{i,k}^n}{B_{i,k}^{n+1}\Delta z_{i,k}^{n+1}} - \frac{\Delta t}{\Delta x_{i,k}B_{i,k}^{n+1}\Delta z_{i,k}^{n+1}}\left(k_{i,k}^n U_{i,k}^n B_{i,k}^n \Delta z_{i,k}^n - k_{i-1,k}^n U_{i-1,k}^n B_{i-1,k}^n \Delta z_{i-1,k}^n\right)$$

$$- \frac{\Delta t}{\Delta x_{i,k}B_{i,k}^{n+1}\Delta z_{i,k}^{n+1}}\left(k_{i,k}^n W_{i,k}^n B_{i,k}^n \Delta z_{i,k}^n - k_{i-1,k}^n W_{i-1,k}^n B_{i-1,k}^n \Delta z_{i-1,k}^n\right)$$

$$+ \frac{\Delta t B_{i,k}^n \Delta z_{i,k}^n}{B_{i,k}^{n+1}\Delta z_{i,k}^{n+1}}\left(P_{i,k}^n + G_{i,k}^n - \varepsilon_{i,k}^n + P_{k\,i,k}^n\right) \tag{2-103}$$

Where the terms *P* and *G* are calculated using the explicit differences shown below.

$$P_{i,k}^n = \nu_t \left(\frac{0.5\cdot(U_{k,i}^n + U_{k,i-1}^n) - 0.5\cdot(U_{k+1,i}^n + U_{k+1,i-1}^n)}{\Delta z_{k+1/2,i}^n}\right)^2 \tag{2-104}$$

$$G_{i,k}^n = \nu_t g \left(\frac{\rho_{k+1,i}^n - \rho_{k,i}^n}{\Delta z_{k,i}^n \rho_w} \right) \tag{2-105}$$

Equation 2-102 is calculated for all of the layers in a segment except for the top and bottom layer.

Next the partial derivatives in equation 2-99 are replaced with the following differences.

$$\frac{\partial}{\partial t}(kB\Delta z)\Big|_{i,k} = \frac{k_{i,k}^{n+1}B_{i,k}^{n+1}\Delta z_{i,k}^{n+1} - k_{i,k}^* B_{i,k}^{n+1}\Delta z_{i,k}^{n+1}}{\Delta t} \tag{2-106}$$

$$\left[B \frac{\nu_t}{\sigma_k} \frac{\partial k}{\partial z}\Big|^{z+\Delta z} - B \frac{\nu_t}{\sigma_k} \frac{\partial k}{\partial z}\Big|^z \right]\Bigg|_{i,k} =$$

$$B_{i,k+1/2}^n \frac{\nu_{t\,i,k+1/2}^n}{\sigma_k} \left(\frac{k_{i,k+1}^{n+1} - k_{i,k}^{n+1}}{\Delta z_{i,k+1/2}^{n+1}} \right) + B_{i,k-1/2}^n \frac{\nu_{t\,i,k-1/2}^n}{\sigma_k} \left(\frac{k_{i,k}^{n+1} - k_{i,k-1}^{n+1}}{\Delta z_{i,k-1/2}^{n+1}} \right) \tag{2-107}$$

The resulting equation can then be simplified to a tridiagonal matrix solution format,

$$AT \cdot k_{k-1}^{n+1} + VT \cdot k_k^{n+1} + CT \cdot k_{k+1}^{n+1} = DT \tag{2-108}$$

where

$$AT = -\frac{\Delta t}{B_{i,k}^{n+1}\Delta z_{i,k}^{n+1}} \left(\frac{B_{i,k-1/2}^n \nu_{t\,i,k-1/2}^n}{\Delta z_{i,k-1/2}^{n+1}\sigma_k} \right)$$

$$VT = \frac{\Delta t}{B_{i,k}^{n+1}\Delta z_{i,k}^{n+1}} \left(1 + \frac{B_{i,k+1/2}^n \nu_{t\,i,k+1/2}^n}{\Delta z_{i,k+1/2}^{n+1}} + \frac{B_{i,k-1/2}^n \nu_{t\,i,k-1/2}^n}{\Delta z_{i,k-1/2}^{n+1}} \right)$$

$$CT = -\frac{\Delta t}{B_{i,k}^{n+1}\Delta z_{i,k}^{n+1}} \left(\frac{B_{i,k+1/2}^n \nu_{t\,i,k+1/2}^n}{\Delta z_{i,k+1/2}^{n+1}\sigma_k} \right)$$

$$DT = k_{i,k}^* \frac{B_{i,k}^n \Delta z_{i,k}^n}{B_{i,k}^{n+1}\Delta z_{i,k}^{n+1}}$$

and $\frac{B_{i,k}^n \Delta z_{i,k}^n}{B_{i,k}^{n+1}\Delta z_{i,k}^{n+1}} = 1$ except at the top layer. The boundary conditions at the top and bottom layers are implemented using the method shown in the following section. Then k^{n+1} can be found by solving the equations using the Thomas algorithm.

The turbulent dissipation is found using the same procedure. Equation 2-90 is split as shown below:

$$\frac{\partial \varepsilon B}{\partial t} + \frac{\partial (\varepsilon UB)}{\partial x} + \frac{\partial (\varepsilon WB)}{\partial z} = B \left(C_{\varepsilon 1} \frac{\varepsilon}{k} P - C_{\varepsilon 2} \frac{(\varepsilon)^2}{k} + P_e \right) \tag{2-109}$$

$$\frac{\partial \varepsilon B}{\partial t} = \frac{\partial}{\partial z} \left(B \frac{\nu_t}{\sigma_\varepsilon} \frac{\partial \varepsilon}{\partial z} \right) \tag{2-110}$$

These equations are then averaged over a layer.

$$\underbrace{\frac{1}{\Delta z}\frac{\partial}{\partial t}(\varepsilon B\Delta z)}_{\text{unsteady}} + \underbrace{\frac{1}{\Delta z}\frac{\partial}{\partial x}(\varepsilon UB\Delta z)}_{\text{convection}} + \underbrace{\frac{1}{\Delta z}\frac{\partial}{\partial z}(\varepsilon WB\Delta z)}_{\text{convection}} =$$

$$\underbrace{\frac{1}{\Delta z}B\Delta z \left(C_{\varepsilon 1} \frac{\varepsilon}{k} P - C_{\varepsilon 2} \frac{(\varepsilon)^2}{k} + P_e \right)}_{\text{source/sink}} \tag{2-111}$$

$$\underbrace{\frac{1}{\Delta z}\frac{\partial}{\partial t}(\varepsilon B\Delta z)}_{\text{unsteady}} = \underbrace{\frac{1}{\Delta z}\left[B \frac{\nu_t}{\sigma_k} \frac{\partial \varepsilon}{\partial z}\Big|^{z+\Delta z} - B \frac{\nu_t}{\sigma_k} \frac{\partial \varepsilon}{\partial z}\Big|^z \right]}_{\text{diffusion}} \tag{2-112}$$

The partial derivatives in equation 2-111 are replaced with finite differences using similar schemes to those used in the turbulent kinetic energy solution. This results in the explicit solution for ε^* shown below.

$$\varepsilon* = \frac{\varepsilon_{i,k}^n B_{i,k}^n \Delta z_{i,k}^n}{B_{i,k}^{n+1} \Delta z_{i,k}^{n+1}} - \frac{\Delta t}{\Delta x_{i,k} B_{i,k}^{n+1} \Delta z_{i,k}^{n+1}} \left(\varepsilon_{i,k}^n U_{i,k}^n B_{i,k}^n \Delta z_{i,k}^n - \varepsilon_{i-1,k}^n U_{i-1,k}^n B_{i-1,k}^n \Delta z_{i-1,k}^n \right)$$

$$- \frac{\Delta t}{\Delta x_{i,k} B_{i,k}^{n+1} \Delta z_{i,k}^n} \left(\varepsilon_{i,k}^n W_{i,k}^n B_{i,k}^n \Delta z_{i,k}^n - \varepsilon_{i-1,k}^n W_{i-1,k}^n B_{i-1,k}^n \Delta z_{i-1,k}^n \right)$$

$$+ \frac{\Delta t B_{i,k}^n \Delta z_{i,k}^n}{B_{i,k}^{n+1} \Delta z_{i,k}^{n+1}} \left(C_{\varepsilon 1} \frac{\varepsilon_{i,k}^n}{k_{i,k}^n} P_{i,k}^n + C_{\varepsilon 2} \frac{(\varepsilon_{i,k}^n)^2}{k_{i,k}^n} + P_{e\,i,k}^{\,n} \right) \qquad \textbf{(2-113)}$$

where ε^* is the turbulent dissipation at the next time step before the application of equation 2-112. Equation 2-113 is calculated for all of the layers in a segment except for the top and bottom layer.

Next the partial derivatives in equation 2-112 are replaced with finite differences using similar schemes to those used in the turbulent kinetic energy solution. This again results in a set of equations in a tridiagonal format.

$$AT \cdot \varepsilon_{k-1}^{n+1} + VT \cdot \varepsilon_k^{n+1} + CT \cdot \varepsilon_{k+1}^{n+1} = DT \qquad \textbf{(2-114)}$$

where

$$AT = -\frac{\Delta t}{B_{i,k}^{n+1} \Delta z_{i,k}^{n+1}} \left(\frac{B_{i,k-1/2}^n v_{t\,i,k-1/2}^n}{\Delta z_{i,k-1/2}^{n+1} \sigma_k} \right)$$

$$VT = \frac{\Delta t}{B_{i,k}^{n+1} \Delta z_{i,k}^{n+1}} \left(1 + \frac{B_{i,k+1/2}^n v_{t\,i,k+1/2}^n}{\Delta z_{i,k+1/2}^{n+1}} + \frac{B_{i,k-1/2}^n v_{t\,i,k-1/2}^n}{\Delta z_{i,k-1/2}^{n+1}} \right)$$

$$CT = -\frac{\Delta t}{B_{i,k}^{n+1} \Delta z_{i,k}^{n+1}} \left(\frac{B_{i,k+1/2}^n v_{t\,i,k+1/2}^n}{\Delta z_{i,k+1/2}^{n+1} \sigma_k} \right)$$

$$DT = \varepsilon_{i,k}^* \frac{B_{i,k}^n \Delta z_{i,k}^n}{B_{i,k}^{n+1} \Delta z_{i,k}^{n+1}}$$

and $\frac{B_{i,k}^n \Delta z_{i,k}^n}{B_{i,k}^{n+1} \Delta z_{i,k}^{n+1}} = 1$ except at the top layer. These equations are solved for ε^{n+1} using the Thomas algorithm.

Implicit Vertical Convection

The second method is very similar to the technique developed above. The only difference is that the vertical convection term is integrated into the implicit part of the solution. First equation 2-99 is split into horizontal and vertical components as shown below:

$$\frac{\partial kB}{\partial t} + \frac{\partial (kUB)}{\partial x} = B(P + G - \varepsilon + P_k) \qquad \textbf{(2-115)}$$

$$\frac{\partial kB}{\partial t} + \frac{\partial (kWB)}{\partial z} = \frac{\partial}{\partial z} \left(B \frac{v_t}{\sigma_k} \frac{\partial k}{\partial z} \right) \qquad \textbf{(2-116)}$$

Next each equation is averaged over a layer.

$$\underbrace{\frac{1}{\Delta z} \frac{\partial}{\partial t} (kB\Delta z)}_{\text{unsteady}} + \underbrace{\frac{1}{\Delta z} \frac{\partial}{\partial x} (kUB\Delta z)}_{\text{convection}} = \underbrace{\frac{1}{\Delta z} B\Delta z (P + G - \varepsilon + P_k)}_{\text{source/sink}} \qquad \textbf{(2-117)}$$

$$\underbrace{\frac{1}{\Delta z}\frac{\partial}{\partial t}(kB\Delta z)}_{\text{unsteady}} + \underbrace{\frac{1}{\Delta z}\frac{\partial}{\partial z}(kWB\Delta z)}_{\text{convection}} = \underbrace{\frac{1}{\Delta z}B\frac{\nu_t}{\sigma_k}\frac{\partial k}{\partial z}\Big|_z^{z+\Delta z}}_{\text{diffusion}}$$ (2-118)

Then the differences developed in the previous section, equations 2-100 and 2-101, are substituted into equation 2-117. The resulting equation can then be rearranged and simplified in order to explicitly solve for k^* as shown in the equation below.

$$k* = \frac{k_{i,k}^n B_{i,k}^n \Delta z_{i,k}^n}{B_{i,k}^{n+1}\Delta z_{i,k}^{n+1}} - \frac{\Delta t}{\Delta x_{i,k}B_{i,k}^{n+1}\Delta z_{i,k}^{n+1}}\left(k_{i,k}^n U_{i,k}^n B_{i,k}^n \Delta z_{i,k}^n - k_{i-1,k}^n U_{i-1,k}^n B_{i-1,k}^n \Delta z_{i-1,k}^n\right)$$
$$+ \frac{\Delta t B_{i,k}^n \Delta z_{i,k}^n}{B_{i,k}^{n+1}\Delta z_{i,k}^{n+1}}\left(P_{i,k}^n + G_{i,k}^n - \varepsilon_{i,k}^n + P_{k_{i,k}}^{\ n}\right)$$ (2-119)

where k^* is the kinetic turbulent energy at the next time step before the application of equation 2-118. Equation 2-119 is calculated for all of the layers in a segment except for the top and bottom layer.

Next the finite differences developed in the previous section, equations 2-106 and 2-107, along with the finite difference for the vertical convective term,

$$\frac{\partial}{\partial z}(kWB\Delta z) = \frac{k_{i,k+1/2}^{n+1}W_{i,k}^n B_{i,k}^n \Delta z_{i,k}^{n+1} - k_{i,k-1/2}^{n+1}W_{i,k}^n B_{i,k}^n \Delta z_{i,k}^{n+1}}{\Delta z_k^{n+1}}$$ (2-120)

$$k_{i,k+1/2}^{n+1} = \frac{k_{i,k+1}^{n+1}+k_{i,k}^{n+1}}{2}$$ (2-121)

$$k_{i,k-1/2}^{n+1} = \frac{k_{i,k}^{n+1}+k_{i,k-1}^{n+1}}{2}$$ (2-122)

are substituted into equation 2-118.

The resulting equation can then be simplified to a tridiagonal matrix solution format,

$$AT \cdot k_{k-1}^{n+1} + VT \cdot k_k^{n+1} + CT \cdot k_{k+1}^{n+1} = DT$$ (2-123)

where

$$AT = -\frac{\Delta t}{B_{i,k}^{n+1}\Delta z_{i,k}^{n+1}}\left(\frac{W_{i,k-1/2}^n B_{i,k-1/2}^n}{2} + \frac{B_{i,k-1/2}^n \nu_{t\,i,k-1/2}^n}{\Delta z_{i,k-1/2}^{n+1}\sigma_k}\right)$$

$$VT = \frac{\Delta t}{B_{i,k}^{n+1}\Delta z_{i,k}^{n+1}}\left(1 + \frac{B_{i,k}^{n+1}\Delta z_{i,k}^{n+1}}{\Delta t} + \frac{W_{i,k+1/2}^n B_{i,k+1/2}^n}{2} - \frac{W_{i,k-1/2}^n B_{i,k+1/2}^n}{2} + \frac{B_{i,k+1/2}^n \nu_{t\,i,k+1/2}^n}{\Delta z_{i,k+1/2}^{n+1}}\right.$$
$$\left. + \frac{B_{i,k-1/2}^n \nu_{t\,i,k-1/2}^n}{\Delta z_{i,k-1/2}^{n+1}}\right)$$

$$CT = -\frac{\Delta t}{B_{i,k}^{n+1}\Delta z_{i,k}^{n+1}}\left(\frac{W_{i,k+1/2}^n B_{i,k+1/2}^n \Delta z_{i,k}^{n+1}}{2\Delta z_{i,k}^{n+1}} - \frac{B_{i,k+1/2}^n \nu_{t\,i,k+1/2}^n}{\Delta z_{i,k+1/2}^{n+1}\sigma_k}\right)$$

$$DT = k_{i,k}^* \frac{B_{i,k}^n \Delta z_{i,k}^n}{B_{i,k}^{n+1}\Delta z_{i,k}^{n+1}}$$

and $\frac{B_{i,k}^n \Delta z_{i,k}^n}{B_{i,k}^{n+1}\Delta z_{i,k}^{n+1}} = 1$ except at the top layer. The boundary conditions at the top and bottom layers are implemented using the method shown in the following section. Then k^{n+1} is found by solving the equations using the Thomas algorithm.

The turbulent dissipation is found using the same procedure. Equation 2-99 is split as shown below:

$$\frac{\partial \varepsilon B}{\partial t} + \frac{\partial (\varepsilon UB)}{\partial x} = B \left(C_{\varepsilon 1} \frac{\varepsilon}{k} P - C_{\varepsilon 2} \frac{(\varepsilon)^2}{k} + P_e \right) \tag{2-124}$$

$$\frac{\partial \varepsilon B}{\partial t} + \frac{\partial (\varepsilon WB)}{\partial z} = \frac{\partial}{\partial z} \left(B \frac{v_t}{\sigma_\varepsilon} \frac{\partial \varepsilon}{\partial z} \right) \tag{2-125}$$

These equations are then averaged over a layer.

$$\underbrace{\frac{1}{\Delta z} \frac{\partial}{\partial t} (\varepsilon B \Delta z)}_{\text{unsteady}} + \underbrace{\frac{1}{\Delta z} \frac{\partial}{\partial x} (\varepsilon U B \Delta z)}_{\text{convection}} = \underbrace{\frac{1}{\Delta z} B \Delta z \left(C_{\varepsilon 1} \frac{\varepsilon}{k} P - C_{\varepsilon 2} \frac{(\varepsilon)^2}{k} + P_e \right)}_{\text{source/sink}} \tag{2-126}$$

$$\underbrace{\frac{1}{\Delta z} \frac{\partial}{\partial t} (\varepsilon B \Delta z)}_{\text{unsteady}} + \underbrace{\frac{1}{\Delta z} \frac{\partial}{\partial z} (\varepsilon W B \Delta z)}_{\text{unsteady}} = \underbrace{\frac{1}{\Delta z} B \frac{v_t}{\sigma_\varepsilon} \frac{\partial \varepsilon}{\partial z} \Big|_z^{z+\Delta z}}_{\text{diffusion}} \tag{2-127}$$

The partial derivatives in equation 2-111 are replaced with finite differences using similar schemes to those used in the turbulent kinetic energy solution. This results in the explicit solution for ε^* shown below.

$$\varepsilon *= \frac{\varepsilon_{i,k}^n B_{i,k}^n \Delta z_{i,k}^n}{B_{i,k}^{n+1} \Delta z_{i,k}^{n+1}} - \frac{\Delta t}{\Delta x B_{i,k}^{n+1} \Delta z_{i,k}^{n+1}} \left(\varepsilon_{i,k}^n U_{i,k}^n B_{i,k}^n \Delta z_{i,k}^n - \varepsilon_{i-1,k}^n U_{i-1,k}^n B_{i-1,k}^n \Delta z_{i-1,k}^n \right)$$
$$+ \frac{\Delta t B_{i,k}^n \Delta z_{i,k}^n}{B_{i,k}^{n+1} \Delta z_{i,k}^{n+1}} \left(C_{\varepsilon 1} \frac{\varepsilon_{i,k}^n}{k_{i,k}^n} P_{k,i}^n + C_{\varepsilon 2} \frac{(\varepsilon_{i,k}^n)^2}{k_{i,k}^n} + P_{e\,i,k}^{\,n} \right) \tag{2-128}$$

Where ε^* is the turbulent dissipation at the next time step before the application of equation 2-126. Equation 2-128 is calculated for all of the layers in a segment except for the top and bottom layer.

Next the partial derivatives in equation 2-127 are replaced with finite differences using similar schemes to those used in the turbulent kinetic energy solution. This again results in a set of equations in a tridiagonal format.

$$AT \cdot \varepsilon_{k-1}^{n+1} + VT \cdot \varepsilon_k^{n+1} + CT \cdot \varepsilon_{k+1}^{n+1} = DT \tag{2-129}$$

where

$$AT = -\frac{\Delta t}{B_{i,k}^{n+1} \Delta z_{i,k}^{n+1}} \left(\frac{W_{i,k-1/2}^n B_{i,k-1/2}^n}{2} + \frac{B_{i,k-1/2}^n v_{t\,i,k-1/2}^n}{\Delta z_{i,k-1/2}^{n+1} \sigma_k} \right)$$

$$VT = \frac{\Delta t}{B_{i,k}^{n+1} \Delta z_{i,k}^{n+1}} \left(1 + \frac{B_{i,k}^{n+1} \Delta z_{i,k}^{n+1}}{\Delta t} + \frac{W_{i,k+1/2}^n B_{i,k+1/2}^n}{2} - \frac{W_{i,k-1/2}^n B_{i,k+1/2}^n}{2} + \frac{B_{i,k+1/2}^n v_{t\,i,k+1/2}^n}{\Delta z_{i,k+1/2}^{n+1}} \right.$$
$$\left. + \frac{B_{i,k-1/2}^n v_{t\,i,k-1/2}^n}{\Delta z_{i,k-1/2}^{n+1}} \right)$$

$$CT = -\frac{\Delta t}{B_{i,k}^{n+1} \Delta z_{i,k}^{n+1}} \left(\frac{W_{i,k+1/2}^n B_{i,k+1/2}^n}{2} - \frac{B_{i,k+1/2}^n v_{t\,i,k+1/2}^n}{\Delta z_{i,k+1/2}^{n+1} \sigma_k} \right)$$

$$DT = \varepsilon_{i,k}^* \frac{B_{i,k}^n \Delta z_{i,k}^n}{B_{i,k}^{n+1} \Delta z_{i,k}^{n+1}}$$

and $\frac{B_{i,k}^n \Delta z_{i,k}^n}{B_{i,k}^{n+1} \Delta z_{i,k}^{n+1}} = 1$ except at the top layer. These equations are then solved for ε^{n+1} using the Thomas algorithm.

Boundary and initial conditions for k-ε model

In order to be able to apply the algorithm developed above to the typical hydraulic problems investigated using CE-QUAL-W2 the appropriate boundary conditions for the bed, free surface, inlet and outlet as well as initial conditions must be specified. This section outlines the boundary conditions and initial conditions implemented in the current version of the k-ε algorithm.

At the bed steep gradients of turbulent kinetic energy and turbulent dissipation are present in the viscous sublayer. To accurately calculate these steep gradients, a large number of grid points are needed in the viscous sublayer and a low Reynolds number version of the k-ε turbulence model must be used. To avoid this problem an empirical law can be used to construct a simple wall function.

To construct a wall function several assumptions must be made about flow in the inner region near the wall. The largest assumption is that the flow parallel to the wall obeys the law of the wall shown below.

$$\frac{U}{U_*} = \frac{1}{\kappa} ln \left(E \frac{y U_*}{\nu} \right) \tag{2-130}$$

Where U_* is the bed friction velocity, κ is the von Karman constant, y is the distance of the grid point from the bed, E is the roughness coefficient and ν is the kinematic viscosity. In addition to the assumption that the flow has a logarithmic velocity profile it is necessary to assume that the total shear stress remains constant in the inner region and is equal to the bed stress. These assumptions can normally be made if the first grid point is in the range of $30 < y^+ < 100$ from the wall (Rodi, 1993).

$$y^+ = \frac{y U_*}{\nu} \tag{2-131}$$

In the range of y^+ specified above the Reynolds stresses are relatively constant. In this region local equilibrium prevails, so if buoyancy effects are negligible then the production equals dissipation which implies that $P = \varepsilon$. It is also assumed that the total shear stress remains constant and is approximately equal to the wall shear stress in this region. Using these assumptions and equation 1 it is possible to derive the equation for turbulent kinetic energy at the first grid point shown below (Rodi, 1993).

$$k = \frac{U_*^2}{\sqrt{c_\mu}} \tag{2-132}$$

The boundary condition for turbulent dissipation can be determined using $\varepsilon = P = U_*^2 \frac{\partial U}{\partial y}$ where $\frac{\partial U}{\partial y}$ is determined from equation 2-130 and is given below.

$$\varepsilon = \frac{U_*^3}{\kappa y} \tag{2-133}$$

Since y, U, E, κ, ν and E are known, a very simple wall function can be implemented by solving equation 2-130 for U_*. In the current version of the k-ε model U_* was found using a root solver based on the bisection method from Press et al. (1996). Then equations 2-132 and 2-133 are used to determine the turbulent kinetic energy and the turbulent dissipation at the first grid point. This simple approach has some limitations, such as not being able to handle separated flow, but seemed like a reasonable first approximation.

The wall function outlined above is valid for both smooth and rough boundaries. For hydraulically smooth beds the roughness coefficient E is set to 9.535 (Ferziger and Peric, 2002). For rough boundaries a smaller value of E is used. Two options are available in the current algorithm for specifying the roughness coefficient. A uniform constant roughness coefficient value can be applied to all segments or the roughness coefficient can be calculated based on the Manning's coefficients specified in the bathymetry file.

In the first option the user specifies the roughness coefficient and this value is used to calculate the bed friction velocity using equation 2-130. After the bed friction velocity has been determined a new Manning's coefficient is calculated using equation 2-134 below. This method was used primarily for experimental channel test cases where the bed was hydraulically smooth and had a roughness coefficient equal to 9.535.

$$n = \frac{R_h^{1/6}}{\sqrt{\frac{g}{\left(\frac{U_*}{U_m}\right)^2}}} \tag{2-134}$$

In the second option the roughness coefficient is calculated using a Strickler relationship and an approximation of the Nikuradse's data shown in equations 2-135 to 2-137 below (Krishnappan and Lau, 1986).

$$E = exp\left(\frac{(\kappa B_s)}{\left(\frac{U_* k_S}{\nu}\right)}\right) \tag{2-135}$$

$$B_s = \left[5.50 + 2.5\, ln\left(\frac{U_* k_S}{\nu}\right)\right] exp\left\{-0.217\left[ln\left(\frac{U_* k_S}{\nu}\right)\right]^2\right\}$$

$$+ 8.5\left(1 - exp\left\{-0.217\left[ln\left(\frac{U_* k_S}{\nu}\right)\right]^2\right\}\right) \tag{2-136}$$

$$k_s = (n \cdot 24.04)^6 \qquad (k_s \text{ in m}) \tag{2-137}$$

The appropriate boundary condition for the free surface is harder to determine. Unfortunately, there is very little experimental data available for turbulent statistics at the free surface (Rodi, 1993). It is difficult to make such measurements because hot wire anemometers tend to disturb the surface and laser Doppler anemometry systems, LDA, have issues with reflections and refraction caused by the free surface (Swean et al., 1991). In many cases researchers have turned to Direct Navier Stokes simulations for more information on the relationship between turbulent kinetic energy and turbulent dissipation and the free surface (Swean et al., 1991, Cotton et al., 2005).

A first approximation for the boundary conditions at the free surface in absence of a wind induced shear is to use a symmetry plane where both turbulent kinetic energy and turbulent dissipation are found using a zero-gradient condition (Rodi, 1993). However, it is generally thought that the presence of the free surface should reduce the length scale of turbulence and reduce the turbulent dissipation. An attempt to take this into account was made in the empirically determined boundary conditions shown below (Celik and Rodi, 1984).

$$\frac{\partial k}{\partial y} = 0 \tag{2-138}$$

$$\varepsilon = \frac{k^{3/2}}{aH} \tag{2-139}$$

Where a is an empirical constant and H is the depth of the shear layer, in this case the depth of the channel. The coefficient a was originally set to a value of 0.18 by Celik and Rodi (1984) and then later changed to a value of 0.43 by Celik and Rodi (1988).

For a free surface with wind induced surface shear, the boundary conditions similar to those used for wall boundaries are appropriate, equations 2-130, 2-132, and 2-133. The free surface can be seen as a moving wall. The bed friction velocity in equations 2-132 and 2-133 can be replaced with the wind induced surface friction velocity (Rodi, 1993).

Rodi presented a set of boundary conditions that could be used for free surfaces with or without wind induced surface shear. When the wind induced surface shear is large then the following boundary condition is used for turbulent kinetic energy.

$$k = \frac{U_{*S}^2}{\sqrt{C_\mu}}$$
(2-140)

When the surface shear is small, $k_s\sqrt{c_\mu} > U_{*S}^2$, then the symmetry condition for turbulent kinetic energy shown in equation 2-138 is used. Where U_{*S} is the wind induced surface friction velocity. In a similar fashion the turbulent dissipation boundary condition for a free surface with and without wind induced surface shear was developed and is given as

$$\varepsilon = \frac{\left(k_s\sqrt{C_\mu}\right)^{3/2}}{\kappa\left[y + aH\left(1 - \frac{U_{*S}^2}{k_s\sqrt{C_\mu}}\right)\right]}$$
(2-141)

The coefficient a was set to a value of 0.07 by Rodi in 1983. When surface shear is present, equation 2-140 reduces to $\varepsilon = \frac{U_{*S}^3}{\kappa \cdot y}$. When surface shear is not present, equation 2-141 becomes $\varepsilon = \frac{k^{3/2}}{\kappa[y + aH]}$ which is similar to equation 2-139 above.

The original CE-QUALW2 free surface boundary conditions were

$$k = \frac{\left(U_{*S}^2 + U_{*boundary}^2\right)}{\sqrt{C_\mu}}$$

$$\varepsilon = \frac{\left(U_{*S}^3 + U_{*boundary}^3\right)}{\kappa \cdot y}$$

These are similar to the boundary conditions presented in equations 2-140 and 2-141 when wind induced shear is present. The only difference is that both the turbulent kinetic energy and turbulent dissipation boundary conditions include an additional term for the friction velocity of the lateral boundaries.

The initial conditions and inlet boundary conditions are specified by setting the eddy viscosity, turbulent kinetic energy, and turbulent dissipation terms to the following values.

$$\upsilon_t = 1.4 \cdot 10^{-6}$$
$$k = 1.25 \cdot 10^{-7}$$
$$\varepsilon = 1.0 \cdot 10^{-9}$$

The outlet values of turbulent kinetic energy and turbulent dissipation are determined using a zero-gradient approach as shown below

$$\frac{\partial k}{\partial x} = 0$$
$$\frac{\partial \varepsilon}{\partial x} = 0$$

This is done by setting the value of turbulent kinetic energy and turbulent dissipation at the outlet cell equal to the value of the cell in the upstream segment.

Computations of k and ε compared to experimental data are shown in Gould (2006). The experimental data were taken from a uniform open channel experiment conducted by Nakagawa, Neuzu, and Ueda (1975). Figure 29 and Figure 30 show CE-QUAL-W2 model comparisons to the experimental data varying

Manning's friction factor. As shown in Gould (2006), the number of vertical layers used in the model application was very important in being able to match experimental laboratory data.

Turbulent Dissipation
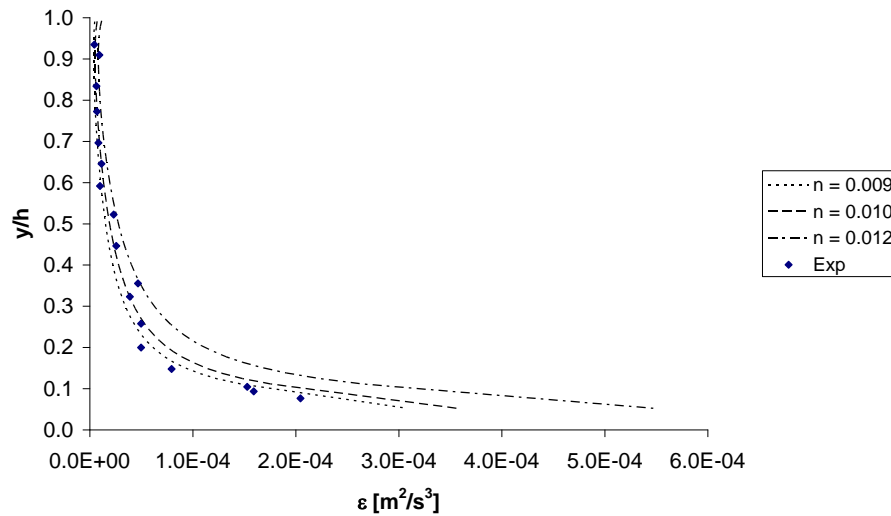
Figure 29. Comparison of CE-QUAL-W2 model predictions of turbulent dissipation with field data from Nakagawa, Neuzu, and Ueda (1975).

Turbulent Kinetic Energy
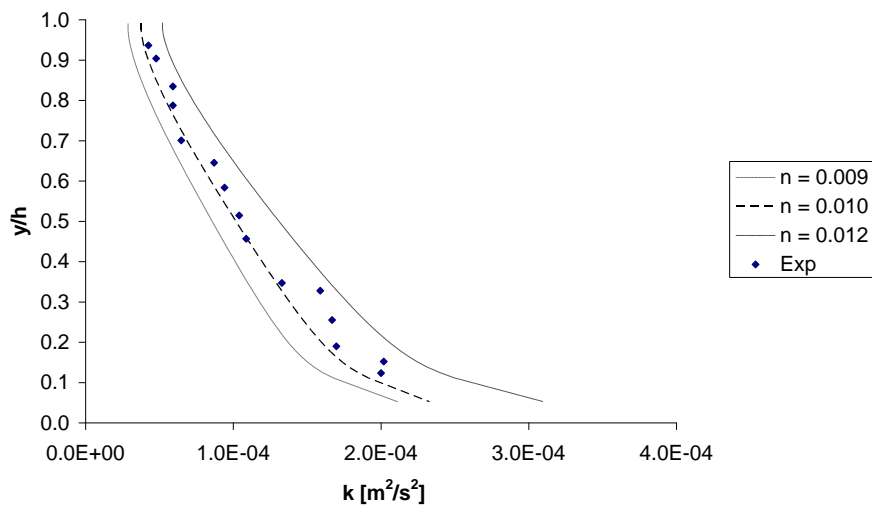
Figure 30. Comparison of CE-QUAL-W2 model predictions of turbulent kinetic energy with field data from Nakagawa, Neuzu, and Ueda (1975).

Effect of Vertical Layer Numbers on Vertical Turbulence

In contrast to other riverine models that assume vertically well-mixed systems, CE-QUAL-W2 accounts for the vertical variation of velocity in a riverine reach. Even though there is an added computational burden of computing the 2D velocity profile, the advantage of making this computation is that the friction factor (Manning's or Chezy) for a segment can be flow or stage invariant depending on the number of vertical layers schematized.

Many 1D hydraulic flow models, such as CE-QUAL-RIV1 and UNET (Barkau, 1997), allow the model user to specify how Manning's friction factor changes with depth. The Mannning's friction factor, *n*, has been thought to vary as a function of depth, Reynolds number, and roughness factor or scale of bed grain size (Ugarte and Madrid, 1994; Soong, et. el., 1995). Some of these formulations for variation of Manning's friction factor with hydraulic radius, *R*, are shown in **Figure 31**:

The figure contains the following equations:

$$Jarrett\,(1984):$$
$$n = 0.39 S^{0.38} R^{-0.16}$$

$$Limerinos\,(1970):$$
$$n = \frac{0.0926\,R^{1/6}}{1.16 + 2\log\left(\dfrac{R}{d_{84}}\right)}$$
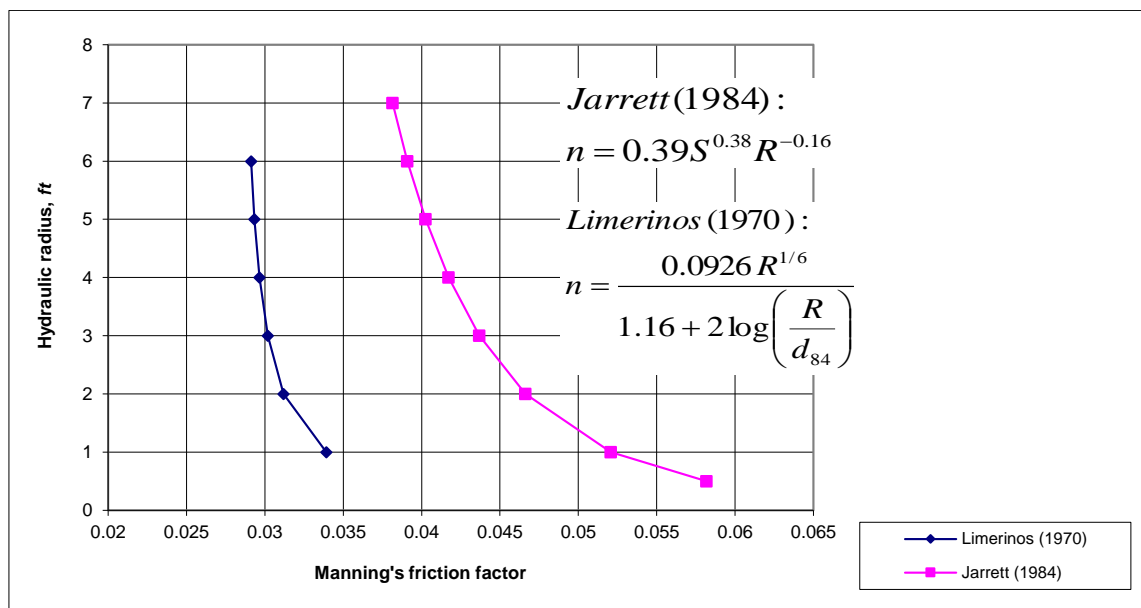
Figure 31. Variation of Manning's friction factor using formulae from Limerinos (1970) and Jarrett (1984, 1985) for a channel slope, S, of 0.0005 and 84th pecentile diameter of the bed material, d_{84}, of 50.

Researchers understand that the friction factor, when representing a hydraulic element with uniform roughness, should be flow invariant with depth (Henderson 1966). However, many assert that the friction factor changes with depth because the friction coefficient is variable with the wetted perimeter. Some investigators reason that it is to be expected that at shallow depths the larger size of the bed material produces a higher overall friction factor than a deeper flow where the sidewalls may have a smaller friction.

Since most researchers used 1D, cross-sectionally averaged flow equations such as Manning's Equation or 1D dynamic hydraulic models, this parameterization itself has been responsible for the seeming variation of Manning's friction factor with depth. For example, all 1D hydraulic models implicitly assume that the rate of transfer of momentum from the bottom of the channel to the top is "infinite" in that regardless of the depth, the shear stress of the bottom is felt even at the surface. For these hydraulic models, even as the depth of the channel increases, they still assume the surface feels the shear stress at the channel bottom and this effect is transferred over the depth of the channel. Therefore, as the water depth increases, the apparent friction factor must be reduced because of the assumption of momentum transfer between the bottom and the surface.

However, in a 2-D, longitudinal-vertical, river model, Manning's friction factor does not have to vary with stage in order to produce the effect that as the river stage increases, the apparent friction decreases. The water surface set-up changes significantly as the number of layers increase. In general, the water surface slope increases as the number of computational layers decreases. This is because the average eddy viscosity in the water column increases as the number of layers decrease until at the limit of a one-layer system, the average vertical eddy viscosity is infinite. The fact that the Manning's friction factor seems to decrease with depth in 1D models is accounted for in modeling the river channel as a 2D, longitudinal-vertical system.

The model allows choosing between six different vertical eddy viscosity formulations. These formulations are shown in **Table** 2. Typical variation of these formulations is shown in **Figure 24** for Manning's friction factor for an open-channel, non-stratified flow regime as compared to theory of steady, uniform channel flow.

The number of vertical layers significantly affects model predictions. For example, **Figure 32** shows a comparison of vertical velocity profiles from a model with one, three, and seven vertical layers using the parabolic eddy viscosity model.
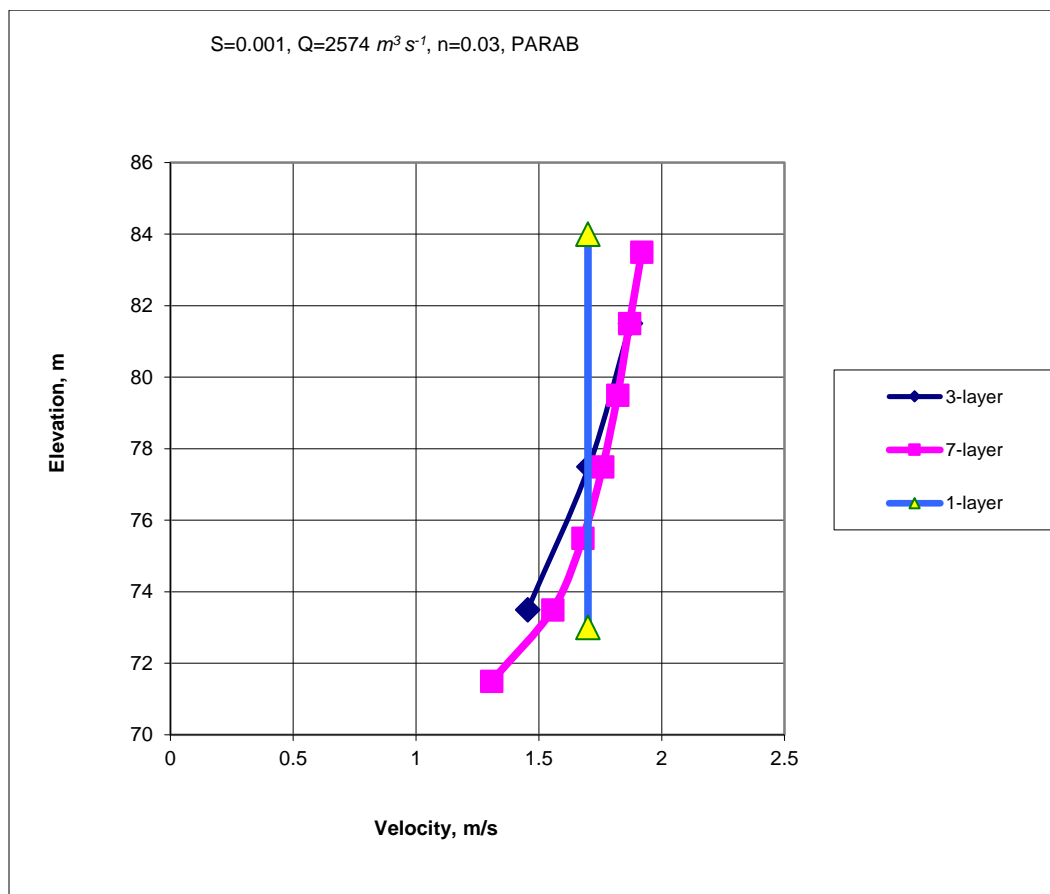
Figure 32. Comparison of vertical velocity predictions with one, three, and seven vertical layers

Figure 33 shows how the change in the number of vertical layers affects the water surface slope over the domain length for a steady-state flow. In order to model the water surface slope of the 1-layer model with the 7-layer model, the apparent value of Manning's friction factor would have to be reduced. Hence, the apparent friction decreases as the number of layers increase.
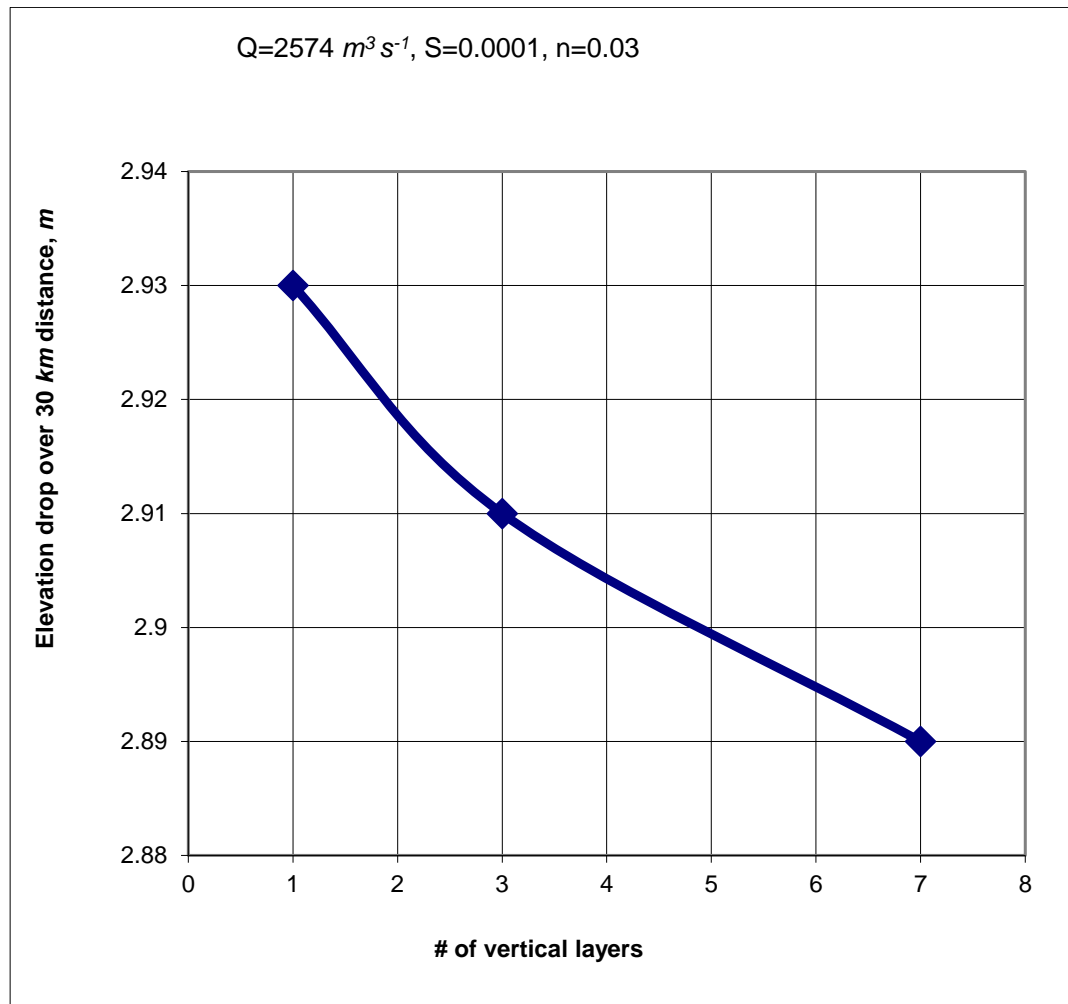
Figure 33. Comparison of elevation drop of W2 model with one, three, and seven vertical layers with same Manning's friction factor.

CE-QUAL-W2 has also been compared to the 1D models DYNHYD (Ambrose et al., 1988) and CE-QUAL-RIV1 (Environmental Laboratory, 1995) by running W2 with only a single vertical layer. The average velocities between the three models agreed well with theory but the water surface slopes are different. W2 predicts an elevation difference of 2.93 m, compared to 2.07 m for DYNHYD and 2.05 m for RIV1 over 30 km for a flow of 2574 $m^3 s^{-1}$, a Manning's n of 0.03, a slope of 0.001, and a channel width of 100 m. Based on steady-state theory, the actual difference should be 2.9 m. Both the DYNHYD and RIV1 models require friction factors greater than expected to correspond to classical theory. This may be a result of these models not incorporating sidewall friction that was important during these test runs where the depth was 15 m and the width was 100 m.

Longitudinal Shear Stress

The longitudinal turbulent shear stress is defined as

$$\frac{\tau_{xx}}{\rho} = \nu_t \frac{\partial U}{\partial x} = A_x \frac{\partial U}{\partial x}$$

(2-142)

where:

A_x = ν_t = longitudinal eddy viscosity

A_x is a user-defined constant or it can be set to scale with the average longitudinal velocity. This turbulence closure approximation is termed a zero-order closure model since no further equations are necessary to solve for the transmission of shear stress within the fluid.

This term is usually of very low magnitude except in areas near boundaries such as at a dam face where the longitudinal velocity goes to zero.

The equation for computing A_x is

$$A_x = \propto \bar{\bar{U}} \Delta z$$

Where α is a user input value, U with double bars are the time-averaged, lateral averaged longitudinal velocity at a segment and layer.

Hydraulic Structures

Pipes

The model user can specify a pipe or culvert between model segments (Berger and Wells, 1999) using a 1D, unsteady hydraulic model that computes the flow between the two linked segments. The model computes the selective withdrawal outflow from the upstream segment with the model user specifying whether the inflow to the downstream segment is treated as mixed over the depth, inflow depth is determined from inflow density, or inflow depth is specified between an upper and lower elevation. The flow between an upstream segment and a downstream segment is shown in **Figure 34**.
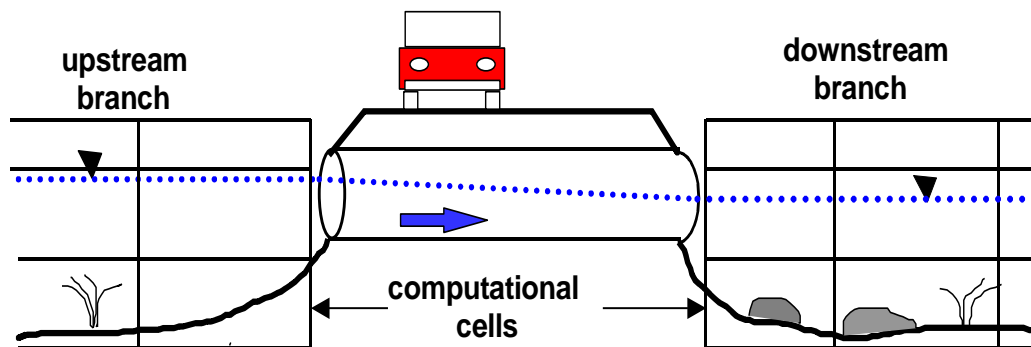
Figure 34. Schematic of linkage of model segments with a culvert.

This model is only appropriate for simple piping systems that are not suddenly under a large hydraulic head. The governing equations for computing the flow and the numerical solution technique are shown below.

The governing equations used to predict flow through culverts are the 1D, time-dependent conservation of momentum and continuity equations (Yen, 1973).

$$\frac{\partial u}{\partial t} + u\frac{\partial u}{\partial x} + g\cos\varphi\frac{\partial h}{\partial x} - g\left(S_o - S_f - S_m\right) = 0 \qquad \textbf{(2-143)}$$

$$\frac{\partial h}{\partial t} + u\frac{\partial h}{\partial x} + \frac{A}{T}\frac{\partial u}{\partial x} = 0 \qquad \textbf{(2-144)}$$

where:
- u = velocity, $m\ s^{-1}$
- t = time, s
- h = piezometric head, m
- g = gravitational acceleration, $m^2\ s^{-1}$
- x = distance along axis of culvert, m
- A = cross-sectional area of culvert filled with water, m^2
- T = width of water level surface, m
- ϕ = angle between culvert axis and horizontal
- S_o = culvert slope
- S_f = friction slope.
- S_m = minor loss slope

The friction slope S_f is estimated using the Manning formula:

$$S_f = \frac{n^2}{R^{4/3}}u|u| \qquad \textbf{(2-145)}$$

where:
- n = Mannings roughness factor
- R = hydraulic radius.

Minor losses due to entrance configuration, gates, valves, and corners are accounted for in the minor loss term S_m:

$$S_m = k\frac{u|u|}{2g}\frac{1}{L} \qquad \textbf{(2-146)}$$

where:
- k = sum of minor loss coefficients
- L = length

Pressurized or full culvert flow is modeled assuming a fictitious water surface width called a Preissmann slot (Yen, 1986). If the culvert is full, the surface width T is zero and the governing equations become singular. Using a Preissmann slot avoids having to switch between the open channel and pressurized flow equations. The slot must be narrow enough to minimize error in the mass and momentum balance but large enough to maintain numerical stability when solving the open channel St. Venant equations. A top width of 0.5% of the diameter is assumed for culverts flowing full.

The advantages of using a Preissmann slot are (Yen, 1986):

1. uses only Saint-Venant equations and avoids switching between the surcharge equation and open-channel flow equations and avoids the associated separate treatment of the boundary conditions
2. no need to define surcharge criteria
3. not necessary to keep inventory of the pipes that are surcharged at different times
4. permits the flow transition to progress computationally reach by reach in a sewer, as in the open-channel case, and hence it can account for the situation when only part of the length of the pipe is full
5. requires few additional assumptions than the standard approach to achieve numerical stability
6. simpler to program

The disadvantages are:

1. introduces a potential accuracy problem in the mass and momentum balance of the flow if the slot is too wide, and stability problems if it is too narrow
2. requires computation of two equations (continuity and momentum) for each of the reaches of the sewer when the sewer is full surcharged, whereas in the standard surcharge computation only one equation is applied to the entire length of the sewer
3. hypothetical rather than real

The Preissmann slot concept has been applied to other models for surcharged flow including the model described by Abbot (1982) and SWMM EXTRAN (Roesner et al. 1988).

The boundary condition used for solving the governing equations is the head or water level at each end of the culvert. However, if the water level at the downstream end of the culvert is less than the critical depth, the critical depth is used. Momentum is not transferred between model segments and the culverts. Initial conditions are the calculated velocities and heads at the previous time step.

The governing equations cannot be solved analytically and an implicit finite difference scheme is used to approximate the solution. The solution method employs the "leap-frog scheme" which calculates the head and velocity at alternating computational nodes (Anderson, et. al., 1984). The finite difference forms of the continuity and momentum equations are:

$$0 = \frac{h_i^{n+1}-h_i^n}{\Delta t} + \theta u_i^n \frac{h_{i+2}^{n+1}-h_{i-2}^{n+1}}{2\Delta x} + (1-\theta)u_i^n \frac{h_{i+2}^n-h_{i-2}^n}{2\Delta x} + \theta \frac{A_i^n}{T_i^n} \frac{u_{i+1}^{n+1}-u_{i-1}^{n+1}}{\Delta x}$$

$$+(1-\theta)\frac{A_i^n}{T_i^n}\frac{u_{i+1}^n-u_{i-1}^n}{\Delta x} \tag{2-147}$$

$$0 = \frac{u_i^{n+1}-u_i^n}{\Delta t} + \theta u_{i+1}^n \frac{u_{i+1}^{n+1}-u_{i-1}^{n+1}}{\Delta x} + (1-\theta)u_{i+1}^n \frac{u_{i+1}^n-u_{i-1}^n}{\Delta x} + \theta g \frac{h_{i+2}^{n+1}-h_i^{n+1}}{\Delta x}$$

$$+(1-\theta)g\frac{h_{i+2}^n - h_i^n}{\Delta x} + \theta g \frac{n^2}{R^{4/3}}u_{i+1}^{n+1}|u_{i+1}^n| + (1-\theta)g\frac{n^2}{R^{4/3}}u_{i+1}^n|u_{i+1}^n|$$

$$+\theta \frac{k}{L}u_{i+1}^{n+1}|u_{i+1}^n| + (1-\theta)\frac{k}{L}u_{i+1}^n|u_{i+1}^n| \tag{2-148}$$

where *n* refers to the time level and *i* references the spatial node **(Figure 35)**.
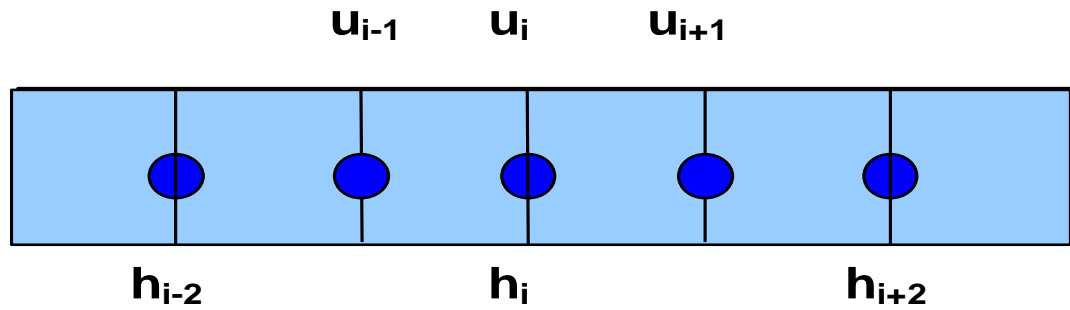
Figure 35. Linkage schematic of model segments with a culvert.

Figure 36 compares flow predictions using the dynamic culvert model with flow data taken within a culvert at NE 47th bridge in the Upper Columbia Slough, Portland, Oregon.   Data was recorded using a flow meter placed directly in a culvert.   The cyclical flows are the result of turning pumps on and off at a downstream pump station. The culvert was calibrated by adjusting the minor loss parameter.
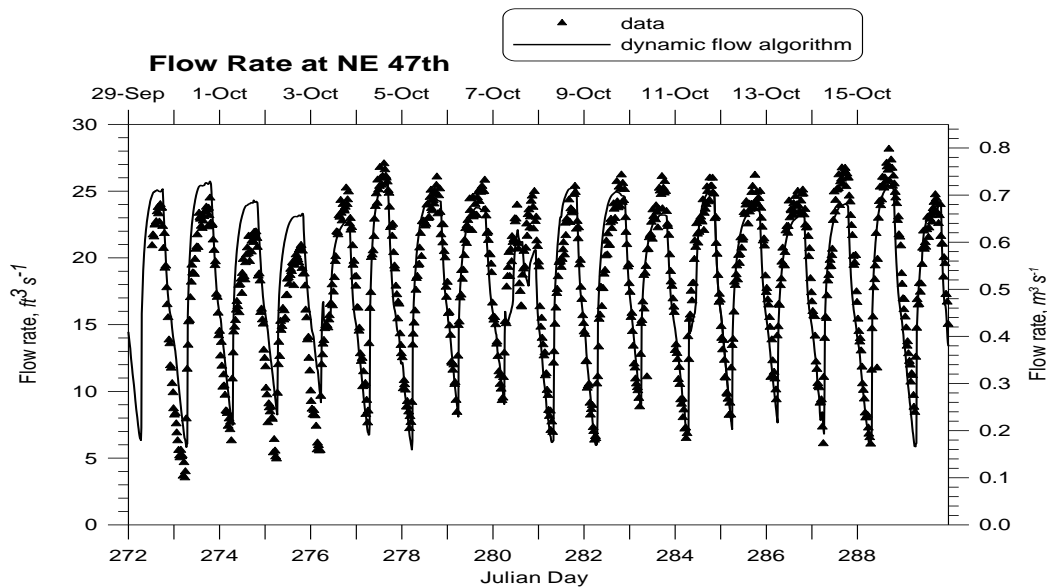
Figure 36. Computed versus observed flow using dynamic culvert model.

Internal Weirs

The model can be used to set internal weirs at specified cell locations. The user specifies the location of the internal weir by providing a segment and layer number. The "weir" effectively acts as a barrier to flow and diffusion of mass/heat across the width of the waterbody as shown in **Figure 37**. This can be used to simulate submerged and curtain weirs within a waterbody.
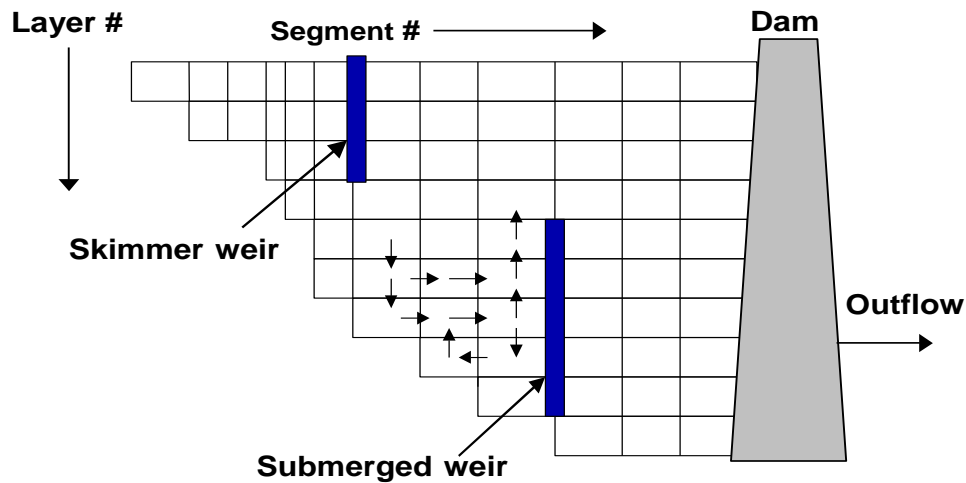
Figure 37. Schematic representation of internal weirs.

Water Level Control or Pumps

Many times, outflows in reservoirs are controlled by water levels. In order to facilitate management of the water body, a water level control or pump algorithm was added to the code. Essentially, this is a pump based on a float controller.

The algorithm allows the user to specify the upstream and downstream segment for water to be transferred at a given flow rate based on the water level at the upstream segment. Reverse flow is not allowed. The withdrawal is treated as a lateral selective withdrawal and the segment that receives the inflow is treated as a tributary.

Outlet Structures

Outflows through hydraulic structures (**Figure 38**) can either be specified or computed by the model based on user-supplied rating curves.

Tainter gate   **Spillway/weir**
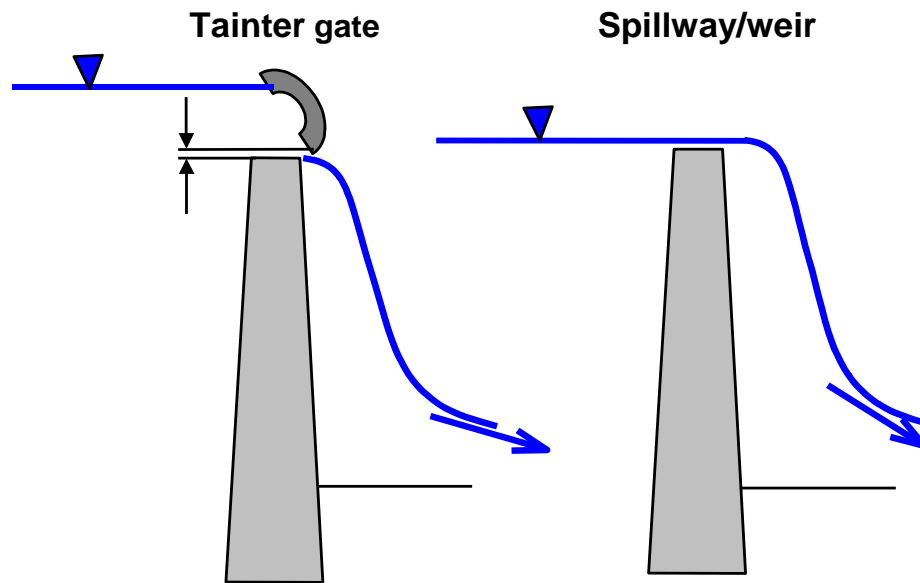
Figure 38. Radial gates and spillway flow.

The UNET model (HEC, 1997a), a one-dimensional unsteady hydraulic model, formally accounts for spillway flow from weirs and spillways. For free or submerged flow from a spillway with a radial gate, UNET uses a general equation of the form:

$$Q_{sp} = C W A^\alpha B^\beta H^\eta \qquad \text{(2-149)}$$

where:

α = empirical coefficient
β = empirical coefficient
η = empirical coefficient
Q_{sp} = flow rate, $m^3\ s^{-1}$
A = trunnion height, m
B = gate opening, m
C = empirical coefficient
W = gate width, m

and

$$H = Z_u - K Z_d - (1 - K) Z_{sp} \qquad \text{(2-150)}$$

where:

Z_u = headwater elevation
Z_d = tailwater elevation
K = 1 for submerged flow and 0 for free flow
Z_{sp} = spillway elevation

This equation was developed based on rating curves for hydraulic control structures in Arizona. Submergence is defined as:

$$\frac{Z_d - Z_{sp}}{Z_u - Z_{sp}} > \frac{2}{3}$$ (2-151)

Note that weir flow is assumed to occur whenever $B = 0.8H$ and is computed as:

$$Q_{weir} = C_w FW\left((1-K)Z_u + KZ_d - Z_{sp}\right)H^{1/2}$$ (2-152)

where:
   C_w = weir coefficient
   $F = 3\left(1 - \frac{[Z_d - Z_{sp}]}{[Z_u - Z_{sp}]}\right)$ when K = 1
   F = 1 when K = 0

For a concrete spillway, HEC (1997a) suggests using a weir coefficient value of 4. Note that the above two equations are considered equivalent whenever $B = 0.8H$.

HEC-RAS, a one-dimensional, steady-state hydraulic model, (HEC, 1997b), includes the ability to model flow over spillways including tainter and sluice gates, broad-crested weirs, and an ogee crest. Ineffective flow area, that area below the weir or gate opening, is used to block a part of the channel until it reaches the level of a spillway or weir.

A summary of the equations used by HEC-RAS (HEC, 1997b) as well as explanations are shown in **Table 4**.

Table 4. HEC-RAS flow rates through weirs and sluice gates.

Condition	Equation	Description
Radial flow gate, flowing freely	$Q = C\sqrt{2g}WT^{T_E}B^{B_E}H^{H_E}$	When the upstream water surface is ≥1.25 times the gate opening height (above the spillway crest), Q = flow, *cfs* C = discharge coefficient (between 0.6 and 0.8) W = gated spillway width, *ft* T = trunnion height (from spillway crest to trunnion pivot point), *ft* B = gate opening height, *ft* H = upstream energy head above spillway crest, Z_u-Z_{sp}, *ft* Z_u = upstream energy grade line elevation, *ft* Z_d = downstream water surface elevation, *ft* Z_{sp} = spillway crest elevation, *ft* T_E = empirical trunnion height exponent, 0.16 B_E = gate opening coefficient, 0.72 H_E = head exponent, 0.62
radial gate flowing under submerged conditions	$Q = 3C\sqrt{2g}WT^{T_E}B^{B_E}H^{H_E}$	When the upstream water surface is ≥1.25 times the gate opening height (above the spillway crest), whenever the tailwater depth divided by the energy depth above the spillway is greater than 0.67 H = Z_u-Z_d
freely flowing sluice gate	$Q = C\sqrt{2gH}WB$	When the upstream water surface is ≥1.25 times the gate opening height above the spillway crest H = upstream energy head above the spillway, Z_u-Z_{sp} C = discharge coefficient, 0.5 to 0.7
submerged sluice gate	$Q = 3C\sqrt{2gH}WB$	When the upstream water surface is ≥1.25 times the gate opening height above the spillway crest, whenever the tailwater depth divided by the energy depth above the spillway is greater than 0.67

Condition	Equation	Description
		$H = Z_u - Z_d$
Low flow through gated structure	$Q = CLH^{\frac{3}{2}}$	When upstream water level is equal to or less than the top of the gate opening, weir flow equation is used $C =$ weir coefficient, 2.6-4.0 depending on broad crested or Ogee spillway and length of spillway crest $H =$ upstream energy head above spillway crest, for an Ogee spillway the value of C is adjusted according to a 1977 Bureau of Reclamation study on variability of C for Ogee spillways, suggested values of C are 2.6 for bridge decks and 3.0 for flow over elevated roadways

Spillways/Weirs

Analysis of flow over weirs has been studied extensively. Martin and McCutcheon (1999) show that a typical relationship between the pool depth and flow over a weir is:

$$Q = C_e W_c h_w^{\eta}$$

(2-153)

where C_e and η are empirical coefficients, W_c is the length of the weir crest, and h_w is the height of the pool above the weir crest. Theoretical calculations of steady-state flow over a weir can be complex depending on whether the weirs are sharp-crested, broad-crested, V-notched, rectangular, Cipolletti, parabolic, or some other type. **Table 5** shows some examples from French (1985) and USBR (2001) on typical equations used for the different weir types. For many regular weir types, formulae exist for accurate estimation of the flow. However, in most cases a rating curve for a given installation is necessary because of the uncertainty of end effects, flow alignments, shallowness in the upstream pool, and other unique features of the installation (Martin and McCutcheon, 1999).

Table 5. List of weir types (French, 1985; USBR, 2001)

Weir type	Weir Equation	Description
Rectangular broad crested weir	$Q = C_D C_v \dfrac{2}{3}\sqrt{\dfrac{2}{3}g}\,WH^{3/2}$	Valid when 0.08 <H/L<0.5 Q = flow rate C_D = discharge coefficient (0.84 to 1.06) C_v = velocity coefficient accounting for neglecting the velocity head in the approach channel (between 1.0 and 1.2) W = width at surface H = upstream head above spillway crest Z_u = upstream energy grade line elevation, *ft* g = gravity acceleration
Rectangular, sharp crested weir	$Q = C_e \dfrac{2}{3}\sqrt{2g}\,BH^{3/2}$	Where B = width at bottom of weir crest Olson and Wright (1990) show that C_e depends on the approach velocity head, $V^2/2g$, and the contraction of streamlines just beyond the weir crest and show that C_e = 0.611+0.075*(H/Z) H = weir head, *ft* Z = weir crest head measured from the channel bottom, *ft* Clay (1995) suggests a simple equation of Q=3.33B$H^{3/2}$ of this form when approach velocities are less than 1 *fps* or Q=3.33B[(H+h)$^{3/2}$-h$_v$$^{3/2}$] h_v = $V^2/2g$ V = approach velocity, *ft s^{-1}*
Parabolic, broad-crested	$Q = C_D C_v \sqrt{\dfrac{3}{4}fg}\,H^2$	f = distance from the bottom point of the weir to the weir focal point, *ft*
Parabolic, sharp-crested	$Q = C_e \dfrac{1}{2}\pi\sqrt{fg}\,H^2$	C_e = effective discharge coefficient
Triangular, broad-crested	$Q = C_D C_v \dfrac{16}{25}\sqrt{\dfrac{2}{5}g}\,tan(0.5\theta)H^{5/2}$	Θ = half angle of the triangular notch
Triangular, sharp-crested	$Q = C_e \dfrac{8}{25}\sqrt{2g}\,tan(0.5\theta)H^{5/2}$	C_e = function of notch angle and varies from 0.59 to 0.57 for angles between 20 and 100 degrees
Trapezoidal, broad-crested	$Q = C_D(Wy_c + my_c^2)[2g(H - y_c)]^{1/2}$	W = top width of trapezoidal weir m = slope of trapezoidal weir y_c = depth of water at the weir H = energy head upstream of weir
Trapezoidal, sharp-crested	$Q = C_e \dfrac{2}{3}\sqrt{2g}(B + \dfrac{4}{5}H\ tan\,0.5\theta)H^{1/2}$	B= bottom width of trapezoidal weir Θ= angle of the trapezoid at a convergence point of the 2 sides
Truncated triangular, broad-crested	$Q = C_D C_v \dfrac{2}{3}\sqrt{\dfrac{2}{3}g}\,W(H - 0.5H_b)^{3/2}$	Use when H > 1.25H_b, otherwise use equation for broad crested triangular weir H_b = depth from the bottom of the truncated triangular weir to the top of the triangle and the beginning of the rectangular section
Truncated triangular, sharp-crested	$Q = C_e \dfrac{4}{15}\sqrt{2g}\dfrac{W}{H_b}(H^{2.5} - (H - H_b)^{2.5})$	Use when H > H_b, otherwise use equation for sharp crested triangular weir
Cipoletti	$Q = C_D C_v \dfrac{2}{3}\sqrt{2g}\,WH^{3/2}$	A modification of the contracted, rectangular, sharp-crested weir with a trapezoidal control section and sides sloping outward with slopes of 4:1 W = top width of weir $C_D\cong$0.63 C_v varies from 1 to 1.2 and is a function of C_D and the ratio of area upstream of the control section and at the control section

Weir type	Weir Equation	Description
Proportional or sutro weir	$Q = C_D B \sqrt{2ga}\left(H - \frac{1}{3}a\right)$	B = bottom width of weir a = distance from weir bottom to top of the rectangular weir section C_D = drag coefficient, 0.597-0.619 for symmetrical Sutro weir, 0.625- 0.603 for unsymmetrical Sutro weir

Since all weirs in practice are calibrated and a head discharge relationship is usually determined, the flow versus head relationship is used rather than an equation from **Table 5**. The user must then analyze the weir or spillway and input a relationship based on the weir or spillway geometry. The model accepts equations in the form of a power function for freely flowing conditions:

$$Q = \alpha_1 \Delta h^{\beta_1} \qquad\qquad \textbf{(A-2-154)}$$

where:

    α_1 = empirical parameter
    β_1 = empirical parameter
    Δh = Z_u-Z_{sp}
    Z_u = upstream head
    Z_{sp} = spillway crest elevation

and for submerged conditions

$$Q = \alpha_2 \Delta h^{\beta_2} \qquad\qquad \textbf{(A-2-155)}$$

where:

    α_2 = empirical parameter
    β_2 = empirical parameter
    Δh = Z_u-Z_d
    Z_u = upstream head
    Z_d = downstream head

Submerged conditions are defined when the tailwater depth over the upstream energy head (static head and velocity head) is greater than 0.67 (HEC, 1997b).   Even though negative flow rates are possible using the second equation whenever $Z_d > Z_u$, these results should be used with caution since rarely are rating curves done for reverse flow over a spillway. The user needs to ensure there is a smooth transition between submerged flow conditions and free flowing conditions by proper choice of model coefficients. The following discussion shows how to generate a smooth flow transition from free flowing to submerged flow conditions (**Figure 39**).

Figure 39. Flow rate over a spillway or weir for submerged and free flowing conditions.

Consider the following weir flow condition in **Figure 40**.

Figure 40. Flow at a submerged weir.

In order to have a smooth transition, the two flows must be equal at the transition point. Using

$$H_2 - H_{weir} = 0.67(\Delta h_1 + \frac{u^2}{2g}) \approx 0.67(H_1 - H_{weir}) \qquad \textbf{(2-156)}$$

and substituting the rating curves for free flow and submerged conditions and solving for α_2 results in:

$$\alpha_2 = \frac{\alpha_1(H_1 - H_{weir})^{\beta_1 - \beta_2}}{(0.33)^{\beta_2}}$$

(2-157)

In many cases a weir can be set as the downstream boundary condition of a river. In CE-QUAL-W2, the user can specify the weir crest as the channel bottom elevation, such that the weir equation is of the form:

$$Q = \alpha_1 H^{\beta_1}$$

(2-158)

where H is the depth of the water at the weir. Setting this in the form of a stage-discharge relationship:

$$H = aQ^b = \left(\frac{Q}{\alpha_1}\right)^{\frac{1}{\beta_1}}$$

(2-159)

where a and b are empirical coefficients. Writing this equation in a form compatible with the stage discharge relationship using the a and b coefficients,

$$H = \left(\frac{1}{\alpha_1}\right)^{\frac{1}{\beta_1}} Q^{\frac{1}{\beta_1}}$$

(2-160)

Then the a and b coefficients become

$$a = \left(\frac{1}{\alpha_1}\right)^{\frac{1}{\beta_1}}$$

(2-161)

$$b = \frac{1}{\beta_1}$$

(2-162)

or vice versa:

$$\alpha_1 = a^{-\beta_1}$$

(2-163)

$$\beta_1 = \frac{1}{b}$$

(2-164)

allows the user to set a weir-rating curve that reproduces the stage discharge relationship at a downstream boundary.

A dynamic weir or spillway crest elevation can also be used to simulate dynamic raising of flashboards. These are designated in the model as gates.

Gates

For a gated structure or sluice gate, a more complex rating curve is required based on the opening and the head difference between the upstream and downstream condition (the spillway crest if free flow and the tailwater elevation if submerged flow).

The following equation is used for freely flowing conditions:

$$Q = \alpha_1 \Delta h^{\beta_1} B^{\gamma_1}$$

(2-165)

where:

  α_1 = empirical coefficient
  β_1 = empirical coefficient
  γ_1 = empirical coefficient
  Δh = Z_u - Z_{sp}
  Z_u = upstream head
  Z_{sp} = spillway crest elevation

and the following equation is used for submerged flow:

$$Q = \alpha_2 \Delta h^{\beta_2} B^{\gamma_2} \qquad \text{(2-166)}$$

where:

  α_2 = empirical coefficient
  β_2 = empirical coefficient
  γ_2 = empirical coefficient
  Δh = Z_u - Z_d
  Z_d = downstream head
  B = gate opening, m

In defining these parameters, the user also has to generate a time series file with the gate opening in m where a gate opening of 0 m is closed.   Whenever the gate opening is equal to or greater than 0.8Δh, a weir equation is used with no functional dependency on the gate opening. In this case, a rating curve must be supplied when the gate acts like a weir. **Figure 41** shows the flow rate dependence on the gate opening.

Gate:Q=2B$^{0.72}$$\Delta$h$^{0.62}$
Weir:Q=1.75Δh$^{1.5}$

Free flow condition
weir flow

Gate flow equation

Gate opening, BGATE, m

Flow rate, $m^3\ s^{-1}$
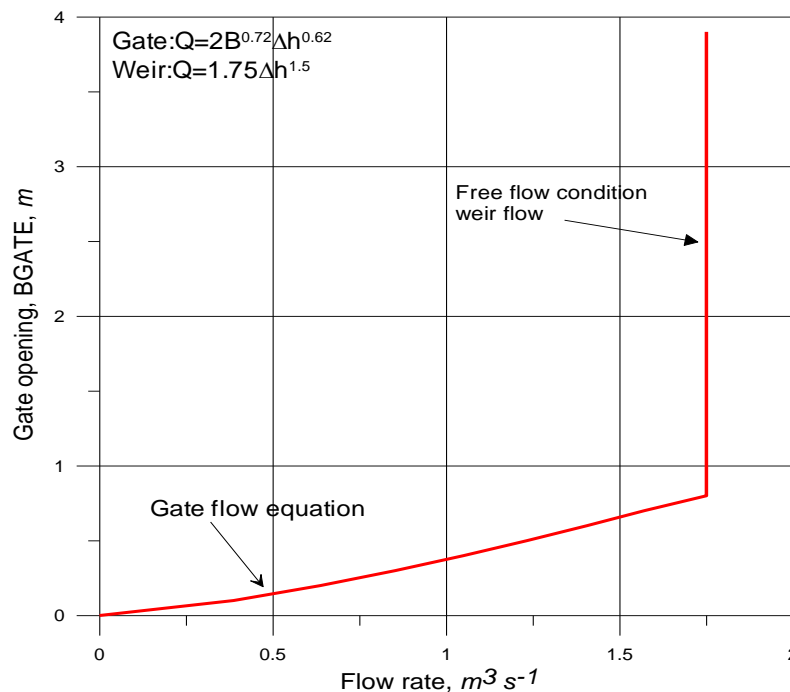
Figure 41. Flow rate variation with gate opening.

In some reservoir systems, an outlet valve is connected to the reservoir and a head-discharge relationship is used based on the gate opening or number of gate turns. In this case, the outlet level is usually at a

different elevation than the withdrawal elevation. The above gate formulation can still be used if no reverse flow occurs through the needle valve. This situation is illustrated in **Figure 42**. In this case, the elevation of the outflow is required in addition to the elevation at which the outflow is taken if a rating curve is used in the model. This use is described in the section on gates in the control file.
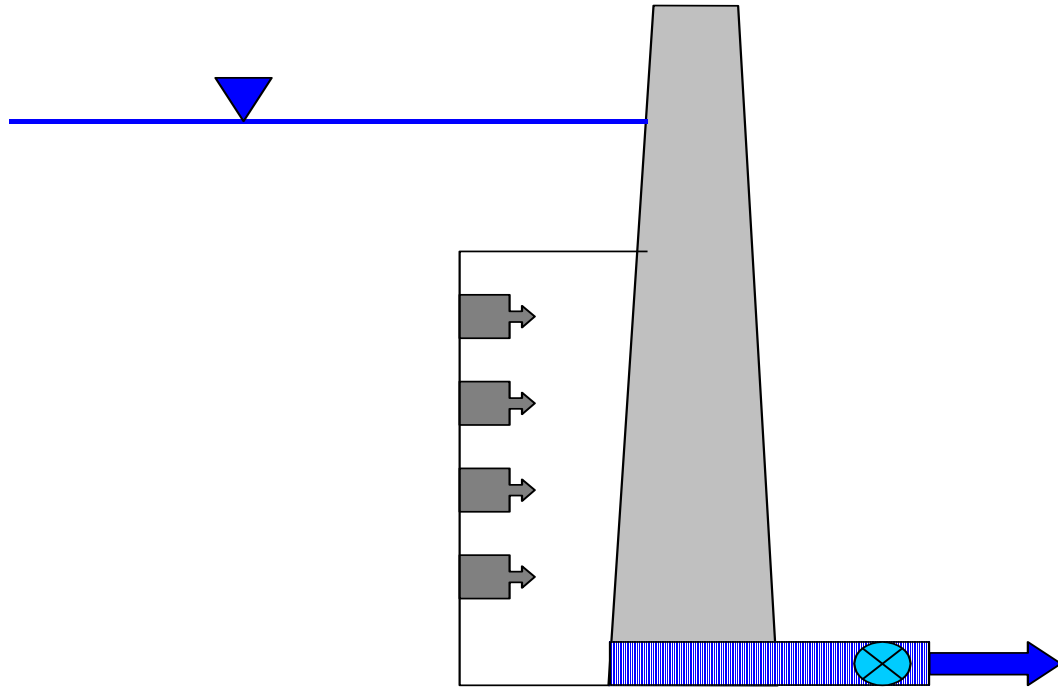
Figure 42. Selective withdrawal with outflow connected to a valve with a gate.

The user can insert weirs and/or spillways, specify connectivity to other model segments, and insert the ratings curve parameters for each weir/spillway. The model treats each spillway, weir, or gate as a selective withdrawal outflow and uses the selective withdrawal algorithm for determining water flow from each vertical layer adjacent to the structure. Inflows from hydraulic control structures are treated as tributary inflows where the user must specify whether the inflow is placed according to density, equally distributed between all vertical layers, or distributed between a given elevation range.

Weir equations are used when gates are open and the open gate does not interfere with the flow (when $B \geq 0.8\Delta h$).

Gates can also be used to move flows around to different parts of the model domain – different branches. In that case the specification of gate openings is interpreted as specification of flow rates.

Branch Momentum Exchange

Starting with CE-QUAL-W2 Version 3, CE-QUAL-W2 conserves longitudinal momentum at branch intersections (**Figure 43**). The vector component of velocity in the x-direction of the main channel, U_x, can be computed from the channel orientations. The x-direction component is $U_x=U cos\beta$ where U is the longitudinal velocity of the tributary at the downstream segment that intersects the main branch and β is the difference in the angle between the main stem and tributary segments.
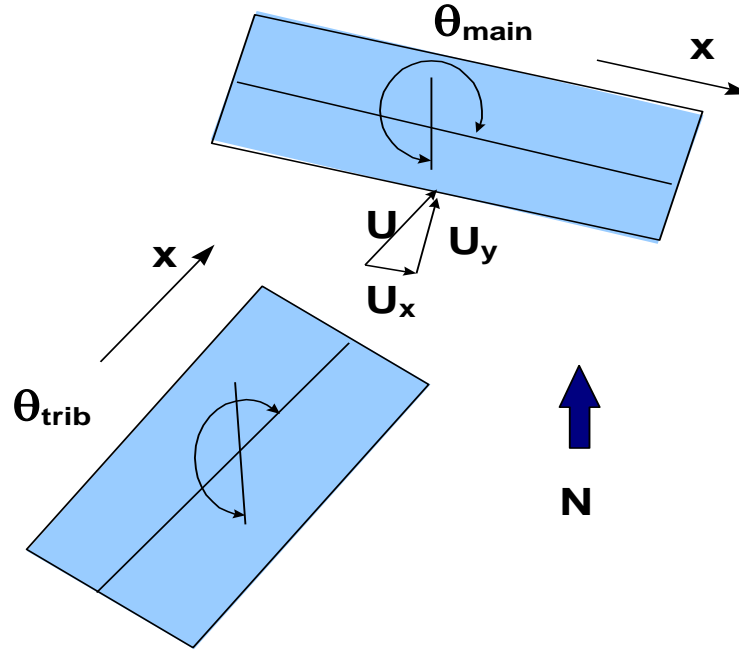
Figure 43. Schematic of branch connection.

The conservation of momentum about a control volume, the main stem segment, would result in an additional source of momentum. Lai (1986) shows that the correction to the x-momentum equation would be:

$$qBU_x \tag{2-167}$$

where:

   q = lateral inflow per unit length

This arises from re-deriving the momentum equations and assuming that all the fluid entering the segment is moving at the velocity U_x. The correction to the x-momentum equation is:

$$\frac{\partial UB}{\partial t} + \frac{\partial UUB}{\partial x} + \frac{\partial WUB}{\partial z} = gB\sin\alpha + g\cos\alpha B\frac{\partial \eta}{\partial x} - \frac{g\cos\alpha B}{\rho}\int_{\eta}^{z}\frac{\partial \rho}{\partial x}dz$$
$$+ \frac{1}{\rho}\frac{\partial B\tau_{xx}}{\partial x} + \frac{1}{\rho}\frac{\partial B\tau_{xz}}{\partial z} + \underbrace{qBU_x}_{\substack{\text{side tributary}\\\text{momentum}}} \tag{2-168}$$

Lateral Inflows

Wells (1997) proposed accounting for the cross-shear as a result of the y component of the velocity of a side branch in the computation of the vertical eddy viscosity. This was implemented by increasing the cross-shear velocity gradient. In Version 2, wind shear across the lateral axis of a segment also increased the vertical mixing by affecting the computation of A_z. Analogous to wind shear, an additional side shear is included in the calculation of the vertical eddy viscosity:

$$A_z = \kappa \left(\frac{l^2}{2}\right) \sqrt{\left(\frac{\partial U}{\partial z}\right)^2 + \left(\frac{\tau_{wy} e^{-2kz} + \tau_{trib}}{\rho A_z}\right)^2} \, e^{(-CR_i)} \qquad \textbf{(2-169)}$$

where:

$$\tau_{trib} \cong \rho \frac{f_i}{8} U_y^2$$
f_i = is an interfacial friction factor, ≈ 0.01
$$U_y = \frac{\sum Q_{in_y}}{\Delta z \Delta x}$$

$$\sum Q_{in_y} = [U_{br} \Delta z B] + \left[\sum Q_{trib}\right]$$

U_{br} = $U_{br}\sin(\Theta_{main}-\Theta_{branch})$
Δz = inflow cell layer height
B = inflow cell width
Δx = inflow cell segment length
Q_{trib} = tributary flow rate assumed to be at right angles to the main channel

This side shear effect is only computed when the vertical mixing algorithm chosen by the user is W2 or W2N.

AUXILIARY FUNCTIONS

Density

Accurate hydrodynamic calculations require accurate water densities. Water densities are affected by variations in temperature and solids concentrations given by:

$$\rho = \rho_T + \Delta\rho_S \tag{2-170}$$

where:

ρ = density, *kg m^{-3}*
ρ_T = water density as a function of temperature, *kg m^{-3}*
$\Delta\rho_S$ = density increment due to solids, *kg m^{-3}*

A variety of formulations has been proposed to describe water density variations due to temperatures. The following relationship is used in the model (Gill, 1982):

$$\begin{aligned}\rho_{T_w} = {}& 999.842594 + 6.793952x10^{-2}T_w \\ & - 9.095290x10^{-3}T_w^2 + 1.001685x10^{-4}T_w^3 \\ & - 1.120083x10^{-6}T_w^4 + 6.536332x10^{-9}T_w^5\end{aligned} \tag{2-171}$$

Suspended and dissolved solids also affect density. For most applications, dissolved solids will be in the form of total dissolved solids. For estuarine applications, salinity should be specified. The effect of dissolved solids on density is calculated using either of these variables with the choice specified by the variable [WTYPE]. Density effects due to total dissolved solids are given by Ford and Johnson (1983):

$$\Delta\rho_{TDS} = (8.221x10^{-4} - 3.87x10^{-6}T_w + 4.99x10^{-8}T_w^2)\Phi_{TDS} \tag{2-172}$$

where:

ρ_{TDS} = TDS concentration, *g m^{-3}*

and for salinity (Gill, 1982):

$$\begin{aligned}\Delta\rho_{sal} = {}& (0.824493 - 4.0899x10^{-3}T_w + 7.6438x10^{-5}T_w^2 \\ & -8.2467x10^{-7}T_w^3 + 5.3875x10^{-9}T_w^4)\Phi_{sal} \\ & +(-5.72466x10^{-3} + 1.0227x10^{-4}T_w \\ & -1.6546x10^{-6}T_w^2)\Phi_{sal}^{1.5} + 4.8314x10^{-4}\Phi_{sal}^2\end{aligned} \tag{2-173}$$

where:

Φ_{sal} = salinity, *kg m^{-3}*

The suspended solids effects are given by Ford and Johnson (1983):

$$\Delta\rho_{ss} = \Phi_{ss}\left(1 - \frac{1}{SG}\right)x10^{-3} \tag{2-174}$$

where:

Φ_{ss} = suspended solids concentration, *g m^{-3}*

SG = specific gravity of suspended solids

Assuming a specific gravity of 2.65, the above relationship is simplified to:

$$\Delta\rho_{ss} = 0.00062\Phi_{ss} \tag{2-175}$$

The total effect of solids is then:

$$\Delta\rho_{s} = (\Delta\rho_{sal} or \Delta\rho_{tds}) + \Delta\rho_{ss} \tag{2-176}$$

Selective Withdrawal

In order to model the complicated outlet hydraulics in a reservoir, special selective withdrawal algorithms are often used (Brooks and Koh, 1969, Davis et al. 1987). These allow the computation of flow from multiple vertical layers without having to solve the full-vertical momentum equation.

Selective withdrawal is applied to all structure outflows where layer locations and outflows at each layer are calculated based on the total outflow **[QOUT]**, structure type **[SINKC]**, elevation **[ESTR]**, and computed upstream density gradients. The selective withdrawal computation uses these values to compute vertical withdrawal zone limits and outflows. It also sums the outflows for multiple structures. In addition, all out-flows – such as withdrawals and hydraulic structures – use selective withdrawal theory to compute the withdrawal envelope.

Outflow distribution is calculated in the subroutine SELECTIVE_WITHDRAWAL. This routine first calculates limits of withdrawal based on either a user specified point or line sink approximation for outlet geometry **[SINKC]**. The empirical expression for point sink withdrawal limits is:

$$d = \left(\frac{c_{bi}Q}{N}\right)^{0.33} \tag{2-177}$$

and for a line sink:

$$d = \left(\frac{2c_{bi}q}{N}\right)^{0.5} \tag{2-178}$$

where:
   d = withdrawal zone half height, m
   Q = total outflow, $m^3\ s^{-1}$
   N = internal buoyancy frequency, Hz, $N = \sqrt{-\frac{g}{\rho}\frac{d\rho}{dz}}$
   q = outflow per unit width, $m^2\ s^{-1}$, q=Q/W where W is the outlet width of the line sink
   c_{bi} = boundary interference coefficient

The point sink approximation assumes approach flow is radial both longitudinally and vertically while the line sink approximation assumes flow approaches the outlet radially in the vertical. The boundary interference coefficient is two near a physical boundary and one elsewhere.

Velocities are determined using a quadratic shape function:

AUXILIARY FUNCTIONS

$$V_k = 1 - \left[\frac{(\rho_k - \rho_o)}{(\rho_l - \rho_o)}\right]^2 \tag{2-179}$$

where:

V_k = normalized velocity in layer k

ρ_k = density in layer k, *kg m^{-3}*

ρ_o = density in the outlet layer, *kg m^{-3}*

ρ_l = density of the withdrawal limit layer, *kg m^{-3}*

The shape function generates a maximum velocity at the outlet level with velocities approaching zero at withdrawal limits. During non-stratified periods, outflow from top to bottom is uniform. Uniform flows also result from large outflows during periods of mild stratification. As stratification develops, withdrawal limits decrease and outflow is weighted towards the outlet elevation.

Withdrawal limits can be varied by specifying a line sink and changing the effective width. Small outlet widths result in nearly uniform outflows, while large widths limit outflows to the outlet layer.

Sediment Resuspension

This algorithm is based on work from Kang et al. (1982) where the bottom shear stress is computed based on wind speed, wind fetch and depth. The wind blowing across a water surface creates wind waves that have orbital motion that decays with depth. The model user inputs a critical shear stress for detachment of the particles. If the critical shear stress is exceeded, then particles are resuspended. The approach of Kang et al. (1982) consists of the following steps:

1. Computation of the wave height, H_s in m,

$$H_s = \frac{W^2}{g} 0.283 \, tanh\left[0.53\left(\frac{gH}{W^2}\right)^{0.75}\right] tanh\left[\frac{0.0125\left(\frac{gF}{W^2}\right)^{0.42}}{tanh\left[0.53\left(\frac{gH}{W^2}\right)^{0.75}\right]}\right] \tag{2-180}$$

where W is the wind velocity (m/s), F is the fetch (m), H is the mean depth (m)

2. Computation of wave period, T_s in s,

$$T_s = \frac{2\pi W}{g} 1.2 \, tanh\left[0.833\left(\frac{gH}{W^2}\right)^{0.375}\right] tanh\left[\frac{0.077\left(\frac{gF}{W^2}\right)^{0.25}}{tanh\left[0.833\left(\frac{gH}{W^2}\right)^{0.375}\right]}\right] \tag{2-181}$$

3. Computation of the wavelength, L in m, iteratively from the following equation:

$$L = \frac{gT_s^2}{2\pi} tanh\left[\frac{2\pi H}{L}\right] \tag{2-182}$$

4. Computation of the orbital velocity, $\bar{U}$ in cm/s,

$$\bar{U} = \frac{\pi H_s}{T_s} \frac{100}{sinh(2\pi H/L)} \tag{2-183}$$

5. Computation of bottom shear stress, τ in dynes/cm^2,

$$\tau = 0.003\bar{U}^2$$ **(2-184)**

6. Computation of actual bottom scour rate of suspended solids, ε in mass of sediments scoured per area or g/m^2,

$$\varepsilon = 0 \quad \tau \leq \tau_c$$ **(2-185)**

$$\varepsilon = \frac{\alpha_o}{t_d^2}(\tau - \tau_c)^3 \quad \tau > \tau_c$$ **(2-186)**

where α_o is an empirical constant=0.008, t_d=7, and τ_c is the user-defined critical shear stress in dynes/cm^2.

Resuspension supposedly only occurs during the first hour of the wind shear greater than the critical shear stress. Hence, the rate of resuspension per time, E in $g/m^2/hour$, would be

$E = \frac{\varepsilon}{1hr}$ for the first hour and nothing after that. The resulting concentration of suspended solids in the entire water column, c in mg/l, if distributed evenly over the entire volume would then be

$$c = \frac{10000\varepsilon A_{bottom}}{V} = \frac{10000\varepsilon}{H}.$$

where A_{bottom} is the surface area of the bottom and V is the volume of the water column above the bottom (=HA_{bottom}). Chapra (1997) also uses this approach and provides an example calculation.

3.   Particle Tracking Algorithm

The original particle tracking algorithm in CE-QUAL-W2 was developed by Goodwin et al. (2001) for use in a smart-particle tracking algorithm predicting movement of fish in a southern reservoir in the USA. A description from Goodwin et al. (2001) of the algorithm is reproduced below:

> The particle-tracking algorithm used was developed by Chapman et al. (1994) to predict transport and fate of floatables and suspended and dissolved materials in three dimensions. The algorithm was simplified for use in CE-QUAL-W2 by deleting portions of the model relating to surface transport of floatables and suspended and dissolved materials. In addition, transport equations for lateral movement were deleted because CE-QUAL-W2 computes forcing functions only in the longitudinal and vertical directions. The following equations are used for particle tracking in CE-QUAL-W2 based on velocity:

$$X^{t+1} = X^t + U^t(Z^t,X^t) * \Delta t$$ **(3-1**)
$$Z^{t+1} = Z^t + W^t(Z^t,X^t) * \Delta t$$ **(3-2)**

where
X^{t+1} =   longitudinal position of particle at time t+1 (m); defined as
$x_{Node(k,i)} + \Delta x$ at time t+1,
Z^{t+1} =   vertical position of particle at time t+1 (m); defined as
$z_{Node(k,i)} + \Delta z$ at time t+1,

Node(k,i)	=	node above, upstream, and closest to particle's position defined as the upper-left node (Figure 1) of the rectangular cell formed by intersection of vertical layer k and longitudinal segment i,
$x_{Node(k,i)}$	=	longitudinal position of Node(k,i) (m),
Δx	=	offset (downstream) from Node(k,i) to particle's position (m),
$z_{Node(k,i)}$	=	vertical position of Node(k,i) (m),
Δz	=	offset (below) from Node(k,i) to particle's position (m),
X^t	=	longitudinal position of particle at time t (m); defined as $x_{Node(k,i)} + \Delta x$ at time t,
Z^t	=	vertical position of particle at time t (m); defined as $z_{Node(k,i)} + \Delta z$ at time t,
$U^t(Z^t,X^t)$	=	interpolated horizontal flow velocity (m/s) at location (Z^t,X^t),
$W^t(Z^t,X^t)$	=	interpolated vertical flow velocity (m/s) at location (Z^t,X^t), and
Δt	=	time interval between time t and time t+1 (seconds).
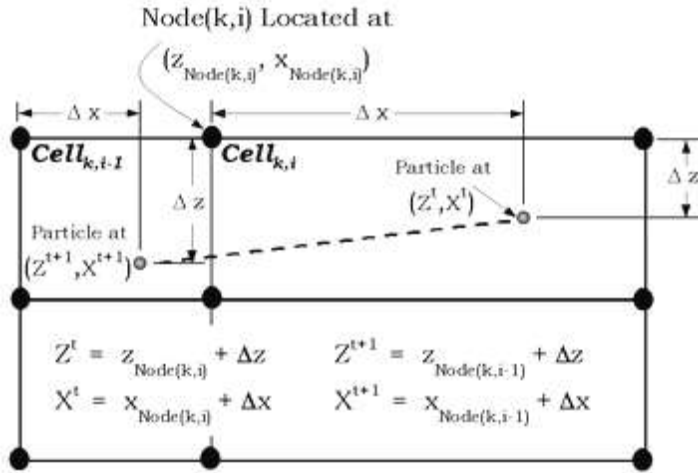
Figure 44. From Goodwin et al. (2001) illustrating the particle transport through the CE-QUAL-W2 grid.

After X^{t+1} and Z^{t+1} are calculated, boundary checks are performed to determine if the particle's new position exceeds either the longitudinal or vertical boundaries of the cell containing X^t and Z^t or any system boundary. An algorithm is activated to determine the appropriate cell in which to place the particle if the particle's new position exceeds the boundaries of its cell from the previous time step. Once the appropriate cell is found, k, i, Node$_{k,i}$, $x_{Node(k,i)}$, $z_{Node(k,i)}$, Δx, and Δz are updated for the particle at t+1 and stored. Since the displacement of a particle is proportional to the time step used, it's possible the displacement calculated in equations (1) and/or (2) could position the particle outside system boundaries. To correct for this, the model places a particle near the boundary at a user-specified distance if X^{t+1} or Z^{t+1} exceeds the system boundaries.

In addition, a random movement of the particle is added to the velocity movement. The randomness added to the particle movement is based on the intensity of turbulence in a system. Following the work of Dunsbergen and Stalling (1993) and Chapman et al. (1994), the transport in x and z including the translation by velocity and random turbulent transport are shown below:

$$X^{t+1} = X^t + U\Delta t + R\sqrt{6D_x\Delta t} \qquad \text{(3-3)}$$
$$Z^{t+1} = Z^t + W\Delta t + R\sqrt{6D_z\Delta t} \qquad \text{(3-4)}$$

where R represents a random number having a uniform distribution with zero mean and unit variance, D_x and D_z are the longitudinal and vertical mass/heat dispersion coefficients. The use of the uniform rather than a Gaussian distribution saves computational time and does not affect the resulting random distribution (Hathhorn, 1997).

The value of D_x is specified in the control file, **w2_con.npt**, whereas the value of D_z is computed based on the turbulence closure model used, such as the kε turbulence model (for example in **w2_con.npt** the user can set AZC=TKE). The choice of D_x can lead to high values of random movement in x if D_x is high. In all cases the maximum movement of a particle is constrained by the grid cell height, Δz, and segment length, Δx.

Also the particles move in the lateral direction based on the following equation assuming that the lateral dispersion coefficient is the same as the longitudinal coefficient:

$$Y^{t+1} = Y^t + V\Delta t + R\sqrt{6D_x\Delta t} \qquad\qquad \textbf{(3-5)}$$

The value of V is based on any lateral inflows or outflows at a segment.

The location of the particles in the grid are identified by its segment (I) and layer (K) location as well as X, Y, and Z coordinates within each layer. Figure 45 and Figure 46 show the x, y, and z coordinate reference locations within the cells for the particle algorithm for the plan view and side view, respectively. Figure 47 shows the definition sketch for lateral velocities in a layer. The standard CE-QUAL-W2 designation for longitudinal (positive downstream or increasing segment number) and vertical velocities (positive downward) in followed in this algorithm. Initial x, y, and z are given for each particle released into a segment and layer. The user specifies x and z, but y is chosen as the middle of a layer, i.e., y=B/2 where B is the layer width.
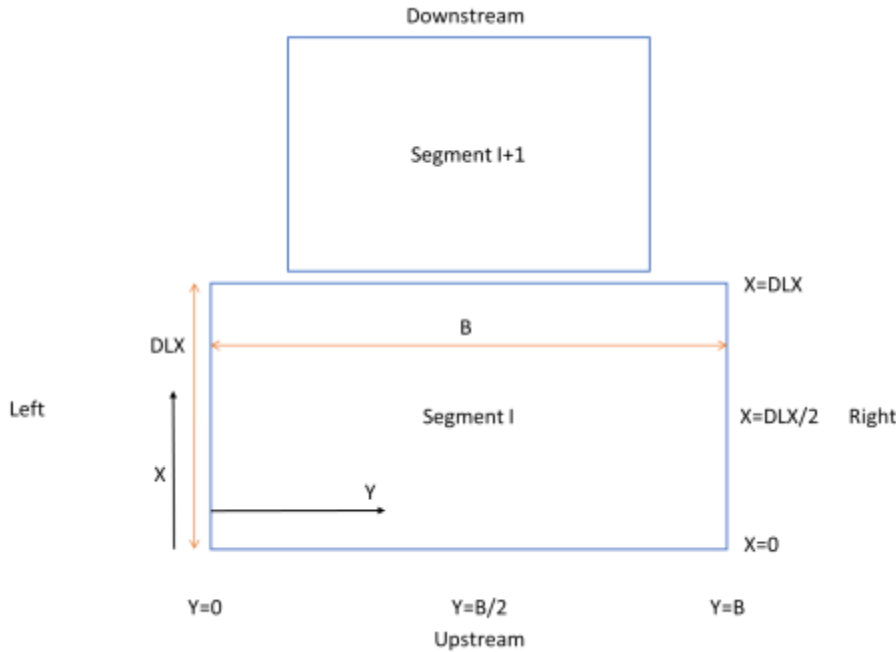
Figure 45. Plan view of x and y coordinates within a layer (K) and segment (I). DLX is the segment length and B is the segment width at the given layer K.
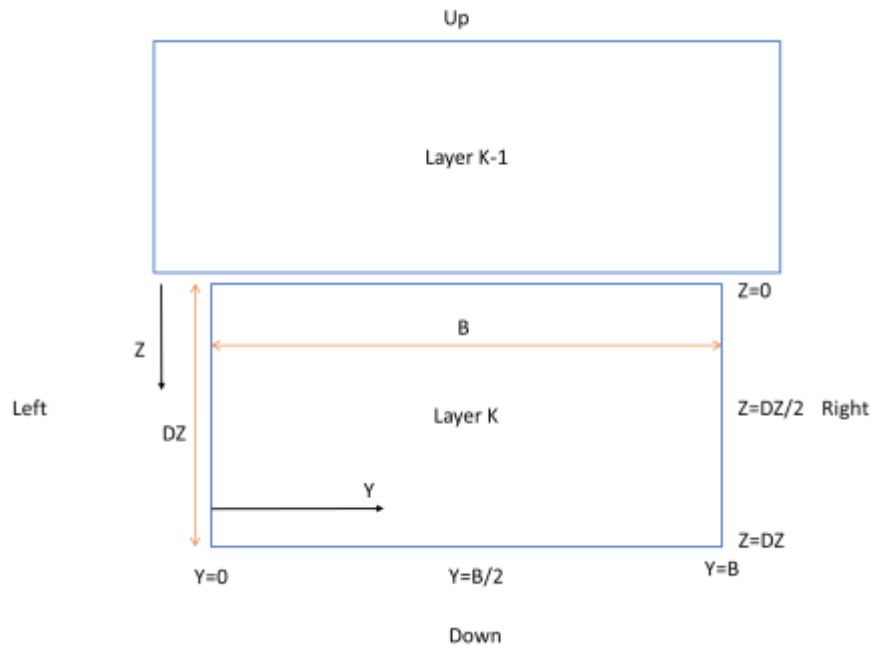
Figure 46. Side view of z and y coordinates within a layer (K) and segment (I). DZ is the layer thickness and B is the layer width.
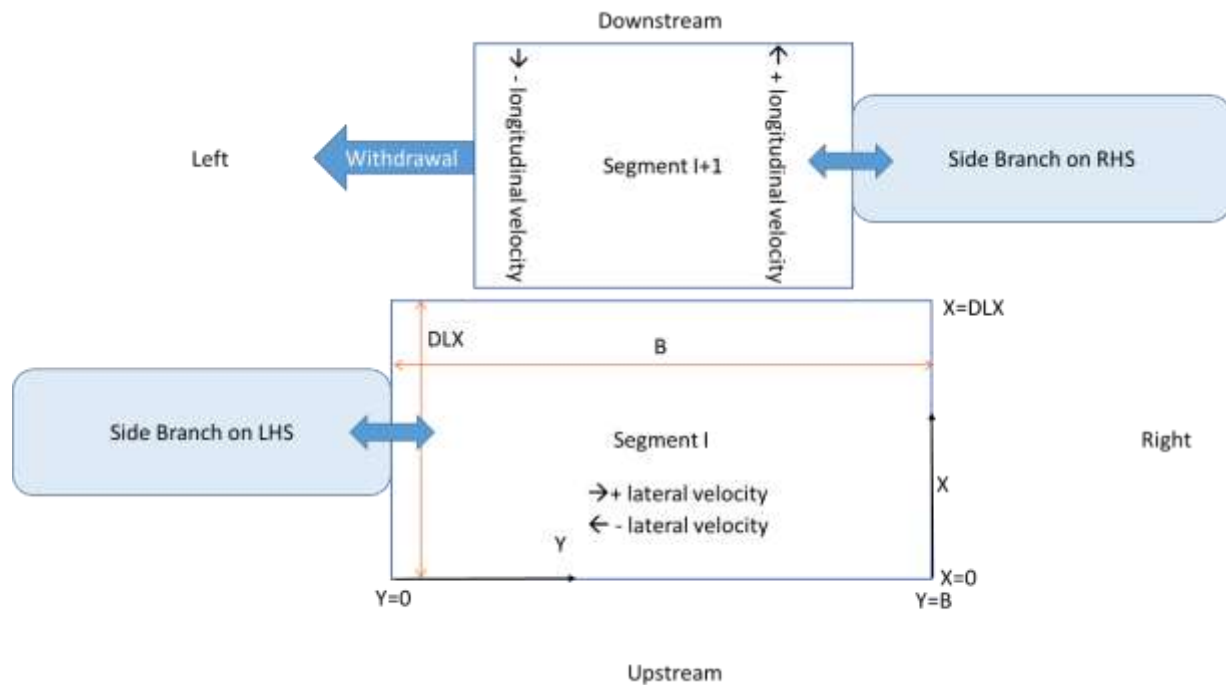
Figure 47. Definition sketch for lateral and longitudinal velocities within the cells. Withdrawals are always assumed to be on the LHS (left hand side) of the segment.

4.   Temperature and Water Quality Modeling

Authors and contributors: Scott A. Wells, Tom M. Cole, Chris Berger, Stewart Rounds, Annette Sullivan, S. Prakash, J. A. Vandenberg, E. M. Buchak, Lillian Jeznach, John Tobiason, Zhong Zhang

This section of the User's Manual documents the governing equation for constituent mass and energy (temperature) and the source/sink terms for temperature and each water quality state variable. There is also a section on the computation of vertical and longitudinal dispersion coefficients.

Turbulent Advection-Diffusion Equation

As in the momentum equation, time-averaged variables for velocity are introduced (**Figure 48**) and concentration (**Figure 49**).
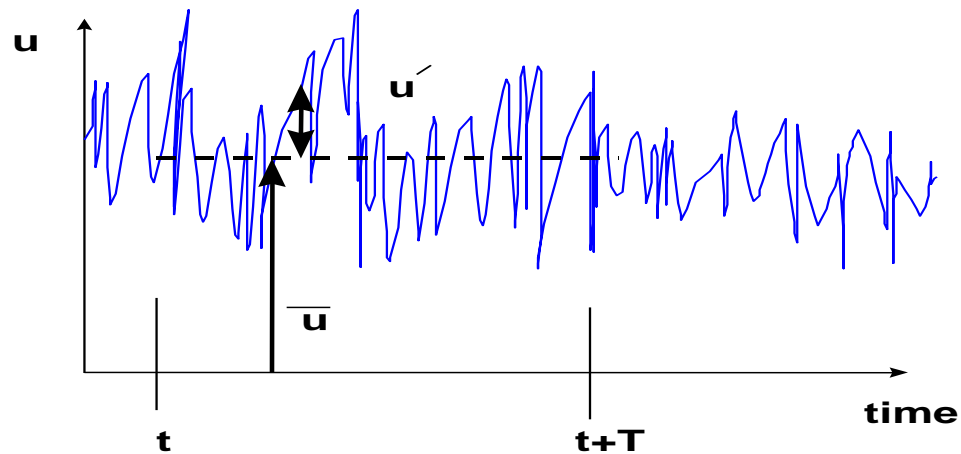
Figure 48. Velocity variability with time.
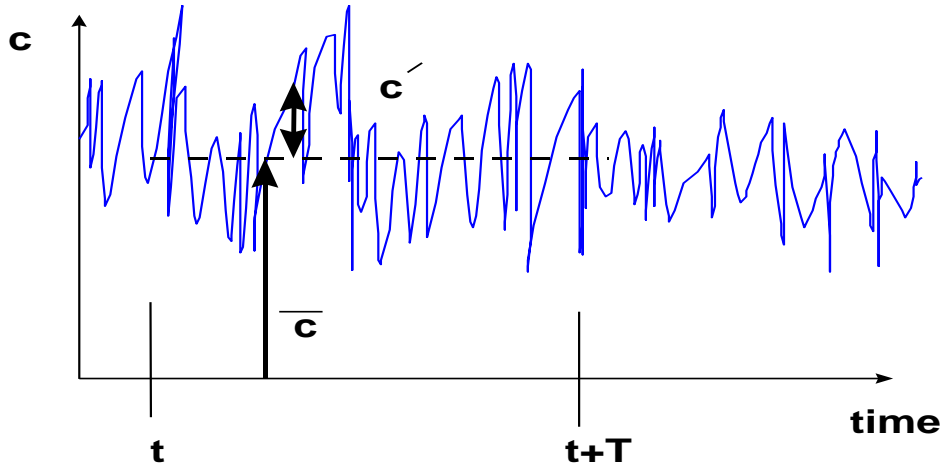
Figure 49. Concentration variability with time.

The instantaneous velocity and concentration are decomposed into a mean and an unsteady component:

$$\frac{1}{T} \int_t^{t+T} u(t) \ dt \tag{4-1}$$

Similarly for w, v, and c:

$$v = \bar{v} + v^{'}$$
$$w = \bar{w} + w^{'}$$

$$c = \bar{c} + c^{'} \tag{4-2}$$

Substituting these into the 3D governing equation and time averaging:

$$\frac{\partial \bar{c}}{\partial t} + \underbrace{\bar{u}\frac{\partial \bar{c}}{\partial x} + \bar{v}\frac{\partial \bar{c}}{\partial y} + \bar{w}\frac{\partial \bar{c}}{\partial z}}_{\text{transport by mean advection}} = \underbrace{D\left[\frac{\partial^2 \bar{c}}{\partial x^2} + \frac{\partial^2 \bar{c}}{\partial y^2} + \frac{\partial^2 \bar{c}}{\partial z^2}\right]}_{\text{molecular diffusive transport}}$$

$$\underbrace{-\frac{\partial}{\partial x}\left(\overline{u'c'}\right) - \frac{\partial}{\partial y}\left(\overline{v'c'}\right) - \frac{\partial}{\partial z}\left(\overline{w'c'}\right)}_{\text{turbulent mass tranport}} + \bar{S} \tag{4-3}$$

The new terms in the governing equation represent mass transport by turbulent eddies. As the intensity of turbulence increases, turbulent mass transport increases. Notice also that all velocities and concentrations are time averaged. The following turbulent mass fluxes are defined as:

$$\bar{J}_t = \left(\overline{u'c'}, \overline{v'c'}, \overline{w'c'}\right) \tag{4-4}$$

where:

$$\overline{(u'c')} = -E_x \frac{\partial \bar{c}}{\partial x}$$

$$\overline{(v'c')} = -E_y \frac{\partial \bar{c}}{\partial y}$$

$$\overline{(w'c')} = -E_z \frac{\partial \bar{c}}{\partial z}$$

Substituting into the above equation:

$$\frac{\partial \bar{c}}{\partial t} + \bar{u}\frac{\partial \bar{c}}{\partial x} + \bar{v}\frac{\partial \bar{c}}{\partial y} + \bar{w}\frac{\partial \bar{c}}{\partial z} = \frac{\partial}{\partial x}\left[(E_x + D)\frac{\partial \bar{c}}{\partial x}\right] + \frac{\partial}{\partial y}\left[(E_y + D)\frac{\partial \bar{c}}{\partial y}\right] + \frac{\partial}{\partial z}\left[(E_z + D)\frac{\partial \bar{c}}{\partial z}\right] + \bar{S}$$

(4-5)

In turbulent fluids, E_x, E_y, and E_z >> D, and D can be neglected except at interfaces where turbulence goes to zero. The turbulent diffusion coefficients can be thought of as the product of the velocity scale of turbulence and the length scale of that turbulence. These coefficients are related to the turbulent eddy viscosity. One is turbulent mass transport, the other is turbulent momentum transport between adjacent control volumes. In general, these turbulent diffusion coefficients are non-isotropic and non-homogeneous.

Temperature and Water Quality Transport

Spatial averages across the lateral dimension of the channel of the turbulent time-averaged quantities can now be introduced:

$$\overline{c} = \overline{\overline{c}} + c''$$
$$\overline{u} = \overline{\overline{u}} + u'' \qquad\qquad\qquad \textbf{(4-6)}$$
$$\overline{w} = \overline{\overline{w}} + w''$$

where the double overbar is a spatial average over y and the double prime is the deviation from the spatial mean as illustrated in **Figure 50** for velocity and **Figure 51** for constituent concentrations.
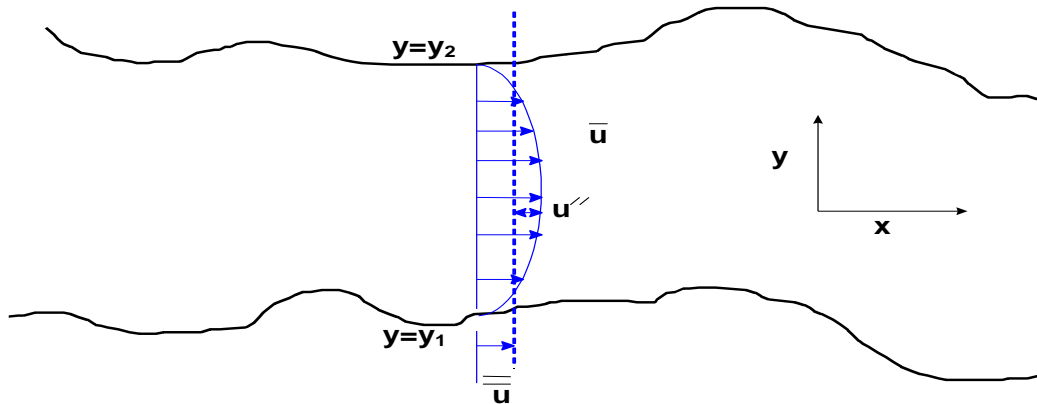
Figure 50. Lateral average of the velocity field.
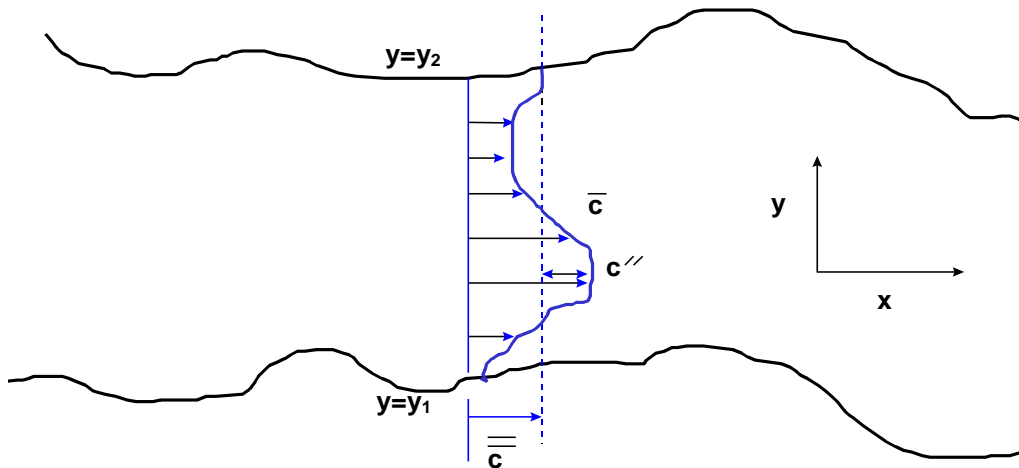
Figure 51.   Lateral average of the concentration field.

These are substituted into the governing equation and then the governing equation is integrated over the width such that:

$$\overbrace{\qquad\qquad\qquad\qquad}^{\text{mass transfer at side boundaries}}$$

$$\frac{\partial B\bar{\bar{c}}}{\partial t} + \frac{\partial B\bar{\bar{u}}\bar{\bar{c}}}{\partial x} + \frac{\partial B\bar{\bar{w}}\bar{\bar{c}}}{\partial z} = -B\left(\bar{\bar{v}}\bar{\bar{c}}|_{y2} - \bar{\bar{v}}\bar{\bar{c}}|_{y1} + \overline{c'v'}|y2 - \overline{c'v'}|y1\right)$$

$$+\frac{\partial}{\partial x}\left((D+E_x)B\frac{\partial\bar{\bar{c}}}{\partial x}\right) + \frac{\partial}{\partial z}\left((D+E_z)B\frac{\partial\bar{\bar{c}}}{\partial z}\right) - \left[\frac{\partial B\overline{u''c''}}{\partial x} + \frac{\partial B\overline{w''c''}}{\partial z}\right] + \bar{r}B \qquad \textbf{(4-7)}$$

Note how the following terms are simplified:

$$\frac{1}{B}\int_{y1}^{y2}\frac{\partial(\bar{\bar{c}}+c'')}{\partial t}dy = \frac{1}{B}\int_{y1}^{y2}\frac{\partial(\bar{\bar{c}})}{\partial t}dy + \frac{1}{B}\int_{y1}^{y2}\frac{\partial(c'')}{\partial t}dy$$

$$= \frac{1}{B}\frac{\partial}{\partial t}\int_{y1}^{y2}\bar{\bar{c}}\,dy + \frac{1}{B}\frac{\partial}{\partial t}\int_{y1}^{y2}c''\,dy = \frac{1}{B}\frac{\partial B\bar{\bar{c}}}{\partial t} \qquad \textbf{(4-8)}$$

$$\frac{1}{B}\int_{y1}^{y2}\frac{\partial(\bar{\bar{u}}+u'')(\bar{\bar{c}}+c'')}{\partial x}dy = \frac{1}{B}\int_{y1}^{y2}\frac{\partial(\bar{\bar{c}}\bar{\bar{u}})}{\partial t}dy + \frac{1}{B}\int_{y1}^{y2}\frac{\partial(c''u'')}{\partial t}dy$$

$$= \frac{1}{B}\frac{\partial}{\partial x}\int_{y1}^{y2}\bar{\bar{c}}\bar{\bar{u}}\,dy + \frac{1}{B}\frac{\partial}{\partial x}\int_{y1}^{y2}c''u''\,dy = \frac{1}{B}\frac{\partial B\bar{\bar{u}}\bar{\bar{c}}}{\partial t} + \frac{1}{B}\frac{\partial B\overline{u''c''}}{\partial x} \qquad \textbf{(4-9)}$$

The spatial average of any double primed variable goes to zero by definition. The turbulent dispersion coefficients are defined as:

$$\overline{u''c''} = -D_x\frac{\partial\bar{\bar{c}}}{\partial x} \qquad \textbf{(4-10)}$$

$$\overline{w''c''} = -D_z\frac{\partial\bar{\bar{c}}}{\partial z}$$

The dispersion terms are a result of lateral averaging of the velocity field. In general, except at an interface, $D_x \gg E_x \gg D$ and similarly for $D_z \gg E_z \gg D$. Substituting in for the dispersion coefficients and using q to be the net mass transport from lateral boundaries, this equation becomes:

$$\frac{\partial B\bar{\bar{c}}}{\partial t} + \frac{\partial B\bar{\bar{u}}\bar{\bar{c}}}{\partial x} + \frac{\partial B\bar{\bar{w}}\bar{\bar{c}}}{\partial z} = qB + \frac{\partial}{\partial x}\left(D_xB\frac{\partial\bar{\bar{c}}}{\partial x}\right) + \frac{\partial}{\partial z}\left(D_zB\frac{\partial\bar{\bar{c}}}{\partial z}\right) + \bar{r}B \qquad \textbf{(4-11)}$$

If the overbars are dropped and replaced with capitals, c is replaced with Φ, then the following equation is obtained:

$$\frac{\partial B\Phi}{\partial t} + \frac{\partial UB\Phi}{\partial x} + \frac{\partial WB\Phi}{\partial z} - \frac{\partial}{\partial x}\left[BD_x\frac{\partial\Phi}{\partial x}\right] - \frac{\partial}{\partial z}\left[BD_z\frac{\partial\Phi}{\partial z}\right] = q_\Phi B + S_\Phi B \qquad \textbf{(4-12)}$$

where:
    Φ = laterally averaged constituent concentration, $g\ m^{-3}$
    D_x = longitudinal temperature and constituent dispersion coefficient, $m^2\ sec^{-1}$
    D_z = vertical temperature and constituent dispersion coefficient, $m^2\ sec^{-1}$
    q_Φ = lateral inflow or outflow mass flow rate of constituent per unit volume, $g\ m^{-3}\ sec^{-1}$
    S_Φ = laterally averaged source/sink term, $g\ m^{-3}\ sec^{-1}$

Note that this can be concentration or temperature since the concentration of heat can be determined to be $\rho c_p T$ where ρ is the fluid density, c_p is the specific heat of water, and T is the temperature. In this case

the source-sink term for temperature would be $S_T = -\frac{\partial \varphi}{\partial z}$ where φ is the heat flux in units of W/m² transmitted through the waterbody.

The following must be known in order to solve the equation:

1. laterally-averaged velocity field the from momentum equations
2. appropriate boundary and initial conditions
3. D_x and D_z
4. laterally-averaged source/sink terms

Determination of D_z and D_x

The specification of D_x, the longitudinal dispersion coefficient, is a user-defined input. The preprocessor though does a check on the magnitude of this value by computing D_x based on an approach by Okubo (1971):

$$D_x = 5.84 X 10^{-4} \Delta x^{1.1}$$

where D_x is in m²/s and the longitudinal grid spacing Δx is in m. D_x can also be set to be a function of the mean velocity or this value can be space and time invariant. D_x can be computed dynamically using

$$D_x = \beta \overline{\overline{U}} \Delta z$$

Where β is a user input value, U with double bars are the time-averaged, lateral averaged longitudinal velocity at a segment and layer. Hence, the dispersion coefficient scales with the average longitudinal velocity.

D_z is internally computed within the CE-QUAL-W2 model using the Reynold's analogy, where D_z is computed from A_z, the vertical eddy viscosity, from

$$D_z = 0.14 A_z$$

Temperature Auxiliary Functions

Heat Exchange

Surface Heat Exchange

The surface heat exchange is treated as a flux boundary condition at the water surface. Surface heat exchange can be formulated as a term by-term process (see Figure 52) using the explicit adjacent cell transport computation as long as the integration timestep is shorter than or equal to the frequency of the meteorological data. Surface heat exchange processes depending on water surface temperatures are computed using computations from the prior time step.

Surface heat transfer terms
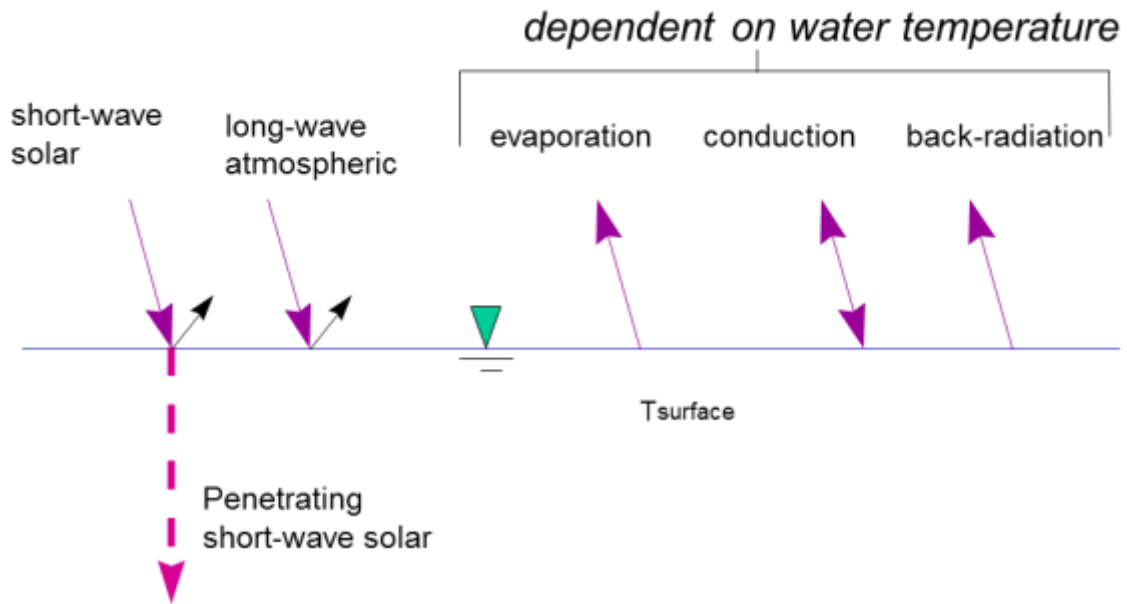
Figure 52. Surface heat exchange term-by-term formulation.

Term-by-term surface heat exchange is computed as:

$$\Phi_n = \Phi_s - \Phi_{sr} + \Phi_a - \Phi_{ar} - \Phi_{br} - \Phi_e - \Phi_c \tag{4-13}$$

where:

ϕ_n: net surface heat flux, *W m^{-2}*
ϕ_s: incoming short-wave solar radiation, *W m^{-2}*
ϕ_{sr}: reflected short-wave solar radiation, *W m^{-2}*
ϕ_{sn}: net short-wave solar radiation, ϕ_s-ϕ_{sr}, *W m^{-2}*
ϕ_a: incoming long-wave atmospheric radiation, *W m^{-2}*
ϕ_{ar}: reflected atmospheric long-wave radiation, *W m^{-2}*
ϕ_{br}: back long-wave radiation, *W m^{-2}*
ϕ_e: evaporative heat loss, *W m^{-2}*
ϕ_c: conductive heat loss, *W m^{-2}*

The short-wave solar radiation is either measured directly or computed from sun angle relationships and cloud cover. Annear and Wells (2007) provide an overview of formulae for short wave solar radiation. If the model user chooses the internally computed short wave solar, the model computes the net clear sky solar radiation ϕ_s (net short-wave solar radiation in Btu/ft^2/day) using the EPA (1971) relationship:

$$\phi_s = 24(2.044A_o + 0.1296A_o^2 - 1.941E - 3A_o^3 + 7.591E - 6A_o^4)*0.1314 \tag{4-14}$$

Note that this equation includes the average reflection loss of short-wave solar radiation. The total clear sky solar radiation was calculated using a least-squares fit polynomial regression of the solar altitude A_o

(degrees), which is the angle of inclination of the sun relative to the horizon from an observer's perspective (Wunderlich, 1972) using

$$A_o = ASin[Sin(Lat)Sin(\delta) + Cos(Lat)Cos(\delta)Cos(H)]$$ **(4-15)**

where *Lat* is the latitude, δ is the solar declination, and *H* is the local hour angle. The local hour angle *H* (radians), is the angular position of the sun for a given location at a specific time during the day and was calculated from Ryan and Stolzenbach (1972) using

$$H = \frac{2\pi}{24}\left[HOUR - (Long - \varphi)\frac{24}{360} + EQT - 12.0\right]$$ **(4-16)**

where *HOUR* is the local hour, φ is standard meridian, *Long* is the longitude, and *EQT* is the equation of time. The equation of time *EQT* (hours), represents the difference between true solar time and mean solar time due to seasonal variations in the orbital velocity of the earth (Ryan and Stolzenbach, 1972). DiLaura (1984) calculated *EQT* as

$$EQT = 0.170Sin[4\pi(INT(Jday) - 80)/373]$$
$$-0.129Sin[2\pi(INT(Jday) - 8)/355]$$ **(4-17)**

where *Jday* is the Julian day as a floating-point value on a scale of 1 to 365 days for a year (366 for a leap year) and *INT* is the integer function. The local hour *HOUR* (hours), was calculated using the time during the day (Wunderlich, 1972), such as

$$HOUR = 24(Jday - INT(Jday))$$ **(4-18)**

EPA (1971) calculated the standard meridian φ (degrees), as

$$\varphi = 15.0 * INT\left(\frac{Long}{15.0}\right)$$ **(4-19)**

where *Long* is the longitude. The time zones calculate a more appropriate standard meridian than the longitude, so the variable *TZ* (hours), the time zone relative to Greenwich Mean Time (GMT) was used to improve the calculation of the standard meridian in the above equation, such that

$$\varphi = -15.0 * INT(TZ)$$ **(4-20)**

The solar declination angle δ (radians) was calculated by Spencer (1971) as:

$$\delta = 0.006918 - 0.399912Cos(\tau_d) + 0.070257Sin(\tau_d)$$
$$-0.006758Cos(2\tau_d) + 0.000907Sin(2\tau_d)$$
$$-0.002697Cos(3\tau_d) + 0.001480Sin(3\tau_d)$$ **(4-21)**

where τ_d is the angular fraction of the year which Spencer (1971) calculated as

$$\tau_d = \frac{2\pi(INT(Jday) - 1)}{365}$$ **(4-22)**

Cloud cover reduction of clear sky solar radiation uses the following relationship (Wunderlich, 1972): $\phi_{s\_net} = \phi_{s\_clearsky}(1 - 0.65C^2)$ where C is the cloud cover fraction between 0 and 1.

The long wave atmospheric radiation is computed from air temperature and cloud cover or air vapor pressure using Brunt's formula. The right-hand terms are all water surface temperature dependent.

Water surface back radiation is computed as:

$$\phi_{br} = \varepsilon\sigma(T_s + 273.15)^4$$ **(4-23)**

where:

ε = emissivity of water, 0.97
σ = Stephan-Boltzman constant, *5.67 x 10^{-8} W m^{-2} {}^oK^{-4}*
T_s = water surface temperature, ^oC

Like the remaining terms, it is computed for each surface layer cell on each iteration timestep.

Evaporative heat loss is computed as:

$$\phi_e = f(W_z)(e_s - e_a)$$ **(4-24)**

where:

$f(Wz)$ = evaporative wind speed function at wind height of z, *W m^{-2} mm Hg^{-1}*
e_s = saturation vapor pressure at the water surface, *mm Hg*
e_a = atmospheric vapor pressure, *mm Hg*

Evaporative heat loss depends on air temperature and dew point temperature or relative humidity. Surface vapor pressure is computed from the surface temperature for each surface cell on each iteration.

Surface heat conduction is computed as:

$$\phi_c = C_c f(W_z)(T_s - T_a)$$ **(4-25)**

where:

C_c = Bowen's coefficient, *0.47 mm Hg {}^oC^{-1}*
T_a = air temperature, ^oC

Short wave solar radiation penetrates the surface and decays exponentially with depth according to Bear's Law (see Figure 53):

$$\phi_s(z) = (1 - \beta)\phi_{sn}e^{-\eta z}$$ **(4-26)**

where:

$\phi_s(z)$ = short wave radiation at depth z, *W m^{-2}*
β = fraction absorbed at the water surface
η = extinction coefficient, *m^{-1}*
ϕ_{sn} = net short-wave radiation reaching the surface, *W m^{-2}*
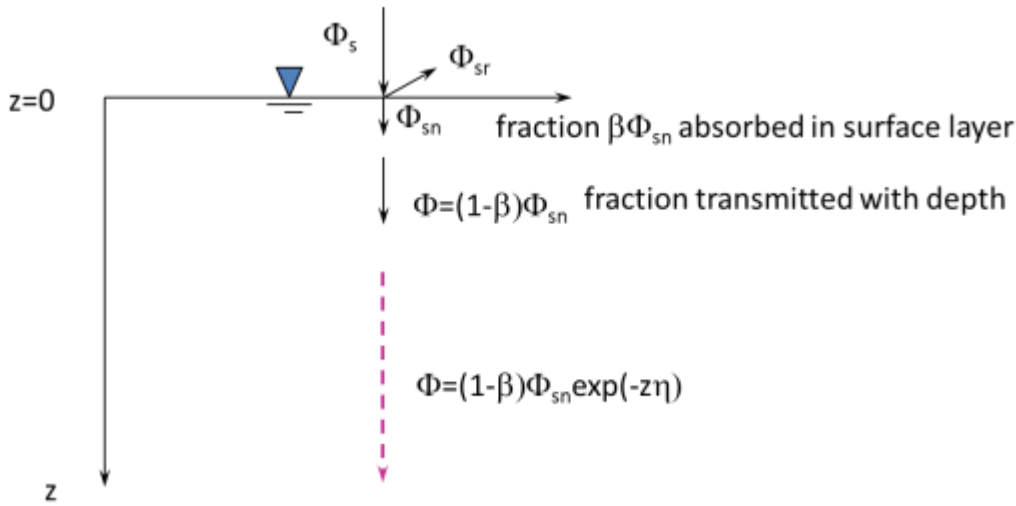
Figure 53. Short-wave solar penetration in a water body.

Evaporation Models for f(W)

Aside from the problems of measuring meteorological data and obtaining representative meteorological data for a waterbody, evaporative wind speed function, *f(Wz),* chosen by the model user can affect surface temperatures especially in the summer. Various formulations of *f(Wz)* have been catalogued and examined in Edinger et al. (1974).

The model user can include different evaporation formulations using an evaporation wind speed formula of the form

$$f(W_z) = a + bW_z^c \tag{4-27}$$

where:
  f(Wz) = wind speed function with wind measured at height z, *W m^{-2} mm Hg^{-1}*
       a = empirical coefficient, 9.2 default
       b = empirical coefficient, 0.46 default
       c = empirical coefficient, 2 default
     W$_z$ = wind speed measured at 2 *m* above the ground, *m s^{-1}*

The function is used in computing both evaporative water and heat loss. The default values for a, b, and c are the ones suggested in Edinger et. al. (1974). The model assumes that the wind is measured at a 2m height. The following equation converts b from any measurement height to 2 *m*:

$$b_{2m} = \alpha^c b_z \tag{4-28}$$

where b_z is *b* measured at *z m* and α is the conversion factor between the wind at *z* and the wind at 2*m* using

$$\frac{W_{2m}}{W_z} = \frac{ln\left(\frac{2}{z_0}\right)}{ln\left(\frac{z}{z_0}\right)} = \frac{1}{\alpha} \tag{4-29}$$

where:

W_{2m} = wind speed at elevation 2 m, $m\ s^{-1}$
W_z = wind speed at height z, $m\ s^{-1}$
z_0 = wind roughness height

Note that wind roughness height, z_o, is a model input parameter since Version 3.6. Typical roughness values include 0.003 *ft* (0.001 m) for wind < 5 *mph* (2.3 m/s) and 0.015 ft (0.005 m) for wind > 5 *mph (2.3 m/s)*. The roughness values can range from 0.0005 ft to 0.03 *ft (0.00015-0.01 m).*

The Ryan-Harleman (1974) evaporation model formulation has also been included in the model using:

$$f(W_z) = a + bW_z \qquad\qquad\qquad \textbf{(4-30)}$$

where:

b = 4.1 *W m^{-2} mm Hg^{-1} m^{-1} s^{-1}*
$a = \lambda(\,T_{sv} - T_{av}\,)^{1/3}$, where s is surface temperature and a is air temperature
λ = 3.59 *W m^2 mm Hg* $°C^{1/3}$
$T_v = T^*\left(1 - 0.378\left[\frac{e}{p}\right]\right)^{-1}$, K
p = atmospheric pressure, assumed to be 760 *mm Hg*

For the Lake Hefner model, a = 0 and b = 4.99 *W m^{-2} mm Hg^{-1} m^{-1} s^{-1}*.

If the virtual temperature difference, T_v, is negative or less than that computed using the Lake Hefner model, *f(W)* reverts to the Lake Hefner evaporation model. **Figure 54** shows a comparison of the Ryan-Harleman model with the model's default formulation.

Adams et al. (1981) recommended that the Lake Hefner model be used for natural lakes (**Table 6**).
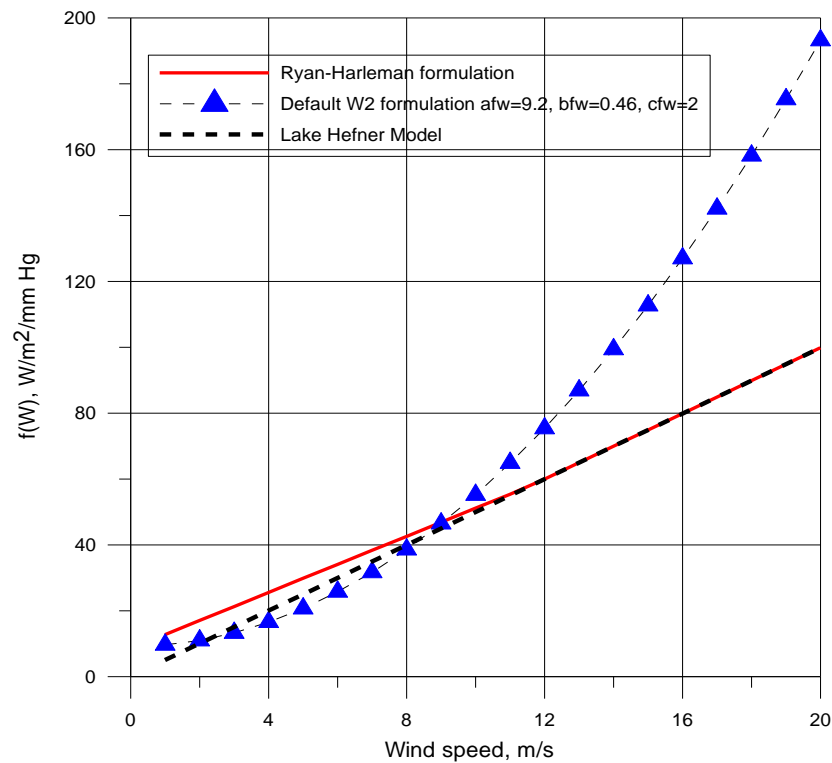
Figure 54. Comparison of the wind speed formualtion for Ryan-Harleman and W2 default (for T_{air}=15ºC, T_{dew}=-5ºC, $T_{surface}$=25ºC).

Summaries of several evaporation formulations are shown below in **Table 6** as adapted from Adams, et al. (1981).

Table 6. Typical Evaporation Formulae for Lakes and Reservoirs

Name	Time	Waterbody	φ_e	f(W)	Remarks
Lake Hefner	3 *hrs* and *day*	Lake Hefner, OK, 2587 *acres*	$17.2W_2(e_s-e_2)$	$5.06W_2$	good agreement with lake data from several lakes in US and Russia
Kohler	*day*	Lake Hefner OK, 2587 *acres*	$17.5W_2(e_s-e_2)$	$5.14W_2$	essentially the same as Lake Hefner formula
Zaykov	-	ponds and small reservoirs	$(1.3+14W_2)(e_s-e_2)$	$0.1708+ 4.11W_2$	based on Russian work
Meyer	*month*	small lakes and reservoirs	$(80+10W_2)(e_s-e_2)$	$10.512+2.94W_2$	e_a obtained daily from mean morning and evening measurements of air temperature and relative humidity

Name	Time	Waterbody	φ_e	f(W)	Remarks
Mor-ton	*month*	Class A pan	$(73.5+14.7W_2)\ (e_s-e_2)$	$9.658+4.32W_2$	data from meteoro-logical stations, measurement heights assumed
Rohwer	*day*	pans, 85 *ft* dia tank, 1300 *acre* reservoir	$(67+10W_2)\ (e_s-e_2)$	$8.8+2.94W_2$	extensive pan meas-urements using dif-ferent pans, corre-lated with tank and reservoir data

φ_e	= evaporation at sea-level with wind corrected to 2 *m*, BTU $ft^{-2}\ day^{-1}$
W	= wind, *mph*
e	= vapor pressure, *mm Hg*
$W\ m^{-2}$	= 0.1314*BTU $ft^{-2}\ day^{-1}$
10 *mb*	= 7.5006151 *mm Hg*

The mass evaporation rate is computed by dividing evaporative heat loss by the latent heat of evaporation of water. Surface heat exchange always includes evaporative heat loss in the heat budget, but the user may choose to exclude it in the water budget. For many reservoirs, inflow rates are determined from storage estimates that implicitly include evaporation.

Equilibrium Temperature

Another option in lieu of the term-by-term formulation presented above is to use a linearized form of the heat flux expression that is a linear function of surface temperature. The equilibrium temperature, T_E, is defined as the temperature at which the net rate of surface heat exchange is zero (see Figure 55) or is the temperature a water body is seeking if it is starting at a surface temperature of T_s.

$$\phi_n = -K(T_s - T_E)$$
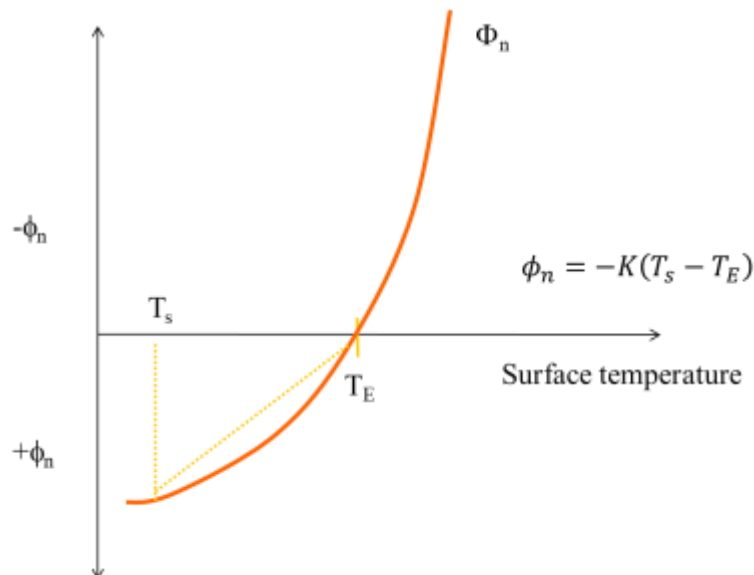
Figure 55. Concept of the equilibrium temperature, T_E, where the net surface heat flux is defined as zero.

Linearization of the term-by-term heat balance along with the definition of equilibrium temperature allows expressing the net rate of surface heat exchange, ϕ_n, as:

$$\phi_n = -K(T_s - T_E) \tag{4-31}$$

where:

ϕ_n = net rate of surface heat exchange, $W\,m^{-2}$
K = coefficient of surface heat exchange, $W\,m^{-2}\,^\circ C^{-1}$
T_w = water surface temperature, $^\circ C$
T_E = equilibrium temperature, $^\circ C$

Seven separate heat exchange processes are summarized in the coefficient of surface heat exchange and equilibrium temperature. The linearization is examined in detail by Brady, et al. (1969) and Edinger et al. (1974).

How to compute T_E and K?
- Compute T_E directly from $\varphi_n = 0$
- Compute K directly from $K = -\varphi_n/(T_s - T_E)$

Or these can be approximated as shown below:

Estimating T_E and K:

T_E: compute from heat flux equation where $\varphi_n = 0$ or approximate technique (Brady et al., 1969):

$$T_E = \frac{\varphi_{sn}}{23 + f(W)(\beta + 0.255)} + T_d$$

where:

φ_{sn}: net short wave solar in Btu/ft^2/day
T_d: dew point temperature $^\circ$F
$f(W)$: wind speed function = $17W_2$ Lake Hefner model, in Btu/ft^2/day/mm Hg
$\beta = 0.255 - 0.0085T^* + 0.000204T^{*2}$
$T^* = 0.5(T_w + T_d)$
T_w: water surface temperature
T_d: dew point temperature
W_2: wind speed at 2 m in mph
K: compute from slope of net flux vs temperature or use approximate formula (Brady et al., 1969):

$$K = 23 + (\beta_w + 0.255)17W_2$$

where: $\beta_w = 0.255 - 0.0085T_w + 0.000204T_w^2$ and units of K are in Btu/ft^2/day/$^\circ$F and are converted to W/m^2/$^\circ$C.

Sediment Heat Exchange

Sediment heat exchange with water is generally small compared to surface heat exchange and many previous modelers have neglected it. Investigations on several reservoirs have shown the process must be included to accurately reproduce hypolimnetic temperatures primarily because of the reduction in numerical

diffusion that previously swamped the numerical solution. The formulation is similar to surface heat exchange:

$$H_{sw} = -K_{sw}(T_w - T_s)$$

(4-32)

where:

H_{sw} = rate of sediment/water heat exchange, $W\ m^{-2}$
K_{sw} = coefficient of sediment/water heat exchange, $W\ m^{-2}\ {}^{\circ}C^{-1}$
T_w = water temperature, ${}^{\circ}C$
T_s = sediment temperature, ${}^{\circ}C$

Previous applications used a value of 0.3 $W\ m^{-2}\ {}^{\circ}C^{-1}$ for K_{sw} that is approximately two orders of magnitude smaller than the surface heat exchange coefficient. Average yearly air temperature is a good estimate of T_s.

Dynamic Shading

Solar Altitude and Azimuth

The declination angle, δ, is computed from Spencer (1971):

$$\delta = 0.006918 - 0.399912\,cos(\tau_d) + 0.070257\,sin(\tau_d) - 0.006758\,cos(2\tau_d) +$$
$$0.000907\,sin(2\tau_d) - 0.0022697\,cos(3\tau_d) + 0.001480\,sin(3\tau_d)$$

(4-33)

where:

$$\tau_d = \frac{2\pi(JD_i - 1)}{365}$$

JD_i = Julian date integer value

The local hour is calculated as:

$$HOUR = 24(JD_r - JD_i)$$

(4-34)

where:

JD_i = Julian date integer value
JD_r = Julian date floating-point value

An equation of time, EQT, correction is needed to calculate the local hour angle. The equation of time represents the difference between true and mean solar time due to seasonal variations in the earth's orbital velocity (DiLaura, D.L 1984) and is given as:

$$EQT = 0.17\,sin\frac{4\pi(JD_i - 80)}{373} - 0.129\,sin\frac{2\pi(JD_i - 8)}{355}$$

(4-35)

where:

JD_i = Julian date integer value

The local hour angle, H, is calculated as:

$$H = \frac{2\pi}{24}\left[HOUR + (Long - \varphi)\frac{24}{360} + EQT - 12\right]$$
(4-36)

The solar altitude, A_o, is the angle of inclination of the sun relative to the horizon from an observer's perspective as shown in **Figure 56**.
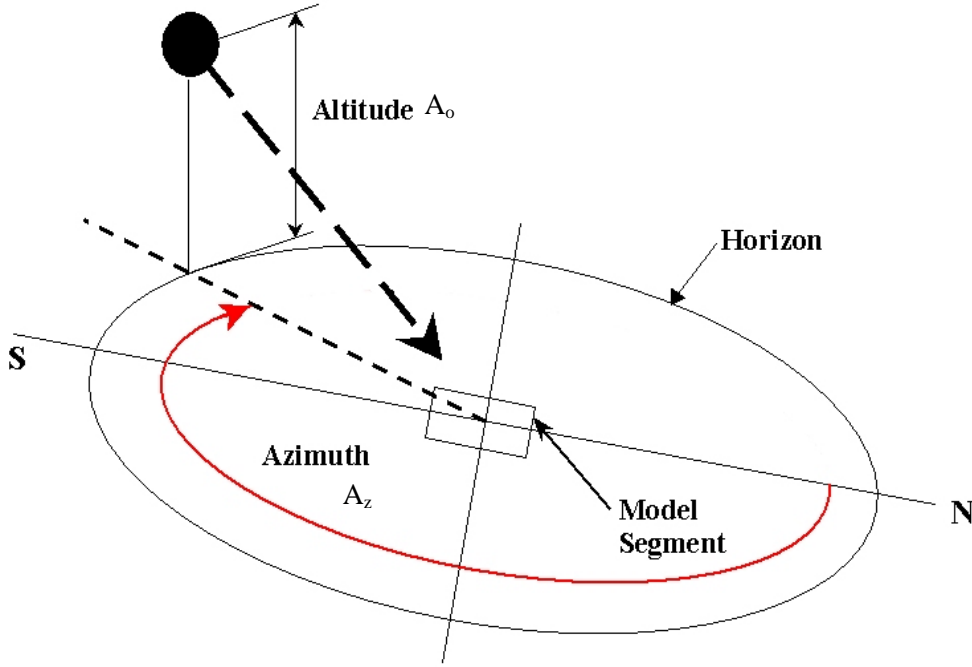
Figure 56. Schematic of solar altitude, A_o, and azimuth, A_z.

A_o is calculated from Wunderlich (1972):

$$A_o = A \sin\left[\sin\left(lat * \frac{\pi}{180}\right)\sin(\delta) + \cos\left(lat * \frac{\pi}{180}\right)\cos(\delta)\cos(H)\right]$$
(4-37)

The solar azimuth is the direction of the sun with respect to a North-South axis measured clockwise from the North as shown in **Figure 57**. The solar azimuth is computed as (Nautical Almanac, 2001):

$$X = \frac{\sin(\delta)\cos\left(\frac{Lat*\pi}{180}\right) - \cos(\delta)\cos(H)\sin\left(\frac{Lat*\pi}{180}\right)}{\cos A_o}$$
(4-38)

$$\text{If } X > 1, X = 1$$

If $X < -1, X = -1$ (4-39)

$$A = A \cos X$$
(4-40)

$$AZ = 2\pi - A$$

If $H < 0, AZ = A$ (4-41)

After computing the solar altitude and azimuth, the impact of shading (**Figure 57**) on short-wave solar radiation is computed as follows.
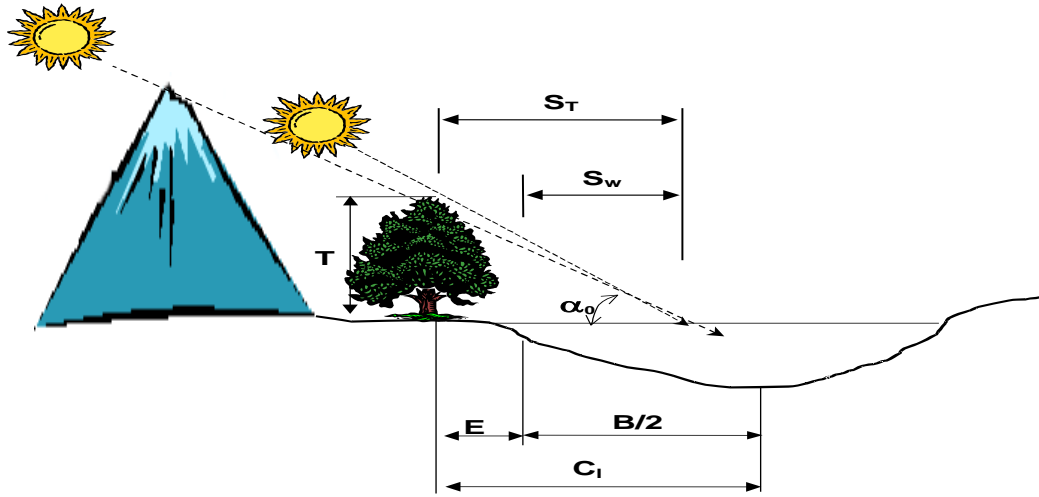
Figure 57. Schematic of topographic and vegetative shading, solar altitude (α_0), and vegetation height (*T*) and their effect on shadow length.

Topographic Shading

The algorithm uses the position of the sun to determine which topographic inclination angle coincides with the direction of incoming solar radiation. The algorithm determines the closest two inclination angles in the direction of the incoming solar radiation and uses them to linearly interpolate an inclination angle for the specific direction of the incoming solar radiation. The calculated inclination angle is then used to determine if vegetative or topographic shading dominates at that time. If the solar altitude is below the calculated topographic inclination angle, then topographic shading dominates and the short-wave solar radiation is reduced by 90% for complete shade. This allows for 10% of the incoming solar radiation as a result of diffuse radiation even when in the shade. If the solar altitude is above the calculated inclination angle, then vegetative shading dominates.

Vegetative Shading

If the topographic angle is less than the solar altitude, vegetative shade dominates and the algorithm calculates the shading influence by determining how far the shadow extends over the water. **Figure 58** and **Figure 59** show schematics of the azimuth angle, segment orientation and computed shadow lengths. The tree shadow length, S_T, is calculated using the tree height, *T*, and solar altitude, A_0, using Equation 206. Then the length of the shadow cast over the water is calculated using Equation 207 where *E* is the distance between the tree and the edge of water and Θ_0 is the segment orientation. The shadow length, S_N, perpendicular to the edge of the water is then calculated using Equation 208. Refer to **Figure 58** and **Figure 59** for diagrams showing the distance calculated in Equations 206 to 208.

$$S_T = \frac{T}{tan\,A_0} \tag{4-42}$$

$$S_W = S_T - \frac{E}{sin(\Theta_0 - \alpha_A)} \tag{4-43}$$

$$S_N = S_W \sin(\Theta_0 - \alpha_A)$$ **(4-44)**

Simplifying Equations 206 to 208:

$$S_N = \frac{T * \sin(\Theta_0 - \alpha_A)}{\tan A_0} - E$$ **(4-45)**

A shading reduction factor is applied in cases where a model segment has potential shading along only part of its segment length or the vegetation density is low. For example, if shade-producing vegetation exists along only half the length of a segment and is 100% opaque, a shade reduction factor of 0.5 is used. If shading is due to vegetation along only half of a segment with 80% opaqueness, a value of 0.4 is used.

The shade factor, $sfact$, is the shadow length perpendicular to the edge of the water, S_N, multiplied by the shade reduction factor, SRF, and divided by the segment width:

$$sfact = SRF \frac{S_N}{B}$$ **(4-46)**

The amount of shade that should be applied to the incoming short-wave solar radiation is calculated as:

$$Shade = (1 - sfact)$$ **(4-47)**

The short-wave solar radiation [SRO] computed by the model is reduced by the shade variable:

$$SRO_{net} = SRO * Shade$$ **(4-48)**
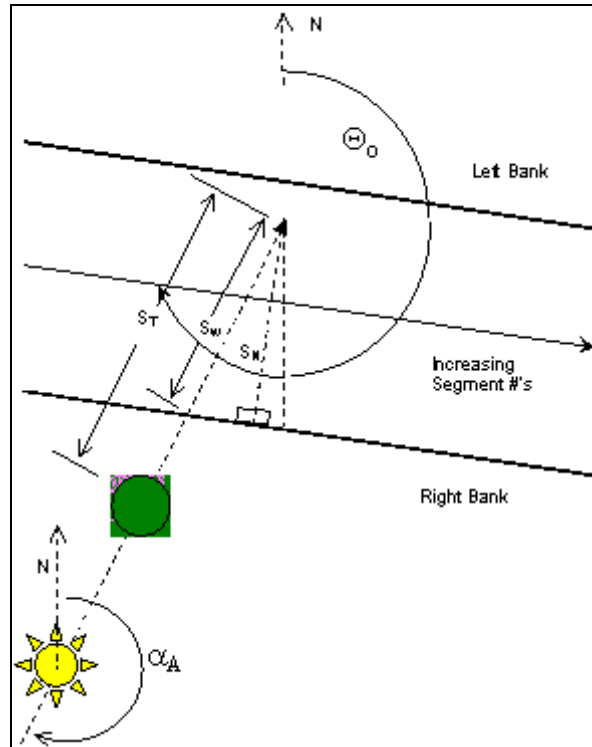
Figure 58. Azimuth angle, α_A, and stream orientation, Θ_0.
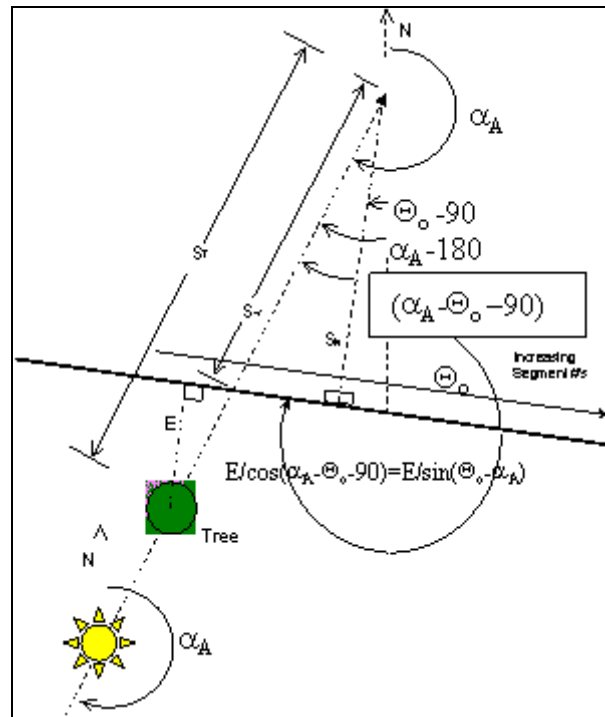
Figure 59. **Relationship between azimuth, stream orientation, and shadow length.**

Data Requirements

Topography and vegetation data are stored in a user-defined input file. An example input file is shown in Appendix C. The file includes tree top elevations for both stream banks. The file also includes the distance from the centerline of the river to the controlling vegetation and the shade reduction factor (explained below) for both stream banks. The shade file has vegetation characteristics recorded by the left and right banks of the stream. The convention used for defining left or right bank is dependent on looking down-stream in the system, the 'Left Bank' is on the left and the 'Right Bank' is to the right.

The shade algorithm reads in 18 topographic inclination angles surrounding each segment center-point. The inclination angles can be determined using topographical maps, Digital Elevation Models (DEM), or contour plots. The steepest inclination angle for each of the 18 locations surrounding a segment should be selected since this angle will control the topographic shading. The first inclination angle is taken from directly North of a segment (orientation angle 0.0) and moves clockwise to the East with increasing orientation angles around the segment in 20° increments.

How far away from the centerline of the river the topography should be analyzed will depend on the system. Wide flat river systems will utilize longer distances for identifying influencing topography than a narrow river canyon. In addition, rather than restricting the code to orientation angles only toward the south appropriate for the Northern hemisphere, using orientation angles that surround a segment allows the algorithm to be used in both the northern and southern hemispheres.

In addition, the user can specify dynamic shading reduction factors as a function of time. Usually, these would correspond to the times for leaf growth and fall for deciduous trees.

The topography and vegetation information is first read in from the input file. Then, using the segment orientation angle, Θ_0, and the solar azimuth, α_A, the bank that has the sun behind it is computed. The criteria used for determining the bank with the sun behind it was modified from Chen (1996) because the segment orientation angle is determined differently in CE-QUAL-W2. **Table 7** shows the criteria used in the model.

Table 7. Criteria for determining sunward bank

Sunward Bank	$0° < \Theta_0 \leq 180°$	$180° < \Theta_0 \leq 360°$
Left	$\alpha_A < \Theta_0$ or $\alpha_A > \Theta_0 + 180°$	$\Theta_0 - 180° < \alpha_A < \Theta_0$
Right	$\Theta_0 < \alpha_A < \Theta_0 + 180°$	$\alpha_A > \Theta_0$ or $\alpha_A < \Theta_0 - 180°$

Ice Cover

Ice thickness, onset, and loss of ice cover play an important role in the heat budget of northern waterbodies. At high latitudes, ice cover may remain until late spring or early summer and prevent warming due to absorption of short-wave solar radiation.

The ice model is based on an ice cover with ice-to-air heat exchange, conduction through the ice, conduction between underlying water, and a "melt temperature" layer on the ice bottom (Ashton, 1979). The overall heat balance for the water-to-ice-to-air system is:

$$\rho_i L_f \frac{\Delta h}{\Delta t} = h_{ai}(T_i - T_e) - h_{wi}(T_w - T_m)$$

(4-49)

where:

ρ_i = density of ice, *kg m^{-3}*
L_f = latent heat of fusion of ice, *J kg^{-1}*
$\Delta h / \Delta t$ = change in ice thickness (h) with time (t), *m sec^{-1}*
h_{ai} = coefficient of ice-to-air heat exchange, *W m^{-2} $^{\circ}C^{-1}$*
h_{wi} = coefficient of water-to-ice heat exchange through the melt layer, *W m^{-2} $^{\circ}C^{-1}$*
T_i = ice temperature, $^{\circ}C$
T_e = equilibrium temperature of ice-to-air heat exchange, $^{\circ}C$
T_w = water temperature below ice, $^{\circ}C$
T_m = melt temperature, $0^{\circ}C$

The ice-to-air coefficient of surface heat exchange, h$_{ai}$, and its equilibrium temperature, T_{ei}, are computed the same as for surface heat exchange in Edinger, et al. (1974) because heat balance of the thin, ice surface water layer is the same as the net rate of surface heat exchange presented previously. The coefficient of water-to-ice exchange, h_{wi}, depends on turbulence and water movement under ice and their effect on melt layer thickness. It is a function of water velocity for rivers but must be empirically adjusted for reservoirs.

Ice temperature in the ice-heat balance is computed by equating the rate of surface heat transfer between ice and air to the rate of heat conduction through ice:

$$h_{ai}(T_i - T_{ei}) = \frac{-k_i(T_i - T_m)}{h}$$

(4-50)

where:

k_i = molecular heat conductivity of ice, *W m^{-1} $^{\circ}C^{-1}$*

When solved for ice temperature, T_i, and inserted in the overall ice-heat balance, the ice thickness relationship becomes:

$$\frac{\rho_i L_f \Delta h}{\Delta t} = \frac{(T_M - T_{ei})}{\frac{h}{k_i} + \frac{1}{h_{ia}}} - h_{wi}(T_w - T_m)$$

(4-51)

from which ice thickness can be computed for each longitudinal segment. Heat from water to ice transferred by the last term is removed in the water temperature transport computations.

Variations in the onset of ice cover and seasonal growth and melt over the waterbody depend on locations and temperatures of inflows and outflows, evaporative wind variations over the ice surface, and effects of

OVERVIEW

water movement on the ice-to-water exchange coefficient. Ice will often form in reservoir branches before forming in the main pool and remain longer due to these effects.

A second, more detailed algorithm for computing ice growth and decay has been developed for the model. The algorithm consists of a series of one-dimensional, quasi steady-state, thermodynamic calculations for each timestep. This algorithm is similar to those of Maykut and Untersteiner (1971), Wake (1977) and Patterson and Hamblin (1988). The detailed algorithm provides a more accurate representation of the upper part of the ice temperature profile resulting in a more accurate calculation of ice surface temperature and rate of ice freezing and melting.

The ice surface temperature, T_s, is iteratively computed at each timestep using the upper boundary condition as follows. Assuming linear thermal gradients and using finite difference approximations, heat fluxes through the ice, q_i, and at the ice-water interface, q_{iw}, are computed. Ice thickness at time t, $\theta(t)$, is determined by ice melt at the air-ice interface, $\Delta\vartheta_{ai}$, and ice growth and melt at the ice-water interface, $\Delta\vartheta_{iw}$. The series of computations for ice cover is presented below.

Initial Ice Formation

Formation of ice requires lowering the surface water temperature to the freezing point by normal surface heat exchange processes. With further heat removal, ice begins to form on the water surface. This is indicated by a negative water surface temperature. The negative water surface temperature is then converted to equivalent ice thickness and equivalent heat is added to the heat source and sink term for water. The computation is done once for each segment beginning with the ice-free period:

$$\theta_0 = \frac{-T_{wn}\rho_w C_{P_w}h}{\rho_i L_f} \tag{4-52}$$

where:

Θ_0 = thickness of initial ice formation during a timestep, m
T_{wn} = local temporary negative water temperature, ^oC
  h = layer thickness, m
  ρ_w = density of water, $kg\ m^{-3}$
  C_{P_w} = specific heat of water, $J\ kg^{-1}\ {}^oC^{-1}$
  ρ_i = density of ice, $kg\ m^{-3}$
  L_f = latent heat of fusion, $J\ kg^{-1}$

Air-Ice Flux Boundary Condition and Ice Surface Temperature Approximation

The ice surface temperature, T_s, must be known to calculate the heat components, H_{br}, H_e, H_c, and the thermal gradient in the ice since the components and gradient all are either explicitly or implicitly a function of T_s. Except during the active thawing season when ice surface temperature is constant at 0ºC, T_s must be computed at each timestep using the upper boundary condition. The approximate value for T_s is obtained by linearizing the ice thickness across the timestep and solving for T_s.

$$T_s^n \approx \frac{\theta^{n-1}}{K_i}[H_{sn}^n + H_{an}^n - H_{br}(T_s^n) - H_e(T_s^n) - H_c(T_s^n)] \tag{4-53}$$

$$H_{sn} + H_{an} - H_{br} - H_e - H_c + q_i = \rho_i L_f \frac{d\theta_{ai}}{dt}, for\, T_s = 0^oC \tag{4-54}$$

$$q_i = K_i \frac{T_f - T_s(t)}{\theta(t)} \qquad \textbf{(4-55)}$$

where:

K_i = thermal conductivity of ice, $W\ m^{-1}\ {}^{\circ}C^{-1}$
T_f = freezing point temperature, ${}^{\circ}C$
n = time level
Θ = thickness of ice, m
q_i = heat flux through ice, $W\ m^{-2}$

Absorbed Solar Radiation by Water Under Ice

Although the amount of penetrated solar radiation is relatively small, it is an important component of the heat budget since it is the only heat source to the water column when ice is present and may contribute significantly to ice melting at the ice-water interface. The amount of solar radiation absorbed by water under the ice cover may be expressed as:

$$H_{ps} = H_s(1 - ALB)(1 - \beta_i)e^{-\gamma_i \theta(t)} \qquad \textbf{(4-56)}$$

where:

H_{ps} = solar radiation absorbed by water under ice cover, $W\ m^{-2}$
H_s = incident solar radiation, $W\ m^{-2}$
ALB_i = ice albedo
β_i = fraction of the incoming solar radiation absorbed in the ice surface
γ_i = ice extinction coefficient, m^{-1}

Ice Melt at Air-Ice Interface

The solution for T_s holds as long as net surface heat exchange, $H_n(T_s)$, remains negative corresponding to surface cooling, and surface melting cannot occur. If $H_n(T_s)$ becomes positive corresponding to a net gain of heat at the surface, q_i must become negative and an equilibrium solution can only exist if $T_s > T_f$. This situation is not possible as melting will occur at the surface before equilibrium is reached (Patterson and Hamblin, 1988). Because of a quasi-steady approximation, heat, which in reality is used to melt ice at the surface, is stored internally producing an unrealistic temperature profile. Stored energy is used for melting at each timestep and since total energy input is the same, net error is small. Stored energy used for melting ice is expressed as:

$$\rho_i C_{p_i} \frac{T_s(t)}{2} \theta(t) = \rho_i L_f \Delta\theta_{ai} \qquad \textbf{(4-57)}$$

where:

C_{pi} = specific heat of ice, $J\ kg^{-1}\ {}^{\circ}C^{-1}$
Θ_{ai} = ice melt at the air-ice interface, m^{-1}

Ice-Water Flux Boundary Condition Formulation

Both ice growth and melt may occur at the ice-water interface. The interface temperature, T_f, is fixed by the water properties. Flux of heat in the ice at the interface therefore depends on T_f and the surface temperature T_s through the heat flux q_i. Independently, heat flux from the water to ice, q_{iw}, depends only on

OVERVIEW

conditions beneath the ice. An imbalance between these fluxes provides a mechanism for freezing or melting. Thus,

$$q_i - q_{iw} = \rho_i L_f \frac{d\theta_{iw}}{dt}$$

(4-58)

where:

Θ_{iw} = ice growth/melt at the ice-water interface

The coefficient of water-to-ice exchange, K_{wi}, depends on turbulence and water movement under the ice and their effect on melt layer thickness. It is known to be a function of water velocity for rivers and streams but must be empirically adjusted for reservoirs. The heat flux at the ice-water interface is:

$$q_{iw} = h_{wi}\big(T_w(t) - T_f\big)$$

(4-59)

where:

T_w = water temperature in the uppermost layer under the ice, $^\circ C$

Finally, ice growth or melt at the ice-water interface is:

$$\Delta\theta_{iw}^n = \frac{1}{\rho_i L_f}\left[K_i \frac{T_f - T_s^n}{\theta^{n-1}} - h_{wi}(T_w^n - T_f)\right]$$

(4-60)

Freezing Temperature of Ice

In general, the temperature at which water freezes, T_f, is set to 0°C for fresh water. If the model is set to SALT [See WTYPEC input], the freezing temperature is affected by the salinity. In the model, when WTYPEC=SALT, the TDS state variable is in units of ppt and the equations used for computing the freezing temperature are computed from the following equations:

For TDS < 35 ppt,
$$T_f = -0.0545TDS$$
(4-61)

For TDS > 35 ppt:
$$T_f = -0.3146 - 0.0417TDS - -0.000166TDS^2$$
(4-62)

Gain and Loss of Water

As ice is formed, water is removed from the waterbody. There is a removal of 0.917 m^3 of water for every 1 m^3 of ice formed. The reverse occurs as ice melts and comes back into the water body. Currently, the model does not account for ablation nor on snow accumulation even though this would be easy to add to the code.

Water is conserved in forming and melting ice from the waterbody. Hence, dissolved substances in the water are concentrated as ice forms. When the ice melts, the model assumes the ice temperature is 0°C and is pure ice with no dissolved constituents. This process is shown below in Figure 60.

Currently snow accretion is not accounted for, nor is sublimation loss; ice is assumed to have no dissolved substances

IceVolume=Existing IceVolume+ Change in ice thickness*DLX*B*0.917 if increasing ice thickness
IceVolume=Existing IceVolume+ (Change in ice thickness/Total ice thickness)* IceVolume*0.917 if decreasing ice thickness

Ice Thickness

ICE

Ice melt water formation=
(Change in ice thickness/Total ice thickness)* IceVolume*0.917/DLT

Ice formation water loss=
(Change in ice thickness*DLX*B*0.917)/DLT

WATER

Note: removal of 0.917 m3 of water for every 1 m3 of ice formed and vice versa

Figure 60. Ice formation and melting water balance.

Overview of Kinetic Source/Sink Term

In order to solve the 2D advection-diffusion equation, the source/sink term, S_Φ, must be specified. The model solves for temperature and a user specified number of water quality variables. Water quality state variables along with their kinetic source/sink terms are shown in **Table 8**. The user can specify any number of generic constituents **[NGC]**, suspended solids groups **[NSS]**, CBOD groups **[NBOD]**, algal groups **[NAL]**, macrophyte groups **[NMC]**, zooplankton groups **[NZP]**, and periphyton/epiphyton groups **[NEP]**.

OVERVIEW

Table 8. CE-QUAL-W2 Water Quality State Variables

Constituent	Internal Source	Internal Sink
Total dissolved solids		
generic constituent, no interactions with other state variables bacteria tracer water age contaminants N_2 gas (Total Dissolved Gas) volatile contaminant	0 and 1st order increase reaeration	settling 0 and 1st order decay gas transfer (volatilization) photodegradation
Inorganic suspended solids		sedimentation
bioavailable P measured as one of the following ortho-P dissolved P SRP	algal/epiphyton respiration labile/refractory particulate/dissolved organic matter sediment release CBOD decay	algal/epiphyton growth adsorption onto inorganic suspended solids
ammonium	sediment release algal/epiphyton/macrophyte excretion labile/refractory dissolved/ particulate organic matter decay CBOD decay	algal/epiphyton/macrophyte growth nitrification
nitrate-nitrite	nitrification	denitrification algal/epiphyton/macrophyte growth
dissolved silica	anoxic sediment release particulate biogenic silica decay	algal/epiphyton growth adsorption onto suspended solids
particulate biogenic silica	algal/epiphyton mortality	settling decay
Iron and Mn	anoxic sediment release	oxic water column settling
labile dissolved organic matter	algal/epiphyton/macrophyte mortality excretion	Decay
refractory dissolved organic matter	labile dissolved organic matter decay	Decay
labile particulate organic matter	algal/epiphyton/macrophyte mortality	settling decay
refractory particulate organic matter	labile particulate organic matter decay	settling decay
Total P in labile dissolved organic matter	algal/epiphyton/macrophyte mortality excretion	Decay
Total P in refractory dissolved organic matter	labile dissolved organic matter decay	Decay
Total P in labile particulate organic matter	algal/epiphyton/macrophyte mortality	settling decay
Total P in refractory particulate organic matter	labile particulate organic matter decay	settling decay
Total N in labile dissolved organic matter	algal/epiphyton/macrophyte mortality excretion	Decay
Total N in refractory dissolved organic matter	labile dissolved organic matter decay	Decay
Total N in labile particulate organic matter	algal/epiphyton/macrophyte mortality	settling decay
Total N in refractory particulate organic matter	labile particulate organic matter decay	settling decay
CBOD		decay, settling
CBOD-P (Total P in organic matter represented by CBOD)		decay, settling
CBOD-N (Total N in organic matter represented by CBOD)		decay, settling

Constituent	Internal Source	Internal Sink
algae	algal growth	respiration excretion mortality settling
algae toxins - intracellular	Internal toxin production	leakage and decay
algae toxins - extracellular	Leakage of intracellular toxin	decay
epiphyton (periphyton)	epiphyton (periphyton) growth	respiration excretion mortality settling
zooplankton	zooplankton growth	transport settling excretion mortality
macrophytes	macrophyte growth	respiration mortality excretion
dissolved oxygen	surface exchange algal/epiphyton (periphyton) growth	surface exchange algal/epiphyton/macrophyte/zooplankton respiration nitrification CBOD decay 0 and 1st order SOD labile/refractory dissolved/ particulate organic matter decay
total inorganic carbon	labile/refractory dissolved/ particulate organic matter decay sediment release surface exchange algal respiration	surface exchange algal/epiphyton (periphyton) growth CBOD decay
alkalinity		[dynamic alkalinity can also be computed based on biological reactions otherwise it is treated as conservative]
methane	sediment diagenesis	Surface exchange
hydrogen sulfide	sediment diagenesis	Surface exchange
Mature fine tailings (about 70% water and 30% fine clay – can take centuries to consolidate; from oil sands mining operation; another inorganic suspended solids group)		consolidation
sediment (1st order sediment model)	settling of algae, LPOM, RPOM, epiphyton burial	decay, focusing of sediments
sediment diagenesis model with state variables in the sediment	Organic matter settling to the sediment and sediment diagenesis	Release to overlying water (C, N, P)

In addition to these water quality state variables, the model also solves for pH and the carbonate cycle (CO_2, HCO_3, H_2CO_3) as part of the set of derived water quality variables.

The constituent transport relationships described in this section of the User's Manual document the transport of constituents with their kinetic reaction rates expressed in source and sink terms. All sources/sinks (both internal and external) for water temperature are contained in the internal code array [TSS]. The sources/sinks for constituents are separated into two arrays, [CSSB] and [CSSK]. [CSSB] contains boundary sources/sinks. [CSSK] contains internal sources/sinks due to kinetic interactions. The division of terms allows kinetic sources/sinks to be updated at different frequencies than boundary sources/sinks -

consistent with coarser time scales associated with biological and chemical processes as opposed to hydro-dynamics. Computational time is also reduced. The frequency at which kinetic sources/sinks [CSSK] are updated is specified by the parameter **[CUF]**.

The source/sink term [CSSK] represents a mass rate of change (model code internal units of *grams m^{-3} sec^{-1}*) of a constituent due to kinetic reactions where concentrations are expressed as *grams meter^{-3}* or mg/l. All of the rate terms in the following discussion are in units of *sec^{-1}* since these are the units used in the code. However, all rate units input into the model from the control file are in units of *day^{-1}* and are then converted to *sec^{-1}* before being used in the code.

Generic Constituent

Any number of generic constituents **[NGC]** can be defined that can settle, decay (using either zero order and/or first order decay and/or photochemical reactions), transfer across the air/water interface, and/or be released from the sediment during anoxic conditions (just for the zero order SOD model). The user sup-plies a zero and/or 1st order decay coefficient with or without an Arrhenius temperature dependence func-tion, and/or a settling velocity and/or a photodegradation coefficient and/or coefficients for volatilization. Gas transfer (or volatilization) requires setting the reaeration coefficient (by making it a fraction of the dis-solved oxygen gas transfer rate) and a saturated gas concentration. Generic constituents do not interact with the hydrodynamics nor any other water quality state variables.
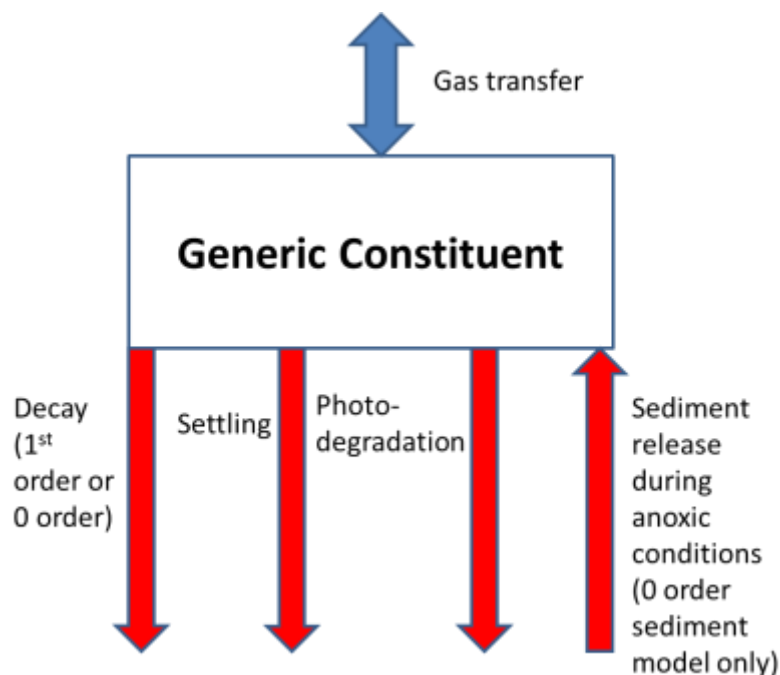
Figure 61. Internal flux for generic constituent compartment.

Referring to Figure 61, the source/sink term for a generic constituent is:

$$S_g = -K_0\theta^{(T-20)} - K_1\theta^{(T-20)}\Phi_g - \omega_g \frac{\partial \Phi_g}{\partial z} - \alpha I_o(1-\beta)e^{-\lambda z}\Phi_g + \frac{A_{sur}}{V_{sur}}K_L(\Phi_s - \Phi_g) +$$

$$K_{sedrel}SOD\frac{A}{V} \qquad\qquad \textbf{(4-63)}$$

where:

   Θ_g = temperature rate multiplier
   T = water temperature, $^{\circ}C$
   α = photodegradation parameter, m^2/J
   I_o = radiation at surface, W/m^2
   λ = light extinction coefficient, m^{-1}
   β = fraction of short wave solar absorbed on the surface
   ω_g = settling velocity, $m\ s^{-1}$
   K_0 = zero order decay coefficient, $g\ m^{-3}\ s^{-1}$ at $20^{\circ}C$
   K_1 = first order decay coefficient, s^{-1} at $20^{\circ}C$
   Φ_g = generic constituent concentration, $g\ m^{-3}$
   Φ_s = generic constituent concentration gas saturation in the atmosphere, $g\ m^{-3}$
   A_{sur} = surface area, m^2
   V_{sur} = surface volume, m^3
   A = cell bottom surface area, m^2
   V = cell volume, m^3
   K_L = surface gas transfer coefficient, m/s
   K_{sedrel} = sediment release as a fraction of SOD (zero order model), (-)
   SOD = temperature corrected sediment oxygen demand (zero order model), m/s

Photodegradation can be an important mechanism for constituents such as fecal coliforms (Mitchell and Chamberlain, 1978; Auer and Niehaus, 1993) and for dissolved organic matter (Moran and Zepp, 1996; Reche et al., 1999). The photo decay rate can be modeled as a pseudo 1st order decay (k_{light}) rate, as described by

$$\frac{\delta C}{dt} = -k_{light} \times C$$

Where k_{light} is the first-order decay coefficient (sec^{-1}) and C is the constituent concentration (g/m^3). Chamberlin and Mitchell (1978) defined the light induced decay of coliforms based on Beer's Law and a proportionality constant as

$$k_{light} = \propto I_0 e^{-\lambda z}$$

Where α is the user defined proportionality constant for the effect of incident light on a specific constituent or organism in the case of fecal coliforms (cm^2/cal), I$_0$ is the incident light energy at the water surface (cal/cm^2-day), λ is the light attenuation coefficient per unit depth (m^{-1}) and z is the depth below the water surface (m). Table 9 shows a selection of α values reported in the literature for coliforms (Bowie et al., 1985). The CE-QUAL-W2 model uses units of W/m^2 for radiation, hence the corresponding units of alpha as used in the CE-QUAL-W2 model are m^2/J.

Table 9. Comparison of α estimates based on Chamberlin and Mitchell (1978) with additional values (Bowie et al., 1985)

Organism	Study	α (cm²/cal)	α (m²/J)	Data Source
Coliform Group	14 field studies (mean)	0.481	1.15E-05	Gameson and Gould (1975)

Organism	Study	α (cm²/cal)	α (m²/J)	Data Source
Coliform Group	24 field studies (mean)	0.168	4.01E-06	Foxworthy and Kneeling (1969)
Coliform Group	61 laboratory studies (mean)	0.136	3.25E-06	Gameson and Gould (1975)
Fecal Coliform	Estimated from field and laboratory studies (mean of salt and freshwater)	0.042	1.00E-06	Mancini (1978)
Fecal Coliforms	22 chamber studies in freshwater (mean)	0.005	1.19E-07	Lantrip (1983)
Total Coliforms	22 chamber studies in freshwater (mean)	0.004	9.55E-08	Lantrip (1983)

A conservative tracer, coliform bacteria, N_2 gas (and Total Dissolved Gas), a volatile generic constituent, and water age are some of the state variables that can be modeled using the generic constituent and are described further below.

Conservative Tracer

A conservative constituent is included to allow dye study simulations, movements of conservative materials through the waterbody, and as an aid in calibrating and testing flow regimes. As a conservative material, this constituent has no internal sources or sinks and the rate term [CSSK] is set to zero.

$$S_{tracer} = 0 \qquad\qquad\qquad \textbf{(4-64)}$$

Volatile Generic Constituent

The loss of a volatile generic constituent, such as a hydrocarbon, by volatilization from the water surface is simulated using the same algorithms as used for N_2.

The rate at which a generic constituent molecule enters and leaves the water surface is described by

$$S_{vol} = \frac{A_{sur}}{Vol_{cell}} K_{Lg}\left(\phi_{sg} - \phi_g\right) = \frac{1}{h_{KT}} K_{Lg}\left(\phi_{sg} - \phi_g\right)$$

where:
K_{Lg} = the surface gas transfer coefficient for a generic constituent (m/s)
A_{sur} = the surface area of the surface layer computational cell (m2)
Vol_{cell} = the volume of the surface layer computational cell (m3)
h_{KT} = depth of the surface layer (K=KT) computational cell (m)
ϕ_g = the liquid phase generic constituent concentration (g/m³)
ϕ_{sg} = the hypothetical saturation liquid phase generic constituent concentration if in equilibrium with the gas concentration (g/m³) based on the gas phase concentration and the Henry's law constant.

The gas transfer rate coefficient (K_{Lg}) is an overall gas transfer rate coefficient, reflecting the composite effect of the individual gas transfer rate constants in both interfacial liquid and gas zones and of Henry's law constant. The gas transfer rate of a generic constituent at the water surface can be estimated based on the reaeration rate for oxygen, as calculated using

$$K_{Lg} = K_{LO2}\sqrt{(\frac{D_g}{D_{O2}})}$$

where K_{LO2} is the reaeration coefficient for oxygen (m/s), D_g is the molecular diffusion coefficient for a generic constituent, and D_{O2} is the molecular diffusion coefficient for oxygen. The molecular diffusion coefficients can be related to their molecular weights as described by

$$\frac{D_g}{D_{O2}} = \sqrt{\frac{MW_{O2}}{MW_g}}$$

The above 2 equations can be combined to generalize the reaeration coefficient for any generic constituent based on its molecular weight and the reaeration coefficient for oxygen:

$$K_{Lg} = K_{LO2}(\frac{MW_{O2}}{MW_g})^{0.25} = K_{LO2} \times CGKLF$$

where CGKLF is the unitless user defined gas transfer factor that indicates the fraction of the surface reparation coefficient, K_{LO2}, for dissolved oxygen gas transfer, as calculated in

$$(\frac{MW_{O2}}{MW_g})^{0.25} = CGKLF$$

Therefore, the only values required to estimate hydrocarbon volatilization are the molecular weights of oxygen and the generic constituent of interest as well as the reaeration coefficient for oxygen, which is internally calculated in the gas transfer subroutine.

CGKLF values for common hydrocarbons as well as for nitrogen and carbon dioxide are shown in Table 10. The values are calculated based on their respective molecular weights and the molecular weight of oxygen (32.00 g/mol).

Table 10. CGKLF input values for hydrocarbons, CO_2, and N_2.

Chemical	MW (g/mole)	CGKLF
Nitrogen	28.01	1.034
Carbon Dioxide	44	0.923
Benzene	78.11	0.800
MTBE	88.15	0.776
Toluene	92.13	0.768
Ethylbenzene	106.16	0.741

For a volatile hydrocarbon, it can often be assumed that the saturation liquid phase concentration ($\phi'g$) is negligible, since there is no significant concentration of the hydrocarbon in the gas phase (atmosphere). Therefore the modified source/sink equation for a volatile generic constituent that includes volatilization from the top layer (water surface) along with possible zero and first order decay is described by

$$S_{gVol} = -k_0\theta_g^{(T-20)} - k_1\theta_g^{(T-20)}\phi_g - \frac{1}{h_{KT}}K_{LO2}CGKLF\phi_g$$

Where S_{gVol} is the source/sink term for the volatile generic constituent concentration ($gm^{-3}s^{-1}$), ϕ_g is the volatile generic constituent concentration (g/m^3), and other terms are as defined previously.

Bacteria with decay and photodegradation

Coliform bacteria are commonly used as an indicator of pathogen contamination. Safety standards and criteria for drinking and recreational purposes are based upon coliform concentrations. Predictions of coliform bacteria are important because of their impact on recreation and water supply.
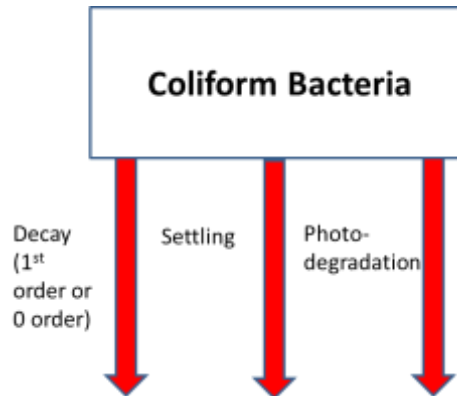
Figure 62. Internal flux for coliform bacteria.

Total coliform, fecal coliform, fecal streptococci, and/or any other type of bacteria that do not interact with other state variables can be simulated. Referring to Figure 62, the rate equation for bacteria is (including photodegradation):

$$S_g = -K_{col}\theta^{(T-20)}\Phi_{col} \underbrace{-\omega_{col}\frac{\partial \Phi_{col}}{\partial z}}_{\text{settling}} \underbrace{-\alpha I_o(1-\beta)e^{-\lambda z}\Phi_{col}}_{\text{photodegradation}}$$

$\underbrace{\phantom{-K_{col}\theta^{(T-20)}\Phi_{col}}}_{\text{1st-order decay}}$

(4-65)

where:

Θ = temperature factor (Q10)
T = water temperature, ^{o}C
K_{col} = coliform mortality rate, sec^{-1} at $20^{o}C$
Φ_{col} = coliform concentration, $g\ m^{-3}$
ω_{col} = bacteria settling velocity, $m\ s^{-1}$
α = photodegradation parameter, m^2/J
I_o = radiation at surface, W/m^2
λ = light extinction coefficient, m^{-1}
β = fraction of short wave solar absorbed on the surface
z = water depth, m

The Q_{10} formulation arises from a doubling of the reaction rate with each 10ºC increase in temperature. This doubling rate has not been found at lower temperatures (Hargrave 1972) and is quite variable for various reactions (Giese 1968). Modeling coliform bacteria is discussed in detail in Zison, et al. (1978).

N₂ dissolved gas and TDG

N₂ gas is a state variable and is modeled by internally computing the N2 gas saturation as a function of temperature and air humidity and internally computing the gas transfer coefficient (for reaeration). The sink term is just gas transfer as shown in Figure 63 and is

$$S_{N2} = \frac{A_{sur}}{V_{sur}} K_{LN2}(\Phi_{sN2} - \Phi_{N2})$$ (4-66)

where:

Φ_{N2} = N2 generic constituent concentration, $g\ m^{-3}$

Φ_{sN2} = N2 gas saturation concentration in the atmosphere, $g\ m^{-3}$

A_{sur} = surface area, m^2

V_{sur} = surface volume, m^3

K_{LN2} = surface gas transfer coefficient for N₂, m/s

Nitrogen gas is a slightly soluble gas, like oxygen. Its gas transfer characteristics are also like oxygen in being controlled by turbulence on the liquid film (Chapra, 1997).

The value of K_{LN2} can be determined from the reaeration formulae presented in the preceding section. The basic physics of gas transfer are the same for N_2 and O_2 since they are both liquid-controlled gases. Using the Higbie-Penetration theory (Chapra, 1997),

$$K_{LN2} = K_{LO2}\sqrt{\frac{D_{N2}}{D_{O2}}}$$

where D_{N2} and D_{O2} are the molecular diffusion coefficients for oxygen and nitrogen, respectively. Using the relationship that

$$\frac{D_{N2}}{D_{O2}} = \sqrt{\frac{MW_{O2}}{MW_{N2}}}$$

$$K_{LN2} = K_{LO2}\left(\frac{MW_{O2}}{MW_{N2}}\right)^{0.25} = 1.034 K_{LO2}$$

where MW is the molecular weight and MW_{O2}=32 g/mole and MW_{N2}=28 g/mole.
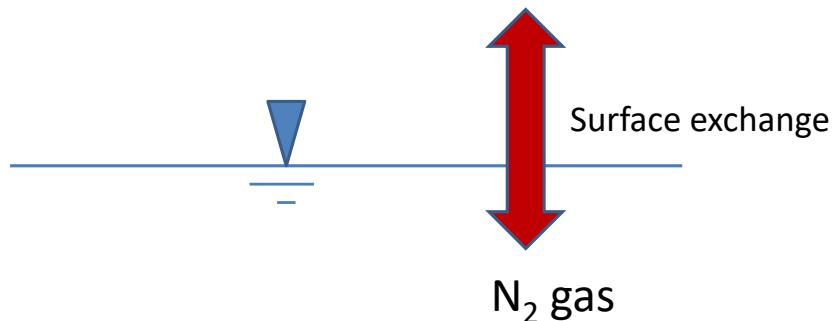
Figure 63. N₂ gas exchange.

The value of N₂ saturation, Φ_{sN2}, is determined using Henry's Law. Henry's Law can be written as

$$x_{N2} = K_H P_{N2}$$

where X_{N2} is the mole fraction of Nitrogen gas, K_H is Henry's Law constant in moles/atm and P_{N2} is the partial pressure of N_2 gas in the atmosphere in atm. Nitrogen gas is assumed to be 79% of the total gas composition in the atmosphere for dry air. Also, in order to account for atmospheric pressure changes with altitude, the following relationship is used in CE-QUAL-W2 to correct the atmospheric pressure:

$$P(atm) = \left[1 - \frac{Altitude, km}{44.3}\right]^{5.25}$$

where altitude is the altitude of the water body in km. Since atmospheric pressure is not an input variable to CE-QUAL-W2 (except when using the SYSTDG algorithm for TDG generation at hydropower facilities – see under **Dissolved Oxygen/Dam Reaeration**), the atmospheric pressure is assumed to be 1 atm at sea level.

The mole fraction of N_2 gas is related to the mass concentration as follows:

$$x_{N2} = \frac{n_{N2}}{n_{H2O} + n_{N2} + \dots}$$

where n_{N2} is the number of moles of N_2, n_{H2O} is the number of moles of water (the dominant term). Neglecting all terms in the denominator except n_{H2O}, which is 55.6 moles/liter (=1000 g/18 g/mole), then the concentration of N_2 is C_{N2}:

$$C_{N2} = n_{N2} \frac{28g}{mole} \frac{10^3 mg}{g}$$

Combining the last 2 equations with Henry's Law, we obtain

$$C_{N2} = 55.6 * 28 * 10^3 P_{N2} K_H = 1.5568E6 P_{N2} K_H$$

The Henry's Law constant is temperature dependent. Using the data of K_H versus temperature in Tchobanoglous and Schroeder (1987),

$K_H(atm^{-1})= 1.8816E-005 - 4.116E-007 * T + 4.6E-009 * T^2$

where T is the surface temperature in $^\circ$C. This relationship is shown in Figure 64.
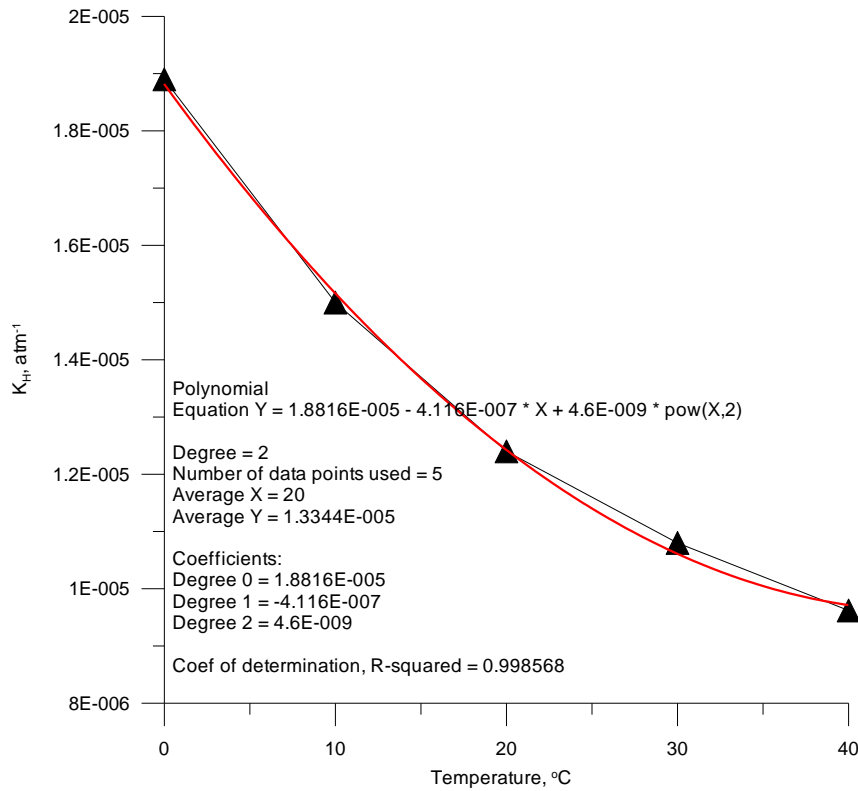
Figure 64. Henry's Law constant dependence on temperature.

The %N_2 in the atmosphere needs to be corrected for water vapor in the atmosphere. The 79% N_2 is based on dry air. The total pressure of dry air can be determined by taking the total atmospheric pressure minus the contribution of water vapor.

The vapor pressure is computed using the air temperature in ^oC as (Chapra, 1997)

$$P_{watervapor}(mmHg) = 4.596 \, exp\left(\frac{17.27T}{237.3 + T}\right)$$

Then $P_{watervapor}$ is converted to atm by multiplying by the conversion factor 0.00136. Since this pressure is at saturation or at 100% humidity, the actual $P_{watervapor}$ is then multiplied by the relative humidity fraction. Since the CE-QUAL-W2 model does not use relative humidity, the relative humidity (RH) was computed based on dew point temperature, T_d, and air temperature, T: (Singh, 1992)

$$RH = \left[\frac{112 - 0.1T + T_d}{112 + 0.9T}\right]^8$$

where all temperatures are in ^oC.

Figure 65 shows the $P_{watervapor}$ as a function of air temperature and relative humidity.
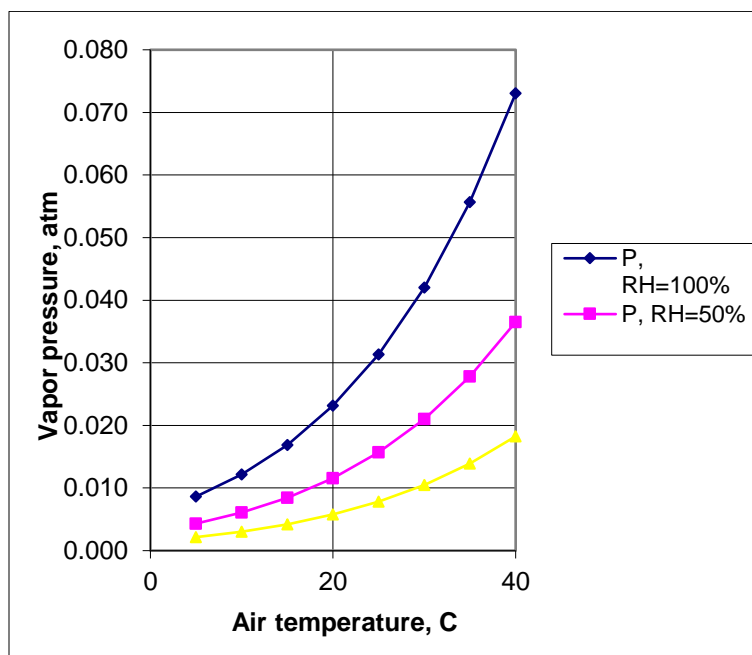
Figure 65. Vapor pressure as a function of air temperature and relative humidity.

The %N_2 is then 0.79(1-RH*$P_{watervapor}$). The term (1-RH*$P_{watervapor}$) is shown in Figure 66 as a function of air temperature and relative humidity.

Also, the increase of salinity can affect the N_2 saturation value. This may be important for estuaries, but this effect is not included in the model at this time. The higher the salinity, the less amount of N_2 the water can hold.

Once N_2 gas is used in the model, the derived constituent TDG% can also turned ON and used in the any derived constituent output. TDG, % is computed from

$$TDG, \% = \left(\frac{0.79 * N2 \; concentration}{N2 \; saturation \; concentration} + \frac{0.21 * O2 \; concentration}{O2 \; saturation \; concentration} \right) 100$$

N_2 gas can be entrained at hydropower facilities and at dams. Algorithms for adding dissolved gas at these facilities is outlined under **Dissolved Oxygen/Dam Reaeration**.
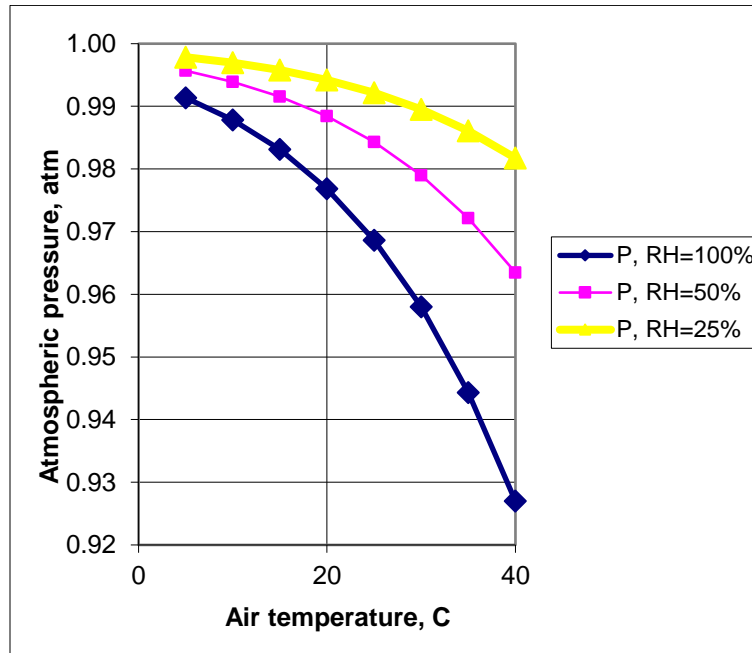
Figure 66. Atmospheric pressure correction as a result of vapor pressure correction assuming original atmospheric pressure is 1 atm.

Water Age or Residence time

The water age is used to compute how long water has remained in the modeled domain. This is accomplished by using only a zero-order decay rate set to –1 day^{-1}. This results in a state variable that increases by 1 day^{-1}, which is an exact representation of water age or hydraulic residence time. This is a very useful state variable when looking at hydrodynamics.

$$S_{age} = -1 \; day^{-1}$$ **(4-67)**

An example of water age for a reservoir in Washington, USA is shown Figure 67, where new water comes in the main inflow but acts as an interflow through the reservoir.
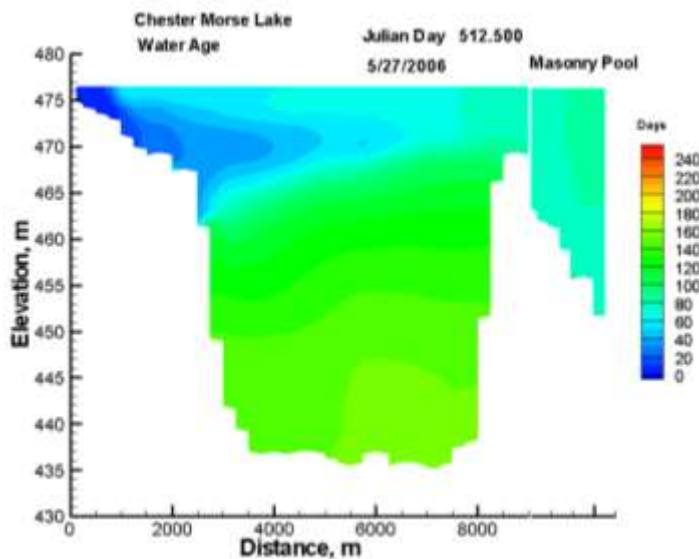
Figure 67. Water age in Chester Morse Lake, WA.

Dissolved Gas Pressure

The model computes dissolved gas pressure (DGP in atm) which is used to compute Total Dissolved Gas (TDG) from TDG=100*DGP/PALT where PALT is the atmospheric pressure in atm at the water surface. The sources of the dissolved gas include hydraulic structures or transport and the sinks of dissolved gas are transport and reaeration. This state variable can be used in lieu of using dissolved oxygen and dissolved nitrogen gas as state variables if the model user is only interested in modeling production of dissolved gas at spillways and the gas transfer downstream. If the model user is using dissolved oxygen and nitrogen, then this variable should not be used to compute TDG.

The DGP exchange at the air-water interface is modeled as a first order rate process.

$$\frac{dDGP}{dt} = -k_{DGP}(DGP - P_{atm})$$

where
DGP = dissolved gas pressure, atm
P_{atm} = barometric pressure, atm
k_{DGP}= air/water gas exchange rate, d^{-1}.

Air/water gas exchange rate for DGP for lakes or estuaries is calculated by:

$$k_{DGP} = DGPO2\frac{K_L}{H}$$

where K_L is the reaeration coefficient in m/d, H is the depth of the surface layer in m, and DGPO2 is the ratio of dissolved gas to oxygen surface transfer ratio. Computations of K_L are shown in **Lake Reaeration Equations**. A typical value of DGPKL would be 1.027 assuming 0.21 O_2 and 0.79 N_2 gas composition.

In SYSTDG model, air/water gas exchange rate for DGP is a function of the wind speed or user defined constant exchange coefficient, whichever is largest. Therefore, k_{DGP} is corrected by:

$$k_{DGP} = max(k_{DGP}, MINKL)$$

MINKL is the minimum air/water gas exchange rate for DGP, m d^{-1}.

Besides calculating the TDG through simulating N2 and DO, The TDG saturation can also calculated from normalizing the DGP by the local barometric pressure, P_{atm}.

$$TDG\% = 100\frac{DGP}{P_{atm}}$$

Water Column CH$_4$, H$_2$S, SO$_4$

Methane (CH$_4$) and hydrogen sulfide (H$_2$S) constituents are state variables for the water column. CH$_4$ is modeled as mg/l as C. H2S is modeled as mg/l as S. For both constituents, the anaerobic release from the sediments, aerobic decay, and reaeration were modeled (Figure 68 and Figure 69).
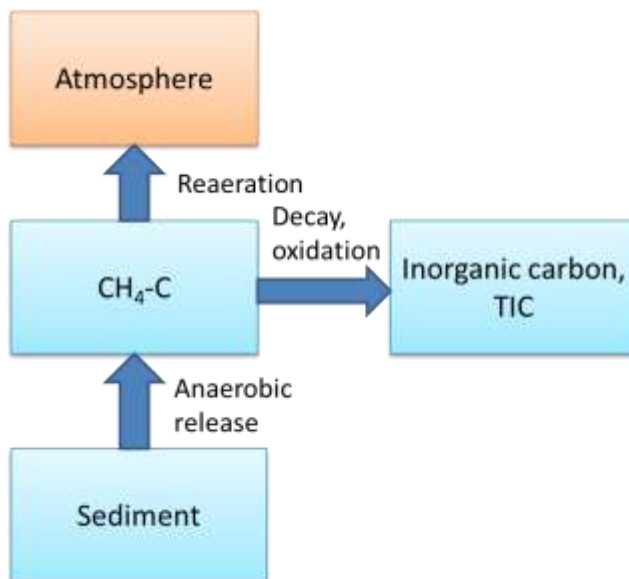
Figure 68. Sources and sinks for methane.
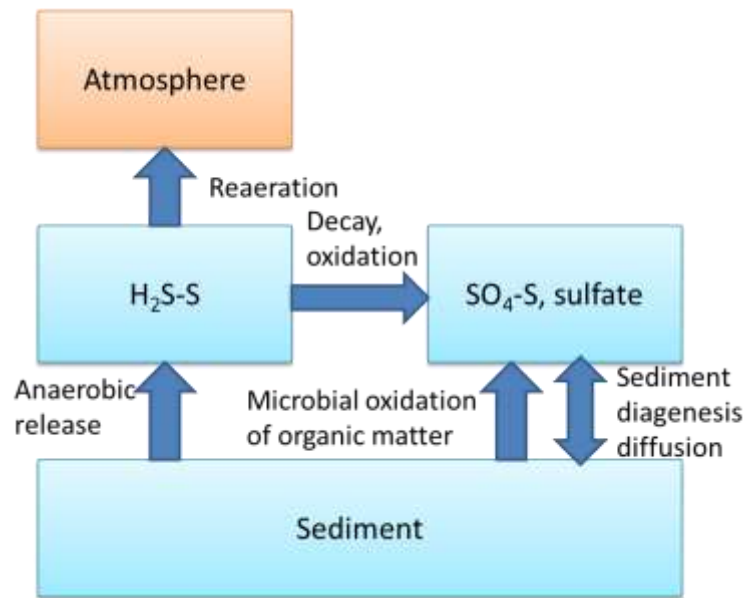
Figure 69. Sources and sinks for hydrogen sulfide and sulfate.

The rate equations for methane and hydrogen sulfide were identical, except for different parameter values and assuming saturation values in the atmosphere of 0 mg/l for both gases:

$$S = SOD\gamma_{OM}\delta_{SODR}\underbrace{\frac{A_{sed}}{V}}_{\text{0-order sediment release}} + \underbrace{A_{sur}K_L(-\Phi)}_{\text{reaeration}} - \underbrace{\Theta^{T-20}K\Phi_C}_{\text{decay}}$$

where:

A_{sed} = sediment surface area, m^2

A_{sur} = surface area of surface computational cell, m^2

SOD = zero-order sediment oxygen demand, $g\ m^{-2}\ sec^{-1}$

K_L = interfacial exchange rate, $m\ sec^{-1}$

γ_{OM} = organic matter temperature rate multiplier

δ_{SODR} = sediment release rate of H₂S or CH₄, fraction of zero-order SOD

Φ = constituent concentration (H₂S or CH₄), $g\ m^{-3}$

Θ = temperature rate multiplier

T = temperature, $°C$

K = decay rate, sec^{-1}

When the sediment diagenesis model is active, the release rates of CH4 and H2S are computed directly from this model rather than using the zero-order SOD model. The specification of TIC sources and sinks is detailed in the section on Total inorganic carbon. Specification of the SO4 release from sediments is specified as a fraction of the zero-order sediment oxygen demand or if the sediment diagenesis module is active is computed directly from pore water release and diffusion into or out from the sediments.

The basic physics of gas transfer are the same for H₂S, CH₄ and O₂. Using the penetration theory for gas transfer, i.e., $K_a = 2\sqrt{\frac{Df}{\pi}}\frac{1}{h}$ where f is the turbulence frequency of surface renewal, D is the molecular diffusion coefficient for O₂ and h is the depth, once the reaeration coefficient for dissolved oxygen is determined, then the value of the reaeration coefficient k_{H2S} for H₂S is determined from the following equation (Thibodeaux, 1996):

$$k_{H2S} = k_{O2} \sqrt{\frac{D_{H2S}}{D_{O2}}}$$

Using

$$\frac{D_A}{D_B} = \sqrt{\frac{MW_B}{MW_A}}$$ where MW is the molecular weight of the component

then

$$k_{H2S} = k_{O2} \left(\frac{MW_{O2}}{MW_{H2S}}\right)^{0.25}.$$

Given the molecular weights of oxygen and hydrogen sulfide:

MW_{O2}=32.00 g/mol
MW_{H2S}=34.08 g/mol
the reaeration coefficient for hydrogen sulfide is:

$$k_{H2S} = k_{O2} \left(\frac{MW_{O2}}{MW_{H2S}}\right)^{0.25} = k_{O2} \times 0.984$$

Similarly, the reaeration coefficient for methane is:
MW_{CH4}=16.04 g/mol
The reaeration coefficient k_{CH4} is:

$$k_{CH4} = k_{O2} \left(\frac{MW_{O2}}{MW_{CH4}}\right)^{0.25} = k_{O2} \times 1.188$$

Water Column Fe(II), FeOOH, Mn(II), and MnO2

The state variables of Fe and Mn in the water column are Fe(II), FeOOH, Mn(II), and MnO_2. These interact with the sediments in the sediment diagenesis model. In the water column the processes active are shown in Figure 70 for Fe and Figure 71 for Mn.
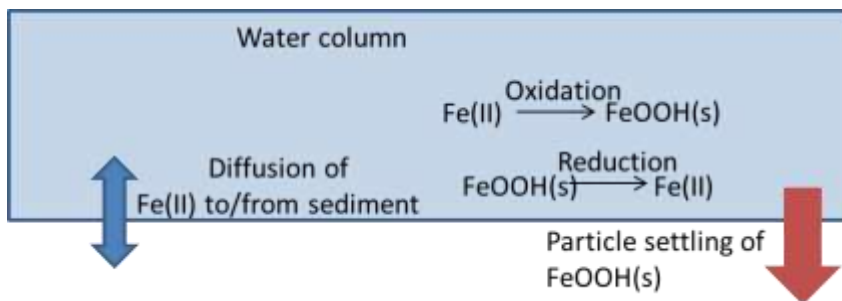
Figure 70. Sources and sinks of Fe in the water column.
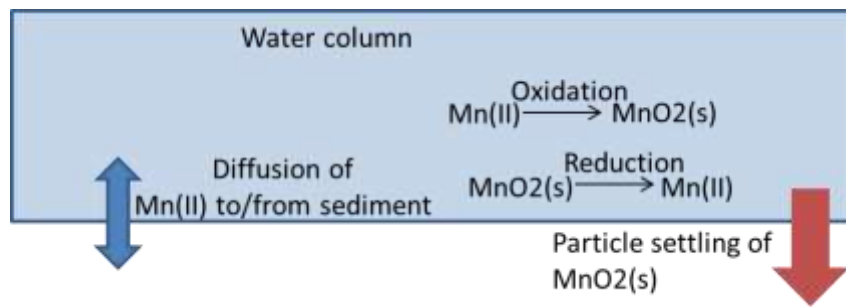
Figure 71. Sources and sinks of Mn in the water column.

Inorganic Suspended Solids

Inorganic suspended solids [ISS] are important in water quality simulations because of their influence on density, light penetration, and nutrient availability. Increased solids concentrations reduce light penetration in the water column thus affecting temperature that in turn affects biological and chemical reaction rates. Dissolved phosphorus and silica concentrations can also be affected by solids through sorption and settling. Light and nutrient availability largely control algal production.

The settling velocity of each inorganic suspended solids compartment is a user-defined parameter. Usually this is determined from Stokes' settling velocity for a particular sediment diameter and specific gravity. Any number of inorganic suspended solids groups can be modeled.
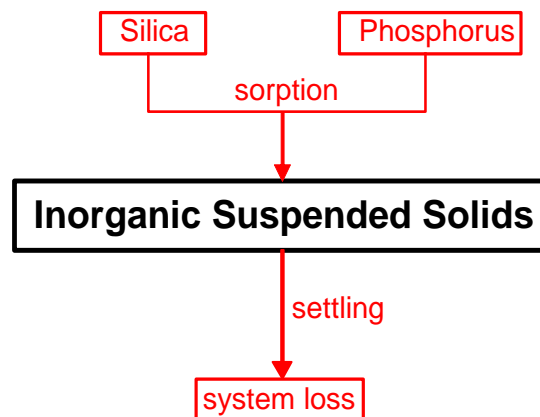
Figure 72. Internal flux for inorganic suspended solids.

Referring to **Figure 72**, the rate equation for inorganic suspended solids is:

$$S_{ISS} = \omega_{ISS} \frac{\partial \Phi_{ISS}}{\partial z} \qquad\qquad \textbf{(4-68)}$$

where:

    z = layer thickness, m
  ω_{ISS} = settling velocity, $m\ sec^{-1}$
  Φ_{ISS} = inorganic suspended solids concentration, $g\ m^{-3}$

In the finite difference representation of suspended solids concentrations, solids settling from layer [K]-1 serve as a source for the layer below it [K]. Lateral averaging results in homogeneous solids concentrations laterally. Concentrations of suspended solids, though, generally decrease with distance away from the dominant flow path, and this effect is not included in the model. The rate term for inorganic suspended solids is evaluated in the subroutine SUSPENDED_SOLIDS.

In the sediment diagenesis model for Version 4.22 and earlier, there was a group for Mature Fine Tailings that was added as a generic constituent. The current model now sets this state variable as a suspended solids group.

Total Dissolved Solids or Salinity

Total dissolved solids (TDS) affect water density and ionic strength, thereby affecting water movements, pH, and the distribution of carbonate species. Dissolved solids are normally expressed as TDS in freshwater applications. Estuarine applications normally use salinity. Either TDS or salinity can be used with the choice indicated by the parameter [WTYPEC] specified in the control file. The choice is then reflected in the computation of density and ionic strength. If TDS is used, the units are $g\ m^{-3}$, while salinity is $kg\ m^{-3}$. It is important to keep in mind that TDS and salinity are not necessarily equivalent. In the model, both are treated conservatively with the rate term set to zero.

Labile DOM

Because of the importance of dissolved oxygen in aquatic systems, all constituents exerting an oxygen demand must be included in kinetic formulations. This demand is often measured in rivers as the biochemical oxygen demand (BOD), which includes microbial respiration and metabolism of various organic and inorganic compounds. However, production of these materials occurs as well as decomposition, requiring the major components of BOD be modeled individually. One of these constituents is dissolved organic matter (DOM), which is composed of labile and refractory components. DOM is modeled as two separate compartments because of the different decomposition rates of the two groups.
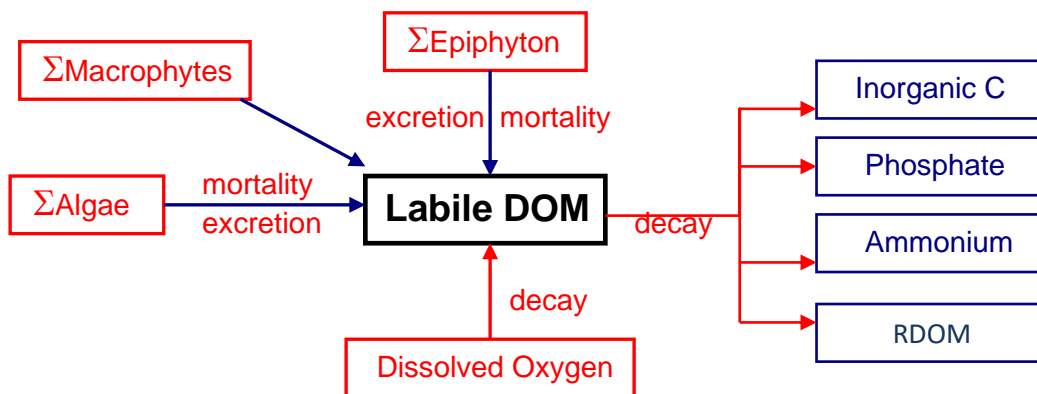
Figure 73. Internal flux between labile DOM and other compartments

Referring to Figure 73, the rate equation for labile DOM is:

$$S_{LDOM} = \underbrace{\sum K_{ae}\Phi_a}_{\text{algal excretion}} + \underbrace{\sum (1 - P_{am})K_{am}\Phi_a}_{\text{algal mortality}} + \underbrace{\sum K_{ee}\Phi_e}_{\text{epiphyton excretion}}$$

$$+ \underbrace{\sum (1 - P_{em})K_{em}\Phi_e}_{\text{epiphyton mortality}} - \underbrace{\gamma_{OM}K_{LDOM}\Phi_{LDOM}}_{\text{labiole DOM decay}} - \underbrace{K_{L \to R}\Phi_{LDOM}}_{\substack{\text{labile to refractory} \\ \text{DOM decay}}} + \underbrace{\sum (1 - P_{mm})K_{mm}\Phi_{macro}}_{\text{macrophyte mortality/excretion}}$$

(4-69)

where:

P_{am} = pattern coefficient for algal mortality
P_{em} = pattern coefficient for epiphyton mortality
P_{mm} = partitioning coefficient for macrophyte mortality
γ_{OM} = temperature rate multiplier for organic matter decay
K_{ae} = algal excretion rate, sec^{-1}
K_{am} = algal mortality rate, sec^{-1}
K_{ee} = epiphyton excretion rate, sec^{-1}
K_{em} = epiphyton mortality rate, sec^{-1}
K_{mm} = macrophyte mortality rate, sec^{-1}
K_{LDOM} = labile DOM decay rate, sec^{-1}
$K_{L \to R}$ = labile to refractory DOM transfer rate, sec^{-1}
Φ_a = algal concentration, $g\ m^{-3}$
Φ_e = epiphyton concentration, $g\ m^{-3}$
Φ_{LDOM} = labile DOM concentration, $g\ m^{-3}$
Φ_{macro} = marophyte concentration, $g\ m^{-3}$

Refractory DOM

Refractory DOM is composed of compounds in the aquatic environment that slowly decompose exerting oxygen demand over long periods. Internally, refractory DOM is produced from the decomposition of labile DOM.
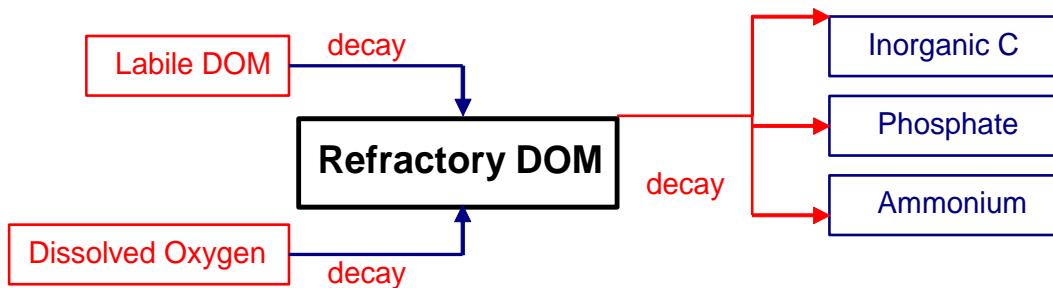
Figure 74. Internal flux between refractory DOM and other compartments.

Referring to **Figure 74**, the rate equation for refractory DOM is:

$$S_{RDOM} = \underbrace{K_{L \to R}\Phi_{LDOM}}_{\substack{\text{labile to refractory} \\ \text{DOM decay}}} - \underbrace{\gamma_{OM}K_{RDOM}\Phi_{RDOM}}_{\text{decay}}$$ **(4-70)**

where:

γ_{OM} = temperature rate multiplier

K_{RDOM} = refractory DOM decay rate, sec^{-1}

$K_{L\square R}$ = transfer rate from labile DOM, sec^{-1}

Φ_{LDOM} = labile DOM concentration, $g\ m^{-3}$

Φ_{RDOM} = refractory DOM concentration, $g\ m^{-3}$

and the rate terms are evaluated in subroutine REFRACTORY_DOM.

Labile Particulate Organic Matter

Labile particulate organic matter (LPOM) represents particulate organic material in the water column. When decaying, particulate organic matter is a source of refractory particulate organic matter, nitrogen, phosphorus, and inorganic carbon. A stoichiometric relationship is used for mineralization of ammonium, phosphorus, and inorganic carbon, and an oxygen demand is exerted as LPOM decomposes. When LPOM settles to the bottom, it accumulates and decays in the sediment compartment or the sediment diagenesis compartment if they are activated for the simulation.
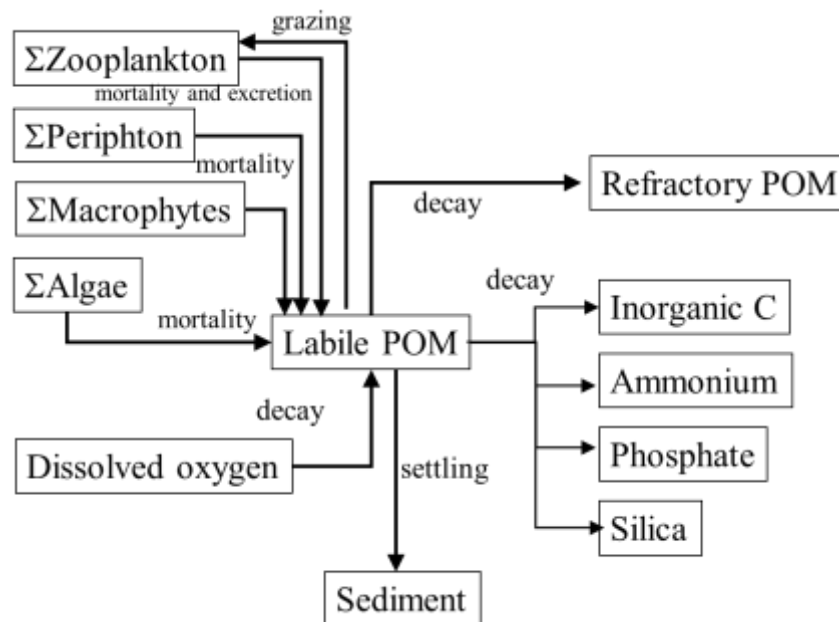
Figure 75. Internal flux between Labile POM and other compartments.

Referring to **Figure 75**, the rate equation for LPOM is:

$$S_{LPOM} = \sum P_{am}\underbrace{K_{am}}\Phi_a + \sum P_{em}\underbrace{K_{em}}\Phi_e - K_{LPOM}\gamma_{OM}\Phi_{LPOM}$$

<div align="center">algal mortality   epiphyton mortality   decay</div>

$$- K_{L\to R}\underbrace{\Phi_{LPOM}} - \omega_{POM}\frac{\partial \Phi_{LPOM}}{\partial z} + \sum P_{mm}\underbrace{K_{mm}}\Phi_{macro} + \sum \underbrace{K_{zm}}\Phi_{zoo} +$$

<div align="center">labile to refractory   settling   macrophyte mortality   zooplankton mortality
POM decay</div>

$$\sum K_{zg}(1 - \underbrace{Z_{effic}})\Phi_{zoo} - \sum K_{zg}\left(\frac{\sigma_{pom}}{\sum\sigma_{zoo}\Phi_{zoo} + \sum\sigma_{alg}\Phi_a + \sigma_{pom}\Phi_{LPOM}}\right)\Phi_{LPOM}\Phi_{zoo}$$

<div align="center">zooplankton excretion   zooplankton ingestion of LPOM</div>

<div align="right">**(4-71)**</div>

where:

P_{am}	=	partition coefficient for algal mortality
P_{em}	=	partition coefficient for epiphyton mortality
P_{mm}	=	partition coefficient for macrophyte mortality
P_{zoopp}	=	partition coefficient for zooplankton LPOM grazing
γ_{OM}	=	temperature rate multiplier for organic matter
ω_{POM}	=	POM settling rate, $m\ sec^{-1}$
K_{am}	=	algal mortality rate, sec^{-1}
K_{em}	=	epiphyton mortality rate, sec^{-1}
K_{mm}	=	macrophyte mortality rate, sec^{-1}
K_{mz}	=	zooplankton mortality rate, sec^{-1}
K_{zg}	=	zooplankton growth rate, sec^{-1}
K_{LPOM}	=	labile POM decay rate, sec^{-1}
K_{effic}	=	Zooplankton ingestion efficiency
$K_{L\to R}$	=	transfer rate from labile POM to refractory POM, sec^{-1}
Φ_a	=	algal concentration, $g\ m^{-3}$
Φ_e	=	periphyton/epiphyton concentration, $g\ m^{-3}$
Φ_{macro}	=	macrophyte concentration, $g\ m^{-3}$
Φ_{LPOM}	=	detritus concentration, $g\ m^{-3}$
Φ_{zoo}	=	zooplankton concentration, $g\ m^{-3}$
σ_{pom}	=	zooplankton preference fraction for particulate organic matter
σ_{alg}	=	zooplankton preference fraction for algae
σ_{zoo}	=	zooplankton preference fraction for zooplankton

and the rate terms are evaluated in subroutine POM. POM settling and accumulation in the sediment compartment is handled identically to the algal compartment.

Refractory Particulate Organic Matter

Refractory POM is slowly decaying non-living, organic matter that settles. The source/sink terms are first order decay, the conversion of LPOM to RPOM, and sedimentation. The settled organic matter becomes part of the first order sediment model or the sediment diagenesis model if they are active.
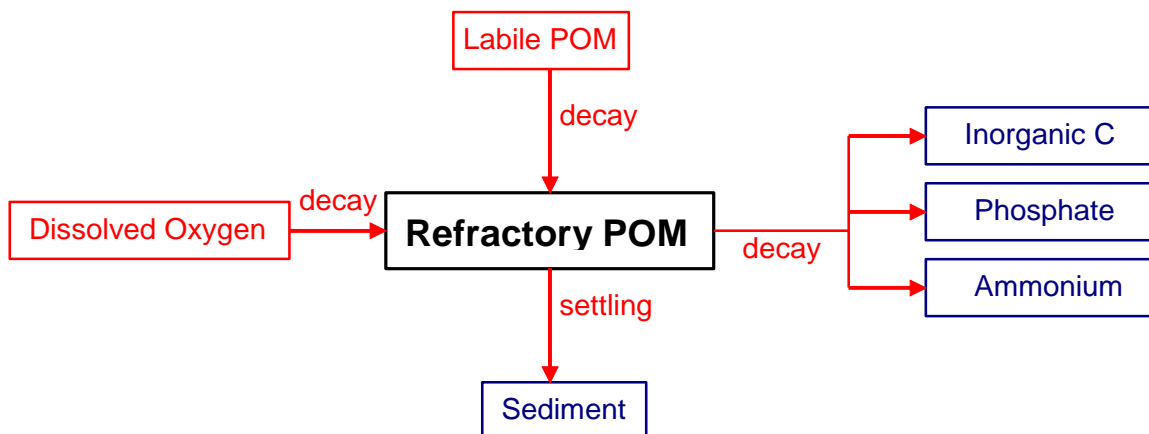
Figure 76. Internal flux between refractory POM and other compartments.

Referring to **Figure 76**, the rate equation for labile POM is:

$$S_{RPOM} = \underbrace{K_{L \to R}\Phi_{LPOM}}_{\substack{\text{labile to refractory}\\\text{POM decay}}} - \underbrace{\gamma_{OM}K_{RPOM}\Phi_{RPOM}}_{\text{decay}} - \underbrace{\omega_{RPOM}\frac{\partial \Phi_{RPOM}}{\partial z}}_{\text{settling}} \tag{4-72}$$

where:

γ_{OM} = temperature rate multiplier
$K_{L \to R}$ = transfer rate from labile POM to refractory POM, sec^{-1}
K_{RPOM} = refractory POM decay rate, sec^{-1}
ω_{POM} = POM settling velocity, m/sec^{-1}
Φ_{LPOM} = labile POM concentration, $g\ m^{-3}$
Φ_{RPOM} = refractory POM concentration, $g\ m^{-3}$

Organic Matter Variable Stoichiometry

The CE-QUAL-W2 model includes a feature starting with V3.5 which allows for the variable stoichiometry of organic matter. Past versions of W2 models have used fixed stoichiometric constants for the ratios of nitrogen and phosphorus to organic matter.

Eight constituents were required to simulate the amount of nitrogen and phosphorus in labile dissolved organic matter (LDOM), refractory organic matter (RDOM), labile particulate organic matter (LPOM), and refractory particulate organic matter (RPOM). These constituents are summarized in Table 11. Hence, all inputs of organic matter accumulate N and P according to the stoichiometry of the incoming organic matter.

Table 11. Constituents used for variable stoichiometry of organic matter.

Abbreviation	Constituent
LDOM-P	Labile Dissolved Organic Matter – Phosphorus
RDOM-P	Refractory Dissolved Organic Matter – Phosphorus
LPOM-P	Labile Particulate Organic Matter – Phosphorus
RPOM-P	Refractory Particulate Organic Matter – Phosphorus

LDOM-N	Labile Dissolved Organic Matter – Nitrogen
RDOM-N	Refractory Dissolved Organic Matter – Nitrogen
LPOM-N	Labile Particulate Organic Matter – Nitrogen
RPOM-N	Refractory Particulate Organic Matter – Nitrogen

Labile Dissolved Organic Matter – Phosphorus (LDOM-P)

LDOM-P is the amount of phosphorus in labile dissolved organic matter. The rate equation of LDOM-P is:

$$S_{\text{LDOM-P}} = \underbrace{\sum K_{ae}\delta_{\text{Pa}}\Phi_a}_{\text{algal excretion}} + \underbrace{\sum (1-P_{am})K_{am}\delta_{\text{Pa}}\Phi_a}_{\text{algal mortality}} + \underbrace{\sum K_{ee}\delta_{\text{Pe}}\Phi_e}_{\text{epiphyton excretion}}$$

$$+ \underbrace{\sum (1-P_{em})K_{em}\delta_{\text{Pe}}\Phi_e}_{\text{epiphyton mortality}} + \underbrace{\sum (1-P_{mm})K_{mm}\delta_{\text{Pm}}\Phi_m}_{\text{macrophyte mortality}} - \underbrace{K_{LDOM}\gamma_{\text{OM}}\Phi_{LDOM-P}}_{\text{labile DOM-P decay}} - \underbrace{K_{L\to R}\gamma_{\text{OM}}\Phi_{LDOM-P}}_{\substack{\text{labile to refractory}\\\text{DOM-P decay}}} \textbf{(4-73)}$$

where:

P_{am} = pattern coefficient for algal mortality
P_{em} = pattern coefficient for periphyton/epiphyton mortality
γ_{OM} = temperature rate multiplier for organic matter decay
$\delta_{\text{P-LDOM}}$ = LDOM stoichiometric ratio for phosphorus
δ_{Pe} = periphyton/epiphyton stoichiometric coefficient for phosphorus
δ_{Pa} = algal stoichiometric coefficient for phosphorus
δ_{Pm} = macrophyte stoichiometric coefficient for phosphorus
K_{ae} = algal excretion rate, sec^{-1}
K_{am} = algal mortality rate, sec^{-1}
K_{ee} = periphyton/epiphyton excretion rate, sec^{-1}
K_{em} = periphyton/epiphyton mortality rate, sec^{-1}
K_{mm} = macrophyte mortality rate, sec^{-1}
K_{LDOM} = labile DOM decay rate, sec^{-1}
$K_{L\to R}$ = labile to refractory DOM transfer rate, sec^{-1}
Φ_a = algal concentration, $g\ m^{-3}$
Φ_m = macrophyte concentration, $g\ m^{-3}$
Φ_e = periphyton/epiphyton concentration, $g\ m^{-3}$
Φ_{LDOM-P} = labile DOM-P concentration, $g\ m^{-3}$

Refractory Dissolved Organic Matter – Phosphorus (RDOM-P)

RDOM-P is the amount of phosphorus in refractory dissolved organic matter. The rate equation of RDOM-P is:

$$S_{RDOM-P} = \underbrace{K_{L\to R}\Phi_{LDOM-P}}_{\substack{\text{labile to refractory}\\\text{DOM decay}}} - \underbrace{\gamma_{OM}K_{RDOM}\Phi_{RDOM-P}}_{\text{decay}} \qquad \textbf{(4-74)}$$

where:
Φ_{LDOM-P} = labile DOM-P concentration, $g\ m^{-3}$
Φ_{RDOM-P} = refractory DOM-P concentration, $g\ m^{-3}$
γ_{OM} = temperature rate multiplier for organic matter

K_{LROM}= refractory POM decay rate, sec^{-1}
$K_{L \to R}$= transfer rate from labile POM to refractory POM, sec^{-1}

Labile Particulate Organic Matter – Phosphorus (LPOM-P)

LPOM-P is the amount of phosphorus in refractory dissolved organic matter. The rate equation of LPOM-P is:

$$S_{LPOM-P} = \underbrace{\sum P_{am} K_{am} \delta_{Pa} \Phi_a}_{\text{algal mortality}} + \underbrace{\sum P_{em} K_{em} \delta_{Pe} \Phi_e}_{\text{epiphyton mortality}} + \underbrace{\sum P_{mm} P_{mpom} K_{mm} \delta_{Pm} \Phi_m}_{\text{macrophyte mortality}} + \underbrace{\sum K_{zm} \delta_{Pz} \Phi_{zoo}}_{\text{zooplankton mortality}}$$

$$\underbrace{- K_{LPOM} \gamma_{OM} \Phi_{LPOM-P}}_{\text{decay}} \underbrace{- K_{L \to R} \Phi_{LPOM-P}}_{\substack{\text{labile to refractory} \\ \text{POM decay}}} + \underbrace{\sum K_{zg}(1 - Z_{effic}) \delta_{Pz} \Phi_{zoo}}_{\text{zooplankton excretion}} \qquad \textbf{(4-75)}$$

$$\underbrace{-\sum K_{zg} \frac{\Phi_{LPOM-P}}{\Phi_{LPOM}} \left(\frac{\sigma_{pom} \Phi_{LPOM}}{\sum \sigma_{zoo} \Phi_{zoo} + \sum \sigma_{alg} \Phi_a + \sigma_{pom} \Phi_{LPOM}} \right) \Phi_{zoo}}_{\text{zooplankton ingestion}} \underbrace{- \omega_{POM} \frac{\partial \Phi_{LPOM-P}}{\partial z}}_{\text{settling}}$$

where:
P_{am}= partition coefficient for algal mortality
P_{em}= partition coefficient for epiphyton mortality
P_{mm}= partition coefficient for macrophyte mortality
P_{mpom}=partition coefficient for RPOM and LPOM from macrophyte mortality
γ_{OM} = temperature rate multiplier for organic matter
σ_{alg}= Zooplankton preference fraction for algae
σ_{pom}= Zooplankton preference fraction for particulate organic matter
ω_{POM}= POM settling rate, $m\ sec^{-1}$
K_{am}= algal mortality rate, sec^{-1}
K_{em}= epiphyton mortality rate, sec^{-1}
K_{zm}= zooplankton mortality rate, sec^{-1}
K_{mm}= macrophyte mortality rate, sec^{-1}
K_{LPOM}= labile POM decay rate, sec^{-1}
$K_{L \to R}$= transfer rate from labile POM to refractory POM, sec^{-1}
Φ_a= algal concentration, $g\ m^{-3}$
Φ_{zoo}= zooplankton concentration, $g\ m^{-3}$
Φ_e= epiphyton concentration, $g\ m^{-3}$
Φ_{LPOM}= LPOM concentration, $g\ m^{-3}$
Φ_{LPOM-P}= LPOM-P concentration, $g\ m^{-3}$
K_{effic} = Zooplankton ingestion efficiency
σ_{zoo} = zooplankton preference fraction for zooplankton

Refractory Particulate Organic Matter – Phosphorus (RPOM-P)

RPOM-P is the amount of phosphorus in refractory dissolved organic matter. The rate equation of RPOM-P is:

$$S_{RPOM} = \underbrace{K_{L \to R} \Phi_{LPOM-P}}_{\substack{\text{labile to refractory} \\ \text{POM decay}}} - \underbrace{\gamma_{OM} K_{RPOM} \Phi_{RPOM-P}}_{\text{decay}} + \underbrace{\sum P_{mm}(1 - P_{mpom}) K_{mm} \delta_{Pm} \Phi_m}_{\text{macrophyte mortality}}$$

$$\qquad \textbf{(4-76)}$$

$$- \underbrace{\omega_{POM} \frac{\partial \Phi_{RPOM-P}}{\partial z}}_{\text{settling}}$$

where:

P$_{mm}$= partition coefficient for macrophyte mortality

P_{mpom} =partition coefficient for RPOM and LPOM from macrophyte mortality

δ_{Pm} = macrophyte stoichiometric coefficient for phosphorus

γ_{OM}= temperature rate multiplier

K$_{L \to R}$= transfer rate from labile POM to refractory POM, sec^{-1}

K$_{RPOM}$= refractory POM decay rate, sec^{-1}

K$_{mm}$= macrophyte mortality rate, sec^{-1}

ω_{POM}= POM settling velocity, m/sec^{-1}

$\Phi_{LPOM\text{-}P}$= labile POM phosphorus concentration, $g\ m^{-3}$

$\Phi_{RPOM\text{-}P}$= refractory POM phosphorus concentration, $g\ m^{-3}$

Labile Dissolved Organic Matter – Nitrogen (LDOM-N)

LDOM-N is the amount of nitrogen in labile dissolved organic matter. The rate equation of LDOM-N is:

$$S_{\text{LDOM-N}} = \underbrace{\sum K_{ae}\delta_{Na}\Phi_a}_{\text{algal excretion}} + \underbrace{\sum(1-P_{am})K_{am}\delta_{Na}\Phi_a}_{\text{algal mortality}} + \underbrace{\sum K_{ee}\delta_{Ne}\Phi_e}_{\text{epiphyton excretion}}$$

$$+ \underbrace{\sum(1-P_{em})K_{em}\delta_{Ne}\Phi_e}_{\text{epiphyton mortality}} + \underbrace{\sum(1-P_{mm})K_{mm}\delta_{Nm}\Phi_m}_{\text{macrophyte mortality}} - \underbrace{K_{LDOM}\gamma_{OM}\Phi_{LDOM-N}}_{\text{labile DOM-N decay}} -$$

$$\underbrace{K_{L \to R}\gamma_{OM}\Phi_{LDOM-N}}_{\substack{\text{labile to refractory} \\ \text{DOM-N decay}}}$$

(4-77)

where:

P_{am} = pattern coefficient for algal mortality

P_{em} = pattern coefficient for epiphyton mortality

γ_{OM} = temperature rate multiplier for organic matter decay

$\delta_{\text{P-LDOM}}$ =LDOM stoichiometric ratio for nitrogen

δ_{Ne} = epiphyton stoichiometric coefficient for nitrogen

δ_{Na} = algal stoichiometric coefficient for nitrogen

δ_{Nm} = macrophyte stoichiometric coefficient for nitrogen

K_{ae} = algal excretion rate, sec^{-1}

K_{am} = algal mortality rate, sec^{-1}

K_{ee} = epiphyton excretion rate, sec^{-1}

K_{em} = epiphyton mortality rate, sec^{-1}

K_{mm} = macrophyte mortality rate, sec^{-1}

   K_{LDOM} = labile DOM decay rate, sec^{-1}

$K_{L \to R}$ = labile to refractory DOM transfer rate, sec^{-1}

Φ_a = algal concentration, $g\ m^{-3}$

Φ_m = macrophyte concentration, $g\ m^{-3}$

Φ_e = epiphyton concentration, $g\ m^{-3}$

$\Phi_{LDOM\text{-}N}$= labile DOM-N concentration, $g\ m^{-3}$

Refractory Dissolved Organic Matter – Nitrogen (RDOM-N)

RDOM-N is the amount of nitrogen in refractory dissolved organic matter. The rate equation of RDOM-N is:

$$S_{RDOM-N} = \underbrace{K_{L \to R} \Phi_{LDOM-N}}_{\substack{\text{labile to refractory} \\ \text{DOM decay}}} - \underbrace{\gamma_{OM} K_{RDOM} \Phi_{RDOM-N}}_{\text{decay}} \tag{4-78}$$

where:

$K_{L \to R}$ = labile to refractory DOM transfer rate, sec^{-1}
K_{RDOM} = refractory DOM decay rate, sec^{-1}
γ_{OM} = temperature rate multiplier for organic matter decay
Φ_{LDOM-N} = labile DOM-N concentration, $g\ m^{-3}$
Φ_{RDOM-N} = refractory DOM-N concentration, $g\ m^{-3}$

Labile Particulate Organic Matter – Nitrogen (LPOM-N)

LPOM-N is the amount of nitrogen in refractory dissolved organic matter. The rate equation of LPOM-N is:

$$S_{LPOM-N} = \underbrace{\sum P_{am} K_{am} \delta_{Na} \Phi_a}_{\text{algal mortality}} + \underbrace{\sum P_{em} K_{em} \delta_{Ne} \Phi_e}_{\text{epiphyton mortality}} + \underbrace{\sum P_{mm} P_{mpom} K_{mm} \delta_{Nm} \Phi_m}_{\text{macrophyte mortality}} + \underbrace{K_{zm} \delta_{Nz} \Phi_{zoo}}_{\text{zooplankton mortality}}$$

$$- \underbrace{K_{LPOM} \gamma_{OM} \Phi_{LPOM-N}}_{\text{decay}} - \underbrace{K_{L \to R} \Phi_{LPOM-N}}_{\substack{\text{labile to refractory} \\ \text{POM decay}}} + \underbrace{K_{zg} (1 - Z_{effic}) \delta_{Nz} \Phi_{zoo}}_{\text{zooplankton}}$$

$$- \underbrace{K_{zg} \frac{\Phi_{LPOM-N}}{\Phi_{LPOM}} \left(\frac{\sigma_{pom} \Phi_{LPOM}}{\sum \sigma_{alg} \Phi_a + \sum \sigma_{zoo} \Phi_{zoo} + \sigma_{pom} \Phi_{LPOM}} \right) \Phi_{zoo}}_{\text{zooplankton ingestion}} - \underbrace{\omega_{POM} \frac{\partial \Phi_{LPOM-N}}{\partial z}}_{\text{settling}}$$

$$\tag{4-79}$$

where:

P_{am} = partition coefficient for algal mortality
P_{em} = partition coefficient for periphyton/epiphyton mortality
P_{mm} = partition coefficient for macrophyte mortality
P_{mpom} = partition coefficient for RPOM and LPOM from macrophyte mortality
γ_{OM} = temperature rate multiplier for organic matter
σ_{alg} = Zooplankton preference fraction for algae
σ_{pom} = Zooplankton preference fraction for particulate organic matter
ω_{POM} = POM settling rate, $m\ sec^{-1}$
K_{am} = algal mortality rate, sec^{-1}
K_{em} = epiphyton mortality rate, sec^{-1}
K_{zm} = zooplankton mortality rate, sec^{-1}
K_{mm} = macrophyte mortality rate, sec^{-1}
K_{LPOM} = labile POM decay rate, sec^{-1}
$K_{L \to R}$ = transfer rate from labile POM to refractory POM, sec^{-1}

Φ_a = algal concentration, *g m⁻³*

Φ_{zoo} = algal concentration, *g m⁻³*

Φ_e = epiphyton concentration, *g m⁻³*

Φ_{LPOM}= LPOM concentration, *g m⁻³*

Φ_{LPOM-N}= LPOM-N concentration, *g m⁻³*

K_{effic} = Zooplankton ingestion efficiency

σ_{zoo} = zooplankton preference fraction for zooplankton

Refractory Particulate Organic Matter – Nitrogen (RPOM-N)

RPOM-N is the amount of nitrogen in refractory dissolved organic matter. The rate equation of RPOM-N is:

$$S_{RPOM} = \underbrace{K_{L \to R} \Phi_{LPOM-N}}_{\substack{\text{labile to refractory} \\ \text{POM decay}}} - \underbrace{\gamma_{OM} K_{RPOM} \Phi_{RPOM-N}}_{\text{decay}} + \underbrace{\sum P_{mm}\left(1 - P_{mpom}\right)K_{mm}\delta_{Nm}\Phi_m}_{\text{macrophyte mortality}}$$

$$\underbrace{- \omega_{POM} \frac{\partial \Phi_{RPOM-N}}{\partial z}}_{\text{settling}}$$

(4-80)

where:

P_{mm} = partition coefficient for macrophyte mortality

P_{mpom} = partition coefficient for RPOM and LPOM from macrophyte mortality

γ_{OM} = temperature rate multiplier

δ_{Nm} = macrophyte stoichiometric coefficient for nitrogen

$K_{L \to R}$ = transfer rate from labile POM to refractory POM, *sec⁻¹*

K_{RPOM} = refractory POM decay rate, *sec⁻¹*

K_{mm} = macrophyte mortality rate, *sec⁻¹*

ω_{RPOM} = POM settling velocity, *m/ sec⁻¹*

Φ_{LPOM-N}= labile POM-N concentration, *g m⁻³*

Φ_{RPOM-N}= refractory POM-N concentration, *g m⁻³*

Organic Carbon Constituents

Zhong Zhang

The organic matter state variables (LPOM, RPOM, RDOM, LDOM) are based on organic matter, dry weight. The CE-QUAL-W2 model also can use organic matter as C. Many other models use this concept also since organic matter is rarely measured in the field, whereas C is. Hence, instead of LDOM, LPOM, RDOM, and RPOM, the model user can use LDOC, LPOC, RDOC, and RPOC.

Organic matter is difficult for laboratories to measure directly. However, collective water quality parameters such as organic carbon, organic nitrogen and organic phosphorous are often measured. Besides simulating organic matter described in the current version of W2, the model includes an option for directly simulating organic carbon constituents without organic matter. The four organic carbon state variables in W2 are refractory and labile dissolved organic carbon (RDOC and LDOC) and refractory and labile particulate organic carbon (RPOC and LPOC).

The model representation of LPOC kinetics is shown in Figure 77. LPOC gains through algae death and grazing, and is lost through decay, hydrolysis, and settling. LPOC increases from the excretion of the zooplankton. The latter is limited by the assimilation efficiency of zooplankton.
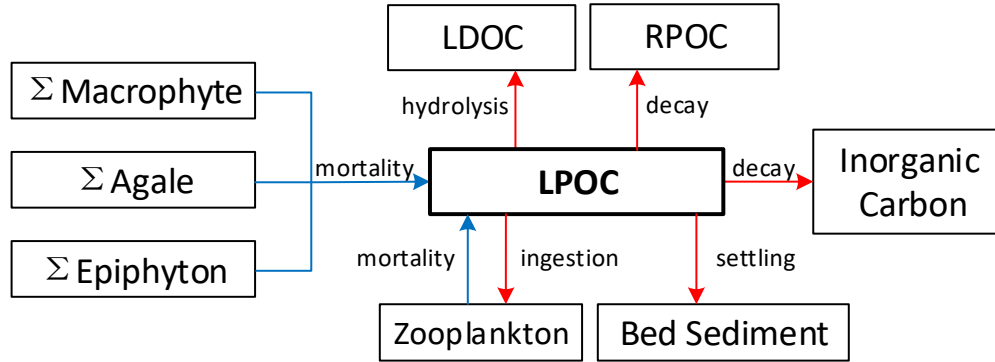
Figure 77.Kinetics of LPOC in the water column.

The kinetic source/sink term for LPOC is

$$
S_{LPOC} = \underbrace{\sum K_{am}\,\delta_{ca}\,\Phi_a P_{am}}_{\text{algal mortality}} + \underbrace{\sum K_{em}\,\delta_{ce}\,\Phi_e P_{em}}_{\text{epiphyton mortality}} - \underbrace{\omega_{LPOM}\,\frac{\partial\,\Phi_{LPOC}}{\partial\,\mathrm{z}}}_{\text{settling}}
$$

$$
\underbrace{-\,\gamma_{OM} K_{LPOC}\Phi_{LPOC}}_{\text{LPOC decay}} + \underbrace{\gamma_{OM} K_{LPOC\rightarrow RPOC}\Phi_{LPOC}}_{\text{labile to refractory POC transfer}} + \underbrace{\gamma_{OM} K_{LPOM\rightarrow LDOM}\Phi_{LPOC}}_{\text{LPOC hydrolysis}}
$$

$$
+\,\underbrace{\sum K_{mm}\,\delta_{cm}\,\Phi_{macro} P_{mm} P_{mmLPOM}}_{\text{macrophyte mortality}} + \underbrace{K_{zm}\,\delta_{cz}\,\Phi_{zoo}}_{\text{zooplankton mortality}}
$$

$$
-\sum\underbrace{\left(Z_u\,\delta_{cz}\,\Phi_{zoo}\,\frac{\Phi_{LPOM}}{\sum\sigma_{alg}\Phi_a + \Phi_{LPOM} + \sum\sigma_{zoo}\Phi_{zoo}} \right)}_{\text{zooplankton growth}}
$$

(4-81)

where

Φ_{LPOC} = LPOC concentration, *g-C m*⁻³

P_{am} = fraction of algal mortality into LPOM (0-1)

P_{em} = fraction of epiphyton mortality into LPOM (0-1)

P_{mm} = fraction of macrophyte mortality into LPOM (0-1)

δ_{ca} = stoichiometric ratio of carbon in algae, *g-C/g-D*

δ_{ce} = stoichiometric ratio of carbon in epiphyton, *g-C/g-D*

δ_{cm} = stoichiometric ratio of carbon in macrophyte, *g-C/g-D*

δ_{cz} = stoichiometric ratio of carbon in zooplankton, *g-C/g-D*

δ_{com} = stoichiometric ratio of carbon in organic matter, *g-C/g-D*

K_{LPOC} = LPOC decay rate, s^{-1}

$K_{LPOC \rightarrow RPOC}$ = transfer rate from LPOC to RPOC, s^{-1}.

The model representation of RPOC kinetics is shown in Figure 78. RPOC gains through macrophyte death, and is lost through decay, hydrolysis and settling. RPOC increases from the LPOC decay.
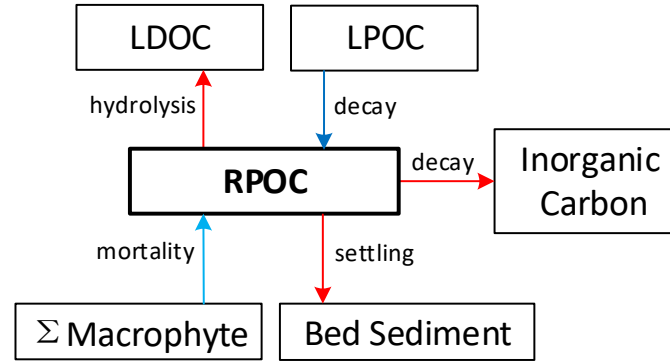
Figure 78. Kinetics of RPOC in the water column.

The kinetic source/sink term for RPOC is

$$S_{RPOC} = \underbrace{\gamma_{OM} K_{LPOC \rightarrow RPOC} \Phi_{LPOC}}_{\text{labile to refractory POC transfer}} - \underbrace{\gamma_{OM} K_{RPOC} \Phi_{RPOC}}_{\text{RPOC decay}} - \underbrace{\omega_{RPOM} \frac{\partial \Phi_{RPOC}}{\partial z}}_{\text{RPOC settling}}$$

$$\underbrace{- \gamma_{OM} K_{RPOM \rightarrow LDOM} \Phi_{RPOC}}_{\text{RPOC hydrolysis}} + \underbrace{\sum K_{mm} \delta_{cm} \Phi_{macro} P_{mm} (1 - P_{mmLPOM})}_{\text{marophyte mortality}}$$

(4-82)

where:

Φ_{RPOC} = RPOC concentration, $g\text{-}C\ m^{-3}$

$K_{LPOC \rightarrow RPOC}$ = transfer rate from LPOC to RPOC, s^{-1}

K_{RPOC} = RPOC decay rate, s^{-1}

The model representation of LDOC kinetics is shown in Figure 79. Particulate fractions (both labile and re-fractory) of organic carbon are hydrolyzed to LDOC, while LDOC mineralizes to CO_2. LDOC gain through algae death and excretion are lost through decay. LDOC oxidation is aerobic and, therefore, reduced at low oxygen concentrations.
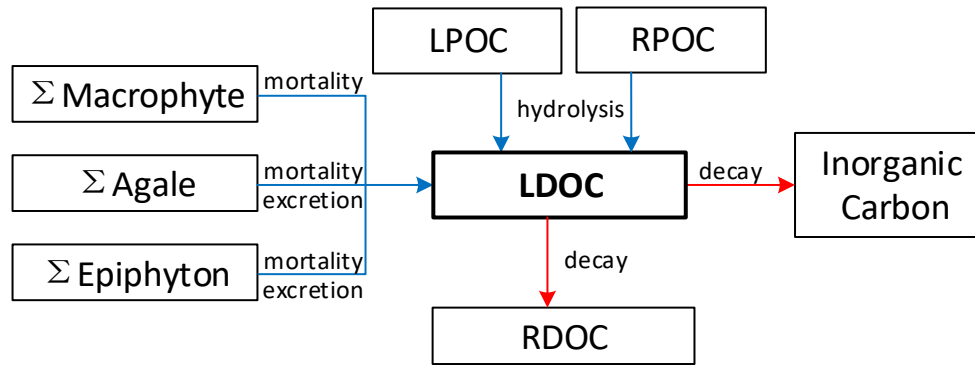
Figure 79. Kinetics of LDOC in the water column.

The kinetic source/sink term for LDOC is

$$S_{LDOC} = \underbrace{\sum K_{am}\, \delta_{ca}\, \Phi_a \left(1 - P_{am}\right)}_{\text{algal mortality}} + \underbrace{\sum K_{ae}\, \delta_{ca}\, \Phi_a}_{\text{algal excretion}} + \underbrace{\sum K_{em}\, \delta_{ce}\, \Phi_e \left(1 - P_{em}\right)}_{\text{epiphyton mortality}}$$

$$+ \underbrace{\sum K_{ee}\, \delta_{ce}\, \Phi_e}_{\text{epiphyton excretion}} - \underbrace{\gamma_{OM} K_{LDOC} \Phi_{LDOC}}_{\text{LDOC decay}} - \underbrace{\gamma_{OM} K_{LDOC \to RDOC} \Phi_{LDOC}}_{\text{labile to refractory DOC transfer}} \qquad \textbf{(4-83)}$$

$$+ \underbrace{\sum K_{mm}\, \delta_{cm}\, \Phi_{macro}\left(1 - P_{mm}\right)}_{\text{macrophyte mortality}} + \underbrace{\gamma_{OM} K_{LPOM \to LDOM} \Phi_{LPOC}}_{\text{LPOC hydrolysis}} + \underbrace{\gamma_{OM} K_{RPOM \to LDOM} \Phi_{RPOC}}_{\text{RPOC hydrolysis}}$$

where

Φ_{LDOC} = LDOC concentration, $g\text{-}C\ m^{-3}$

Φ_{LPOC} = LPOC concentration, $g\text{-}C\ m^{-3}$

Φ_{RPOC} = RPOC concentration, $g\text{-}C\ m^{-3}$

K_{LDOC} = LDOC decay rate, s^{-1}

$K_{LDOC \to RDOC}$ = LDOC to RDOC transfer rate, s^{-1}.

The model representation of RDOC kinetics is shown in Figure 80**Error! Reference source not found.**. RDOC gain through LDOC decay and lost when it mineralizes to CO_2.
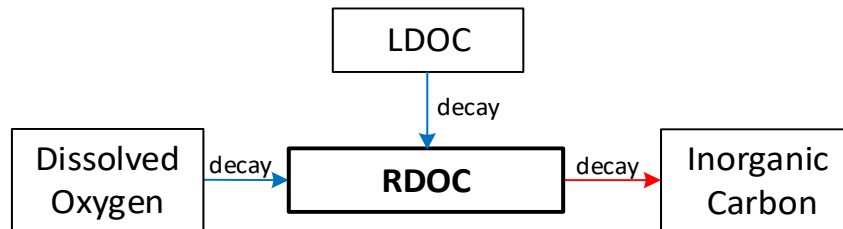
Figure 80. Kinetics of RDOC in the water column.

The kinetic source/sink term for RDOC is

$$S_{RDOC} = \underbrace{\gamma_{OM} K_{LDOC \rightarrow RDOC} \Phi_{LDOC}}_{\text{labile to refractory DOC transfer}} - \underbrace{\gamma_{OM} \mathrm{K}_{RDOC} \Phi_{RDOC}}_{\text{RDOC decay}} \qquad \textbf{(4-84)}$$

where

Φ_{RDOC} = RDOC concentration, *g-C m^{-3}*

K_{RDOC} = RDOC decay rate, *s^{-1}*

$K_{LDOC \rightarrow RDOC}$ = LDOC to RDOC transfer rate, *s^{-1}*.

Carbonaceous Biochemical Oxygen Demand (CBOD)

Any number of CBOD groups with varying decay rates and either particulate or dissolved can be modeled allowing the user to more accurately characterize various CBOD sources. Additionally, different CBOD sources can be tracked separately in the model to determine what affect they have on the receiving water.

Care must be taken when including CBOD in the simulation to ensure that CBOD, DOM, POM, and algal biomass are properly accounted for. CBOD is typically specified as allochthonous inputs and the forms of autochthonous organic matter are kept track of in the various organic matter compartments. This ensures that no "double dipping" occurs. This group can also model dissolved or particulate CBOD by specifying a zero or a finite settling velocity, respectively, for the group. The settled CBOD goes into the 1st order sediment compartment.

In Version 3.6 and earlier, **Figure 81** described the CBOD cycle with fixed stoichiometry of the CBOD in terms of C:N:P. Starting with Version 3.7, code changes were made such that for each CBOD group, the nitrogen and phosphorus corresponding to the CBOD group were modeled as separate constituents. One can still though use the V3.6 and earlier fixed N and P stoichiometry for the BOD groups if one wishes. CBOD-C though is still based on a fixed C stoichiometry.
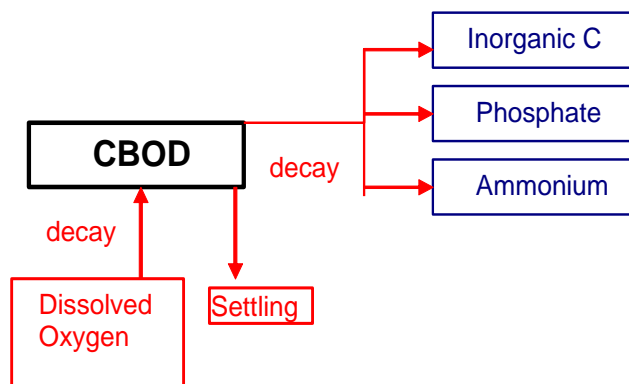
Figure 81. Internal flux between CBOD and other compartments in Version 3.6 and earlier.

The following figure illustrates the CBOD cycle for Version 3.7 and later.
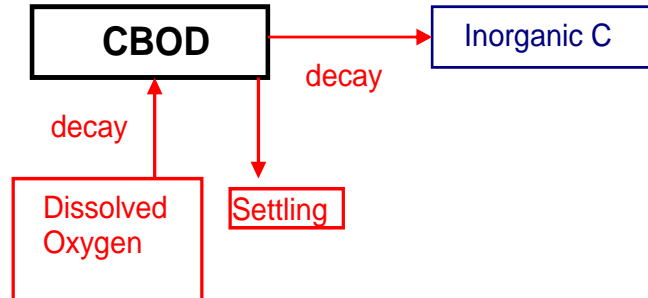
Figure 82. Internal flux between CBOD and other compartments in Version 3.7 and later.

The rate equation for CBOD is:

$$S_{CBOD} = -\underbrace{\Theta^{T-20} \, \mathrm{K}_{BOD} \, R_{BOD} \, \Phi_{CBOD}}_{\text{decay}} - \underbrace{\omega_{CBOD} \frac{\partial R_{BOD} \Phi_{CBOD}}{\partial z}}_{\text{settling}}$$ **(4-85)**

where:

Θ = BOD temperature rate multiplier

T = temperature, $^\circ C$

ω_{CBOD} = CBOD settling velocity, m/sec^{-1}

K_{BOD} = CBOD decay rate, sec^{-1}

R_{BOD} = CBOD conversion from input CBOD to CBOD-ultimate ($CBOD_u$)

Φ_{BOD} = CBOD concentration, $g\ m^{-3}$

Note that the user can enter the 5-day $CBOD_5$ or any other day $CBOD_{day}$ into the CE-QUAL-W2 model. The RBOD term converts to $CBOD_u$ (ultimate or 28 day) internally in the model. The model though will output $CBOD_5$ if you entered $CBOD_5$ as input - not $CBOD_u$. If you use $CBOD_u$ as the input CBOD, then $R_{BOD}=1$ and the output would be $CBOD_u$.

Typical determination of R_{BOD} is based on the following standard CBOD equation: $R_{BOD} = \frac{CBOD_u}{CBOD_t} = \frac{1}{(1 - exp[-K_{BOD}t])}$ where t is the time in days (5 days, for example), K_{BOD} is the BOD decay rate in day^{-1}, and $CBOD_t$ is the CBOD at that time.

Carbonaceous Biochemical Oxygen Demand - Phosphorus (CBODP)

The phosphorus associated with a specific CBOD group is modeled as a separate constituent.

Sources and sinks for carbonaceous biochemical oxygen demand - phosphorus (CBODP) are shown in Figure 83.
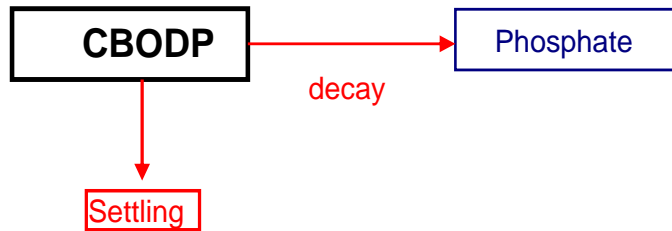
Figure 83. Internal flux between CBODP and other compartments.

The rate equation for CBODP is:

$$S_{CBODP} = -\underbrace{\Theta^{T-20}\, \text{K}_{BOD}\, \Phi_{CBODP}}_{\text{decay}} - \underbrace{\omega_{CBOD}\, \frac{\partial \Phi_{CBODP}}{\partial z}}_{\text{settling}}$$

where:

Θ = BOD temperature rate multiplier

T = temperature, $^{\circ}C$

ω_{CBOD} = CBOD settling velocity, m/sec^{-1}

K_{BOD} = CBOD decay rate, sec^{-1}

Φ_{CBODP} = CBODP concentration, $g\, m^{-3}$

Carbonaceous Biochemical Oxygen Demand - Nitrogen (CBODN)

The nitrogen associated with a specific CBOD group is modeled as a separate constituent. Figure 84 shows the CBODN sources and sinks.
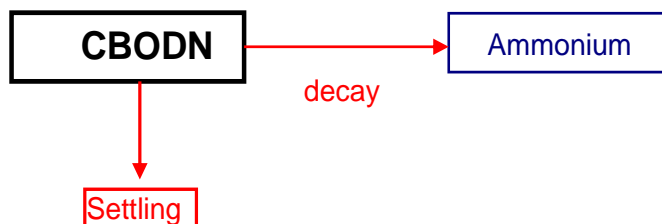
Figure 84. Internal flux between CBODN and other compartments.

The rate equation for CBODN is:

where:

$$S_{CBODN} = - \underbrace{\Theta^{T-20} \, K_{BOD} \, \Phi_{CBODN}}_{\text{decay}} - \underbrace{\omega_{CBOD} \frac{\partial \Phi_{CBODN}}{\partial z}}_{\text{settling}}$$

- Θ = BOD temperature rate multiplier
- T = temperature, ℃
- ω_{CBOD} = CBOD settling velocity, $m\ s^{-1}$
- K_{BOD} = CBOD decay rate, sec^{-1}
- Φ_{CBODN}=CBODN concentration, $g\ m^{-3}$

Algae

An algal community can be represented as a single assemblage or as multiple algae groups. Often, the algal groups might include diatoms, greens, and cyanobacteria. The user has complete freedom in how many and what kinds of algal groups can be included in the simulation through careful specification of the kinetic rate parameters that define the characteristics of each algal group.

Source-sink term for algae
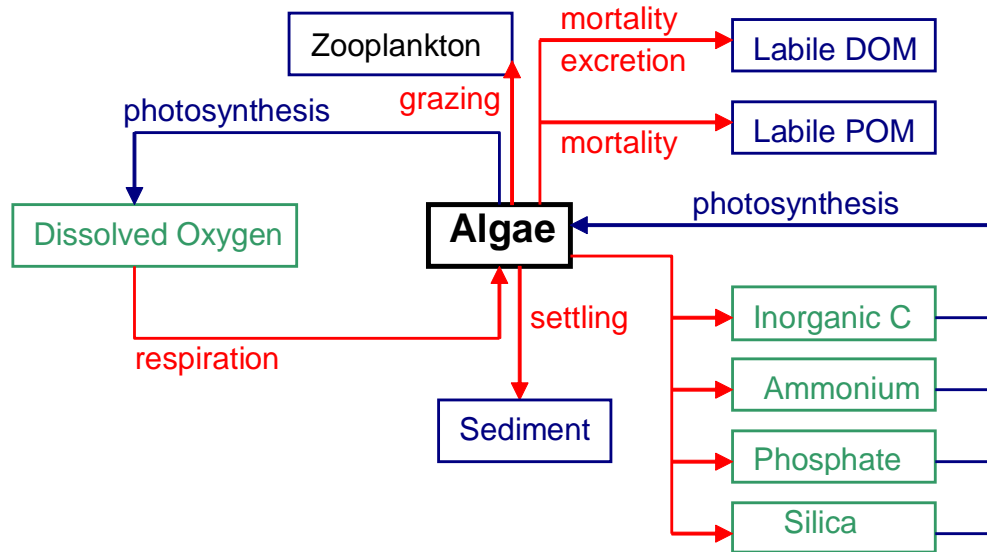
Figure 85. Internal flux between algae and other compartments.

Referring to **Figure 85**, the rate equation for each algal group is:

$$S_a = \underbrace{K_{ag}\Phi_a}_{\text{growth}} - \underbrace{K_{ar}\Phi_a}_{\text{respiration}} - \underbrace{K_{ae}\Phi_a}_{\text{excretion}} - \underbrace{K_{am}\Phi_a}_{\text{mortality}} - \underbrace{\omega_a \frac{\partial \Phi_a}{\partial z}}_{\text{settling}} - \underbrace{\sum\left(Z_\mu \Phi_{zoo} \frac{\sigma_{alg}\Phi_a}{\sum\sigma_{alg}\Phi_a + \sigma_{pom}\Phi_{lpom} + \sum\sigma_{zoo}\Phi_{zoo}}\right)}_{\text{net loss to grazing}} \quad \textbf{(4-86)}$$

where:

- z = cell height

Z_μ = net growth rate of a zooplankton species

$\sigma_{alg}, \sigma_{zoo}$ = zooplankton grazing preference factors for algae (alg) or zooplankton (zoo)

K_{ag} = algal growth rate, sec^{-1}

K_{ar} = algal dark respiration rate, sec^{-1}

K_{ae} = algal excretion rate, sec^{-1}

K_{am} = algal mortality rate, sec^{-1}

ω_a = algal settling rate, $m\ sec^{-1}$

Φ_a = algal concentration, $g\ m^{-3}$

Chlorophyll *a* (chl *a*) is most commonly available as an estimate of algal biomass. To convert chl *a* to algal biomass, chl *a* is typically multiplied by the given algae (as $g\ m^{-3}$ or mg/l dry weight OM)/chl *a* (as µg chlorophyll a/l) ratio. This value can vary widely depending on the makeup of the algal population. Some previous studies determined the conversion factor by regressing particulate organic matter with chlorophyll *a*.

Algal growth rate is computed by modifying a maximum growth rate affected by temperature, light, and nutrient availability:

$$K_{ag} = \gamma_{ar}\gamma_{af}\lambda_{\min}K_{ag\max}$$ **(4-87)**

where:

γ_{ar} = temperature rate multiplier for rising limb of curve

γ_{af} = temperature rate multiplier for falling limb of curve

λ_{min} = multiplier for limiting growth factor (minimum of light, phosphorus, silica, and nitrogen) between 0 and 1

K_{ag} = algal growth rate, sec^{-1}

K_{agmax} = maximum algal growth rate, sec^{-1}

Rate multipliers for algal growth are computed based upon available light, phosphorus, nitrogen, and silica. The rate multiplier, λ, between 0 and 1 for light is based upon the Steele (1962) function:

$$\lambda_l = F(I) = \frac{I}{I_S}e^{-\frac{I}{I_S}+1}$$ (4-88)

where:

I = available light, $W\ m^{-2}$

I_s = saturating light intensity at maximum photosynthetic rate, $W\ m^{-2}$

λ_l = light limiting factor or F(I)

The above expression allows for simulation of photoinhibition at light intensities greater than the saturation value. However, light penetration decreases with depth:

$$I(z) = (1-\beta)I_0 e^{-\alpha z}$$ (4-89)

where:

I_0 = solar radiation at the water surface, $W\ m^{-2}$

α = attenuation coefficient, m^{-2}

z = depth, m

$(1-\beta)$ = fraction of solar radiation absorbed at the water surface

The average effect of light on algal growth in a particular model cell can be obtained by combining the above two expressions and integrating over the cell depth to obtain (Chapra and Reckhow, 1983):

$$\lambda_l = \frac{e}{\alpha \Delta z}[e^{-\gamma_2} - e^{-\gamma_1}] \tag{4-90}$$

where:

$$\gamma_1 = \frac{(1-\beta)I_o e^{-\alpha d}}{I_s}$$

$$\gamma_2 = \frac{(1-\beta)I_o e^{-\alpha(d+\Delta z)}}{I_s}$$

d: depth at top of model cell, m

The fraction of solar radiation, $(1-\beta)I_o$, is added directly to the surface layer. The attenuation coefficient, α, consists of a baseline value **[EXH2O]** to which the effects of inorganic **[EXINOR]** and organic **[EXORG]** suspended solids, and algae **[EXA]** are added.

Rate multipliers limiting maximum algal growth due to nutrient limitations are computed using the Monod relationship:

$$\lambda_i = \frac{\Phi_i}{P_i + \Phi_i} \tag{4-91}$$

where:

  Φ_i = phosphorus or nitrate + ammonium concentration, $g\ m^{-3}$
  P_i = half-saturation coefficient for phosphorus or nitrate + ammonium, $g\ m^{-3}$

The algal nitrogen preference for ammonium is based upon the following (Thomann and Fitzpatrick, 1982) equation:

$$P_{NH4} = \Phi_{NH4}\frac{\Phi_{NOx}}{(K_{NH4}+\Phi_{NH4})(K_{NH4}+\Phi_{NOx})} + \Phi_{NH4}\frac{K_{NH4}}{(\Phi_{NH4}+\Phi_{NOx})(K_{NH4}+\Phi_{NOx})}$$

$$\tag{4-92}$$

where:
  P_{NH4} = ammonium preference factor
  K_{NH4} = ammonia preference half-saturation coefficient, $g\ m^{-3}$
  Φ_{NH4} = ammonium concentration, $g\ m^{-3}$
  Φ_{NOx} = nitrate-nitrite concentration, $g\ m^{-3}$

This allows algae to use primarily ammonium and gradually switch to nitrate as ammonium concentrations decrease.

Algal dark respiration is computed using the rising limb of the temperature function:

$$K_{ar} = \gamma_{ar}\gamma_{af}K_{armax} \tag{4-93}$$

where:
  γ_{ar} = temperature rate multiplier for rising limb of curve
  γ_{af} = temperature rate multiplier for falling limb of curve
  K_{armax} = maximum dark respiration rate, sec^{-1}

Algal photorespiration (excretion) is evaluated using an inverse relation to the light rate multiplier:

$$K_{ae} = (1 - \lambda_l)\gamma_{ar}\gamma_{af}K_{aemax} \tag{4-94}$$

where:

γ_{ar} = temperature rate multiplier for rising limb of curve

γ_{af} = temperature rate multiplier for falling limb of curve

K_{aemax} = maximum excretion rate constant, sec^{-1}

λ_l = light limiting factor

Excretion rates increase at both low and high light intensities, with excretion products contributing to labile DOM.

Algal mortality is defined as:

$$K_{am} = \gamma_{ar}\gamma_{af}K_{ammax} \tag{4-95}$$

where:

γ_{ar} = temperature rate multiplier for rising limb of curve

γ_{af} = temperature rate multiplier for falling limb of curve

K_{ammax} = maximum mortality rate, sec^{-1}

This mortality rate represents both natural and predator mortality. Algal growth does not occur in the absence of light. Algal growth is not allowed to exceed the limit imposed by nutrient supply over a given timestep. Algal excretion is not allowed to exceed algal growth rates.

Like inorganic solids, settling algae serve as a source for the layer below. Unlike inorganic solids, algae passing to the sediments accumulate within the sediment compartment. POM is also accumulated in this sediment compartment.

Algae vertical migration

This section is based on work by Overman (2019), Overman and Wells (2021), and Cervarich et al. (2020).

Some species of cyanobacteria (which are often responsible for HABs) are able to move vertically in the water column by their own motility, independent of water velocity (Visser et al., 2016). This vertical migration can lead to HABs when colonies accumulate on a water surface and experience increased growth, causing degradation of water quality and environmental health (Belov and Giles, 1997).

Cyanobacteria vertical migration is achieved through a process called buoyancy regulation. Cells regulate their buoyancy either with carbohydrate ballast or gas vesicles (Kromkamp and Walsby, 1990). Carbohydrates are accumulated when cells photosynthesize. This ballast causes a decrease in buoyancy and subsequent sinking. Once cells have stopped photosynthesizing, the carbohydrates are consumed, the ballast depleted, and cells rise again (Kromkamp and Mur, 1984). Chemicals accumulated during photosynthesis also cause gas vesicles contained in cells to collapse through turgor pressure, which decreases buoyancy. Synthesis of new gas vesicles leads to an increase in buoyancy (Kromkamp et al., 1988). Based on these mechanisms, buoyancy regulation and vertical migration are affected by external factors such as light and nutrients. Numerous laboratory and field studies have documented relationships between cyanobacteria buoyancy and irradiance (e.g. Kromkamp and Walsby, 1990; Ibelings et al., 1991; Visser et al., 1997; Wallace and Hamilton, 1999; Brookes and Ganf, 2001; Cui et al., 2016). Because of the threat cyanobacteria poses to environmental and human health and the observed relationship between cyanobacteria movement and

measurable variables, many modeling efforts have focused on predicting vertical migration (see Overman, 2019, for a review).

Two different models were used to calculate a settling velocity for an algae group at each time step rather than using a constant settling velocity. The predefined velocity model is based on a simple sinusoidal function of time that predicts a spatially constant settling velocity for an algae group. The dynamic velocity model uses more complex equations to calculate an algae group's settling velocity based on solar irradiance for each model grid cell. The vertical migration models were added to the Kinetic Rates Module in the Water Quality Subroutine of CE-QUAL-W2.

Predefined Velocity

A simple way to model the vertical movement of cyanobacteria is to assume a velocity function for colonies based on knowledge of their typical movement. Because cyanobacteria vertical migration is due to buoyancy regulation, which is dependent on light, a velocity function that represents changes in light is a logical choice. If cyanobacteria colonies are assumed to migrate vertically on a daily cycle, an equation for colony velocity as a function of time can be used:

$$v_p(t) = A \frac{2\pi}{86,400\,s} cos\left(\frac{2\pi}{86,400\,s}t + \phi\right)$$

where A is migration amplitude and the period is assumed to be one day (86,400 seconds). The value of the phase (ϕ) depends on the initial location of colonies. For example, if $t = 0$ in the simulation corresponds to midnight and colonies are assumed to be at the bottom at that time, the value is $\pi/2$ with positive velocity corresponding to downward movement.

The velocity function can also be dependent on space as well as time, as in Belov and Giles (1997):

$$v_p(t,z) = \begin{cases} A \frac{2\pi}{86,400\,s} cos\left(\frac{2\pi}{86,400\,s}t + \phi\right)e^{-\alpha(H-z)}, & I_0 > 0 \\ A \frac{2\pi}{86,400\,s} cos\left(\frac{2\pi}{86,400\,s}t + \phi\right), & I_0 \leq 0 \end{cases}$$

where, α is the light attenuation coefficient and I_0 is solar irradiance at the water surface, H is a user supplied depth parameter. The addition of the exponential term gives colonies deeper in the water column higher speeds and responds to variations in water clarity when the light attenuation coefficient, α, is variable. The exponential term is only applied during the photoperiod so that the effects of water clarity are only included when there is sunlight present.

Dynamic Velocity

The predefined velocity approach can predict cyanobacteria movement based on the observed tendency of colonies to migrate vertically on a daily cycle; however, it does not reflect the response of colonies to variations in solar irradiance. In order to capture this natural behavior, a model of colony velocity based on relationships between sunlight and cyanobacteria growth and colony density was also tested. Using this approach, the change in cyanobacteria colony density was computed based on the solar irradiance in the model grid cell. This density was then used to solve for the colony's settling velocity via Stokes' law:

$$v = \frac{2gr^2(\rho_c - \rho')}{9\phi n}$$

where g is acceleration due to gravity, r is colony radius, ρ_c is cyanobacteria density, ρ' is density of water, ϕ is form resistance, and n is viscosity of water.

The approach to modeling light-dependent density change was based on models developed by Kromkamp and Walsby (1990) and Visser et al. (1997) in which density increase was modeled using equations similar

to growth kinetic equations with additional calibration coefficients. Kromkamp and Walsby (1990) used a Monod type equation to model density increase with light and a linear relationship was used to model density decrease in the absence of light. Visser et al. (1997) modeled density increase using an exponential term which accounts for photoinhibition and density decrease with a linear term. In the buoyancy model described here, density change was assumed to follow a response to light similar to algal growth kinetics, including photoinhibition:

$$\frac{\partial \rho_c}{\partial t} = c_1 F(I) - c_2$$

where c_1 and c_2 are calibration coefficients. In the absence of light, density decreases at a constant rate. The numerical solution for the above equation is:

$$\rho_{c_i}^{n+1} = (c_1 F(I_i^n) - c_2)\Delta t + \rho_{c_i}^n$$

where Δt is the model timestep.

The function of light, $F(I)$, must account for variations in light intensity over the depth of a model grid cell due to light attenuation with depth. The integral of light over the grid cell is (Chapra, 2008):

$$F(I) = \frac{e}{\alpha \Delta z}[e^{-\gamma_2} - e^{-\gamma_1}]$$

where

$$\gamma_1 = \frac{(1-\beta)I_0}{I_s} e^{-\alpha(i-1)\Delta z}$$

$$\gamma_2 = \frac{(1-\beta)I_0}{I_s} e^{-\alpha(i)\Delta z}$$

where β is the fraction of solar irradiance absorbed at the water surface and α is the light attenuation coefficient (TVA, 1972). The height of the model grid cell is given by Δz, I_0 is irradiance at the water surface, and I_s is the saturating light intensity for the cyanobacteria species.

While the above equations account for changes in colony density due to instantaneous solar irradiance, they do not include information about past growth rates. To address this, an exponentially-decaying weighted average of past growth rates in each grid cell was applied as:

$$\rho_{c_i}^{n+1} = \frac{\sum_{q=-1}^{Q} \rho_{c_i}^{n-q} W^q}{\sum_{q=-1}^{Q} W^q}$$

where the past densities in the grid cell i are multiplied by a weight W and summed. The total number of timesteps over which to average past densities is given by Q. The weight decreases exponentially with time before the present, so that densities predicted at more recent timesteps have greater weights, i.e.:

$$W^q = e^{-k(t^{n+1} - t^{n-q})}$$

where k is the time decay constant for influence of past densities. This is similar to the approach taken by Serizawa et al. (2008).

In the dynamic velocity model, colonies were assumed to have a minimum and maximum allowable density (ρ_{min} and ρ_{max}, respectively) as well as a constant radius based on values found in field studies (Table 12). When predicted densities were greater than the maximum or less than the minimum allowed values, the value was set to ρ_{max} or ρ_{min}, respectively. It was also necessary to define initial densities (ρ_0) for all colonies within a grid cell. Initial colony density, ρ_{0_i} was assumed to vary exponentially from the surface to the bed, following a similar pattern to light decay with depth, as:

$$\rho_{0_i} = \rho_{0_S} + (\rho_{0_B} - \rho_{0_S})(1 - e^{-z_i})$$

where ρ_{0_S} is the initial colony density at the surface and ρ_{0_B} is the initial colony density at the bed.

Table 12. Literature values for biological parameters of cyanobacteria used in models.

Study	Identifier	Minimum density, $kg\ m^{-3}$	Maximum density, $kg\ m^{-3}$	Colony radius, μm	Saturating light intensity, $W\ m^{-2}$
Reynolds (1984)	Cyanobacteria	-	-	25-1000	-
Reynolds et al. (1987)	*M. aeruginosa*	985	1005	120-3200	-
	A. flos-aqua	920	1030	28-100	-
	P, agardhii	985	1085	13.7-18.3	-
Nakamura et al. (1993)	*Microcystis* sp.	-	-	10-300	-
Visser et al. (1997)	*Microcystis* sp.	-	-	-	139
Long et al. (2001)	*M. aeruginosa*	-	-	-	-
Wu and Song (2008)	*M. aeruginosa*	-	-	-	119-244
Wu et al. (2009)	*M. aeruginosa*	-	-	-	65-119
Zhang et al. (2011)	*M. aeruginosa*	-	-	-	75-392
Zhu et al. (2014, 2018)	*Microcystis* sp.	967	997	10-350	-
Rowe et al. (2016)	*Microcystis* sp.	-	-	12.5-370, median: 58.5	-

Algae toxin production

This section is taken from Garstecki (2021) who analyzed modeling cyanotoxin production and fate and transport.

Cyanobacteria are known to produce toxins that can affect water quality in a surface waterbody. But not all genera or species produce toxins. The conceptual model for those species that produce cyanotoxin is shown in Figure 86. The model considers both intracellular and extracellular toxins.
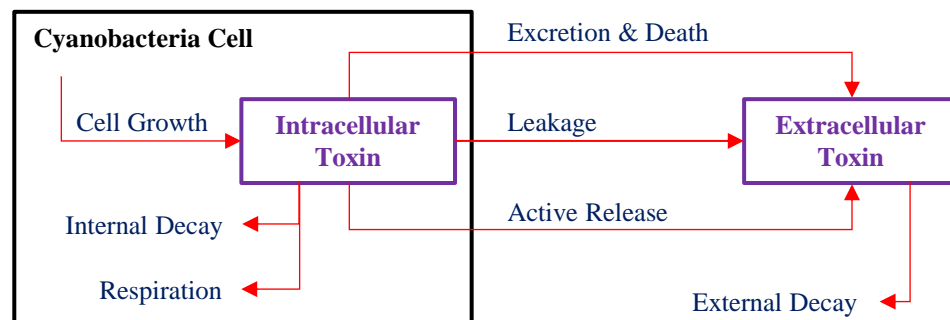
Figure 86. Sources and sinks of the intracellular and extracellular toxins.

The four main toxins used in the model are summarized in Table 13.

Table 13. Main toxins simulated.

	Microcystin (MC)	**Cylindrospermop-sin (CYN)**	**Anatoxin-a (ATX)**	**Saxitoxin (STX)**
Type	Hepatotoxin (liver)	Cytotoxin (several organs)	Neurotoxin (nervous system)	
Toxin Presence	Mostly exist as in-tracellular toxins Extracellular toxins (< 30% of total MC concentrations) Water-soluble and stable	Mostly exist as ex-tracellular toxins (dissolved) Very water-soluble Active release or leaking from cells likely Stable at low light levels	Highly water-soluble Unstable at pH higher than 10 Extracellular mainly through cell lysis Stable at low light levels	Paralytic shellfish tox-ins (accumulate in shellfish) pH and sodium con-centrations affect pro-duction (different re-sponse from different species)
Degrada-tion	Photodegradation (<2 weeks) Biodegradation by bacteria (adsorbed onto sediment)	Photodegradation (half-life of 20 days) UV (half-life of 18 hours)	Biodegradation by bacteria (half-life of 5 days) Basic pH levels (half-life of 14 days)	Natural waters (half-life of 9-28 days) High temperatures de-crease half-life Degradation can lead to toxic variants

Typical health guidelines for these toxins in the State of Oregon are shown in Table 14.

Table 14. Oregon Health Authority Advisory Toxin Levels (Oregon Health Authority, 2020a, 2020b).

	MC	**CYN**	**ATX-a**	**STX**	**Units**	**Notes**
OHA Recreational Use Values	4	8	8	4	µg L^{-1}	Everyone
OHA Drinking Water Guidance Values	1.6	3	3	1.6	µg L^{-1}	Adults
	0.3	0.7	0.7	0.3	µg L^{-1}	Ages 5 years and younger

1. Units for STX are in saxitoxin equivalents: µg STX-eq L^{-1}
2. Advisory levels were provided for all four toxins in 2018, but only MC and CYN in drinking water are regulated under current rules.

The intracellular and extracellular toxin equations used in Ce-QUAl-W2 are shown below:

$$C_{intra} = \sum_{i=1}^{n\ algal\ groups} (CTP) * \Phi_a * \beta \qquad \textbf{(4-96)}$$

$$\frac{dC_{extra}}{dt} = K_{am} * \Phi_a * \beta * (CTP) + k_{release} * C_{intra} - k_{decay} * C_{extra} \qquad \textbf{(4-97)}$$

The intracellular toxin is calculated based only on the concentration of algae present in a model cell and the fraction of algae producing that toxin. The intracellular concentration is summed for all the algal groups that produce that toxin. There are no decay or other rates associated with the intracellular toxin

concentration. The extracellular rate equation is only a function of the death rate of algae, the release rate of intracellular toxin and the extracellular decay. Only one value is allowed for the release rate and decay rate for each toxin being modeled.

Each of the four toxins (microcystin, cylindrospermopsin, anatoxin-a, and saxitoxin) have been added as state variables to the CE-QUAL-W2 code with the option to turn any of them "on" or "off" depending on the cyanobacteria species that grow in the waterbody of interest. Table 15 lists suggested ranges of values to use for each parameter based on literature values and model tests.

Table 15. Model parameter ranges to use in CE-QUAL-W2 toxin model.

Parameter	MC	CYN	ATX-A	STX
CTP, fraction of algae concentration producing toxin	Waterbody dependent, determined by species present			
CTB, ratio of intracellular toxin to dry weight biomass (mg-toxin mg-DW^{-1}) where DW, dry weight	0.0005-0.024	0.0005-0.007	0.001-0.01	0.001-0.004
CTR, release rate day^{-1}	Approx. equal to 0-1 times excretion rate	Approx. equal to 1-2 times excretion rate	Approx. equal to 0-1 times excretion rate	Approx. equal to 0-1 times excretion rate
CTD, extracellular decay rate, day^{-1}	0.05-0.2	0.01-0.06	0.05-0.2	0.01-0.07

Periphyton/Epiphyton

Any number of user defined periphyton/epiphyton groups can be modeled. Similar to the 1st order sediment compartment, periphyton/epiphyton are not transported in the water column.
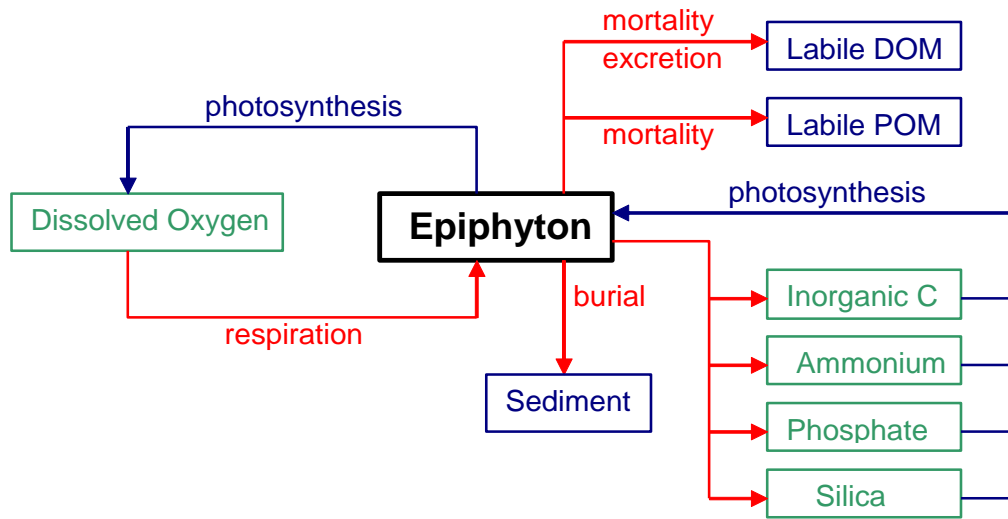
Figure 87. Internal flux between epiphyton and other compartments.

Referring to **Figure 87**, the rate equation for each epiphyton/periphyton group is:

$$S_e = \underbrace{K_{eg}\Phi_e}_{growth} - \underbrace{K_{er}\Phi_e}_{respiration} - \underbrace{K_{ee}\Phi_e}_{excretion} - \underbrace{K_{em}\Phi_e}_{mortality} - \underbrace{K_{eb}\Phi_e}_{burial} \tag{4-98}$$

where:

    K_{eg} = epiphyton growth rate, sec^{-1}
    K_{er} = epiphyton dark respiration rate, sec^{-1}
    K_{ee} = epiphyton excretion rate, sec^{-1}
    K_{em} = epiphyton mortality rate, sec^{-1}
    K_{eb} = epiphyton burial rate, sec^{-1}
    Φ_e = epiphyton concentration, $g\ m^{-3}$

Epiphyton/periphyton growth rate is computed by modifying a maximum growth rate affected by epiphyton/periphyton biomass, temperature, and nutrient availability:

$$K_{eg} = \gamma_{er}\gamma_{ef}\lambda_{min}K_{eg\ max} \tag{4-99}$$

where:

    γ_{er} = temperature rate multiplier for rising limb of curve
    γ_{ef} = temperature rate multiplier for falling limb of curve
    λ_{min} = multiplier for limiting growth factor (minimum of phosphorus, silica, nitrogen, and epiphyton/periphyton biomass) between 0 and 1
    K_{eg} = epiphyton/periphyton growth rate, sec^{-1}
    K_{egmax} = maximum epiphyton/periphyton growth rate, sec^{-1}

Rate multipliers for epiphyton/periphyton growth are computed based upon available light, phosphorus, nitrogen, silica, and epiphyton biomass. Epiphyton/periphyton biomass is included as a surrogate for light limited epiphyton/periphyton self-shading and will be discussed in greater detail below.

The rate multiplier for light is based upon the Steele (1962) function:

$$\lambda_l = F(I) = \frac{I}{I_s} e^{-\frac{I}{I_s}+1} \tag{4-100}$$

where:

    I = available light, $W\ m^{-2}$

    I_s = saturating light intensity at maximum photosynthetic rate, $W\ m^{-2}$

    λ_l = light limiting factor or F(I)

The above expression allows for simulation of photoinhibition at light intensities greater than the saturation value. However, light penetration decreases with depth:

$$I(z) = (1-\beta)I_0 e^{-\alpha z} \tag{4-101}$$

where:

    I_0 = solar radiation at the water surface, $W\ m^{-2}$

    α = attenuation coefficient, m^{-2}

    z = depth, m

    β = fraction of solar radiation absorbed at the water surface

The average effect of light on epiphyton/periphyton growth in a model cell can be obtained by combining the above two expressions and integrating over the cell depth to obtain (Chapra and Reckhow, 1983):

$$\lambda_l = \frac{e}{\alpha \Delta z}[e^{-\gamma_2} - e^{-\gamma_1}] \tag{4-102}$$

where:

$$\gamma_1 = \frac{(1-\beta)I_o e^{-\alpha d}}{I_s}$$

$$\gamma_2 = \frac{(1-\beta)I_o e^{-\alpha(d+\Delta z)}}{I_s}$$

d =depth at the top of computational cell, *m.*

The attenuation coefficient, λ, is computed from a baseline value **[EXH2O]** to which the effects of inorganic **[EXINOR]** and organic **[EXORG]** suspended solids, as well as the extinction of each algal group, are added. Epiphyton/periphyton self-shading are accounted for in the biomass limitation formulation.

Rate multipliers limiting epiphyton growth due to nutrient limitations are computed using the Monod relationship:

$$\lambda_i = \frac{\Phi_i}{P_i + \Phi_i} \tag{4-103}$$

where:

    λ_i = phosphorus or nitrate + ammonium concentration, $g\ m^{-3}$

    P_i = half-saturation coefficient for phosphorus or nitrate + ammonium, $g\ m^{-3}$

The epiphyton/periphyton preference for ammonium can be modeled using the following (Thomann and Fitzpatrick, 1982):

$$P_{NH4} = \Phi_{NH4} \frac{\Phi_{NOx}}{(K_{NH4}+\Phi_{NH4})(K_{NH4}+\Phi_{NOx})} + \Phi_{NH4} \frac{K_{NH4}}{(\Phi_{NH4}+\Phi_{NOx})(K_{NH4}+\Phi_{NOx})}$$ (4-104)

P_{NH4} = ammonium preference factor
K_{NH4} = ammonia preference half-saturation coefficient, $g\ m^{-3}$
Φ_{NH4} = ammonium concentration, $g\ m^{-3}$
Φ_{NOx} = nitrate-nitrite concentration, $g\ m^{-3}$

Epiphyton/periphyton dark respiration is computed using the rising limb of the temperature function:

$$K_{er} = \gamma_{er}\gamma_{ef}K_{er\ max}$$ (4-105)

where:

γ_{er} = temperature rate multiplier for rising limb of the curve
γ_{er} = temperature rate multiplier for falling limb of the curve
K_{armax} = maximum dark respiration rate, sec^{-1}

Epiphyton/periphyton excretion is evaluated using an inverse relation to the light rate multiplier:

$$K_{ee} = (1 - \lambda_l)\gamma_{er}\gamma_{ef}K_{ee\max}$$ (4-106)

where:

λ_l = light limiting factor
γ_{er} = temperature rate multiplier for rising limb of the curve
γ_{er} = temperature rate multiplier for falling limb of the curve
K_{eemax} = maximum excretion rate constant, sec^{-1}

Excretion rates increase at both low and high light intensities, with excretion products contributing to labile DOM.

Epiphyton/periphyton mortality is defined as:

$$K_{em} = \gamma_{er}\gamma_{ef}K_{em\ max}$$ (4-107)

where:

γ_{er} = temperature rate multiplier for rising limb of the curve
γ_{er} = temperature rate multiplier for falling limb of the curve
K_{emmax} = maximum mortality rate, sec^{-1}

This mortality rate represents both natural and predator mortality. Epiphyton/periphyton growth does not occur in the absence of light. Epiphyton/periphyton growth is not allowed to exceed the limit imposed by nutrient supply over a given timestep. Epiphyton/periphyton excretion is not allowed to exceed epiphyton/periphyton growth rates.

The epiphyton/periphyton burial rate represents the burial of dead epiphyton/periphyton to the organic sediment compartment. The epiphyton/periphyton become part of the 1st-order sediment compartment. Epiphyton/periphyton though that die (mortality) become a part of the labile particulate organic matter and the labile dissolved organic matter pool. The user defines the fraction of the dead epiphyton (EPOM) that goes to the LPOM pool. This POM is then transported in the water column. Currently, there is no sloughing of epiphyton/periphyton into the water column as a function of velocity shear. This is a function of the biomass limitation term.

The burial of periphyton organic matter goes into first order sediment which is tied to the sediment diagenesis model
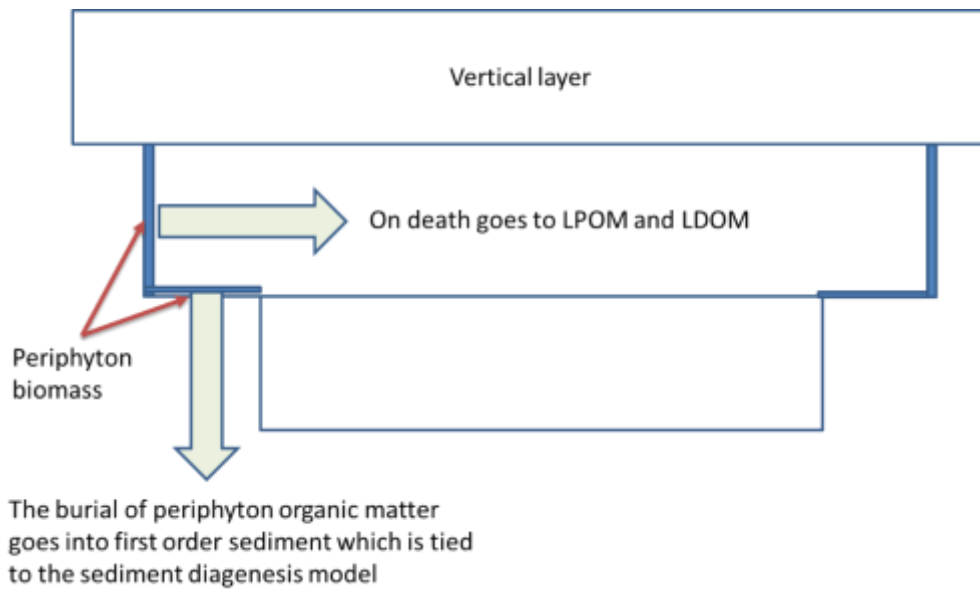
Figure 88. How epiphyton/periphyton transfer organic matter to the water column at death and to the sediment during burial.

The epiphyton/periphyton biomass is controlled by a biomass limitation equation based on Monod kinetics. The biomass limitation function, f [BLIM], varies from 0 to 1 and is multiplied with the growth rate. This function is defined as

$$f = \left[1 - \frac{B}{B+K_B} \right]$$ **(4-108)**

where:

  B = epiphyton areal biomass, g/m^2 [**EPD**]
  K_b = epiphyton areal biomass half-saturation coefficient, g/m^2 [**EHS**]

The areal biomass is calculated as $B = \Phi_e \frac{V}{A}$ **(4-109)**

where:

  A = computational cell surface area including side walls and bottom area, m^2
  V = computational cell volume, m^3
  Φ_e = epiphyton concentration, $g\ m^{-3}$

The biomass limitation is a surrogate calibration parameter for light limitation due to self-shading.

Macrophytes

The macrophyte model consists of two parts: a section describing the water quality compartment and a section describing the hydrodynamic compartment. Bother of these sections are from Berger (2000) and Berger and Wells (2008). Chris Berger is the primary author of this section.

The macrophyte model was designed to simulate multiple submerged macrophyte species. It does not differentiate between plant parts. The nutrient fluxes for the water quality component of the macrophyte

compartment are shown in Figure 89. Light, temperature, carbon dioxide, ammonia-nitrogen (only ammo-nia is used as a N source for macrophytes), and ortho-phosphorus may limit growth. Depending on the macrophyte species, nitrogen and phosphorus may be obtained from the sediments or the water column. If they are obtained from the sediments, the sediments are assumed to be an infinite pool that cannot limit growth. Plants grow upwards from the sediment through model layers. Growth upward is accomplished by moving the growth of a layer to the layer above if the concentration in the layer is greater than a threshold concentration and the concentration in the upper layer is less than the same threshold concentration. Mac-rophyte shading is modeled by making light attenuation a function of macrophyte concentration.
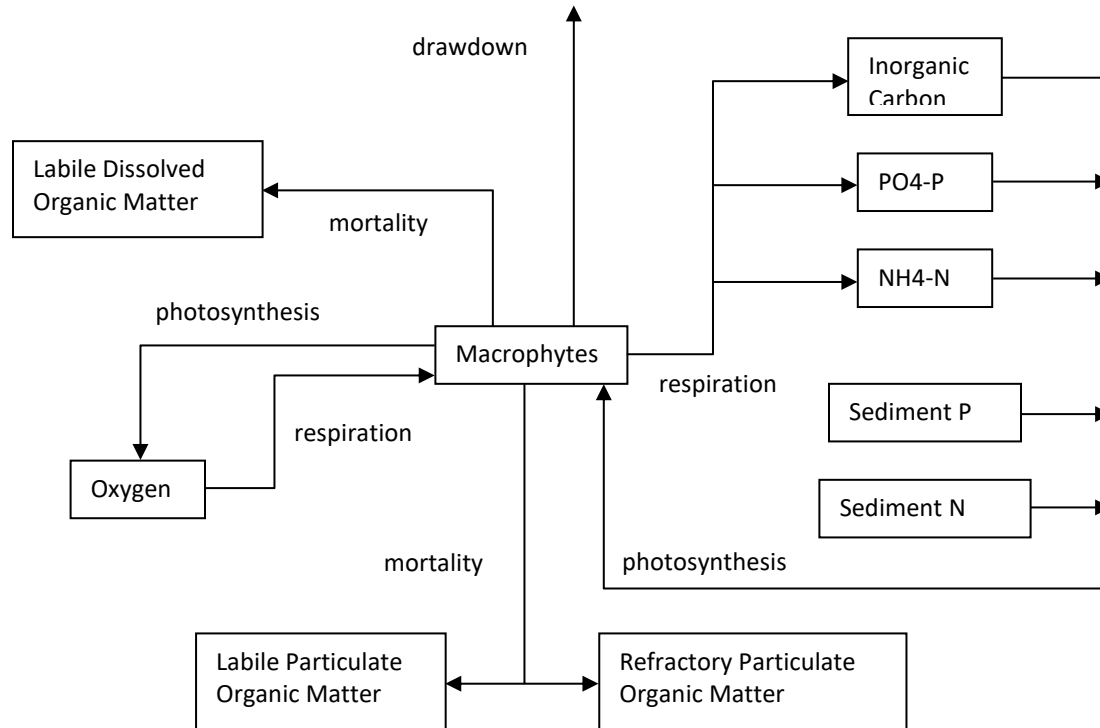
Figure 89. Nutrient fluxes for the macrophyte compartment in CE-QUAL-W2.

The macrophyte growth rate is modeled as follows:

$$S_{macro} = \mu_{mmax}\underbrace{f(I,N,P,C)\gamma_1\gamma_2\Phi_{macro}}_{growth} - \underbrace{K_{mr}\gamma_1\Phi_{macro}}_{respiration} - \underbrace{K_{mm}\Phi_{macro}}_{mortality} \qquad \textbf{(4-110)}$$

where:
S_{macro}: macrophyte growth rate density (g/m^3/s)
I : solar radiation (W/m^2)
$f(I,N,P,C)$: Growth limiting function between 0 and 1
$\mu_{m\,max}$: maximum macrophyte growth rate (input unit: d^{-1}; internal calculation unit: s^{-1})
K$_{mr}$: maximum respiration rate (input unit: d^{-1}; internal calculation unit: s^{-1})
K$_{mm}$: mortality/excretion rate (input unit: d^{-1}; internal calculation unit: s^{-1})
γ_1: ascending temperature rate multiplier

KINETICS

γ_2: descending temperature rate multiplier
γ_1: growth limiting factor due to photosynthesis
Φ_{macro}: macrophyte concentration (g/m³)

Growth rate, respiration rate, and mortality/excretion rate are temperature dependent. Temperature effects are modeled using the equations developed by Thornton and Lessem (1978) which are currently used in the phytoplankton compartment of CE-QUAL-W2. The growth limiting function f(I,N,P,C) is the minimum of the light f(I), nitrogen f(N), phosphorus f(P), and carbon f(C) limiting functions such that $f(I, N, P, C) = minimum(f(I), f(N), f(P), f(C))$.

All the limiting functions are unit-less and have a value between 0 and 1. The limiting functions for the nutrients have the following Michaelis-Menten form

$$f(S) = \frac{S}{K_S + S}$$
(4-111)

where S (mg/l) is the nutrient concentration and K_s (mg/l) is the half-saturation concentration. Light limitation was modeled with a hyperbolic equation which as the same form as the Michaelis-Menten function:

$$f(I) = \frac{I}{I + I_h}$$
(4-112)

where I: solar radiation (W/m²), I_h: half-saturation coefficient for solar radiation (W/m²). This function is frequently used in the absence of photo-inhibition (Carr et al., 1997).

The net light extinction coefficient γ (m⁻¹) was modeled as a function of macrophyte plant tissue concentration giving

$$\gamma = \varepsilon_{H_2O} + \varepsilon_{iss}\Phi_{iss} + \varepsilon_{oss}\Phi_{oss} + \sum_{\substack{\text{of} \\ \text{macrophyte} \\ \text{groups}}} \varepsilon_{mac}\Phi_{mac} + \sum_{\substack{\text{of} \\ \text{algae} \\ \text{groups}}} \varepsilon_{alg\,ae}\Phi_{alg\,ae}$$
(4-113)

where:
ε_{H_2O} = light extinction exclusive of suspended solids, m⁻¹
ε_{iss} = light extinction due to inorganic suspended solids, m³ m⁻¹ g⁻¹
ε_{oss} = light extinction due to non-living organic suspended solids, m³ m⁻¹ g⁻¹
ε_{mac} = light extinction due to macrophytes, m³ m⁻¹ g⁻¹
$\varepsilon_{alg\,ae}$ = light extinction due to algae, m³ m⁻¹ g⁻¹
Φ_{iss} = inorganic suspended solids concentration, g m⁻³
Φ_{oss} = organic suspended solids concentration, g m⁻³
Φ_{mac} = macrophyte plant tissue concentration, g m⁻³
$\Phi_{alg\,ae}$ = algae concentration, g m⁻³

Modeling of flow through macrophytes incorporated the following concepts:

- Porosity of the macrophytes was calculated through determination of the blockage area of the vegetation normal to the direction of flow
- The drag of individual stems and leaves were totaled to determine the total drag force in a model cell
- The effective Mannings n was calculated by combining the effect of bed shear and the drag force on the plants

Modeling Frictional Force

The total frictional force f was partitioned into a bottom friction component f_b and a vegetation drag component f_v giving

$$f = f_b + f_v \qquad\qquad\qquad \textbf{(4-114)}$$

Bottom shear τ_b was simulated using Manning's friction factor

$$\tau_b = \frac{\rho_w g n^2}{R^{1/3}} U|U| \qquad\qquad\qquad \textbf{(4-115)}$$

where:

ρ_w: density of water
g: gravitational constant
U: water velocity
R: hydraulic radius
n: Manning's friction factor.

The Columbia Slough model has already been calibrated for the no macrophytes condition. Manning's friction factor for the model segments was typically around 0.03.

Vegetative drag caused by macrophytes was modeled in a manner similar to that used by Petryk and Bosmajian (1975) where the drag force D_i on the ith plant is

$$D_i = C_d A_i \left(\frac{\rho_w U^2}{2} \right)$$

where:
A_i: area of plant projected normal to the direction of flow
C_d: drag coefficient.

The total drag force in a model cell due to vegetation is

$$\sum D_i = C_d \left(\frac{\rho_w U^2}{2} \right) \sum A_i$$

The total plant area normal to the direction of flow $\sum A_i$ was estimated using biomass to surface area ratios from Sher-Kaul et al. (1995) and surface area to volume ratios from Sand-Jensen and Borum (1991). The projected area normal to flow would then be $\varepsilon \sum A_i$ and the total drag was then

$$\sum D_i = C_d \left(\frac{\rho_w U^2}{2} \right) \sum A_i$$

The drag coefficient C_d was a calibration parameter but has been shown to be of the order of 1.0 for vegetation (Hsi and Nath, 1968; Hoerner, 1965; Petryk, 1969).

The effective Mannings n of each model cell was calculated in the manner used by Petryk and Bosmajian (1975) with

$$n = n_b \sqrt{1 + \frac{C_d \sum A_i}{2gAL} \frac{1}{n_b^2} R^{4/3}} \qquad\qquad\qquad \textbf{(4-116)}$$

where
n_b: Mannings friction factor due to bed shear only.

This derivation is shown in more detail in Berger and Wells (2008).

$$\frac{\partial U\varphi B}{\partial x} + \frac{\partial W\varphi B}{\partial z} = q\varphi B \tag{4-120}$$

where:
q - lateral inflow/outflow per unit volume (T^{-1}).

The new free water surface equation is

$$\frac{\partial B_\eta \varphi \eta}{\partial t} = \frac{\partial}{\partial x}\int_\eta^h U\varphi B dz - \int_\eta^h q\varphi B dz \tag{4-121}$$

with
B_η – time and spatially varying surface width, meters
η - free water surface elevation, meters

The constituent transport equation could also be affected by the reduction of cross-sectional area due to macrophytes giving

$$\frac{\partial \varphi BC}{\partial t} + \frac{\partial U\varphi BC}{\partial x} + \frac{\partial W\varphi BC}{\partial z} - \frac{\partial}{\partial x}\varphi BD_x\frac{\partial C}{\partial x} - \frac{\partial}{\partial z}\varphi BD_z\frac{\partial C}{\partial z} = q_\varphi \varphi B + S_K\varphi B \tag{4-122}$$

where:
C - constituent concentration, mg/l
D_x- longitudinal temperature and constituent dispersion coefficient, m^2/sec
D_z- vertical temperature and constituent dispersion coefficient, m^2/sec
q_φ- lateral inflow or outflow mass flow rate of constituent per unit volume, mg/l/sec
S_K- kinetics source/sink term for constituent concentration, mg/l/sec

The parameter coefficients used in the first application of this model to the Columbia Slough are shown below in Table 16. Descriptions of the input data fields are included in Part 3 of the User Manual.

Table 16. Parameters and values used for macrophytes in the Columbia Slough model.

Variable name in input data file	CE-QUAL-W2 Model value	Coefficient definition (units)
PRNMC	ON or OFF	Macrophyte snapshot output on or off
MACROC	ON or OFF	Macrophyte compartment on or off
EXM	0.01	Light extinction coefficient for organic particles (m/mg/l)
MBMP	40.0	Threshold macrophyte concentration for which growth is moved to the above layer (mg/l)
MMAX	500.0	Maximum macrophyte concentration (mg/l)
MG	0.30	Maximum macrophyte growth rate (day^{-1})
MR	0.05	Macrophyte respiration rate (day^{-1})
MM	0.05	Macrophyte mortality rate (day^{-1})
SATM	20.0	Macrophyte half-saturation light intensity at the maximum photosynthetic rate (Watts/m^2)
MT1	7	Lower temperature bound for macrophyte growth (Celsius)
MT2	15	Lowest temperature at which macrophyte growth processes are near the maximum rate (Celsius)

Variable name in input data file	CE-QUAL-W2 Model value	Coefficient definition (units)
MT3	24	Upper temperature at which macrophyte growth processes are near the maximum rate (Celsius)
MT4	34	Upper lethal temperature for macrophytes(Celsius)
MK1	0.1	Temperature rate multiplier for MT1
MK2	0.99	Temperature rate multiplier for MT2
MK3	0.99	Temperature rate multiplier for MT3
MK4	0.01	Temperature rate multiplier for MT4
MPOM	0.9	Fraction of dead macrophytes which becomes POM, the fraction (1-MPOM) becomes labile DOM
LRPMAC	0.2	Fraction of POM which originates as dead macrophytes becoming labile POM
PSED	0.5	Fraction of phosphorus uptake by macrophytes obtained from sediments
NSED	0.5	Fraction of nitrogen uptake by macrophytes obtained from sediments
MHSP	0	Half-saturation constant for P uptake by macrophytes (mg/l)
MHSN	0	Half-saturation constant for N uptake by macrophytes (mg/l)
MHSC	10	Half-saturation constant for carbon uptake by macrophytes (mg/l)
MACP	0.005	Stoichiometric equivalent between macrophyte biomass and orthophosphate
MACN	0.08	Stoichiometric equivalent between macrophyte biomass and nitrogen
MACC	0.45	Stoichiometric equivalent between macrophyte biomass and carbon
02MR	1.1	Dissolved oxygen requirement for macrophyte respiration
02MG	2.0	Stoichiometric equivalent for dissolved oxygen production during macrophyte photosynthesis
CD	3.0	Macrophyte drag coefficient

Zooplankton

A multiple zooplankton compartment was adapted from the U.S. Army Corps of Engineers reservoir model CE-QUAL-R1 (Environmental Laboratory, 1995) for the CE-QUAL-W2 model. Zooplankton are assumed to be non-motile and are transported only by advection and dispersion. Zooplankton can graze algae, detritus (POM), and other zooplankton. Losses occur through mortality and respiration. There is also the possibility of algae vertical settling or floating by setting a settling velocity. There is also the ability to allow dynamic vertical migration. The source/sink term for zooplankton is shown below:

$$S_{zoo} = \underbrace{\gamma_1 \gamma_2 Z_e K_{zmax} \left(\frac{\left(\sum \sigma_{alg} \Phi_a + \sigma_{pom} \Phi_{lpom} + \sum \sigma_{zoo} \Phi_{zoo} \right) - Z_L}{\left(\sum \sigma_{alg} \Phi_a + \sigma_{pom} \Phi_{lpom} + \sum \sigma_{zoo} \Phi_{zoo} \right) + Z_{1/2}} \right) \Phi_{zoo}}_{growth} - \underbrace{(1 - \gamma_2) K_{zm} \Phi_{zoo}}_{mortality}$$

$$- \underbrace{\gamma_1 K_{zr} \Phi_{zoo}}_{respiration} - \underbrace{\omega_{zoo} \frac{\partial \Phi_{zoo}}{\partial z}}_{settling}$$

where:

Φ_{lpom} = Labile particulate organic matter concentration (mg/l)

Φ_{rpom} = Refractory particulate organic matter concentration(mg/l)

Φ_a = Algae concentration (mg/l)

Φ_{zoo} = Zooplankton concentration (mg/l)

K_{zm} = Zooplankton mortality rate (input unit: d^{-1}; internal calculation unit: s^{-1})

K_{zmax}= Maximum ingestion rate for zooplankton (input unit: d^{-1}; internal calculation unit: s^{-1})

K_{zr} = Zooplankton respiration rate (input unit: d^{-1}; internal calculation unit: s^{-1})

$Z_{1/2}$ = Half-saturation coefficient for zooplankton ingestion (mg/l)

Z_e = Zooplankton ingestion efficiency

Z_L = Low threshold concentration for zooplankton feeding (mg/l)

γ_1 = Temperature coefficient for rising limb of curve for zooplankton

γ_2 = Temperature coefficient for falling limb of curve for zooplankton

σ_{alg} = Zooplankton preference fraction for algae

σ_{zoo} = Zooplankton preference fraction for zooplankton

σ_{pom} = Zooplankton preference fraction for particulate organic matter

ω_{zoo} = zooplankton settling velocity

The zooplankton source/sinks are also illustrated in Figure 90. The growth rate is a function of temperature, the maximum growth rate, and a modified Michaelis-Menten equation which includes a low threshold concentration below which zooplankton do not feed. At dissolved oxygen concentrations below 2 mg/l feeding stops, and the mortality rate is doubled. The zooplankton model coefficients described in Table 17.
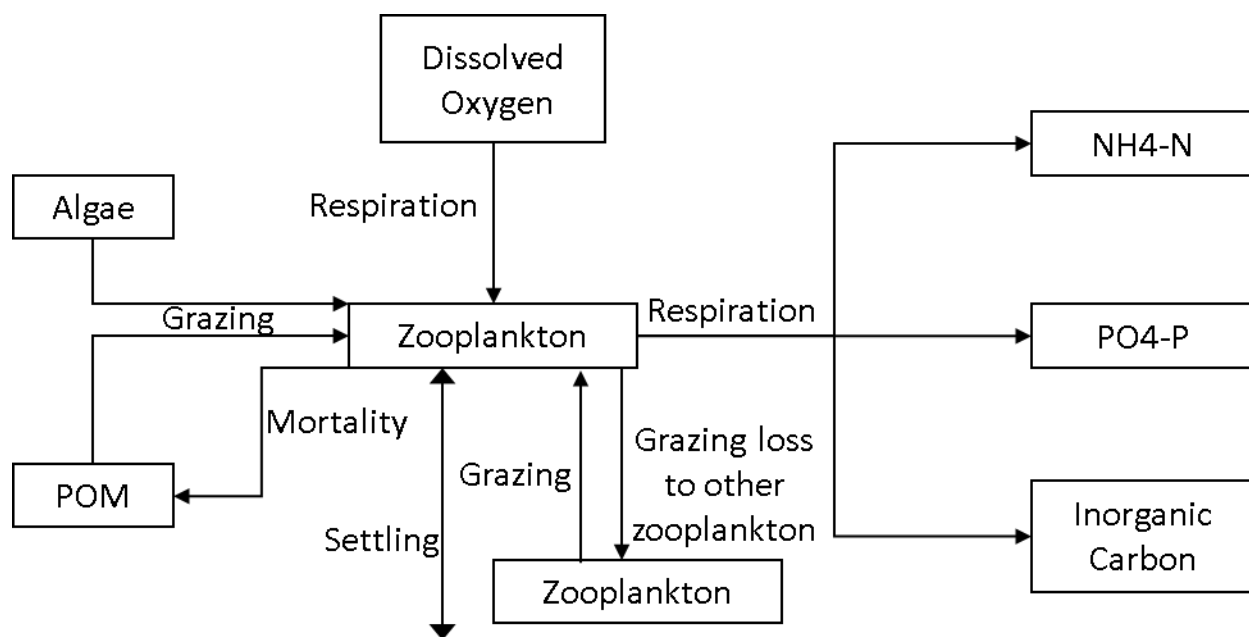
Figure 90. Zooplankton source/sinks.

Table 17. Parameters used in the zooplankton model.

Name	Description
ZMAX	Maximum ingestion rate for zooplankton (1/day input by user, 1/sec internal units)
ZMORT	Maximum nonpredatory mortality rate for zooplankton (1/day input by user, 1/sec internal units).
ZEFFIC	Zooplankton assimilation efficiency or the proportion of food assimilated to food consumed (dimensionless).
PREFA	Preference factor of zooplankton for algae (dimensionless).
PREFP	Preference factor of zooplankton for detritus (dimensionless).

KINETICS

Name	Description
ZRESP	Maximum zooplankton respiration rate (1/day input by user, 1/sec internal units).
ZOOMIN	Threshold food concentration at which zooplankton feeding begins (mg/l).
ZS2P	Zooplankton half-saturation constant for food concentration (mg/l)
ZS	Zooplankton settling velocity (m/day)
ZOOT1	Lower temperature for zooplankton growth (Celsius)
ZOOT2	Lower temperature for maximum zooplankton growth (Celsius)
ZOOT3	Upper temperature for maximum zooplankton growth (Celsius)
ZOOT4	Upper temperature for zooplankton growth (Celsius)
ZOOK1	Fraction of zooplankton growth rate at ZOOT1 (dimensionless)
ZOOK2	Fraction of zooplankton growth rate at ZOOT2 (dimensionless)
ZOOK3	Fraction of zooplankton growth rate at ZOOT3 (dimensionless)
ZOOK4	Fraction of zooplankton growth rate at ZOOT4 (dimensionless)
EXZ	Zooplankton light extinction (m^{-1})
O2ZR	Oxygen stoichiometry for zooplankton respiration
ZP	Stoichiometric equivalent between zooplankton biomass and phosphorus
ZN	Stoichiometric equivalent between zooplankton biomass and nitrogen
ZC	Stoichiometric equivalent between zooplankton biomass and carbon

Phosphorus

Phosphorus is an important element in aquatic ecosystems since it serves as one of the primary nutrients for phytoplankton growth. In many fresh waters, phosphorus is considered to be the nutrient limiting maximum production of phytoplankton biomass (Schindler, 1971; Schindler et al., 1973; Vollenweider, 1968, 1976).

Phosphorus is assumed to be completely available as ortho-phosphate (PO_4) for uptake by phytoplankton. Measurements of soluble reactive phosphorus are closest to the form used in the model. Macrophytes are specified as either taking P from the sediments or from the water column.
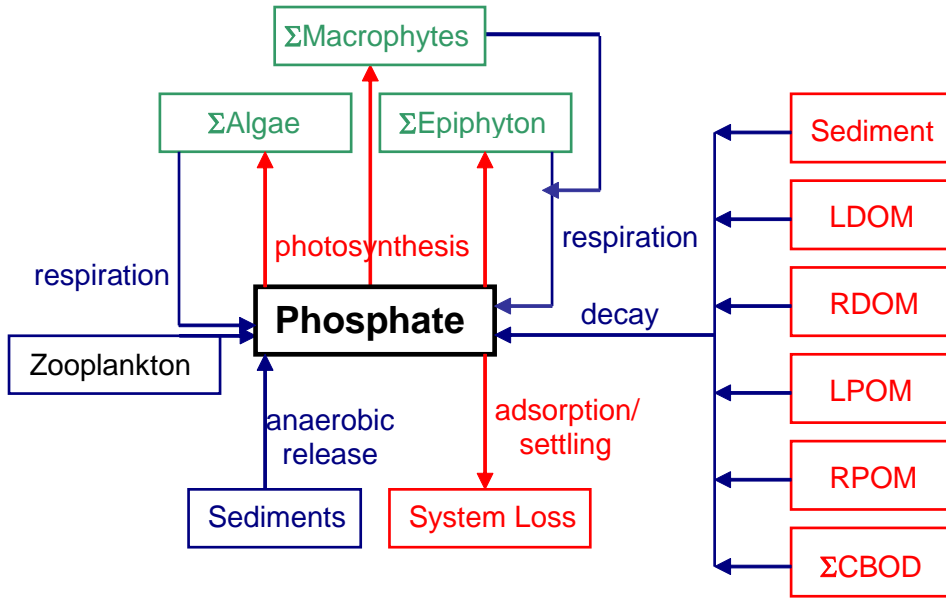
Figure 91. Internal flux between phosphorus and other compartments.

Referring to **Figure 91**, the rate equation for phosphorus is:

$$S_p = \sum(K_{ar} - K_{ag})\delta_{Pa}\Phi_a + \sum(K_{er} - K_{eg})\delta_{Pe}\Phi_e + K_{LDOM}\delta_{POM}\gamma_{OM}\Phi_{LDOM}$$

<div align="center">algal net growth   epiphyton net growth   labile DOM decay</div>

$$+ K_{RDOM}\delta_{POM}\gamma_{OM}\Phi_{RDOM} + K_{LPOM}\delta_{POM}\gamma_{OM}\Phi_{LPOM} + K_{RPOM}\delta_{POM}\gamma_{OM}\Phi_{RPOM}$$

<div align="center">refractory DOM decay   labile POM decay   refractory POM decay</div>

$$+ \sum K_{CBOD}R_{CBOD}\delta_{P-CBOD}\Theta^{T-20}\Phi_{CBOD} + K_s\delta_{POM}\gamma_{OM}\Phi_s + SOD\gamma_{OM}\frac{A_{sed}}{V}$$

<div align="center">CBOD decay   1st-order sediment release   0-order sediment release</div>

$$- \frac{(\sum\varpi_{ISS}\Phi_{ISS} + \omega_{Fe}\Phi_{Fe})P_P}{\Delta z}\Phi_P + \sum(K_{mr} - (1 - f_{psed})K_{mg})\delta_{Pm}\Phi_{macro} + \sum K_{zr}\delta_{Pz}\Phi_{zoo}$$

<div align="center">inorganic solids adsorption   macrophyte net growth   zooplankton respiration</div>

<div align="center">**(4-123)**</div>

where:
- Δz = model cell thickness, m
- A_{sed} = sediment surface area, m^2
- V = cell volume, m^3
- P_P = adsorption coefficient, $m^3\ g^{-1}$
- f_{psed} = fraction of macrophyte phosphorus uptake from sediments
- δ_{Pe} = periphyton/epiphyton stoichiometric coefficient for phosphorus
- δ_{Pa} = algal stoichiometric coefficient for phosphorus
- δ_{Pm} = macrophyte stoichiometric coefficient for phosphorus
- δ_{Pz} = zooplankton stoichiometric coefficient for phosphorus
- δ_{POM} = organic matter stoichiometric coefficient for phosphorus
- δ_{P-CBOD} = phosphorus/CBOD stoichiometric ratio
- γ_{OM} = temperature rate multiplier for organic matter decay
- Θ = temperature rate multiplier for CBOD decay

KINETICS

R_{BOD} = conversion ratio for 5-day CBOD to CBOD ultimate

ω_{ISS} = inorganic suspended solids settling velocity, $m\ sec^{-1}$

ω_{Fe} = particulate organic matter settling velocity, $m\ sec^{-1}$

K_{ag} = algal growth rate, sec^{-1}

K_{ar} = algal dark respiration rate, sec^{-1}

K_{eg} = periphyton/epiphyton growth rate, sec^{-1}

K_{er} = periphyton/epiphyton dark respiration rate, sec^{-1}

K_{mg} = macrophyte growth rate, sec^{-1}

K_{mr} = macrophyte respiration rate, sec^{-1}

K_{zr} = macrophyte respiration rate, sec^{-1}

K_{LDOM} = labile DOM decay rate, sec^{-1}

K_{RDOM} = refractory DOM decay rate, sec^{-1}

K_{LPOM} = labile POM decay rate, sec^{-1}

K_{RPOM} = refractory POM decay rate, sec^{-1}

K_{CBOD} = CBOD decay rate, sec^{-1}

K_{sed} = sediment decay rate, sec^{-1}

SOD = anaerobic sediment release rate, $g\ m^{-2}s^{-1}$

Φ_P = phosphorus concentration, $g\ m^{-3}$

Φ_{Fe} = total iron concentration, $g\ m^{-3}$

Φ_{ISS} = inorganic suspended solids concentration, $g\ m^{-3}$

Φ_a = algal concentration, $g\ m^{-3}$

Φ_e = periphyton/epiphyton concentration, $g\ m^{-3}$

Φ_{LDOM} = labile DOM concentration, $g\ m^{-3}$

Φ_{LPOM} = labile POM concentration, $g\ m^{-3}$

Φ_{RDOM} = refractory DOM concentration, $g\ m^{-3}$

Φ_{RPOM} = refractory POM concentration, $g\ m^{-3}$

Φ_{CBOD} = CBOD concentration, $g\ m^{-3}$

Φ_{sed} = organic sediment concentration, $g\ m^{-3}$

Φ_{macro} = macrophyte concentration, $g\ m^{-3}$

Φ_{zoo} = zooplankton concentration, $g\ m^{-3}$

and the rate terms are evaluated in subroutine PHOSPHORUS. In the model, the PO₄ concentration is in units of PO₄ as P.

The contribution of algae, POM, and DOM to phosphorus is given in the rate equations. However, effects due to settling and contribution from sediments require some additional explanation.

Dissolved inorganic phosphorus adsorbs onto inorganic particulates under oxic conditions and is lost when these materials settle. Loss may be rapid in the upper end of reservoirs in the riverine and transition zones due to greater concentrations of allochthonous particulates. A Langmuir isotherm describes this process. Since phosphorus concentrations are generally small, only the isotherm's linear region is utilized and is represented by the product $P_P\Phi_P$. The adsorbed solids settle at a rate equal to the solids' settling velocity. Adsorption is not allowed to occur if dissolved oxygen concentrations approach anaerobic conditions.

Phosphorus adsorption onto inorganic suspended solids should be used cautiously. In most systems, available phosphorus sites for adsorption onto inflowing inorganic suspended solids are generally already in use, so little adsorption takes place when inorganic suspended solids enter into a reservoir or estuary. The phosphorus formulation needs to be recast with inorganic phosphorus as the state variable that is then partitioned between dissolved and particulate forms. However, phosphorus sorption onto iron hydroxides

that form when anoxic waters come into contact with oxygenated water can be an important mechanism of phosphorus removal from the water column for certain waterbodies.

Sediment contribution of phosphorus to overlying waters can be simulated in three ways:
  (1) The sediment compartment accumulates particulate organic matter and algae, which then decay under oxic conditions. This is modeled as a 1st-order process. However, sediment phosphorus release depends upon sediment age, chemistry, overlying phosphorus concentrations, and other factors not included in the sediment compartment.
  (2) Under anaerobic conditions using the zero-order sediment oxygen model, sediments can be assigned a release rate for phosphorus that is a function of the assigned sediment oxygen demand rate. This rate only changes based on temperature. Phosphorus release is only allowed to occur if the overlying water dissolved oxygen concentration is approaching anaerobic conditions.
  (3) Sediment diagenesis predicts P release under anaerobic conditions. This is a truly predictive model based on organic matter loading to the sediments.

Note that when the sediment diagenesis model is not used, a combination of the first two can be used where organic materials accumulate and decay in the sediments under aerobic conditions and are released based on the SOD zero-order decay rate under anaerobic conditions.

Ammonium

Ammonium is a product of the decay of organic matter, and algae can use ammonium during photosynthesis to form proteins. In many estuarine applications, nitrogen is the limiting nutrient for algal growth. Macrophytes can prefer taking N from the sediments versus the water column. Ammonia can decay in the presence of nitrifying bacteria to Nitrite and Nitrate. Ammonium is viewed as total ammonia, both ammonium (NH_4^+-N) and unionized ammonia (NH_3-N).
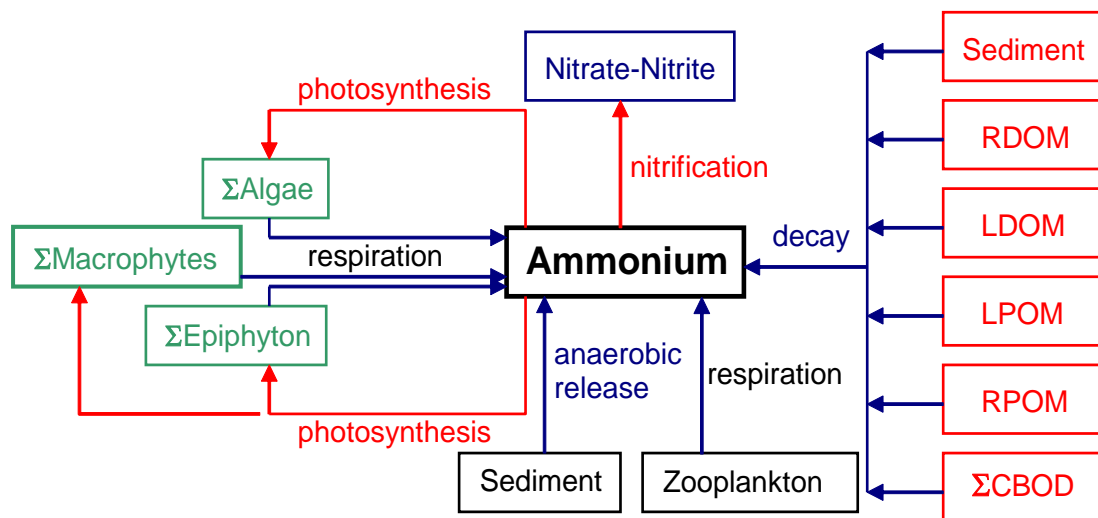
Figure 92. Internal flux between ammonium and other compartments.

Referring to **Figure 92**, the rate equation for ammonium is:

$$S_{NH4} = \sum K_{ar}\delta_{Na}\Phi_s - \sum K_{ag}\delta_{Na}\Phi_a P_{NH4} + \sum K_{er}\delta_{Ne}\Phi_e - \sum K_{eg}\delta_{Ne}\Phi_e P_{NH4}$$
$$\underbrace{\qquad}_{\text{algal respiration}} \quad \underbrace{\qquad}_{\text{algal growth}} \quad \underbrace{\qquad}_{\text{epiphyton respiration}} \quad \underbrace{\qquad}_{\text{epiphyton growth}}$$

$$+ \underbrace{K_{LDOM}\delta_{NOM}\gamma_{OM}\Phi_{LDOM}}_{\text{labile DOM decay}} + \underbrace{K_{RDOM}\delta_{NOM}\gamma_{OM}\Phi_{RDOM}}_{\text{refractory DOM decay}} + \underbrace{K_{LPOM}\delta_{NOM}\gamma_{OM}\Phi_{LPOM}}_{\text{labile POM decay}}$$

$$+ \underbrace{K_{RPOM}\delta_{NOM}\gamma_{OM}\Phi_{RPOM}}_{\text{refractory POM decay}} + \underbrace{K_s\delta_{NOM}\gamma_{OM}\Phi_s}_{\text{1st-order sediment release}} + \underbrace{SOD_{NH4}\gamma_{OM}\frac{A_{sed}}{V}}_{\text{0-order sediment release}}$$

$$+ \underbrace{\sum K_{CBOD}R_{CBOD}\delta_{N-CBOD}\Theta^{T-20}\Phi_{CBOD}}_{\text{CBOD decay}} - \underbrace{K_{NH4}\gamma_{NH4}\Phi_{NH4}}_{\text{nitrification}}$$

$$+ \underbrace{\sum(K_{mr} - (1 - f_{nsed})K_{mg})\delta_{Nm}\Phi_{macro}}_{\text{net macrophyte growth}} + \underbrace{\sum K_{zr}\delta_{Nz}\Phi_{zoo}}_{\text{zooplankton respiration}}$$

(4-124)

where:

A_{sed} = sediment area, m^2
V = volume of cell, m^3
f_{nsed} = fraction of macrophyte nitrogen uptake from sediments
δ_{Na} = algal stoichiometric coefficient for nitrogen
δ_{Ne} = periphyton/epiphyton stoichiometric coefficient for nitrogen
δ_{Nm} = macrophyte stoichiometric coefficient for nitrogen
δ_{Nz} = zooplankton stoichiometric coefficient for nitrogen
δ_{NOM} = organic matter stoichiometric coefficient for nitrogen
δ_{N-CBOD} = CBOD stoichiometric coefficient for nitrogen
γ_{NH4} = temperature rate multiplier for nitrification
γ_{OM} = temperature rate multiplier for organic matter decay
Θ = temperature rate multiplier for CBOD decay
R_{CBOD} = ratio of 5-day CBOD to ultimate CBOD
P_{NH4} = ammonium preference factor
K_{NOx} = nitrate-nitrogen decay rate, sec^{-1}
K_{NH4} = ammonium decay rate, sec^{-1}
K_{ar} = algal dark respiration rate, sec^{-1}
K_{ag} = algal growth rate, sec^{-1}
K_{mg} = macrophyte growth rate, sec^{-1}
K_{mr} = macrophyte respiration rate, sec^{-1}
K_{zr} = zooplankton respiration rate, sec^{-1}
K_{LDOM} = labile DOM decay rate, sec^{-1}
K_{RDOM} = refractory DOM decay rate, sec^{-1}
K_{LPOM} = labile POM decay rate, sec^{-1}
K_{RPOM} = refractory POM decay rate, sec^{-1}
K_{CBOD} = CBOD decay rate, sec^{-1}
K_{sed} = sediment decay rate, sec^{-1}
SOD_{NH4} = sediment ammonium release rate, $g\ m^{-2}\ sec^{-1}$
Φ_{ISS} = inorganic suspended solids concentration, $g\ m^{-3}$
Φ_{NH4} = ammonium concentration, $g\ m^{-3}$
Φ_a = algal concentration, $g\ m^{-3}$
Φ_{LDOM} = labile DOM concentration, $g\ m^{-3}$

Φ_{RDOM} = refractory DOM concentration, $g\ m^{-3}$

Φ_{LPOM} = labile POM concentration, $g\ m^{-3}$

Φ_{RPOM} = refractory POM concentration, $g\ m^{-3}$

Φ_{CBOD} = CBOD concentration, $g\ m^{-3}$

Φ_{macro} = macrophyte concentration, $g\ m^{-3}$

Φ_{zoo} = zooplankton concentration, $g\ m^{-3}$

Φ_{sed} = organic sediment concentration, $g\ m^{-3}$

and the rate terms are evaluated in subroutine AMMONIUM. As with phosphorus, 0-order sediment re-
lease only occurs when dissolved oxygen is less than a minimum value as determined by the transition from
aerobic to anaerobic processes. Either a 0- or 1st-order process or a combination of both may be used for
sediment ammonium release. Also, the sediment diagenesis model computes ammonium release during
anaerobic conditions. In the model, the ammonium concentration is in units of NH_4 as N.

Nitrate-Nitrite

This compartment represents nitrate plus nitrite. Nitrite is an intermediate product in nitrification between
ammonium and nitrate. Nitrate can be used as a source of nitrogen for algae and periphyton/epiphyton
during photosynthesis based on the ammonia-nitrate preference factor for set for each algal and periphy-
ton group.

Nitrogen may be the limiting nutrient for algae in systems with high phosphorus loadings or in estuaries.
Some species of cyanobacteria can fix atmospheric nitrogen for use in photosynthesis. This process can be
included by setting the nitrogen half-saturation concentration for algal growth to zero.
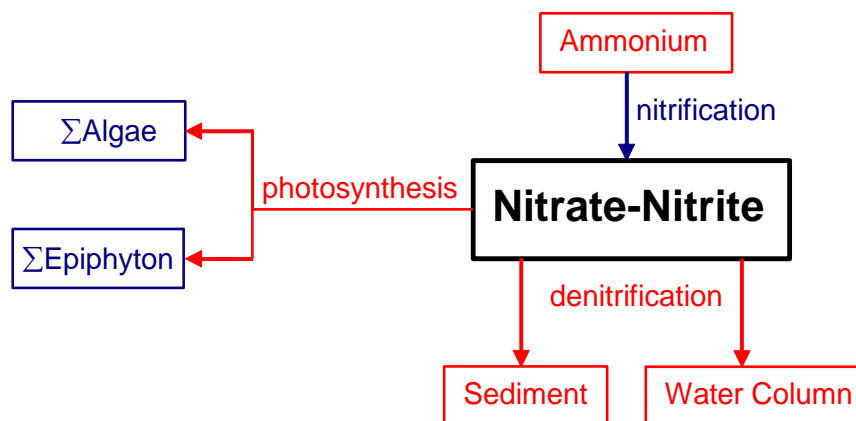
Figure 93. Internal flux between nitrate + nitrite and other compartments.

Referring to **Figure 93**, the rate equation for nitrate-nitrite is:

$$S_{NOx} = K_{NH4}\gamma_{NH4}\Phi_{NH4} - \underbrace{K_{NOx}\gamma_{NOx}\Phi_{NOx}}_{\text{water column denitrification}} - \underbrace{\omega_{NOx}\frac{\partial\Phi_{NOx}}{\partial z}}_{\text{sediment denitrification}}$$

$$- \underbrace{\sum K_{ag}\delta_{Na}\Phi_a(1 - P_{NH4})}_{\text{algal uptake}} - \underbrace{\sum K_{eg}\delta_{Ne}\Phi_e(1 - P_{NH4})}_{\text{epiphyton uptake}}$$

(4-125)

where:

γ_{NH4} = temperature rate multiplier for nitrification
γ_{NOx} = temperature rate multiplier for denitrification
δ_{Ne} = epiphyton stoichiometric coefficient for nitrogen
δ_{Na} = algal stoichiometric coefficient for nitrogen
P_{NH4} = ammonium preference factor
K_{NH4} = nitrification rate, sec^{-1}
K_{NOx} = denitrification rate, sec^{-1}
K_{ag} = algal growth rate, sec^{-1}
ω_{NOx} = sediment transfer velocity, $m\ sec^{-1}$
Φ_{NH4}= ammonia-nitrogen concentration, $g\ m^{-3}$
Φ_{NOx} = nitrate-nitrogen concentration, $g\ m^{-3}$
Φ_a = algal concentration, $g\ m^{-3}$

and the rate terms are evaluated in subroutine NITRATE. Nitrification is only allowed to occur if oxygen is present and is gradually decreased as oxygen is depleted, and denitrification is allowed to occur as oxygen is depleted based on the transition from aerobic to anaerobic processes (see Dissolved Oxygen where the transition to anaerobic processes follows a Monod approach). In the model, the nitrate+nitrite concentration is in units of $NO_3 + NO_2$ as N.

Dissolved Silica

Dissolved silica is an important component of diatoms, providing the structural skeleton. In many cases diatoms can be silica limited. Dissolved silica is taken up by algae based on stoichiometric relationships and is produced by the decay of organic matter containing particulate biogenic silica. Also, dissolved silica is adsorbed onto inorganic suspended solids based on a partitioning coefficient.
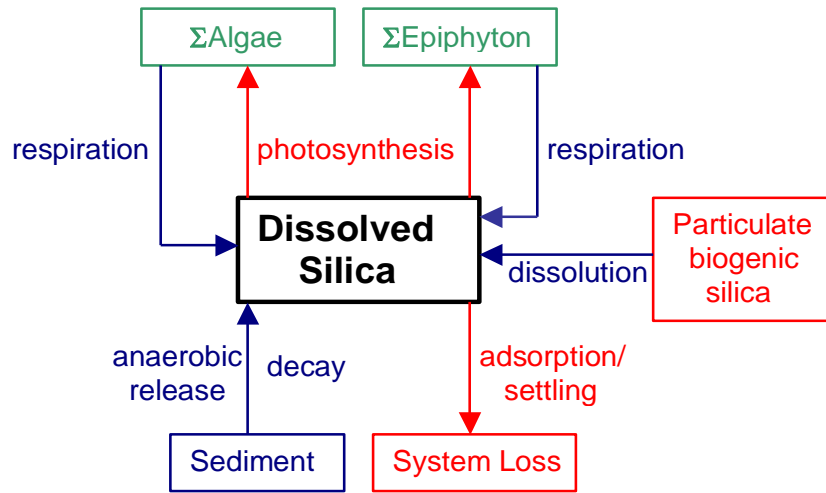
Figure 94. Internal flux between dissolved silica and other compartments.

Referring to **Figure 94**, the rate equation for dissolved silica is:

$$S_{DSi} = -\sum(K_{ag} - K_{ar})\delta_{Sia}\Phi_a - \sum(K_{eg} - K_{er})\delta_{Sie}\Phi_e$$

$$\underbrace{\phantom{-\sum(K_{ag}-K_{ar})\delta_{Sia}\Phi_a}}_{\text{algal uptake}} \qquad \underbrace{\phantom{-\sum(K_{eg}-K_{er})\delta_{Sie}\Phi_e}}_{\text{epiphyton uptake}}$$

$$+ \underbrace{K_{sed}\delta_{SiOM}\gamma_{OM}\Phi_{sed}}_{\text{1st order sediment release}} + \underbrace{SOD\varphi_{Si}\gamma_{OM}\frac{A_{sed}}{V}}_{\text{0-order sediment release}} + \underbrace{K_{PSi}\gamma_{OM}\Phi_{PSi}}_{\substack{\text{particulate biogenic} \\ \text{decay}}}$$

$$\qquad\qquad\qquad\qquad\qquad\qquad\qquad\qquad\qquad\qquad\qquad \text{(4-126)}$$

$$- \underbrace{\frac{P_{Si}(\sum\omega_{ss}\Phi_{ss}+\omega_{POM}\Phi_{POML}+\omega_{POM}\Phi_{POMR}+\omega_{Fe}\Phi_{Fe})}{\Delta z}\Phi_{DSi}}_{\text{inorganic solids adsorption and settling}}$$

where:

θ = temperature rate factor for BOD decay
γ_{OM} = temperature rate multiplier for organic matter decay
φ_{Si} = fraction of SOD for silica release
Δz = computational cell height, m
δ_{Sie} = epiphyton stoichiometric ratio for silica
δ_{Sia} = algal stoichiometric ratio for silica
δ_{SiOM} = sediment organic matter stoichiometric ratio for silica
A_{sed} = sediment area, m^2
V = computational cell volume, m^3
P_{Si} = silica adsorption coefficient, $m^3\,g^{-1}$
SOD = sediment oxygen demand, $g\,m^{-2}\,sec^{-1}$
ω_{ISS} = inorganic suspended solids settling velocity, $m\,sec^{-1}$
K_{ag} = algal growth rate, sec^{-1}
K_{eg} = epiphyton growth rate, sec^{-1}
K_{sed} = sediment decay rate, sec^{-1}
Φ_a = algal concentration, $g\,m^{-3}$
Φ_e = epiphyton concentration, $g\,m^{-3}$
Φ_{sed} = organic sediment mass, g

Φ_{ISS} = inorganic suspended solids concentration, *g m^{-3}*

Φ_{DSi} = dissolved silica concentration, *g m^{-3}*

Φ_{Fe} = total iron concentration, *g m^{-3}*

Particulate Biogenic Silica

Particulate biogenic silica results from diatom mortality and settles and also dissolves to form dissolved silica.
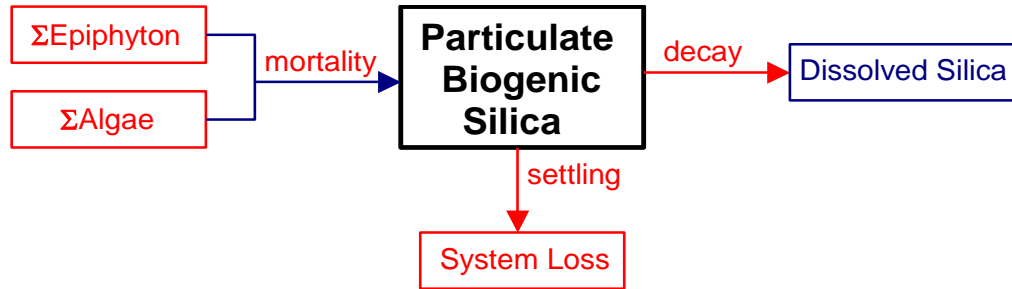
Figure 95. Internal flux between particulate biogenic silica and other compartments

Referring to **Figure 95**, the rate equation for particulate biogenic silica is:

$$S_{PSi} = \underbrace{P_{am}\delta_{Sia}K_{am}\Phi_a}_{\text{algae mortality}} + \underbrace{P_{em}\delta_{Sie}K_{em}\Phi_e}_{\text{epiphyton mortality}} - \underbrace{K_{PSi}\gamma_{OM}\Phi_{PSi}}_{\text{decay}} - \underbrace{\frac{\omega_{PSi}\partial\Phi_{PSi}}{\partial z}}_{\text{settling}} \tag{4-127}$$

where:

P_{am} = partition coefficient for algal mortality

δ_{Sie} = epiphyton stoichiometric coefficient for silica

δ_{Sia} = algal stoichiometric coefficient for silica

γ_{OM} = temperature rate multiplier for organic matter

P_{em} = partition coefficient for periphyton/epiphyton mortality

K_{am} = algal mortality rate, *sec^{-1}*

K_{em} = epiphyton mortality rate, *sec^{-1}*

K_{PSi} = particulate biogenic silica decay rate, *sec^{-1}*

ω_{PSi} = particulate biogenic silica settling rate, *m sec^{-1}*

Φ_e = epiphyton concentration, *g m^{-3}*

Φ_a = algal concentration, *g m^{-3}*

Φ_{PSi} = particulate biogenic silica concentration, *g m^{-3}*

Dissolved Oxygen

Oxygen is one of the most important elements in aquatic ecosystems. It is essential for higher forms of life, controls many chemical reactions through oxidation, and is a surrogate variable indicating the general health of aquatic systems.

CE-QUAL-W2 includes both aerobic and anaerobic processes. The ability to model anaerobic periods is important since it provides information on potential problems with water quality. Simulations can be used to identify possibilities for both metalimnetic and hypolimnetic oxygen depletion and its impact on various water control management alternatives. If a single variable were to be measured in aquatic systems that would provide maximum information about the system state, it would be dissolved oxygen.
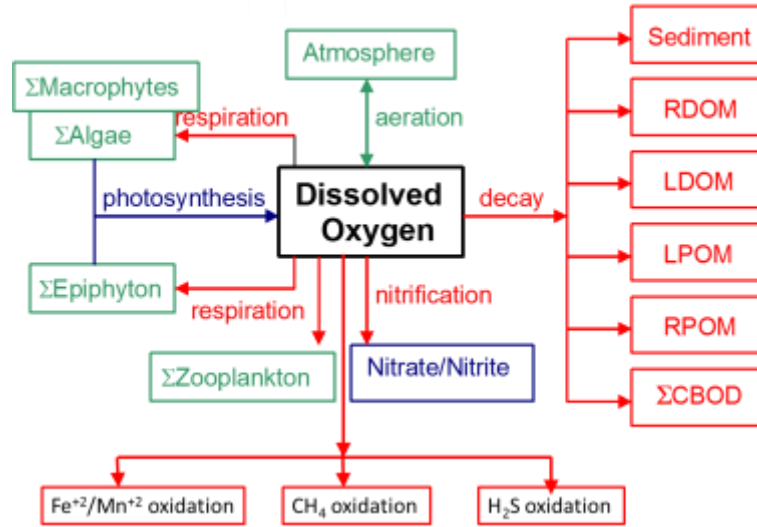
Figure 96. Internal flux between dissolved oxygen and other compartments.

Referring to **Figure 96**, the rate equation for dissolved oxygen is:

$$S_{DO} = \sum(K_{ag} - K_{ar})\delta_{OMa}\Phi_a + \sum(K_{eg} - K_{er})\delta_{OMe}\Phi_e + \frac{A_{sur}}{V_{sur}}K_L(\Phi_{S_{DO}} - \Phi_{DO})$$

$$\underbrace{\phantom{\sum(K_{ag} - K_{ar})\delta_{OMa}\Phi_a}}_{\text{algal net production}} \quad \underbrace{\phantom{\sum(K_{eg} - K_{er})\delta_{OMe}\Phi_e}}_{\text{epiphyton net production}} \quad \underbrace{}_{\text{aeration}}$$

$$- K_{RPOM}\delta_{OM}\gamma_{OM}\Phi_{RPOM} - K_{LPOM}\delta_{OM}\gamma_{OM}\Phi_{LPOM} - K_{LDOM}\gamma_{OM}\delta_{OM}\Phi_{LDOM}$$

$$\underbrace{}_{\text{refractory POM decay}} \quad \underbrace{}_{\text{labile POM decay}} \quad \underbrace{}_{\text{labile DOM decay}}$$

$$- K_{RDOM}\delta_{OM}\gamma_{OM}\Phi_{RDOM} - K_s\delta_{OM}\gamma_{OM}\Phi_{sed} - SOD\gamma_{OM}\frac{A_{sed}}{V}$$

$$\underbrace{}_{\text{refractory DOM decay}} \quad \underbrace{}_{\text{1st-order sediment decay}} \quad \underbrace{}_{\text{0-order SOD}}$$

$$- \sum K_{CBOD}R_{CBOD}\Theta^{T-20}\Phi_{CBOD} - K_{NH4}\delta_{NH4}\gamma_{NH4}\Phi_{NH4} + \sum(K_{mg} - K_{mr})\delta_{OMmac}\Phi_{macro}$$

$$\underbrace{}_{\text{CBOD decay}} \quad \underbrace{}_{\text{nitrification}} \quad \underbrace{}_{\text{macrophyte net production}}$$

$$- \sum\gamma_{zoo}K_{zr}\delta_{OMzoo}\Phi_{zoo} - \delta_{H2S-O2}K_{H2S}\Phi_{H2S} - \delta_{CH4-O2}K_{CH4}\Phi_{CH4} - \delta_{Fe2-O2}K_{Fe2}\Phi_{Fe2}$$

$$\underbrace{}_{\text{zooplankton respiration}} \quad \underbrace{}_{\text{oxidation}}$$

$$- \delta_{Mn2-O2}K_{Mn2}\Phi_{Mn2}$$

$$\underbrace{}_{\text{oxidation}}$$

(4-128)

where:

δ_{OMa} = oxygen stoichiometric coefficient for algal organic matter

δ_{OMe} = oxygen stoichiometric coefficient for periphyton/epiphyton organic matter

δ_{OMmac} = oxygen stoichiometric coefficient for macrophyte organic matter

δ_{OM} = oxygen stoichiometric coefficient for organic matter

δ_{NH4} = oxygen stoichiometric coefficient for nitrification

δ_{Fe2-O2} = oxygen stoichiometric coefficient for Fe^{+2}

δ_{Mn2-O2}= oxygen stoichiometric coefficient for Mn^{+2}

δ_{H2S-O2} = oxygen stoichiometric coefficient for H_2S

δ_{CH4-O2} = oxygen stoichiometric coefficient for CH_4

δ_{OMzoo} = oxygen stoichiometric coefficient for zooplankton

γ_{NH4} = temperature rate multiplier for nitrification

γ_{OM} = temperature rate multiplier for organic matter decay

γ_{zoo} = temperature rate multiplier for zooplankton

R_{BOD} = conversion from CBOD in the model to CBOD ultimate

Θ = BOD temperature rate multiplier

V = volume of computational cell, m^3

T = temperature, ℃

A_{sed} = sediment surface area, m^2

A_{sur} = water surface area, m^2

K_{ag} = algal growth rate, sec^{-1}

K_{ar} = algal dark respiration rate, sec^{-1}

K_{eg} = epiphyton growth rate, sec^{-1}

K_{er} = epiphyton dark respiration rate, sec^{-1}

K_{mg} = macrophyte growth rate, sec^{-1}

K_{mr} = macrophyte dark respiration rate, sec^{-1}

K_{zr} = zooplankton respiration rate, sec^{-1}

K_{NH4} = ammonia decay (nitrification) rate, sec^{-1}

K_{Fe2} = Fe^{+2} oxidation rate, sec^{-1}

K_{Mn2} = Mn^{+2} oxidation rate, sec^{-1}

K_{CH4} = CH_4 oxidation rate, sec^{-1}

K_{H2S} = H_2S oxidation rate, sec^{-1}

K_{LDOM} = labile DOM decay rate, sec^{-1}

K_{RDOM} = refractory DOM decay rate, sec^{-1}

K_{LPOM} = labile POM decay rate, sec^{-1}

K_{RPOM} = refractory POM decay rate, sec^{-1}

K_{BOD} = CBOD decay rate, sec^{-1}

K_{sed} = sediment decay rate, sec^{-1}

SOD = sediment oxygen demand, $g\ m^{-2}\ sec^{-1}$

K_L = interfacial exchange rate for oxygen, $m\ sec^{-1}$

Φ_{NH4} = ammonia-nitrogen concentration, $g\ m^{-3}$

Φ_a = algal concentration, $g\ m^{-3}$

Φ_e = periphyton/epiphyton concentration, $g\ m^{-3}$

Φ_{zoo} = zooplankton concentration, $g\ m^{-3}$

Φ_{macr} = macrophyte concentration, $g\ m^{-3}$

Φ_{LDOM} = labile DOM concentration, $g\ m^{-3}$

Φ_{RDOM} = refractory DOM concentration, $g\ m^{-3}$

Φ_{LPOM} = labile POM concentration, $g\ m^{-3}$

Φ_{RPOM} = refractory POM concentration, $g\ m^{-3}$

Φ_{BOD} = CBOD concentration, $g\ m^{-3}$

Φ_{sed} = organic sediment concentration, $g\ m^{-3}$

Φ_{DO} = dissolved oxygen concentration, $g\ m^{-3}$

Φ_{Fe2} = reduced Fe concentration, $g\ m^{-3}$

Φ_{Mn2} = reduced Mn concentration, $g\ m^{-3}$

Φ_{CH4} = CH_4 concentration, $g\ m^{-3}$

Φ_{H2S} = H_2S concentration, $g\ m^{-3}$

Φs_{DO} = saturation DO concentration, $g\ m^{-3}$

and the rate terms are evaluated in subroutine DISSOLVED_OXYGEN. Decay is not allowed to occur when dissolved oxygen concentrations are zero. A Monod formulation is used to move gradually from oxic to anoxic conditions. This is accomplished by reducing temperature rate multipliers eventually to zero as dissolved oxygen concentrations are zero.

This reduction of oxic reactions as dissolved oxygen levels approach zero is based on specification of a dissolved oxygen half-saturation constant in the following equation:

$$\text{Rate Reduction} = \frac{\Phi_{DO}}{K_{DO} + \Phi_{DO}}$$ where Φ_{DO} is the concentration of dissolved oxygen and K_{DO} is a half-saturation dissolved oxygen concentration when oxic reactions are half of their maximum without limitation of oxygen conditions.

Since reaeration in waterbodies are dependent on surface layer turbulence, the reaeration formulae for riverine, lake/reservoir, and estuarine systems are different. Surface layer turbulence for riverine waterbodies are dependent on boundary shear, while for lake or reservoir waterbodies, wind stress is usually the primary component of surface layer turbulence. In the following sections, formulae for reaeration as a function of wind speed and boundary shear are presented. The user can select a different formulation for each waterbody type. The reason for selecting a waterbody type is to help the user select a system that best approximates the appropriate theory. The possible water body types are RIVER, LAKE, or ESTUARY. Tchobanoglous and Schroeder (1987) and Thomann and Mueller (1987) show typical ranges for the reaeration coefficient for different water bodies in Table 18.

Table 18. Typical reaeration coefficient values for different water body types (from Tchobanoglous and Schroeder, 1987, and Thomann and Mueller, 1987).

Type of water body	Range in K_L(m/day) or k_a (day^{-1}) at 20°C
Small ponds and backwaters	0.10-0.23 day^{-1}
Sluggish streams and large lakes	0.23-0.35 day^{-1}
Large streams of low velocity	0.35-0.46 day^{-1}
Large streams of normal velocity	0.46-0.69 day^{-1}
Swift streams	0.69-1.15 day^{-1}
Rapids and waterfalls	>1.15 day^{-1}
Tidal river- estuary: Mean tidal depth < 3 m, average tidal velocity of 0.3 m/s	1.2 m/day
Tidal river- estuary: Mean tidal depth < 3 m, average tidal velocity of 1 m/s	2.1 m/day
Tidal river- estuary: Mean tidal depth 3-6 m, average tidal velocity of 0.3 m/s	0.9 m/day
Tidal river- estuary: Mean tidal depth 3-6 m, average tidal velocity of 1 m/s	1.8 m/day
Tidal river- estuary: Mean tidal depth 6-9 m, average tidal velocity of 0.3 m/s	0.7 m/day
Tidal river- estuary: Mean tidal depth 6-9 m, average tidal velocity of 1 m/s	1.5 m/day
Tidal river- estuary: Mean tidal depth >-9 m, average tidal velocity of 0.3 m/s	0.6 m/day
Tidal river- estuary: Mean tidal depth >9 m, average tidal velocity of 1 m/s	1.2 m/day

Note that in the preceding table, for rivers the value for k_a was in day^{-1}, but for estuaries k_L was reported in units of m/day. To convert between k_a in day^{-1} and k_L in m/day, one uses the following:

$$k_a = \frac{k_L A}{V}$$

where A is the surface area and V is the volume of the surface layer. The difference in units has to do with the river correlation using the average depth (V/A) in its correlation. In lakes and reservoirs (and sometimes in estuaries), the transfer coefficient used is not a function of the average depth and is presented in units of L/T.

River Reaeration Equations

Reaeration equations for rivers are given in **Table 19**. Most of these equations in the table are based on field studies of selected streams or laboratory channels. Equations 7 and 8 were developed from Melting and Flores (1999) for a large data set of reaeration coefficients. These may be the best choice for rivers even though other equations have been used extensively.

Recently, Moog and Jirka (1998) suggested that formulations that do not account for channel slope should not be used. Therefore, equations 7 and 8 may again be the best selection of equations for river sections.

Thomann and Mueller (1987) suggested using Equation 1 except for small streams where Equation 3 for flow less than 10 cfs should be used. They also suggested a minimum value of K_L of 0.6 m day^{-1}.

Mills et al. (1985) in a review of water quality reaeration coefficients used a different formulation than equation 3 in **Table 19** based on a 1978 reference at 25ºC:

$$K_a = 7776US \ for \ Q < 10cfs$$
$$K_a = 4665.6US \ for \ \ 10 < Q < 3000cfs$$
$$K_a = 2592US \ for \ \ Q > 3000cfs \tag{4-129}$$

where S is the slope in ft/ft and U is velocity in ft/s

However, Mills et al. (1985) only recommend its use for shallow low-flow streams. Therefore, equation 3 in **Table 19** is exactly the same as the above formulation in the low flow regime (note that the slopes in Equation 3 are in ft/mile and in the above equation are unitless).

Covar (1976) used an approach where the equations of O'Connor-Dobbins, Churchill, and Owens were used together based on the applicability of each equation. The applicability of each equation was based on the velocity of the stream and its depth. This is equation 0 in the following table.

Table 19. River reaeration equations.

#	Equation	Comments	Applicability	Reference
0	Either Eq 1, 2 or 4	K_a – evaluated based on applicability criteria of these equations		Covar (1976)

#	Equation	Comments	Applicability	Reference
1	$$K_a = \frac{K_L}{H} = \frac{(D_{O_2}U)^{1/2}}{H^{3/2}}$$	D_{O2} = H₂O molecular diffusion, $m^2\,s^{-1}$ U = average velocity, $m\,s^{-1}$ H = average channel depth, m	depths between 1-30 ft and velocities between 0.5-1.6 fps	O'Connor and Dobbins (1958)
2	$$K_a = \frac{K_L}{H} = \frac{11.6U}{H^{1.67}}$$	U, $ft\,s^{-1}$ H, ft K_a, day^{-1}	depths between 2-11 ft and velocities between 1.8-5 fps	Churchill, Elmore and Buckingham (1962)
3	$K_a = 0.88US$ for $10 < Q < 300 cfs$ $K_a = 1.8US$ for $1 < Q < 10 cfs$	S, $ft\,mile^{-1}$ U, $ft\,s^{-1}$ K_a, day^{-1}	suggested for use when Q < 10cfs	Tsivoglou and Wallace (1972)
4	$$K_a = \frac{K_L}{H} = \frac{21.6U^{0.67}}{H^{1.85}}$$	U, $ft\,s^{-1}$ H, ft	depths between 0.4-2.4 ft and velocities between 0.1-1.8 fps	Owens et al. (1964)
5	$$K_a = \frac{K_L}{H} = \frac{25u^*}{H}(1+F^{0.5})$$	u^* = shear velocity, $(HSg)^{0.5}$ S = slope of energy grade line F = Froude number, $U/(gH)^{0.5}$		Thackston and Krenkel (1966)
6	$$K_a = \frac{K_L}{H} = \frac{7.62U}{H^{1.33}}$$	U, $ft\,s^{-1}$ H, ft		Langbien and Durum (1967)
7	$K_a = 517(US)^{0.524}Q^{-0.242}$ for $\rightleftarrows Q < 0.556$ $K_a = 596(US)^{0.528}Q^{-0.136}$ for $\rightleftarrows Q > 0.556$	U, $m\,s^{-1}$ S, $m\,m^{-1}$ Q, $m^3 s^{-1}$ K_a, day^{-1}	for pool and riffle streams	Melching and Flores (1999)
8	$K_a = 88(US)^{0.313}D^{-0.353}$ for $Q < 0.556$ $K_a = 142(US)^{0.333}D^{-0.66}W^{-0.243}$ for $Q > 0.556$	U, $m\,s^{-1}$ S, $m\,m^{-1}$ W = stream top width, m D = average depth, m K_a, day^{-1}	for channel-control streams	Melching and Flores (1999)
9	w/ channel slope - $\quad K_a = C_1 U^{C_2} H^{C_3} S^{C_4}$ w/o channel slope - $\quad K_a = C_1 U^{C_2} H^{C_3}$	U, $m\,s^{-1}$ H, m S, non-dimensional K_a, day^{-1} C^1, C_2, C_3, C_4 = user defined parameters	User defined relationship	
10	$$K_a = \frac{K_L}{H} = \frac{5.0u^*}{H}(1+9F^{0.25})$$	u^* = shear velocity, $(HSg)^{0.5}$ S = slope of energy grade line F = Froude number, $U/(gH)^{0.5}$ K_a, day^{-1}		Thackston and Dawson (2001)

Figure 97 shows the functional dependence of these formulae assuming the following relationship between flow (Q, ft³/s), velocity (V, ft/s) and depth (H, ft) (St. John et al., 1984):

V = 0.033 Q^{0.5}
H = 0.475 Q^{0.4}
S = 5.2 *ft/mile*
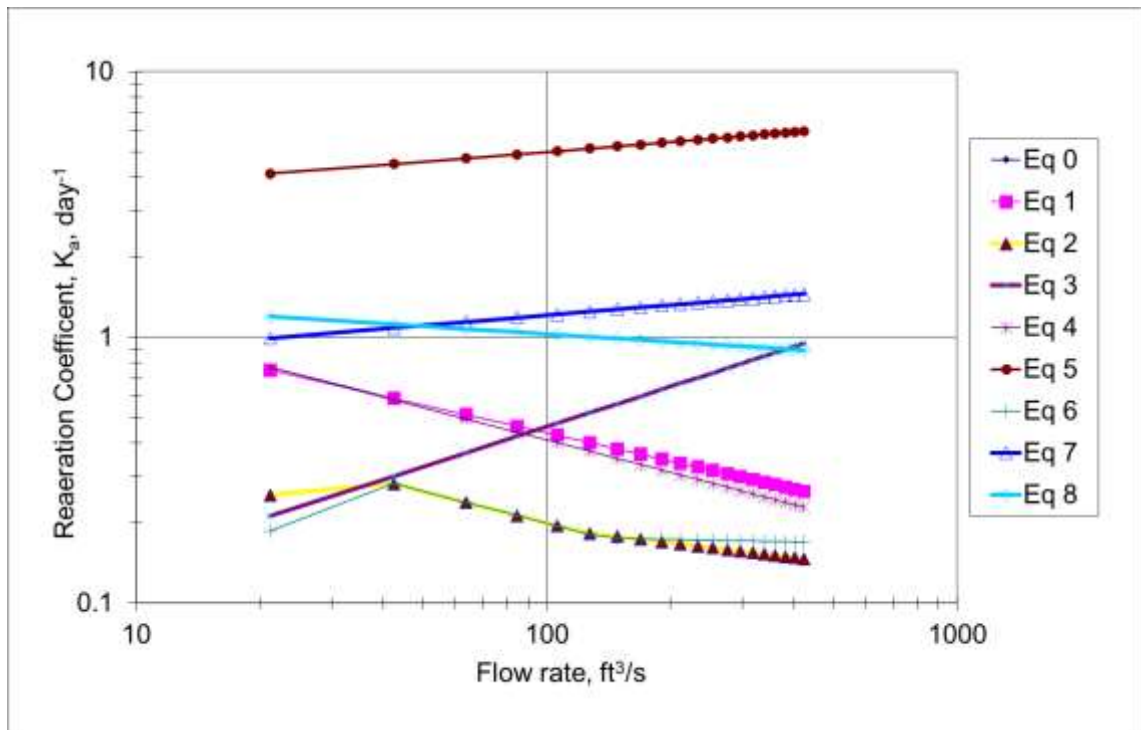
Figure 97. Reaeration coefficient as a function of flow rate.

Lake Reaeration Equations

Wind effects rather than boundary shear more often control reaeration in lakes, reservoirs, and estuarine systems. There have been many wind studies for lakes (e.g., O'Connor, 1983) and open ocean systems. A summary of wind speed formulae for predicting reaeration is shown in **Table 20** based on a 10 m wind measuring height.

Table 20. Lake reaeration equations as a function of wind speed at 20°C.

#	Equation	Comments	Reference
1	$$K_a = \frac{K_L}{H} = \frac{0.864W}{H}$$	W, $m\ s^{-1}$ at 10 m H, m K_L, $m\ day^{-1}$	Broecker et al (1978)
2	$$K_a = \frac{K_L}{H} = \frac{\alpha W^\beta}{H}$$	$\alpha = 0.2$, $\beta = 1$ for W < 3.5 $m\ s^{-1}$ a = 0.057, $\beta = 2$ for W > 3.5 $m\ s^{-1}$ where W is a daily average wind speed	Gelda et al (1996)
3	$$K_a = \frac{K_L}{H}$$ $$= \frac{0.728W^{0.5} - 0.317W + 0.0372W^2}{H}$$	W, $m\ s^{-1}$ at 10 m K_L, $m\ day^{-1}$	Banks and Herrera (1977)
4	$K_a = \frac{K_L}{H} = \frac{\frac{0.0986W^{1.64}}{H}}{}$ [at 20°C] or $$K_a = \frac{K_L}{H} = \frac{0.0986W^{1.64}}{H}\left(\frac{600}{Sc}\right)^{0.5}$$	The latter equation was the original equation used where W is measured at 10 m and Sc is the Schmidt number Sc=(ν/D)= 13750[0.10656 exp(-.0627T)+.00495] T = temperature, ^oC ν=kinematic viscosity D=diffusivity	Wanninkhof et al. (1991)

#	Equation	Comments	Reference
5	$K_a = \dfrac{K_L}{H} = \dfrac{\frac{D_{o2}}{(200-60W^{0.5})10^{-6}}}{H}$	D_{O2} = oxygen molecular diffusivity, $m^2\,s^{-1}$ W, $m\,s^{-1}$ K_L, $m\,s^{-1}$	Kanwisher (1963)
6	$K_a = \dfrac{K_L}{H} = \dfrac{0.5+0.05W^2}{H}$		Cole and Buchak (1995)
7	$K_a = \dfrac{K_L}{H} = \dfrac{0.362\sqrt{W}}{H}$ $W < 5.5 m/s$ $K_a = \dfrac{K_L}{H} = \dfrac{0.0277W^2}{H}$ $W > 5.5 m/s$		Banks (1975)
8	$K_a = \dfrac{K_L}{H} = \dfrac{0.64+0.128W^2}{H}$	Recommended form for WQRSS reservoir model	Smith (1978)
9	$K_a = \dfrac{K_L}{H} = \dfrac{0.156W^{0.63}}{H}$ $W \le 4.1 m/s$ $K_a = \dfrac{K_L}{H} = \dfrac{0.0269W^{1.9}}{H}$ $W > 4.1 m/s$		Liss (1973)
10	$K_a = \dfrac{K_L}{H} = \dfrac{0.0276W^2}{H}$		Downing and Truesdale (1955)
11	$K_a = \dfrac{K_L}{H} = \dfrac{0.0432W^2}{H}$		Kanwisher (1963)
12	$K_a = \dfrac{K_L}{H} = \dfrac{0.319W}{H}$		Yu et al (1977)
13	$K_a = \dfrac{K_L}{H} = \dfrac{0.398}{H}$ $W < 1.6$ $K_a = \dfrac{K_L}{H} = \dfrac{0.155W^2}{H}$ $W \ge 1.6$	W = wind speed, $m\,s^{-1}$	Weiler (1974)
14	$K_a = \dfrac{K_L}{H} = \dfrac{C_1+C_2W^{C_3}}{H}$	User defined relationship where: W, $m\,s^{-1}$ at 10 m K_a, day^{-1} C_1, C_2, C_3 are user defined	

Figure 98 shows how these formulations vary with wind speed.

The definition of wind speed was usually taken at an elevation of 10 m for these formulations. The wind speed at 10 m elevation in the middle of a lake or reservoir, W_{10m}, can be computed from that measured at 10 m on land by using an approach from Fang and Stefan (1994).

$$W_{10m} = W_z f(fetch) \tag{4-130}$$

where:

    W_z = wind speed measured at 10 m height on land, m/s

$$f(fetch) = \frac{ln\frac{10}{z_{o2}}ln\frac{\delta}{z_{o1}}}{ln\frac{10}{z_{o1}}ln\frac{\delta}{z_{o2}}} \simeq \frac{5ZB+4.6052}{3ZB+9.2103} \tag{4-131}$$

where:

    z_{o1} = roughness of land (assume 0.01 m) (Kraus, 1972)

    z_{o2} = roughness of water surface (assume 0.0001 m) (Ford and Stefan, 1980)

    δ = thickness of wind boundary layer over smooth surface that is a function of the fetch length (Elliot, 1958), m

ZB = $0.8\,ln\dfrac{fetch}{2} - 1.0718$

The function *f(fetch)* varies from 1.056 for small lakes to 1.123 for large lakes. The fetch is the length in *m* of the wind over the water surface from one bank to the other.
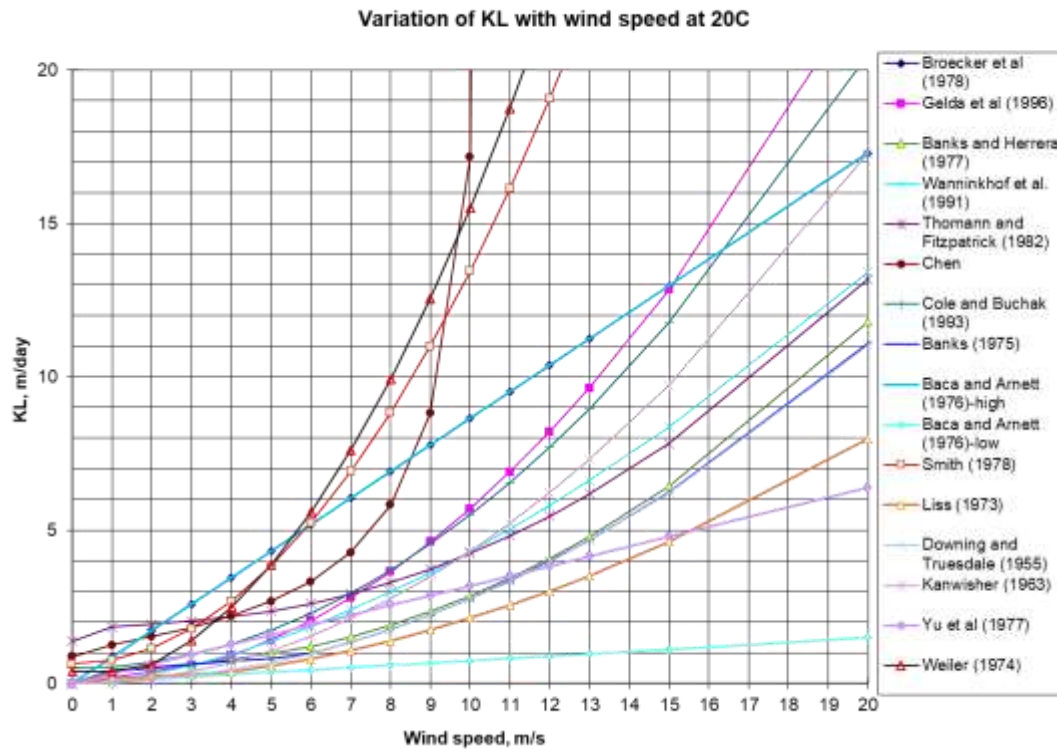
Figure 98. Variation of wind speed and KL for lake/reservoir equations.

Equations for correcting the wind speed to 10 *m* and accounting for fetch dependence are included in the model. This dependence on measuring height, fetch, and wind speed is shown in **Figure 99** and **Figure 100**.
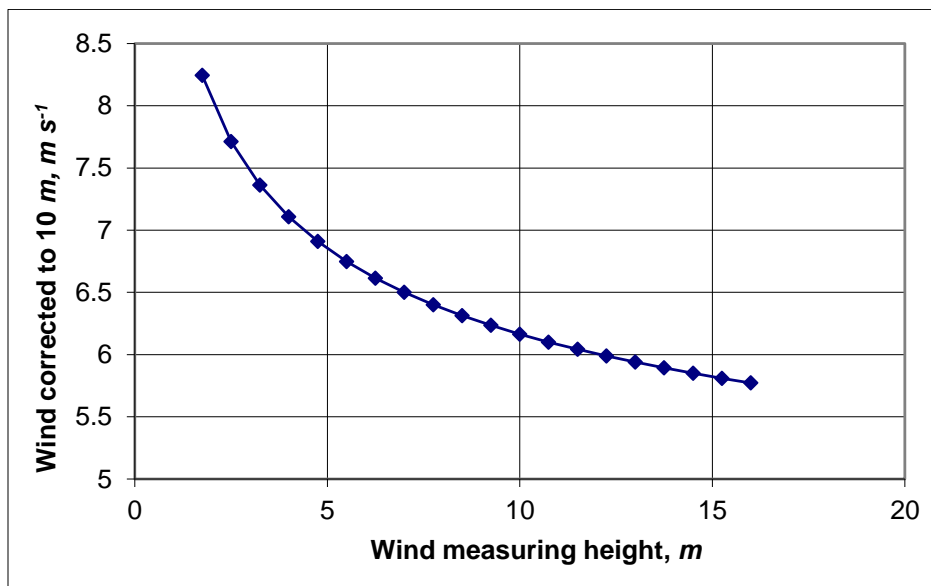
Figure 99. Wind speed of 5 *m s^{-1}* and a fetch of 5 *km* corrected to 10 *m* as a function of measuring height on land.
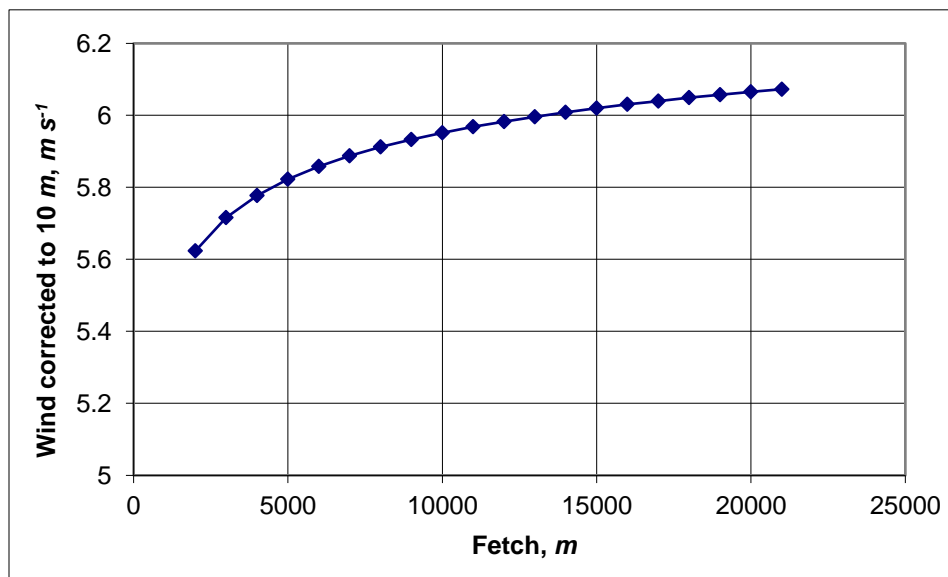
Figure 100. Wind speed of 5 *m s^{-1}* corrected to 10 *m* as a function of fetch.
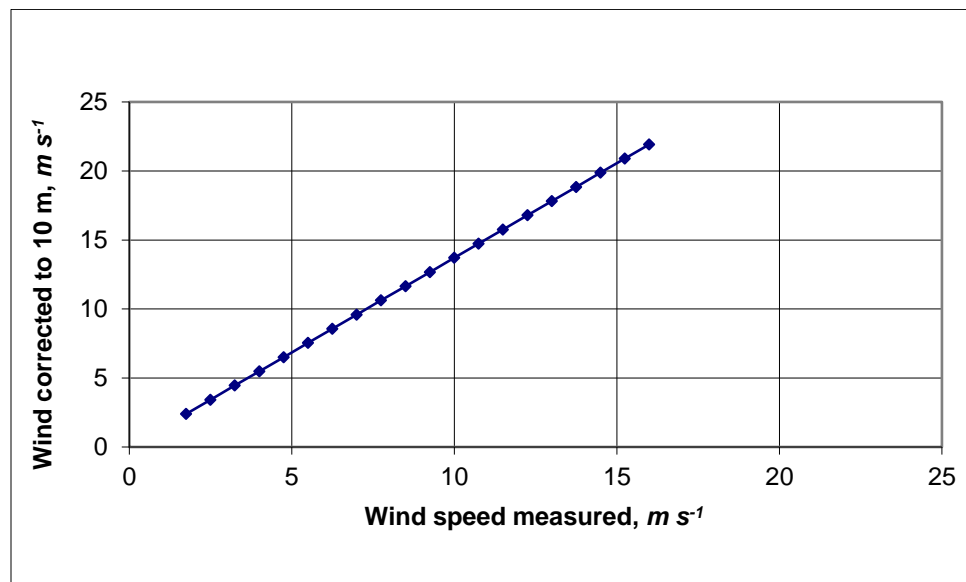
Figure 101. Wind corrected to 10 *m* based on wind measured on land.

Estuarine Equations

For estuarine systems, Thomann and Mueller (1987) and Chapra (1997) suggest using any of the wind formulations in **Table 21** or Equation 1 in **Table 19** using the mean tidal velocity over a tidal cycle for the horizontal velocity. Table 21 shows an additional formulation from Thomann and Fitzpatrick (1982) for estuaries, as well as the approach of Covar (1976) for rivers. Since many texts suggest using the mean tidal velocity, caution should be exercised in using these equations since they are based on the instantaneous velocity in the model.

Table 21. Reaeration equations for estuarine waterbody at 20°C.

#	Equation	Comments	Reference
0	Either Eq 1, 2 or 4 from **Table 19**	Ka is determined based on applicability criteria of each of these 3 formulations	Covar (1976)
1	$K_a = \dfrac{K_L}{H} = \dfrac{0.728W^{0.5} - 0.317W + 0.0372W^2}{H} + 3.93\dfrac{\sqrt{U}}{H^{1.5}}$	U, *m s⁻¹* this formula combines the effect of wind from Banks and Herrera (1977) and estuary tidal flow	Thomann and Fitzpatrick (1982)
2	$K_a = C_1 U^{C_2} H^{C_3} + \dfrac{0.5 + C_4 W^2}{H}$	U, *m s⁻¹* H, *m* W, *m s⁻¹* at 10 *m* K_a, *day⁻¹* C_1, C_2, C_3, and C_4 - user defined parameters	User defined relationship

Chu and Jirka (2003) reported on wind and stream flow induced reaeration and showed that for cases where the time scale tidal flow is >> the time scale for reaeration, then the reaeration process can be described as a steady process and the impacts of stream flow and wind can be additive using:

$$K_L = K_{Lb} + K_{Lw}$$

Where K_{Lb} is the reaeration coefficient (or transfer velocity) due to bottom shear and K_{Lw} is the reaeration coefficient due to wind in m/day.

$$K_{Lb} = 2.150 \left(\frac{u_{*b}^3}{h}\right)^{0.25}$$

Where h is the depth in cm, $u_{*b} = \sqrt{\frac{f}{8}} U$, U is the mean water velocity, f is approximately 0.04.

$K_{Lw} = \alpha u_{*a}$ for smooth surfaces (u_{*a}<20 cm/s)

$\alpha = 4.38E - 5$ when u_{a*} is in units of cm/s

$K_{Lw} = \beta u_{*a}^2$ for rough surfaces
$\beta = 1.83E - 3$ when u_{a*} is in units of cm/s

$u_{*a} = 0.01 U_{10}(8 + 0.65 U_{10})^{1/2}$ from Wu (1980) and U_{10} is wind speed at 10 m in m/s and u_{*a} is in m/s.

Reaeration Temperature Dependence

Reaeration temperature dependence is usually based upon an Arrhenius formulation:

$$K_T = K_{20}\theta^{T-20} \tag{4-132}$$

where Θ is 1.024. This dependency is based on the variation in molecular diffusivity as a function of temperature. The molecular diffusivity of oxygen varies according to temperature based on the following equation:

$$D_{O2} = 4.58E - 11T + 1.2E - 9 \tag{4-133}$$

where:
   D_{O2} = molecular diffusivity of oxygen, $m^2\ sec^{-1}$
      T = temperature, $°C$

Using Equation 1 in Table B-2, the variation of KL as a function of temperature using Equation 43 (assuming D is a constant) and 44 yield similar results (**Figure 102**).

No temperature correction was made to the calculated value of K_L in earlier versions of the model. The latest version includes the correction with theta set to 1.024.
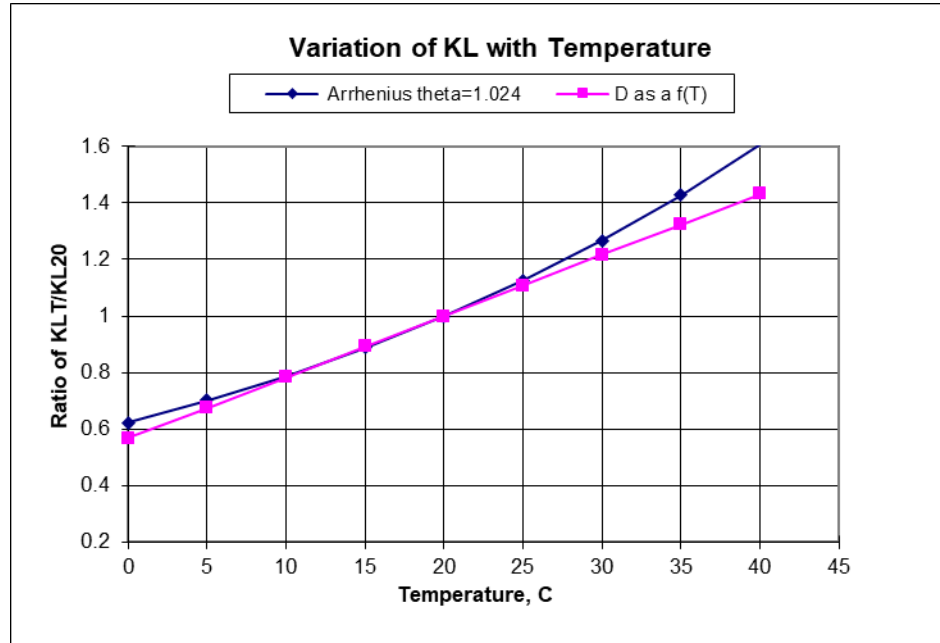
Figure 102. Variation of K_{LT}/K_{L20} as a function of temperature.

Dam Reaeration

Many rivers and reservoirs have spillways or weirs over which water entrains oxygen into a pool below the dam. This section outlines the approach for including oxygen and nitrogen entrainment at dams and weirs.

Small Dams or Weirs

Many rivers have small spillways or weirs over which water flows that entrains oxygen. **Table 22** lists formulae for predicting the entrainment of dissolved oxygen based on empirical data.

Table 22. Formulae for small dam or weir reaeration effects.

Equation	Comments	Reference
$D_a - D_b = \left[1 - \frac{1}{1+0.11ab(1+0.046T)H}\right]D_a$or $\frac{D_a}{D_b} = 1 + 0.11ab(1 + 0.046T)H$	D_a = DO deficit above dam, $g\ m^3$ D_b = DO deficit below dam, $g\ m^3$ T = temperature, ^oC H = height of water fall, ft a = 1.25 in clear to slightly polluted water to 1.00 in polluted water b = 1.00 for weir with free flow b = 1.3 for step weirs or cascades	Barrett et al. (1960)
$D_a - D_b = 0.037HD_a$	D_a = DO deficit above dam, $g\ m^{-3}$ D_b = DO deficit below dam, $g\ m^{-3}$ H = height of water fall, ft only valid for dams less than 15 ft and T between 20 and 25^oC	Mastropietro (1968)
$\frac{D_a}{D_b} = 1 + 0.38ab(1 - 0.11H)(1 + 0.046T)H$	D_a = DO deficit above dam, $g\ m^{-3}$ D_b = DO deficit below dam, $g\ m^{-3}$ T = temperature, ^oC H = height of water fall, m	Butts and Evans (1983)

Equation	Comments	Reference
	a = 1.8 for clean water to 0.65 for gross polluted water b = 0.05 for sluice gates b = 1.0 for sharp crested straight faced weir b = 0.45 for flat broad crested curved face weir b = 0.7 for flat broad crested weir with regular step b = 0.8 for sharp crested vertical face weir b = 0.6 for flat broad crested weir vertical face	

Most of these equations have been used for dams or weirs with heights of fall between 3 and 10 m. These equations do not generally predict supersaturation.

Large Dam Spillways/Gates

The USACE has been involved in gas abatement studies on the Columbia and Snake River system for many years (WES, 1996, 1997). Some of their research efforts have been focused on development of models of gas generation from spillways. These empirical models have been called CriSP 1.6 (Columbia Basin Research, 2000). The gas production equations used in CriSP are empirical correlations between total dissolved gas (TDG), usually measured a mile downstream of the dam after turbulence from the spillway had subsided, and discharge, usually measured in kcfs. The form of these equations is shown in **Table 23**.

Table 23. Equations used in CRiSP model for gas production.

Equation type	Equation	Description of empirical coefficients
Linear function of total spill	$\%TDG = mQ_s + b$	Q_s = total spill, *kcfs* m = empirical coefficient b = empirical coefficient
Bounded exponential of total spill	$\%TDG = a + be^{cQ_s}$	Q_s = total spill, *kcfs* a = empirical coefficient b = empirical coefficient c = empirical coefficient
Bounded exponential of the spill on a per spillway basis	$\%TDG = a + be^{cq_s}$	q_s = spill through an individual spillway, *kcfs* a = empirical coefficient b = empirical coefficient c = empirical coefficient

Examples of some of these correlations are shown in **Table 24**. In many cases, the %TDG in these correlations was constrained to a maximum of 145% and when the flow reached only a few kcfs, there was assumed to be no change in TDG from the forebay to the tailrace. Also, the correlations in **Table 24** sometimes changed from year to year based on changes in operating conditions or structural changes in the spillway or deflectors.

Table 24. Equations used in CRiSP model for gas production for Columbia and Snake Dams.

Dam	Equation	Coefficients
Bonneville	$\%TDG = mQ_s + b$	m = 0.12, b = 105.61
Lower Granite	$\%TDG = a + be^{cq_s}$	a = 138.0; b = -35.8; c = -0.10
Dworshak	$\%TDG = a + be^{cQ_s}$	a = 135.9; b = -71.1; c = -0.4787
Ice Harbor	$\%TDG = a + be^{cQ_s}$	a = 136.8; b = -42.0; c = -0.0340 1995 a = 138.7; b = -79.0; c = -0.0591 1996 a = 130.9; b = -26.5; c = -0.0220 1997 a = 120.9; b = -20.5; c = -0.0230 1998
Hell's Canyon	$\%TDG = a + be^{cQ_s}$	a = 138; b = -36; c = -0.02 [Assumed relationship - no data]

DO Impacts of Spillways

For each spillway, weir, or gate, the user now has the choice of equation to use for computing the effects of hydraulic structures on downstream dissolved oxygen. The equations chosen are shown in **Table 25**. These equations are based on equations from **Table 22** and **Table 23**.

Table 25. Spillways and weirs reaeration

#	Equation type	Equation	Description of empirical coefficients
1	Linear function of spill on a per spillway basis	$\%TDG = aq_s + b$ DO concentration, Φ_{O_2}, is determined from $\Phi_{O_2} = \%TDG\Phi_s$	$\%TDG$ = % total dissolved gas saturation q_s = spill through an individual spillway, kcfs a = empirical coefficient Φ_S = dissolved oxygen saturation
2	empirical coefficients a and b	$\%TDG = a + be^{q_s}$ Φ_{O_2}, is then determined from $\Phi_{O_2} = \%TDG\Phi_{sat}$	q_s = spill through an individual spill-way,*kcfs* a = empirical coefficient b = empirical coefficient c = empirical coefficient Φ_{sat} = dissolved oxygen saturation
3	Reaeration effect for a small height weir or dam (<10 m) empirical coefficients a, b, and c	$\dfrac{D_a}{D_b} = 1 + 0.38ab(1 - 0.11c)(1 + 0.046T)c$ Φ_{O_2} below the dam is then computed from: $\Phi_{O_2} = \Phi_{sat} - D_b$	D_a = DO deficit above dam, $g\ m^{-3}$ D_b = DO deficit below dam T = temperature in ^oC H = height of water fall, m a = 1.8 for clean water to 0.65 for gross polluted water b = 0.05 for sluice gates 1.0 for sharp crested, straight faced weir 0.45 for flat, broad crested, curved face weir 0.7 for flat, broad crested weir with regular step 0.8 for sharp crested, vertical face weir 0.6 for flat, broad crested weir with vertical face Φ_{sat} = dissolved oxygen saturation, $g\ m^{-3}$

Note that for equations 1 and 2, the maximum TDG allowed is 145%. If TDG is computed to be less than 100%, there is no effect of the spillway or gate on reaeration. For each spillway or gate defined in the

model, there is a section to define whether gas effects for nitrogen and dissolved oxygen are computed and, if so, by which formula.

For each spillway or weir, the user turns on the computations and then selects an equation number from **Table 25**. This algorithm only computes gas effects for flow from upstream to downstream. There is no adjustment of nitrogen or dissolved oxygen for reverse flow.

SYSTDG Algorithm

An algorithm for computing TDG from spillways was developed by Scheider and Hamilton (2015a, 2015b) to compute real-time TDG saturation levels in the Columbia River basin, USA. SYSTDG is an empirical regression equation for each spillway at a hydropower facility based on flow rate, tailwater depth, and barometric pressure. This algorithm also incorporates entrainment of water from powerhouse flows and specific TDG relations for each bay. The original development was an Excel-based spreadsheet model. The Corps of Engineers (Zhang and Threadgill, 2019) integrated this into CE-QUAL-W2 for the Columbia and Snake River hydropower facilities.

This review of the SYSTDG model is taken from Zhang and Threadgill (2019) who reviewed and summarized the SYSTDG equations and approach. Table 26 summarizes the SYSTDG TDG regression equations.

Table 26. List of spillway flow TDG production equations in SYSTDG from Scheider and Hamilton (2015b).

No	TDG Production Equation*
1	$TDG_{sp} = P1 * (1 - e^{P3 * Q_{sp}}) + bp$ $\Delta TDG_{sp} = P1 * (1 - e^{P3 * Q_{sp}})$
2	$TDG_{sp} = P1 * (twe - twce)^{P2} * (1 - e^{P3 * q_s}) + P4 + bp$ $\Delta TGP_{sp} = P1 * (twe - twce)^{P2} * (1 - e^{P3 * q_s}) + P4$
3	$TDG_{sp} = P1 * (twe - twce)^{P2} * q_s{}^{P3} + P4 + bp$ $\Delta TGP_{sp} = P1 * (twe - twce)^{P2} * q_s{}^{P3} + P4$
4	$TDG_{sp} = P1 * (twe - twce) + P2 * q_s{}^{P3} + P4 + bp$ $\Delta TGP_{sp} = P1 * (twe - twce) + P2 * q_s{}^{P3} + P4$
5	$TDG_{sp} = P1 * (1 - e^{P2 * q_s}) + P3 * (Temp_{tw} - P4) + bp$ $\Delta TDG_{sp} = P1 * (1 - e^{P2 * q_s}) + P3 * (Temp_{tw} - P4)$

*TDG_{sp} = spillway discharge total gas pressure (mmHg), ΔTGP_{sp} = spillway discharge gas pressure (mmHg), bp = observed barometric pressure (mmHg), twe = observed project tailwater elevation (feet), twce = project specific tailwater channel elevation (feet), twe - twce = tailwater channel depth (feet), $Temp_{tw}$ = tailwater temperature (°C), Q_{sp} = total project spillway discharge (kcfs), q_s = flow weighted specific spillbay discharge (kcfs), P1 - P4 = project specific coefficients (unitless) and are determined from nonlinear regression analyses.

Scheider and Hamilton (2015b) provided coefficient values for 11 federal dams on the Columbia and Snake River system as shown in Table 27.

Table 27. Coefficients for Spillway TDG Production in SYSTDG from Scheider and Hamilton (2015b).

Dam	E1	E2	P1	P2	P3	P4	TWCE	SPAT
Dworshak Dam (DWR) (# of bays known)	0.0	0.0	410.00	0.0	-0.210	-26.70	0.0	-
Dworshak Dam (DWR) (default)	0.0	0.0	288.20	0.0	-0.510	0.0	0.0	-
Dworshak Dam (DWR) (RO)	0.0	0.0	240.00	0.0	-0.32	0.0	0.0	-
Lower Granite Dam (LWG)	1.000	0.0	5.300	1.000	-0.123	0.0	585.0	8
Little Goose Dam (LGS)	1.200	0.0	5.566	1.000	-0.080	0.0	480.0	6
Lower Monumental Dam (LMN)	0.800	0.0	1.000	1.100	0.500	0.0	405.0*	8
Ice Harbor Dam (IHR)	1.000	0.0	0.156	1.345	0.7956	60.970	320.0	8
McNary Dam (MCN)	0.650	0.0	5.620	1.000	-0.119	0.0	228.0	21
John Day Dam (JDA)	0.150	0.0	1.000	1.000	0.671	23.500	135.0	20
Dalles Dam (TDA)	0.0	0.0	4.870	1.000	0.0	-207.51	0.0*	22
Bonneville Dam (BON)	0.0	0.0	1.560	13.660	1.000	23.030	0.0	20
Chief Joseph Dam (CHJ)	0.0	0.0	1.000	1.160	0.260	0.000	743.0	19
Grand Coulee Dam (GCL) (fbe < 1266)	1.380	22.600	0.0	0.0	0.0	312.00	0.0	0
Grand Coulee Dam (GCL) (fbe > =1266)	0.0	0.0	400.00	0.0	-0.020	0.0	0.0	0
Grand Coulee Dam (GCL) (fbe > =1266)	1.0	0.0	316.96	-0.098	1.085	11.4	0.0	0

*For LMN, the value for TWCE in the input tab was 400.00, but the value used in the TDG equation was 405.0. For TDA, the TWCE is specified as 68.0, but in order to fit the equation properly, a value of 0 had to be used (Scheider and Hamilton, 2015a, 2015b).

The unit spillway discharge was a surrogate measure for the velocity, momentum, and exposure time of aerated flow associated with spillway discharge. The higher the unit spillway discharge, the greater the TDG exchange during spillway flows. Flow weighted specific spillbay discharge can be actual measured discharges through each spillbay or computed as a function of the spill pattern:

$$q_s = \frac{\sum_{i=1}^{nb} Q_i^C}{\sum_{i=1}^{nb} Q_i^{(C-1)}}$$ **(4-134)**

Where Q_i = discharge through spillbay i, nb = the number of project spillbays, C = Project and spill pattern specific constant.

Table 28 lists C values for 11 federal dams on the Columbia and Snake River system (Scheider and Hamilton, 2015b) ranging from 1 to 4.01.

Table 28. Spill Pattern Identification with Exponential Coefficient (C) specified in SYSTDG*

Dam	Spill Pattern Name in FPP	Spill Pattern Name in SYSTDG	When to Use this Spill Pattern	C
LWG	Spring SP with RSW	Spring	From April 3-June 20	1
LWG	Summer SP with RSW	Summer	From June 21-August 31	2
LWG	No RSW	No RSW	Use when flows <30 kcfs	2
LGS	Low Crest with SW	Low Crest**	Use when flows >85 kcfs	2
LGS	High Crest with SW	High Crest**	Start of spill season and when flows 35-85 kcfs	2
LGS	No SW	No RSW	Use when flows < 35 kcfs	2
LGS	SW change or closure	Change	Used during the periods that the spillway weir is being changed from Hi to Lo or closed completely.	N/A[1]
LMN	Bulk with RSW	Bulk	Start of spill season and when flows <140 kcfs or full PH does not exist	4
LMN	Uniform with RSW	Uniform	Use when flows >140 kcfs or when full PH exist	2
LMN	No RSW	No RSW	Use when flows < 30 kcfs	2
IHR	45 kcfs/TDG Spill Cap	45 kcfs/SC	When spill operation = 45kcfs/SC	1.2
IHR	30% Spill with RSW	30%	When spill operation = 30%	2
IHR	No RSW	No RSW	Use when flows < 30 kcfs	2
MCN	With TSWs in 19 & 20	With TSW	Use when flows < 259 kcfs and April 10 - June 7	3.01
MCN	No TSW	No TSW	Use when flows > 259 kcfs; and June 8 – Aug 31	4.01
MCN	Navigation with TSW	Navigation	Used when flows are <165 kcfs, and there is a navigational lock-age & the barge want it	2.01
MCN	TSW Removal	Removal	When TSWs are being removed	2.01
JDA	With TSWs in 18 &19	With TSW	Use when spill <305 kcfs and April 10 –August 31	2.01
JDA	No TSW	No TSW	Used before, during and after TSW removal or installation; Also when spill >305 kcfs or flows > 685 kcfs (this is the flood pattern)	1.01
TDA	40% Spill	40%	April 10-August 31	N/A[2]
BON	Vertical gate openings	Vertical Openings	April 10-August 31	2
CHJ	---	Center First	All times	2.01
DWR	---	Spillway1	Use when 1 spillbay is used	N/A[3]
DWR	---	Spillway2	Use when 2 spillbays are used	N/A[3]
DWR	---	RO	Use with Regulating Outlet spill	N/A[3]
DWR	---	No Spill	Use when there is NO spill	N/A[3]
GCL	---	---	No spill pattern is used	-

* Spill pattern name: FPP, SW, RSW, TSW
1. Not currently implemented in SYSTDG.

2. Spillway TDG production equation is a function of tailwater elevation only. No C value is used.
3. C values are not used in DWR TDG production equations.

The interaction of powerhouse flows and the highly aerated spillway flows can be considerable at many dams. The powerhouse discharge can be entrained with the spillway discharge, becoming "gassed" to the same level as the spillway. In SYSTDG, the entrainment of powerhouse flows is computed as a simple linear function of spillway flows. Without spillway discharge, there is no mechanism to attract powerhouse flows into the spillway region and no air-entrainment mechanism to drive local TDG supersaturation. As spillway flows increase relative to powerhouse flows, both bubble production and water entrainment ramp up to a point at which nearly all powerhouse flows are exposed to bubbles entrained at the spillway. Table 29 lists three equations used to calculate the entrainment of powerhouse flow in SYSTDG (Scheider and Hamilton, 2015a).

Table 29. List of powerhouse flow entrainment equations in SYSTDG

Equation #	Powerhouse Flow Entrainment Equation*
1	$Q_{ent} = E1 * Q_{sp} + E2$
2	$Q_{ent} = \min[\,(Q_{tot} / 60)\,,\,1] * E1 * Q_{sp} + E2$
3	$Q_{ent} = \min[\,(Q_{sp} / 20)\,,\,1] * E1 * Q_{sp} + E2$

*Q_{ent} = Total powerhouse flow that is entrained in spillway flow (kcfs), Q_{tot} = total project discharge (powerhouse and spillway) (kcfs), *E1 - E2* = project specific coefficients (unitless).

E_1 and E_2 are model coefficients that represent the site-specific geometric configuration of the spillway in relation to the outflow direction of the powerhouse. Their values for 11 dams on the Columbia and Snake River system are listed in Table 2. Q_{ent} calculated from equations listed in Table 29 must be less than or equal to the total powerhouse discharge:

$$Q_{ent} = \min(Q_{ent},\ Q_{tot} - Q_{sp}\,) \qquad\qquad \textbf{(4-135)}$$

In SYSTDG, the average tailrace mixing TDG pressures generated from a project are computed from the flow weighted average TDG pressures of the spillway and the powerhouse. TDG pressures of flows released from the powerhouse are assumed equivalent to the TDG pressure in the forebay.

$$TDG_{rel} = \frac{TDG_{sp}(Q_{sp}+Q_{ent})+TDG_{ph}(Q_{ph}-Q_{ent})}{Q_{ph}+Q_{sp}} \qquad\qquad \textbf{(4-136)}$$

Where **TDG_{rel}** = project release TGP after mixing (mmHg), **TDG_{sp}** = spillway TGP (mmHg), **TDG_{ph}** = release TGP through the powerhouse turbines (mmHg), **Q_{sp}** = Total project spill (kcfs), **Q_{ph}** = Total flow through powerhouse turbines (kcfs).

The equation above for tailrace TDG during spill events. Q_{ent}, Q_{sp}, Q_{ph} are known (gauged) or assumed (forecast). The entrained powerhouse flow was assumed to be exposed to the same conditions that spillway flows encounter and, hence, achieve the same pressures. The TDG associated with the powerhouse release is generally assumed to be equivalent to the TDG observed in the forebay. TDG_{ph} is either from a gauge

(boundary condition) or routed from upstream of the project (DWR is an exception). TDG_{sp} is computed from the spillway TDG production equations listed in Table 26.

Dissolved Oxygen Saturation Computations

The dissolved oxygen saturation is computed from Mortimer's (1981) formulation:

$$\Phi_{O2_{sat}} = P_{alt}e^{(7.7117-1.31403[ln\{T+45.93\}])}$$

(4-137)

where:

T = water temperature, $°C$

P_{alt} = altitude correction factor=$\left(1 - \frac{H}{44.3}\right)^{5.25}$,

H = elevation of the waterbody, $km\ above\ sea\ level$

The saturation value is also a function of the chlorinity in saline environments. The following equation is used to compute DO saturation for a saltwater waterbody type that includes salinity effects (APHA, 1985; EPA 1985; Thomann and Mueller, 1987).

$$\Phi^*{}_{O2sat} = e^{\left(ln(\Phi_{O2sat})-S\left[1.7674X10^{-2}-\frac{1.0754X10^1}{T}+\frac{2.1407X10^3}{T^2}\right]\right)}$$

(4-138)

where:

S = salinity, $kg\ m^{-3}$

T = temperature, $°K$

The section on N_2 gas under Generic Constituents shows the computation procedure for N2 gas saturation.

Sediments

Organic sediment contributions to nutrients and dissolved oxygen demand are simulated using three methods. The first method uses a constant, or zero-order, release and demand. This method has been frequently used to model sediment demands and nutrient release rates. It does not depend on sediment concentrations or require a separate sediment compartment. However, the formulation is not predictive as the rates do not vary over time except as a result of temperature dependence of the decay rate. As a consequence, results should be interpreted cautiously when evaluating effects of different nutrient loadings on dissolved oxygen in a waterbody.

The second method uses a sediment compartment to accumulate organic sediments and allow their decay aerobically. Nutrient releases and oxygen demand are thus dependent upon sediment accumulation – a 1st-order process. However, there is no release of phosphorus or other diagenesis products when overlying water is anoxic since this sediment compartment is labile, oxic decay of organics on the sediment surface. Either of these methods, or a combination, may be used to simulate effects of organic sediments upon water quality.

The third method is the sediment diagenesis model which is discussed in the section **Sediment Diagenesis Model**, which models both an aerobic and an anaerobic sediment layers.

KINETICS

Zero Order Model

The 0-order process uses a specified sediment oxygen demand and anoxic release rates for phosphorus, ammonium, inorganic carbon, and iron that are temperature dependent. Nutrient releases do not occur when dissolved oxygen concentrations are above a minimum value **[O2LIM]** nor do they occur if the SOD is set to zero. The sediment contribution to inorganic carbon is computed as a fraction of the sediment oxygen demand.
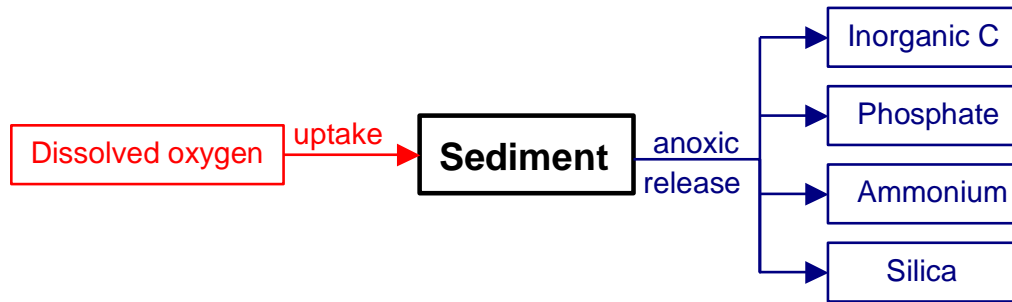
Figure 103. Internal flux between 0-order sediment compartment and other compartments.
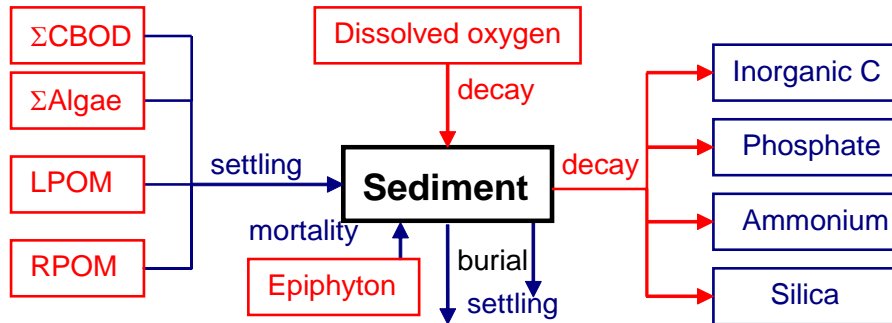
Figure 104. Internal flux between 1st-order sediment compartment and other compartments.

First Order Model

The 1st-order sediment compartment requires specifying inclusion of this compartment in the simulation, a decay rate, and initial conditions. The sediment compartment is not transported, except for focusing of sediments to the bottom by a user-defined settling velocity. Instead, a compartmental equation is written for the sediment compartment that is solved in the subroutine SEDIMENT.

Referring to **Figure 104**, the equation for the 1st-order sediment compartment is:

$$S_{sed} = \underbrace{\frac{\omega_{POMR}A_{bottom}}{Vol_{cell}}\Phi_{POMR}}_{POMR\ sedimentation} + \underbrace{\frac{\omega_{POML}A_{bottom}}{Vol_{cell}}\Phi_{POML}}_{POML\ sedimentation} + \sum \underbrace{\frac{\omega_a A_{bottom}}{Vol_{cell}}\Phi_a}_{algae\ sedimentation} - \underbrace{\gamma_{om}K_s\Phi_s}_{sediment\ decay} + \underbrace{K_{epom}K_{eb}\Phi_e}_{epiphyton\ burial} - $$

$$\underbrace{\frac{\omega_{SED}A_{bottom}}{Vol_{cell}}\Phi_s}_{sediment\ sedimentation} + \underbrace{\frac{\omega_{CBOD}A_{bottom}}{Vol_{cell}}\Phi_{CBOD}}_{CBOD\ sedimentation} - \underbrace{K_{burial}\Phi_s}_{sediment\ burial}$$

(4-139)

where:

γ_{OM} = rate multiplier for organic matter

ω_{POM} = POM settling velocity, $m\ sec^{-1}$

ω_a = algal settling velocity, $m\ sec^{-1}$

ω_{CBOD} = particulate CBOD settling velocity, $m\ sec^{-1}$

ω_{SED} = sediment settling velocity, $m\ sec^{-1}$

K_{sed} = sediment decay rate, sec^{-1}

Φ_a = algal concentration, $g\ m^{-3}$

Φ_{LPOM} = POM labile concentration, $g\ m^{-3}$

Φ_{RPOM} = POM refractory concentration, $g\ m^{-3}$

Φ_s = organic sediment concentration, $g\ m^{-3}$

Vol_{cell} = volume of computational cell, m^3

A_{bottom} =Area of bottom, m^2

Φ_e = ephiphyton concentration, $g\ m^{-3}$

K_{epom} =fraction of ephiphyton that go to particulate fraction and settle into sediment at death

K_{em} = ephiphyton mortality rate

K_{burial} = sediment burial rate, sec^{-1}

Pauer and Auer (2000) claim that nitrification is generally a sediment-based phenomena rather than one existing in the water column. Their argument is based on the study of a samples obtained from a hyper-eutrophic lake-river system which had extremely high ammonia concentrations (2-10 mg/l NH_3-N) and where cell counts indicated much higher nitrifier populations in the sediments rather than in the water column. They question if nitrification is being modeled correctly in many water quality models, where nitrification is treated as occurring in the water column rather than the sediments.

Nitrification rates of water column samples were measured in 2.5 L bottles kept in the dark at 20° Celsius. Rates of nitrification were to be determined by tracking concentrations of nitrogen species in the bottles. Since no change in ammonia or nitrate-nitrite concentrations were noted, the authors assumed that the lack of observable nitrification was due to low nitrifier populations occurring in the water column of the lake and river. Sediment nitrification rates were measured using sediment core samples under similar conditions. Changes in the concentrations of nitrogen species were apparent and an average sediment nitrification rate of 0.34 g N/m²/day was determined. Table 30 summarizes the nitrification rates.

Table 30. Areal nitrification rates of sediment nitrifiers of Onondaga Lake and the Seneca River, New York (Pauer and Auer, 2000).

Reaction	Source	Growth Temperature (Celsius)	Nitrification rate (g N/m²/day)
Nitrification	Onondaga Lake, Seneca River, New York	20°	0.21 to 0.67 (mean=0.34)

Sediment Variable Stoichiometry and Kinetics

Variable stoichiometry of sediments is done automatically within the W2 model. In addition to sediment phosphorus and sediment nitrogen, there is also a sediment carbon compartment. The sediment carbon stoichiometry is variable because organic matter, algae and periphyton/epiphyton may have differing car-

bon stoichiometry. The initial sediment stoichiometry for P, N, and C is based on the given initial stoichiometry for organic matter. The decay rate of sediment in a model cell is the mass averaged decay rate of the LPOM, RPOM, and the CBOD groups.

Sediment Phosphorus

$$S_{Psed} = \underbrace{\frac{\omega_{POMR}A_{bottom}}{Vol_{cell}}\Phi_{RPOM-P}}_{\text{RPOM-P sedimentation}} + \underbrace{\frac{\omega_{POML}A_{bottom}}{Vol_{cell}}\Phi_{LPOM-P}}_{\text{LPOM-P sedimentation}} + \sum\underbrace{\frac{\omega_a A_{bottom}}{Vol_{cell}}\delta_{Pa}\Phi_a}_{\text{algae sedimentation}} - \underbrace{K_s\Phi_{s-P}}_{\text{sediment decay}}$$

$$+\underbrace{\sum K_{epom}K_{em}\delta_{Pe}\Phi_e}_{\text{epiphyton mortality}} - \underbrace{\frac{\omega_{SED}A_{bottom}}{Vol_{cell}}\Phi_{s-P}}_{\text{sediment sedimentation}}$$

where:

ω_{POM} = POM settling velocity, $m\ sec^{-1}$
ω_a = algal settling velocity, $m\ sec^{-1}$
ω_{CBOD} = particulate CBOD settling velocity, $m\ sec^{-1}$
ω_{SED} = sediment settling velocity, $m\ sec^{-1}$
K_{sed} = sediment decay rate, sec^{-1}
Φ_a = algal concentration, $g\ m^{-3}$
δ_{Pe} = epiphyton/periphyton stoichiometric coefficient for phosphorus
δ_{Pa} = algal stoichiometric coefficient for phosphorus
K_{sed} = sediment decay rate, sec^{-1}
Φ_{LPOM-P} = labile POM labile concentration, $g\ m^{-3}$
Φ_{RPOM-P} = refractory POM concentration, $g\ m^{-3}$
Φ_{s-P} = sediment phosphorus concentration, $g\ m^{-3}$
Vol_{cell} = volume of computational cell, m^3
A_{bottom} = Area of bottom, m^2
Φ_e = epiphyton concentration, $g\ m^{-3}$
K_{epom} = fraction of epiphyton that go to particulate fraction and settle into sediment at death
K_{em} = epiphyton mortality rate

Sediment Nitrogen

$$S_{Nsed} = \underbrace{\frac{\omega_{POMR}A_{bottom}}{Vol_{cell}}\Phi_{RPOM-N}}_{\text{RPOM-N sedimentation}} + \underbrace{\frac{\omega_{POML}A_{bottom}}{Vol_{cell}}\Phi_{LPOM-N}}_{\text{LPOM-N sedimentation}} + \sum\underbrace{\frac{\omega_a A_{bottom}}{Vol_{cell}}\delta_{Na}\Phi_a}_{\text{algae sedimentation}} - \underbrace{K_s\Phi_{s-N}}_{\text{sediment decay}}$$

$$+\underbrace{\sum K_{epom}K_{em}\delta_{Ne}\Phi_e}_{\text{epiphyton mortality}} - \underbrace{\frac{\omega_{SED}A_{bottom}}{Vol_{cell}}\Phi_{s-N}}_{\text{sediment sedimentation}} + \underbrace{\frac{\omega_{NO3SED}A_{bottom}}{Vol_{cell}}\Phi_{NO3-N}f_{NO3-SED}}_{\text{diffusion of NO3 into sediments}}$$

where:

ω_{POM} = POM settling velocity, $m\ sec^{-1}$
ω_a = algal settling velocity, $m\ sec^{-1}$
ω_{CBOD} = particulate CBOD settling velocity, $m\ sec^{-1}$

ω_{SED} = sediment settling velocity, $m\ sec^{-1}$

K_{sed} = sediment decay rate, sec^{-1}

Φ_a = algal concentration, $g\ m^{-3}$

δ_{Pe} = epiphyton stoichiometric coefficient for phosphorus

δ_{Pa} = algal stoichiometric coefficient for phosphorus

K_{sed} = sediment decay rate, sec^{-1}

δ_{Ne} = epiphyton stoichiometric coefficient for nitrogen

δ_{Na} = algal stoichiometric coefficient for nitrogen

ω_{NO3} = NO$_3$-N diffusion rate into sediments, $m\ sec^{-1}$

Φ_{LPOM-N} = labile POM concentration, $g\ m^{-3}$

Φ_{RPOM-N} = refractory POM concentration, $g\ m^{-3}$

Φ_{NO3-N} = NO$_3$-N concentration, $g\ m^{-3}$

Φ_{s-N} = sediment nitrogen concentration, $g\ m^{-3}$

Vol$_{cell}$ = volume of computational cell, m^3

A_{bottom}= Area of bottom, m^2

Φ_e = epiphyton concentration, $g\ m^{-3}$

K_{epom}= fraction of epiphyton that go to particulate fraction and settle into sediment at death

K_{em} = epiphyton mortality rate

$f_{NO3-SED}$= fraction of NO$_3$-N diffused into sediments that is incorporated into organic matter in the sediments (the rest, 1- $f_{NO3-SED}$, is denitrified into N$_2$)

Sediment Carbon

$$S_{Csed} = \underbrace{\frac{\omega_{POMR}A_{bottom}}{Vol_{cell}}\gamma_{COM}\Phi_{RPOM}}_{RPOM\ sedimentation} + \underbrace{\frac{\omega_{POML}A_{bottom}}{Vol_{cell}}\gamma_{COM}\Phi_{LPOM}}_{LPOM\ sedimentation} + \sum \underbrace{\frac{\omega_a A_{bottom}}{Vol_{cell}}\delta_{Ca}\Phi_a}_{algae\ sedimentation} - \underbrace{K_s\Phi_{s-C}}_{sediment\ decay}$$

$$+ \sum \underbrace{K_{epom}K_{em}\delta_{Ce}\Phi_e}_{epiphyton\ mortality} - \underbrace{\frac{\omega_{SED}A_{bottom}}{Vol_{cell}}\Phi_{s-C}}_{sediment\ sedimentation}$$

where:

ω_{POML}=Labile POM settling velocity, $m\ sec^{-1}$

ω_{POMR} = Refractory POM settling velocity, $m\ sec^{-1}$

ω_a = algal settling velocity, $m\ sec^{-1}$

ω_{SED} = sediment settling velocity, $m\ sec^{-1}$

K_{sed} = sediment decay rate, sec^{-1}

Φ_a = algal concentration, $g\ m^{-3}$

δ_{Ce} = epiphyton stoichiometric coefficient for carbon

δ_{Ca} = algal stoichiometric coefficient for carbon

γ_{COM} =organic matter stoichiometric coefficient for carbon

K_{sed} = sediment decay rate, sec^{-1}

Φ_{LPOM} = labile POM carbon concentration, $g\ m^{-3}$

Φ_{RPOM} = refractory POM carbon concentration, $g\ m^{-3}$

Φ_{s-C} = sediment carbon concentration, $g\ m^{-3}$

Vol$_{cell}$ = volume of computational cell, m^3

A_{bottom}= Area of bottom, m^2

Φ_e = epiphyton concentration, *g m^{-3}*
K_{epom}= fraction of epiphyton that go to particulate fraction and settle into sediment at death
K_{em} = epiphyton mortality rate

Sediment Diagenesis Model

The sediment diagenesis model in CE-QUAL-W2 Version 4 and later is based on work from ERM and Golder (2011), Prakash et al. (2015), and Berger and Wells (2014) that were supported by CEMA (Cumulative Environmental Management Association, Canada). The ERM and Golder (2011) report is included in the model download package and describes those model processes. Processes described in the Berger and Wells (2014) report are included below.

Sediment Phosphorus

A schematic of the sediment phosphate model is shown in Figure 105.

Figure 106 and Figure 107 show the phosphate sources and sinks in the aerobic and anaerobic compartments, respectively, in the CE-QUAL-W2 model framework.
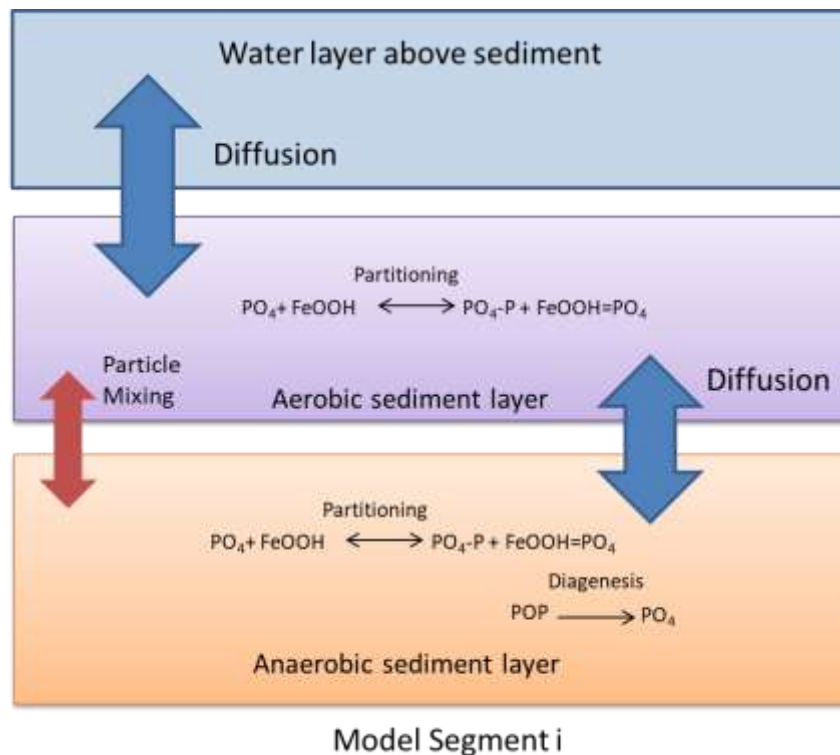
Figure 105. Schematic of sediment phosphate model (DiToro, 2001).
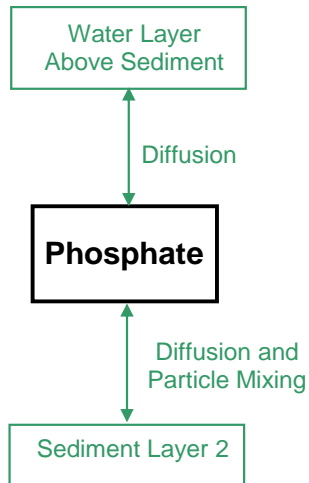
Figure 106. Internal flux between phosphate within the aerobic sediment layer 1 and other compartments.
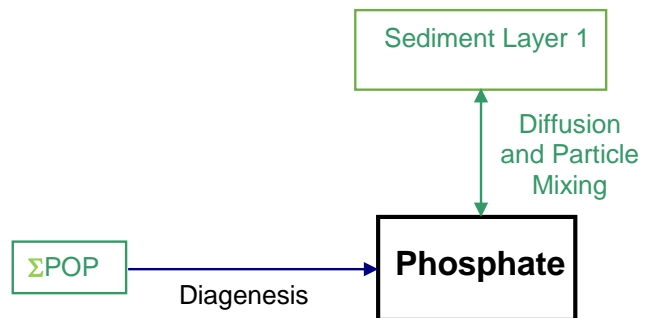
Figure 107. Internal flux between phosphate within the anaerobic sediment layer 2 and other compartments.

Because the aerobic layer is assumed to be very thin, oxidation of particulate organic phosphorus is assumed to be negligible. The source/sink rate equation for phosphate in sediment layer 1 is assumed to be zero:

$$S_{PO41} = 0$$

The rate equation for phosphate in sediment layer 2 is:

KINETICS

$$S_{PO42} = \underbrace{\sum_{i=1}^{3} k_{POPi} \gamma_{POP} \Phi_{POPi}}_{\text{Diagenesis}}$$

where:

γ_{POP} =   particulate organic phosphorus temperature rate multiplier

k_{POPi} = particulate organic phosphorus class i mineralization rate, sec^{-1}

Φ_{POPi}= particulate organic carbon class i concentration, $g\ m^{-3}$

The three classes correspond to labile, refractory, and inert/slow refractory particulate organic phosphorus for i=1, i=2, and i=3, respectively. Phosphate can exist in dissolved and particulate forms. Dissolved oxygen concentrations determine the extent to which dissolved phosphate sorbs to iron oxyhydroxide particulates. Within the aerobic layer phosphate sorbs to iron oxyhydroxide. At low dissolved oxygen concentrations, iron oxyhydroxide is reduced and the sorbed phosphate is released.

Mass balance equations for layer 1 (aerobic) and layer 2 (anaerobic) are:

$$H_1 \frac{d\Phi_{PO41}}{dt} = -K_{L01}(f_d \Phi_{PO41} - \Phi_{PO40}) + K_{L12}(f_d \Phi_{PO42} - f_d \Phi_{PO41})$$
$$+ w_{12}(f_p \Phi_{PO42} - f_p \Phi_{PO41}) - w_2 \Phi_{PO41}$$

$$H_2 \frac{d\Phi_{PO42}}{dt} = -K_{L12}(\Phi_{PO42} - \Phi_{PO41}) - w_{12}(f_p \Phi_{PO42} - f_p \Phi_{PO41}) + w_2(\Phi_{PO41} - \Phi_{PO42})$$
$$+ H_2 S_{PO42}$$

where:

Φ_{PO41} = total phosphate concentration in layer 1, $g\ m^{-3}$

Φ_{PO42}= total phosphate concentration in layer 2, $g\ m^{-3}$

Φ_{PO40} = phosphate concentration in water column, $g\ m^{-3}$

H_1 = height of layer 1, m

H_2 = height of layer 2, m

K_{L01} = mass transfer coefficient between water column and layer 1, $m\ s^{-1}$

K_{L12} = mass transfer coefficient between layer 1 and layer 2, $m\ s^{-1}$

f_d = dissolved fraction of phosphate

f_p = particulate fraction of phosphate

w_{12} = particle mixing velocity between layer 1 and layer 2, $m\ s^{-1}$

w_2 = burial velocity, $m\ s^{-1}$

The implicit finite difference scheme for layer 1 is

$$H_1 \frac{\Phi_{PO41}^{t+\Delta t} - \Phi_{PO41}^{t}}{\Delta t}$$
$$= -K_{L01}(f_d \Phi_{PO41}^{t+\Delta t} - \Phi_{PO40}) + K_{L12}(f_d \Phi_{PO42}^{t+\Delta t} - f_d \Phi_{PO41}^{t+\Delta t})$$
$$+ w_{12}(f_p \Phi_{PO42}^{t+\Delta t} - f_p \Phi_{PO41}^{t+\Delta t}) - w_2 \Phi_{PO41}^{t+\Delta t}$$

Rearranging

$$\left(-\frac{H_1}{\Delta t} - f_d K_{L01} - f_d K_{L12} - w_{12}f_p - w_2\right) \Phi_{PO41}^{t+\Delta t} + (K_{L12}f_d + w_{12}f_p)\Phi_{PO42}^{t+\Delta t}$$
$$= -\frac{H_1}{\Delta t}\Phi_{PO41}^{t} - K_{L01}\Phi_{PO40}$$

And the finite difference scheme for layer 2

$$H_2 \frac{\Phi_{PO42}^{t+\Delta t} - \Phi_{PO42}^t}{\Delta t}$$
$$= -K_{L12}\left(f_d\Phi_{PO42}^{t+\Delta t} - f_d\Phi_{PO41}^{t+\Delta t}\right) - w_{12}\left(f_p\Phi_{PO42}^{t+\Delta t} - f_p\Phi_{PO41}^{t+\Delta t}\right)$$
$$+ w_2\left(\Phi_{PO41}^{t+\Delta t} - \Phi_{PO42}^{t+\Delta t}\right) + H_2 S_{PO42}$$

Rearranging

$$\left(f_d K_{L12} + f_p w_{12} + w_2\right)\Phi_{PO41}^{t+\Delta t} + \left(-\frac{H_2}{\Delta t} - f_d K_{L12} - f_p w_{12} - w_2\right)\Phi_{PO42}^{t+\Delta t}$$
$$= -H_2 S_{PO42} - \frac{H_2}{\Delta t}\Phi_{PO42}^t$$

The fractions associated with dissolved and particulate forms can be calculated with (Chapra, 1997):

$$f_d = \left(\frac{1}{\varphi + K_{dp}(1-\varphi)\rho}\right)$$
$$f_p = \left(\frac{K_{dp}(1-\varphi)\rho}{\varphi + K_{dp}(1-\varphi)\rho}\right)$$

where:
   f_d = dissolved fraction of phosphate
   f_p = particulate fraction of phosphate
   φ = sediment porosity
   ρ = sediment density, *g m⁻³*
      K_{dp} = phosphorus sorption coefficient, *m³ g⁻¹*

Consumption of Dissolved Oxygen due to Sediment Re-suspension

Particulate organic matter in the sediments can be resuspended by turbulence caused by wind or by bottom scour caused by high current velocities. Once particulate organic matter has been re-suspended into an aerobic water column, it will decay and consume dissolved oxygen.

Wind Induced Resuspension

This algorithm for predicting the resuspension of particulate organic matter due to wind is based on work from Kang et al. (1982) where the bottom shear stress is computed based on wind speed, wind fetch and depth. This algorithm is shown in Chapter 2 in the section Sediment Resuspension.

Bottom Scour Resuspension

Following the approach of Edinger (2002) in the 3D model GLLVHT, the CE-QUAL-W2 model can compute the bottom scour of sediment (inorganic or organic) in units of g/m²/s from Nielson (1992) as

$$Bottom\ scour\ rate\ \left[\frac{M}{L^2 T}\right] = V_{scour} C_{bottom}$$

where the scour velocity V_{scour} (m/s) is calculated from

$$V_{scour} = \frac{0.00033 \left(\frac{\theta'}{\theta_c} - 1\right)(S_g - 1)^{0.6} g^{0.6} d^{0.8}}{\nu}$$

and

g = acceleration due to gravity, 9.78 m^2/s

d = particle diameter, m

θ' = Shield's parameter, $\theta' = \frac{\tau_{bottom}}{[g(S_g-1)d]}$

θ_c = critical Shield's parameter [User input for each particle size]

τ_{bottom} = bottom shear stress in m^2/s^2, when using the Chezy coefficient, $\tau_{bottom} = \frac{gU_{bottom}^2}{C^2}$

U_{bottom} = bottom velocity, m/s

C = Chezy coefficient in units, m$^{0.5}$/s

S_g = specific gravity of solid, $\rho_{solid}/\rho_{water}$

ν = molecular viscosity of water, $\nu = 1.79E - 6\exp(-0.0266T)$

C_{bottom} = bottom sediment concentration in mg/l, $C_{bottom} = C_{KB}exp\left(\frac{V_s\Delta z}{D_z}\right)$ or a minimum bottom concentration defined between 1.0 mg/l (0.02 mm particle diameter and S_g=1.2), 3.0 mg/l (0.2 mm particle diameter and S_g=1.8), and 5.0 mg/l (2.0 mm particle diameter and S_g=2.2) [from Schubel et al. (1978)]

V_s = settling velocity of particles, m/s

Δz = vertical grid spacing at the bottom, m

C_{KB} = Bottom concentration of suspended solids, mg/l

D_z = vertical mass turbulent diffusion coefficient, m^2/s

T = water temperature, ^{o}C

The model user can input a value of critical Shields parameter in the control file or one can have the model estimate it based on the following approach.   Cao et al. (2006) used a simple estimate of the critical Shield's parameter based on the particle Reynolds number explicitly. The particle Reynolds number, R, is defined as

$$R = d\sqrt{S_g g d}$$

The critical Shield's criterion is then

$\theta_c = \frac{\left[1+(0.0223R)^{2.8358}\right]^{0.3542}}{3.0946R^{0.6769}}$ for R between 6.6 and 282.8

$\theta_c = 0.1414R^{-0.2306}$ for R < 6.6

$\theta_c = 0.045$ for R > 282.8

Mass Balance Equations for Particulate Organic Matter

The loss of particulate organic matter to the water column due to resuspension needs to be included in the mass balance equations for particulate organic carbon (POC), particulate organic nitrogen (PON), and particulate organic phosphorus (POP). The mass balance equation for POC in the anaerobic layer (layer 2) is (DiToro, 2001):

$$H_2 \frac{d\Phi_{POCi}}{dt} = -k_{POCi}\theta_{POCi}^{(T-20)}\Phi_{POCi}H_2 - w_2\Phi_{POCi} + f_{POCi}J_{POC} - E_{POCi}$$

where:

Φ_{POCi} = POC concentration in reactivity class i in layer 2, $g\ m^{-3}$

H_2 = height of layer 2, m

J_{POC} = depositional flux of POC from water column, $g\ m^{-2}\ s^{-1}$

E_{POCi} = resuspension rate of reactivity class i, $g\ m^{-2}\ s^{-1}$
k_{POCi} = reaction rate of reactivity class i, s^{-1}
f_{POCi} = fraction of J_{POC} that is in reactivity class i
θ_{POCi} = temperature coefficient for reactivity class i
T_2 = temperature of layer 2, $°C$
w_2 = burial velocity, $m\ s^{-1}$

And the finite difference scheme for layer 2

$$H_2 \frac{\Phi_{POCi}^{t+\Delta t} - \Phi_{POCi}^{t}}{\Delta t} = -k_{POCi}\theta_{POCi}^{(T-20)}\Phi_{POCi}^{t+\Delta t}H_2 - w_2\Phi_{POCi}^{t+\Delta t} + f_{POCi}J_{POC} - E_{POCi}$$

Rearranging

$$H_2 \frac{\Phi_{POCi}^{t+\Delta t}}{\Delta t} + k_{POCi}\theta_{POCi}^{(T-20)}\Phi_{POCi}^{t+\Delta t}H_2 + w_2\Phi_{POCi}^{t+\Delta t} = H_2 \frac{\Phi_{POCi}^{t}}{\Delta t} + f_{POCi}J_{POC} - E_{POCi}$$

And solving for $\Phi_{POCi}^{t+\Delta t}$:

$$\Phi_{POCi}^{t+\Delta t} = \left(\Phi_{POCi}^{t} + \frac{\Delta t}{H_2}f_{POCi}J_{POC} - \frac{\Delta t}{H_2}E_{POCi}\right)\left(1 + \frac{w_2\Delta t}{H_2} + k_{POCi}\theta_{POCi}^{(T-20)}\Delta t\right)^{-1}$$

The mass balance equations for PON and POP would be solved for in analogous fashion.

Dynamic Calculation of Sediment pH and Temperature

pH

The dynamic calculation of pH was implemented using a similar approach as a pH model developed by the United States Geological Survey (Sullivan et al, 2013). In order to calculate pH, sediment organic carbon, sediment alkalinity, and sediment temperature also had to be modeled.

Sediment Total Inorganic Carbon

A schematic of the sediment total inorganic carbon model is shown in Figure 108. Figure 109 and Figure 110 show the total inorganic carbon sources and sinks in the aerobic and anaerobic compartments, respectively, in the CE-QUAL-W2 model framework.

KINETICS
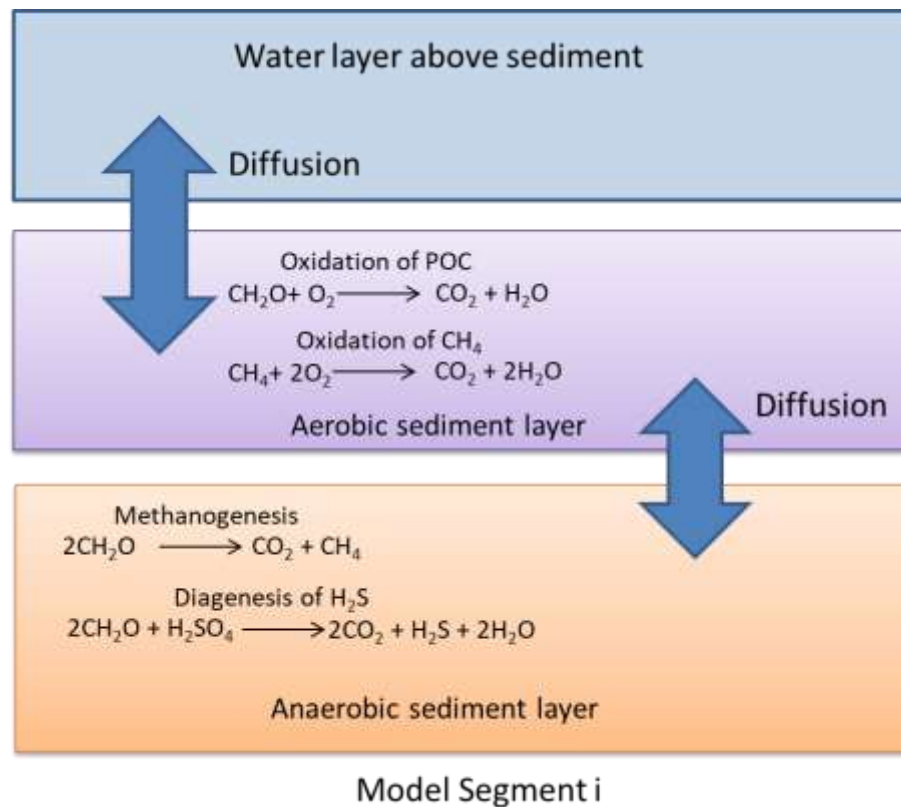
Figure 108. Schematic of sediment inorganic carbon model.
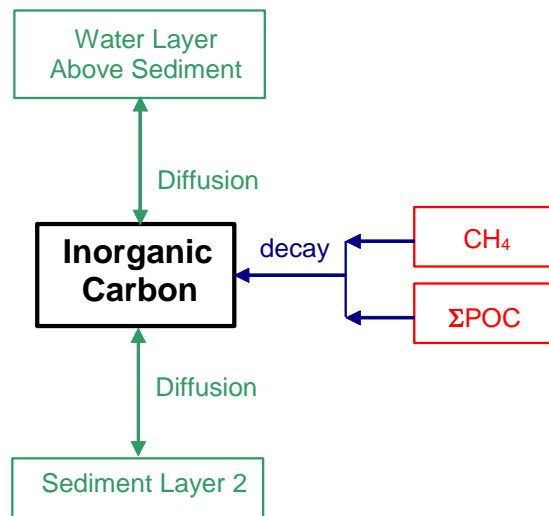
Figure 109 **Internal flux between inorganic carbon within the aerobic sediment layer 1 and other compartments.**
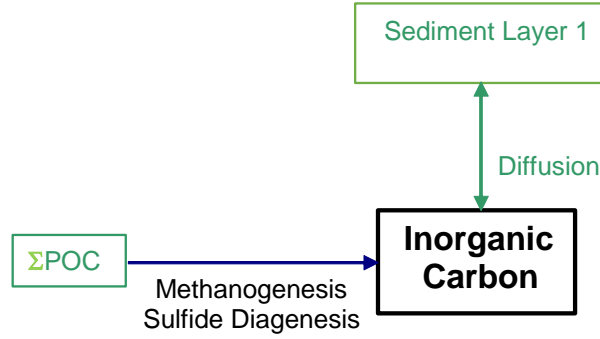
Figure 110 Internal flux between inorganic carbon within the anaerobic sediment layer 2 and other compartments.

The rate equation for total inorganic carbon (TIC) in the aerobic sediment layer 1 is:

$$S_{TIC1} = \underbrace{\sum k_{POC1} \gamma_{POC} \Phi_{POC}}_{\text{POC decay}} + \underbrace{k_{CH41} \gamma_{CH4} \Phi_{CH4}}_{\text{CH4 decay}}$$

where:
γ_{POC} = particulate organic carbon temperature rate multiplier
γ_{CH4} = methane temperature rate multiplier
k_{POC1} = POC decay rate in layer 1, *sec⁻¹*
k_{CH41} = methane decay rate in layer 1, *sec⁻¹*
k_{POCm2} = methanogenesis rate in layer 2, *sec⁻¹*
k_{POCs2} = sulfide diagenesis rate in layer 2, *sec⁻¹*
Φ_{POC} = particulate organic carbon concentration, *g m⁻³*
Φ_{CH4} = methane concentration, *g m⁻³*

The rate equation for TIC in the anaerobic sediment layer 2 is:

$$S_{TIC2} = \underbrace{\sum k_{POCm2} \gamma_{POC} \Phi_{POC}}_{\text{Methanogenesis}} + \underbrace{k_{POCs2} \gamma_{POC} \Phi_{POC}}_{\text{Sulfide Diagenesis}}$$

The mass balances for layer 1 and layer 2 are:

$$H_1 \frac{d\Phi_{TIC1}}{dt} = -K_{L01}(\Phi_{TIC1} - \Phi_{TIC0}) + K_{L12}(\Phi_{TIC2} - \Phi_{TIC1}) + H_1 S_{TIC1}$$

$$H_2 \frac{d\Phi_{TIC2}}{dt} = -K_{L12}(\Phi_{TIC2} - \Phi_{TIC1}) + H_2 S_{TIC2}$$

KINETICS

where:

Φ_{TIC1} = total inorganic carbon concentration in layer 1, $g\ m^{-3}$

Φ_{TIC2} = total inorganic carbon concentration in layer 2, $g\ m^{-3}$

Φ_{TIC0} = total inorganic carbon concentration in water column, $g\ m^{-3}$

H_1 = height of layer 1, m

H_2 = height of layer 2, m

K_{L01} = mass transfer coefficient between water column and layer 1, $m\ s^{-1}$

K_{L12} = mass transfer coefficient between layer 1 and layer 2, $m\ s^{-1}$

The mass transfer coefficient K_{L12} is related to the diffusion coefficient D using

$$K_{L12} = \frac{D}{\Delta z} = \frac{D}{\frac{1}{2}(H_1 + H_2)}$$

The implicit finite difference scheme for layer 1 is

$$H_1 \frac{\Phi_{TIC1}^{t+\Delta t} - \Phi_{TIC1}^t}{\Delta t} = -K_{L01}\left(\Phi_{TIC1}^{t+\Delta t} - \Phi_{TIC0}\right) + K_{L12}\left(\Phi_{TIC2}^{t+\Delta t} - \Phi_{TIC1}^{t+\Delta t}\right) + H_1 S_{TIC1}$$

Rearranging

$$\left(-\frac{H_1}{\Delta t} - K_{L01} - K_{L12}\right)\Phi_{TIC1}^{t+\Delta t} + K_{L12}\Phi_{TIC2}^{t+\Delta t} = -H_1 S_{TIC1} - \frac{H_1}{\Delta t}\Phi_{TIC1}^t - K_{L01}\Phi_{TIC0}$$

And the finite difference scheme for layer 2

$$H_2 \frac{\Phi_{TIC2}^{t+\Delta t} - \Phi_{TIC2}^t}{\Delta t} = -K_{L12}\left(\Phi_{TIC2}^{t+\Delta t} - \Phi_{TIC1}^{t+\Delta t}\right) + H_2 S_{TIC2}$$

Rearranging

$$K_{L12}\Phi_{TIC1}^{t+\Delta t} + \left(-\frac{H_2}{\Delta t} - K_{L12}\right)\Phi_{TIC2}^{t+\Delta t} = -H_2 S_{TIC2} - \frac{H_2}{\Delta t}\Phi_{TIC2}^t$$

Sediment Alkalinity

Sources and sinks for non-conservative sediment alkalinity model is shown in Figure 111. Alkalinity is in units of mg/l as $CaCO_3$.
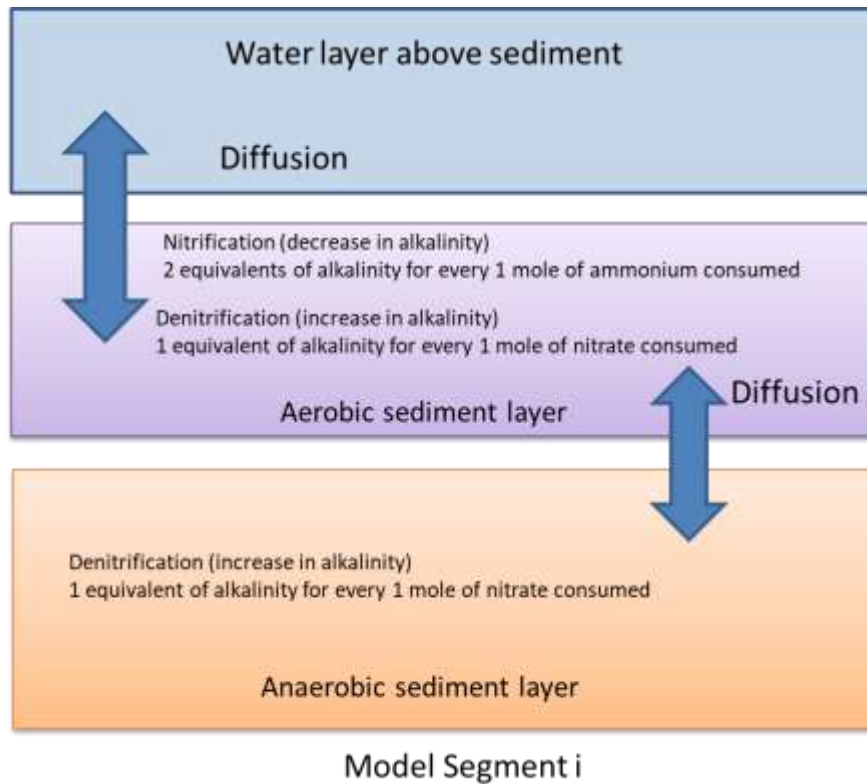
Figure 111. Sources and sinks of the sediment alkalinity model.

The rate equation for alkalinity in the aerobic sediment layer 1 is:

$$S_{ALK1} = -\underbrace{\left(\frac{2 \text{ equivalents alkalinity}}{1 \text{ mole ammonium nitrified}}\right) k_{NH4}\gamma_{NH4}\Phi_{NH4}}_{\text{nitrification}}$$
$$+ \underbrace{\left(\frac{1 \text{ equivalent alkalinity}}{1 \text{ mole nitrate denitrified}}\right) k_{NOx}\gamma_{NOx1}\Phi_{NOx}}_{\text{denitrification}}$$

where:
γ_{NOx} = denitrification temperature rate multiplier
γ_{NH4} = nitrification temperature rate multiplier
k_{NOx1} = denitrification rate in aerobic layer, sec^{-1}
k_{NH4} = nitrification rate, sec^{-1}
Φ_{NOx} = nitrate-nitrite concentration, $g\ m^{-3}$
Φ_{NH4} = ammonium concentration, $g\ m^{-3}$

The rate equation for alkalinity in the anaerobic sediment layer 2 is:

$$S_{ALK2} = \underbrace{\left(\frac{1 \text{ equivalent alkalinity}}{1 \text{ mole nitrate denitrified}}\right) k_{NOx}\gamma_{NOx}\Phi_{NOx}}_{\text{denitrification}}$$

KINETICS

where:
k_{NOx2} = denitrification rate in anaerobic layer, sec^{-1}

The mass balances for layer 1 and layer 2 are:

$$H_1 \frac{d\Phi_{ALK1}}{dt} = -K_{L01}(\Phi_{ALK1} - \Phi_{ALK0}) + K_{L12}(\Phi_{ALK2} - \Phi_{ALK1}) + H_1 S_{ALK1}$$

$$H_2 \frac{d\Phi_{ALK2}}{dt} = -K_{L12}(\Phi_{ALK2} - \Phi_{ALK1}) + H_2 S_{ALK2}$$

where:
Φ_{ALK1} = alkalinity concentration in layer 1, $g\ m^{-3}$
Φ_{ALK2} = alkalinity concentration in layer 2, $g\ m^{-3}$
Φ_{ALK0} = alkalinity concentration in water column, $g\ m^{-3}$
H_1 = height of layer 1, m
H_2 = height of layer 2, m
K_{L01} = mass transfer coefficient between water column and layer 1, $m\ s^{-1}$
K_{L12} = mass transfer coefficient between layer 1 and layer 2, $m\ s^{-1}$

The implicit finite difference scheme of alkalinity is equivalent to that used for inorganic carbon.

Sediment Temperature

A schematic of the sediment temperature model is shown in Figure 112.
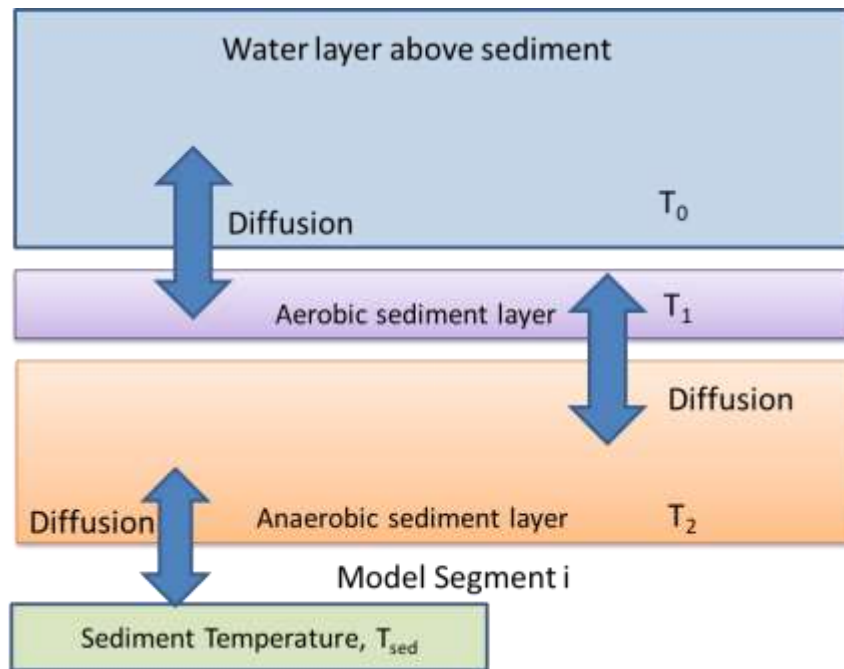
Figure 112. Schematic of sediment temperature model.

The heat balances for the aerobic layer 1 and anaerobic layer 2 are:

$$\rho C_p H_1 \frac{dT_1}{dt} = -K_{L01}\rho C_p(T_1 - T_0) + K_{L12}\rho C_p(T_2 - T_1)$$

$$\rho C_p H_2 \frac{dT_2}{dt} = -K_{L12}\rho C_p(T_2 - T_1) + K_{sw}(T_{sed} - T_2)$$

where:
T_1 = temperature in layer 1, $°C$
T_2 = temperature in layer 2, $°C$
T_0 = temperature in water column, $°C$
T_{sed} = temperature of sediments below anaerobic layer, $°C$
H_1 = height of layer 1, m
H_2 = height of layer 2, m
K_{L01} = heat transfer coefficient between water column and layer 1, $m\ s^{-1}$
K_{L12} = heat transfer coefficient between layer 1 and layer 2, $m\ s^{-1}$
K_{sw} = coefficient of sediment heat exchange between anaerobic layer and sediments below anaerobic layer, $W\ m^{-2}\ °C^{-1}$
ρ = water density, $g\ m^{-3}$
C_p = water density, $J\ g^{-1}\ °C^{-1}$

The implicit finite difference scheme for layer 1 is

$$\rho C_p H_1 \frac{T_1^{t+\Delta t} - T_1^t}{\Delta t} = -K_{L01}\rho C_p\left(T_1^{t+\Delta t} - T_0\right) + K_{L12}\rho C_p\left(T_2^{t+\Delta t} - T_1^{t+\Delta t}\right)$$

Rearranging and cancelling out ρC_p

$$\left(-\frac{H_1}{\Delta t} - K_{L01} - K_{L12}\right)T_1^{t+\Delta t} + K_{L12}T_2^{t+\Delta t} = -\frac{H_1}{\Delta t}T_1^t - K_{L01}T_0$$

And the finite difference scheme for layer 2

$$\rho C_p H_2 \frac{T_2^{t+\Delta t} - T_2^t}{\Delta t} = -K_{L12}\rho C_p\left(T_2^{t+\Delta t} - T_1^{t+\Delta t}\right) + K_{sw}\left(T_{sed} - T_2^{t+\Delta t}\right)$$

Rearranging

$$K_{L12}\rho C_p T_1^{t+\Delta t} + \left(-\frac{\rho C_p H_2}{\Delta t} - \rho C_p K_{L12} + K_{sw}\right)T_2^{t+\Delta t} = -\frac{\rho C_p H_2}{\Delta t}T_2^t - K_{sw}T_{sed}$$

Metal (Fe and Mn) Complexation and Diagenesis

Ferrous Iron Fe(II)

Iron is modeled using two constituents: iron oxyhydroxide, FeOOH(s), and ferrous iron Fe(II). FeOOH(s) is very insoluble and is modeled as a particulate whereas Fe(II) is more soluble. Figure 113 illustrates the iron model within the water column and sediments.
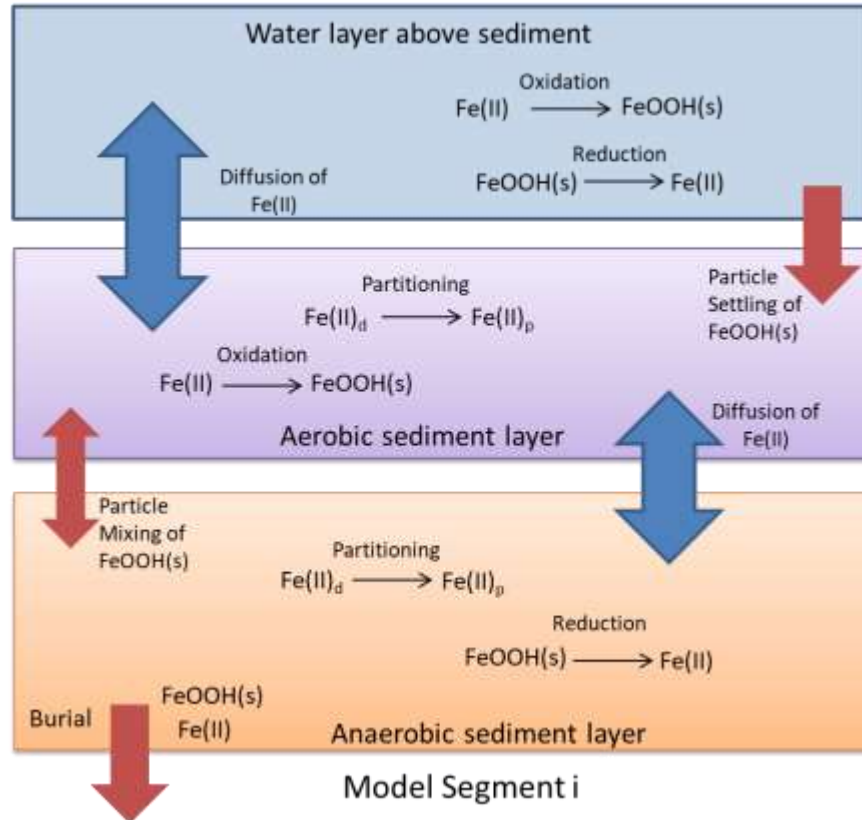
Figure 113. Schematic of iron model (Ditoro, 2001).

The modeling of ferrous iron in the water column was added to CE-QUAL-W2. The rate equation in the water column is:

$$S_{Fe(II)} = \underbrace{-k_{Fe(II)0}\Phi_{DO}10^{2(pH-7)}\Phi_{Fe(II)}}_{\text{Oxidation}} + \underbrace{k_{FeOOH}\left(\frac{K_{FeOOH}}{K_{FeOOH}+\Phi_{DO}}\right)\Phi_{FeOOH}}_{Reduction}$$

where:
k_{FeOOH} = reduction rate in water column, sec^{-1}
$k_{Fe(II)0}$ = oxidation rate in water column, $sec^{-1}(g\ m^{-3})^{-1}$
K_{FeOOH} = half saturation constant for oxygen for this reaction, $g\ m^{-3}$
$\quad\Phi_{DO}$ = dissolved oxygen concentration, $g\ m^{-3}$
$\ \Phi_{Fe(II)}$ = ferrous iron concentration, $g\ m^{-3}$
Φ_{FeOOH} = iron oxyhydroxide concentration, $g\ m^{-3}$
pH = pH in water column

The rate equation for ferrous iron in sediment layer 1 is:

$$S_{Fe(II)1} = \underbrace{-k_{Fe(II)1}\Phi_{DO}10^{2(pH1-7)}f_d\Phi_{Fe(II)1}}_{\text{Oxidation}}$$

where:

f_d = dissolved fraction of ferrous iron

$k_{Fe(II)1}$=ferrous iron oxidation rate in layer 1, $sec^{-1}(g\ m^{-3})^{-1}$

Φ_{DO} = dissolved oxygen concentration, $g\ m^{-3}$

$\Phi_{Fe(II)}$ = ferrous iron concentration, $g\ m^{-3}$

$pH1$ = pH in layer 1

The rate equation for ferrous iron in sediment layer 2 is:

$$S_{Fe(II)2} = \underbrace{k_{FeOOH2}\Phi_{FeOOH}}_{\text{Reduction}}$$

where:

k_{FeOOH2}= ferrous iron reduction rate in layer 2, sec^{-1}

Φ_{FeOOH} = iron oxyhydroxide concentration, $g\ m^{-3}$

Mass balances for the aerobic layer 1 and anaerobic layer 2 are:

$$H_1\frac{d\Phi_{Fe(II)1}}{dt} = -K_{L01}\big(f_d\Phi_{Fe(II)1} - \Phi_{Fe(II)0}\big) + K_{L12}\big(f_d\Phi_{Fe(II)2} - f_d\Phi_{Fe(II)1}\big)$$
$$+ w_{12}\big(f_p\Phi_{Fe(II)2} - f_p\Phi_{Fe(II)1}\big) - w_2\Phi_{Fe(II)1} + H_1 S_{Fe(II)1}$$

$$H_2\frac{d\Phi_{Fe(II)2}}{dt} = -K_{L12}\big(f_d\Phi_{Fe(II)2} - f_d\Phi_{Fe(II)1}\big) - w_{12}\big(f_p\Phi_{Fe(II)2} - f_p\Phi_{Fe(II)1}\big)$$
$$+ w_2\big(\Phi_{Fe(II)1} - \Phi_{Fe(II)2}\big) + H_2 S_{Fe(II)2}$$

where:

$\Phi_{Fe(II)0}$ =ferrous iron concentration in water column, $g\ m^{-3}$

H_1 = height of layer 1, m

H_2 = height of layer 2, m

K_{L01} = mass transfer coefficient between water column and layer 1, $m\ s^{-1}$

K_{L12} = mass transfer coefficient between layer 1 and layer 2, $m\ s^{-1}$

f_d = dissolved fraction of ferrous iron

f_p = particulate fraction of ferrous iron

w_{12} = particle mixing velocity between layer 1 and layer 2, $m\ s^{-1}$

w_2 = burial velocity, $m\ s^{-1}$

The implicit finite difference scheme for layer 1 is

$$H_1\frac{\Phi_{Fe(II)1}^{t+\Delta t} - \Phi_{Fe(II)1}^{t}}{\Delta t}$$
$$= -K_{L01}\big(f_d\Phi_{Fe(II)1}^{t+\Delta t} - \Phi_{Fe(II)0}\big) + K_{L12}\big(f_d\Phi_{Fe(II)2}^{t+\Delta t} - f_d\Phi_{Fe(II)1}^{t+\Delta t}\big)$$
$$+ w_{12}\big(f_p\Phi_{Fe(II)2}^{t+\Delta t} - f_p\Phi_{Fe(II)1}^{t+\Delta t}\big) - w_2\Phi_{Fe(II)1}^{t+\Delta t}$$
$$- H_1 k_{Fe(II)1}\Phi_{DO}10^{2(pH1-7)}f_d\Phi_{Fe(II)1}^{t+\Delta t}$$

KINETICS

Rearranging

$$\left(-\frac{H_1}{\Delta t} - f_d K_{L01} - f_d K_{L12} - w_{12}f_p - w_2 - H_1 k_{Fe(II)1}\Phi_{DO}10^{2(pH1-7)}f_d\right)\Phi_{Fe(II)1}^{t+\Delta t}$$
$$+ \left(K_{L12}f_d + w_{12}f_p\right)\Phi_{Fe(II)2}^{t+\Delta t} = -\frac{H_1}{\Delta t}\Phi_{Fe(II)1}^t - K_{L01}\Phi_{Fe(II)0}$$

And the finite difference scheme for layer 2

$$H_2 \frac{\Phi_{Fe(II)2}^{t+\Delta t} - \Phi_{Fe(II)2}^t}{\Delta t}$$
$$= -K_{L12}\left(f_d \Phi_{Fe(II)2}^{t+\Delta t} - f_d \Phi_{Fe(II)1}^{t+\Delta t}\right) - w_{12}\left(f_p \Phi_{Fe(II)2}^{t+\Delta t} - f_p \Phi_{Fe(II)1}^{t+\Delta t}\right)$$
$$+ w_2\left(\Phi_{Fe(II)1}^{t+\Delta t} - \Phi_{Fe(II)2}^{t+\Delta t}\right) + H_2 S_{Fe(II)2}$$

Rearranging

$$\left(f_d K_{L12} + f_p w_{12} + w_2\right)\Phi_{Fe(II)1}^{t+\Delta t} + \left(-\frac{H_2}{\Delta t} - f_d K_{L12} - f_p w_{12} - w_2\right)\Phi_{Fe(II)2}^{t+\Delta t}$$
$$= -H_2 S_{Fe(II)2} - \frac{H_2}{\Delta t}\Phi_{Fe(II)2}^t$$

The fractions associated with dissolved and particulate forms can be calculated with (Chapra, 1997):

$$f_d = \left(\frac{1}{\varphi + K_{dFe}(1-\varphi)\rho}\right)$$
$$f_p = \left(\frac{K_{dFe}(1-\varphi)\rho}{\varphi + K_{dFe}(1-\varphi)\rho}\right)$$

where:

f_d = dissolved fraction of ferrous iron
f_p = particulate fraction of ferrous iron
φ = sediment porosity
ρ = sediment density, $g\ m^{-3}$
K_{dFe} = ferrous sorption coefficient, $m^3\ g^{-1}$

Iron Oxyhydroxide FeOOH(s)

The rate equation in the water column for iron oxyhydroxide is:

$$S_{FeOOH} = \underbrace{k_{Fe(II)0}\Phi_{DO}10^{2(pH-7)}\Phi_{Fe(II)}}_{\text{Oxidation}} - \underbrace{k_{FeOOH}\left(\frac{K_{FeOOH}}{K_{FeOOH} + \Phi_{DO}}\right)\Phi_{FeOOH}}_{\text{Reduction}}$$

where:
k_{FeOOH}= reduction rate in water column, sec^{-1}
$k_{Fe(II)0}$= oxidation rate in water column, $sec^{-1}(g\ m^{-3})^{-1}$
K_{FeOOH}=half saturation constant for oxygen for this reaction, $g\ m^{-3}$
Φ_{DO} = dissolved oxygen concentration, $g\ m^{-3}$
Φ_{FeOOH} = iron oxyhydroxide concentration, $g\ m^{-3}$

$\Phi_{Fe(II)}$= ferrous iron concentration, $g\ m^{-3}$
pH=pH in water column

The rate equation for iron oxyhydroxide in the aerobic sediment layer 1 is:

$$S_{FeOOH1} = \underbrace{k_{Fe(II)1}\Phi_{DO}10^{2(pH1-7)}f_d\Phi_{Fe(II)1}}_{\text{Oxidation}}$$

where:
f_d = dissolved fraction of ferrous iron
$k_{Fe(II)1}$=ferrous iron oxidation rate in layer 1, $sec^{-1}(g\ m^{-3})^{-1}$
  Φ_{DO} = dissolved oxygen concentration, $g\ m^{-3}$
 $\Phi_{Fe(II)}$ = ferrous iron concentration, $g\ m^{-3}$
$pH1$ = pH in layer 1

The rate equation for iron oxyhydroxide in the anaerobic sediment layer 2 is:

$$S_{FeOOH2} = \underbrace{-k_{FeOOH2}\Phi_{FeOOH}}_{\text{Reduction}}$$

where:
k_{FeOOH2}= ferrous iron reduction rate in layer 2, sec^{-1}
Φ_{FeOOH} = iron oxyhydroxide concentration, $g\ m^{-3}$

Mass balances for layer 1 and layer 2 are:

$$H_1\frac{d\Phi_{FeOOH1}}{dt} = w_{12}(\Phi_{FeOOH2} - \Phi_{FeOOH1}) - w_2\Phi_{FeOOH1} + w_1\Phi_{FeOOH0} + H_1S_{FeOOH1}$$

$$H_2\frac{d\Phi_{FeOOH2}}{dt} = -w_{12}(\Phi_{FeOOH2} - \Phi_{FeOOH1}) + w_2(\Phi_{FeOOH1} - \Phi_{FeOOH2}) + H_2S_{FeOOH2}$$

where:
Φ_{FeOOH0}=iron oxyhydroxide concentration in water column, $g\ m^{-3}$
   H_1 = height of layer 1, m
   H_2 = height of layer 2, m
   w_1 = particle settling velocity, $m\ s^{-1}$
   w_{12} = particle mixing velocity between layer 1 and layer 2, $m\ s^{-1}$
   w_2 = burial velocity, $m\ s^{-1}$

The implicit finite difference scheme for layer 1 is

$$H_1\frac{\Phi_{FeOOH1}^{t+\Delta t} - \Phi_{FeOOH1}^t}{\Delta t}$$
$$= w_{12}\left(\Phi_{FeOOH2}^{t+\Delta t} - \Phi_{FeOOH1}^{t+\Delta t}\right) - w_2\Phi_{FeOOH1}^{t+\Delta t} + w_1\Phi_{FeOOH0}$$
$$+ H_1 k_{Fe(II)1}\Phi_{DO}10^{2(pH1-7)}f_d\Phi_{Fe(II)1}^t$$

Rearranging

KINETICS

$$\left(-\frac{H_1}{\Delta t} - w_{12} - w_2\right)\Phi_{FeOOH1}^{t+\Delta t} + w_{12}\Phi_{FeOOH2}^{t+\Delta t}$$
$$= -\frac{H_1}{\Delta t}\Phi_{FeOOH1}^{t} - w_1\Phi_{FeOOH0} - H_1 k_{Fe(II)1}\Phi_{DO}10^{2(pH1-7)}f_d\Phi_{Fe(II)1}^{t}$$

And the finite difference scheme for layer 2

$$H_2\frac{\Phi_{FeOOH2}^{t+\Delta t} - \Phi_{FeOOH2}^{t}}{\Delta t}$$
$$= -w_{12}\left(\Phi_{FeOOH2}^{t+\Delta t} - \Phi_{FeOOH1}^{t+\Delta t}\right) + w_2\left(\Phi_{FeOOH1}^{t+\Delta t} - \Phi_{FeOOH2}^{t+\Delta t}\right)$$
$$- H_2 k_{FeOOH}\Phi_{FeOOH2}^{t+\Delta t}$$

Rearranging

$$(w_{12} + w_2)\Phi_{FeOOH1}^{t+\Delta t} + \left(-\frac{H_2}{\Delta t} - w_{12} - w_2 - H_2 k_{FeOOH}\right)\Phi_{FeOOH2}^{t+\Delta t} = -\frac{H_2}{\Delta t}\Phi_{FeOOH2}^{t}$$

Manganese Mn(II)

The manganese model within the water column and sediments is illustrated in Figure 114.
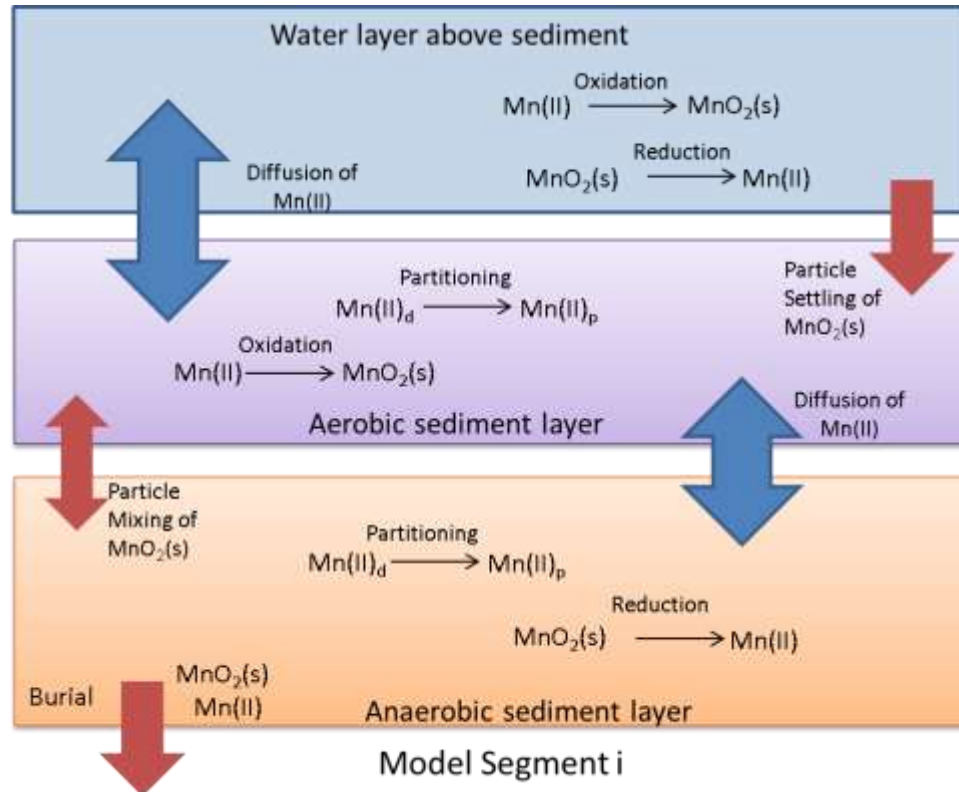
Figure 114. Schematic of manganese model (DiToro, 2001).

The following rate equation is used to model ionic divalent manganese Mn(II) in the water column is:

$$S_{Mn(II)} = \underbrace{-k_{Mn(II)0}\Phi_{DO}10^{2(pH-7)}\Phi_{Mn(II)}}_{\text{Oxidation}} + \underbrace{k_{MnO_2}\left(\frac{K_{MnO_2}}{K_{MnO_2} + \Phi_{DO}}\right)\Phi_{MnO_2}}_{Reduction}$$

where:

k_{MnO_2}=reduction rate in water column, sec^{-1}

$k_{Mn(II)0}$= oxidation rate in water column, $sec^{-1}(g\ m^{-3})^{-1}$

K_{MnO_2}=half saturation constant for oxygen for this reaction, $g\ m^{-3}$

Φ_{DO} = dissolved oxygen concentration, $g\ m^{-3}$

$\Phi_{Mn(II)}$ = Mn(II) concentration, $g\ m^{-3}$

Φ_{MnO_2}= manganese dioxide concentration, $g\ m^{-3}$

pH =pH in water column

The rate equation for Mn(II) in the aerobic sediment layer 1 is:

$$S_{Mn(II)1} = \underbrace{-k_{Mn(II)1}\Phi_{DO}10^{2(pH1-7)}f_d\Phi_{Mn(II)1}}_{\text{Oxidation}}$$

where:

f_d = dissolved fraction of Mn(II)

$k_{Mn(II)1}$= Mn(II) oxidation rate in layer 1, $sec^{-1}(g\ m^{-3})^{-1}$

Φ_{DO} = dissolved oxygen concentration, $g\ m^{-3}$

$\Phi_{Mn(II)1}$ =Mn(II) concentration, $g\ m^{-3}$

$pH1$ = pH in layer 1

The rate equation for manganese dioxide in the anaerobic sediment layer 2 is:

$$S_{Mn(II)2} = \underbrace{k_{MnO_2}\Phi_{MnO_2}}_{Reduction}$$

where:

k_{MnO_2}=manganese dioxide reduction rate in layer 2, sec^{-1}

Φ_{MnO_2} = manganese dioxide concentration, $g\ m^{-3}$

Mass balances for layer 1 and layer 2 are then:

$$H_1\frac{d\Phi_{Mn(II)1}}{dt} = -K_{L01}\left(f_d\Phi_{Mn(II)1} - \Phi_{Mn(II)0}\right) + K_{L12}\left(f_d\Phi_{Mn(II)2} - f_d\Phi_{Mn(II)1}\right)$$
$$+ w_{12}\left(f_p\Phi_{Mn(II)2} - f_p\Phi_{Mn(II)1}\right) - w_2\Phi_{Mn(II)1} + H_1 S_{Mn(II)1}$$

$$H_2\frac{d\Phi_{Mn(II)2}}{dt} = -K_{L12}\left(f_d\Phi_{Mn(II)2} - f_d\Phi_{Mn(II)1}\right) - w_{12}\left(f_p\Phi_{Mn(II)2} - f_p\Phi_{Mn(II)1}\right)$$
$$+ w_2\left(\Phi_{Mn(II)1} - \Phi_{Mn(II)2}\right) + H_2 S_{Mn(II)2}$$

where:

$\Phi_{Mn(II)0}$ =Mn(II) concentration in water column, $g\ m^{-3}$

H_1 = height of layer 1, m

H_2 = height of layer 2, m

KINETICS

K_{L01} = mass transfer coefficient between water column and layer 1, $m\ s^{-1}$
K_{L12} = mass transfer coefficient between layer 1 and layer 2, $m\ s^{-1}$
f_d = dissolved fraction of Mn(II)
f_p = particulate fraction of Mn(II)
w_{12} = particle mixing velocity between layer 1 and layer 2, $m\ s^{-1}$
w_2 = burial velocity, $m\ s^{-1}$

The implicit finite difference scheme for layer 1 is

$$H_1 \frac{\Phi_{Mn(II)1}^{t+\Delta t} - \Phi_{Mn(II)1}^t}{\Delta t}$$
$$= -K_{L01}\left(f_d \Phi_{Mn(II)1}^{t+\Delta t} - \Phi_{Mn(II)0}\right) + K_{L12}\left(f_d \Phi_{Mn(II)2}^{t+\Delta t} - f_d \Phi_{Mn(II)1}^{t+\Delta t}\right)$$
$$+ w_{12}\left(f_p \Phi_{Mn(II)2}^{t+\Delta t} - f_p \Phi_{Mn(II)1}^{t+\Delta t}\right) - w_2 \Phi_{Mn(II)1}^{t+\Delta t}$$
$$- H_1 k_{Mn(II)1} \Phi_{DO} 10^{2(pH1-7)} f_d \Phi_{Mn(II)1}^{t+\Delta t}$$

Rearranging

$$\left(-\frac{H_1}{\Delta t} - f_d K_{L01} - f_d K_{L12} - w_{12} f_p - w_2 - H_1 k_{Mn(II)1} \Phi_{DO} 10^{2(pH1-7)} f_d\right) \Phi_{Mn(II)1}^{t+\Delta t}$$
$$+ \left(K_{L12} f_d + w_{12} f_p\right) \Phi_{Mn(II)2}^{t+\Delta t} = -\frac{H_1}{\Delta t} \Phi_{Mn(II)1}^t - K_{L01} \Phi_{Mn(II)0}$$

And the finite difference scheme for layer 2

$$H_2 \frac{\Phi_{Mn(II)2}^{t+\Delta t} - \Phi_{Mn(II)2}^t}{\Delta t}$$
$$= -K_{L12}\left(f_d \Phi_{Mn(II)2}^{t+\Delta t} - f_d \Phi_{Mn(II)1}^{t+\Delta t}\right) - w_{12}\left(f_p \Phi_{Mn(II)2}^{t+\Delta t} - f_p \Phi_{Mn(II)1}^{t+\Delta t}\right)$$
$$+ w_2\left(\Phi_{Mn(II)1}^{t+\Delta t} - \Phi_{Mn(II)2}^{t+\Delta t}\right) + H_2 S_{Mn(II)2}$$

Rearranging

$$\left(f_d K_{L12} + f_p w_{12} + w_2\right) \Phi_{Mn(II)1}^{t+\Delta t} + \left(-\frac{H_2}{\Delta t} - f_d K_{L12} - f_p w_{12} - w_2\right) \Phi_{Mn(II)2}^{t+\Delta t}$$
$$= -H_2 S_{Mn(II)2} - \frac{H_2}{\Delta t} \Phi_{Mn(II)2}^t$$

The fractions associated with dissolved and particulate forms can be calculated with (Chapra, 1997):

$$f_d = \left(\frac{1}{\varphi + K_{dMn}(1 - \varphi)\rho}\right)$$
$$f_p = \left(\frac{K_{dMn}(1 - \varphi)\rho}{\varphi + K_{dMn}(1 - \varphi)\rho}\right)$$

where

f_d = dissolved fraction of Mn(II)
f_p = particulate fraction of Mn(II)
φ = sediment porosity
ρ = sediment density, $g\ m^{-3}$
K_{dp} = manganese sorption coefficient, $m^3\ g^{-1}$

Manganese Dioxide MnO$_2$

The rate equation in the water column for manganese dioxide is:

$$S_{MnO_2} = \underbrace{k_{Mn(II)0}\Phi_{DO}10^{2(pH-7)}\Phi_{Mn(II)}}_{\text{Oxidation}} - \underbrace{k_{MnO_2}\left(\frac{K_{MnO_2}}{K_{MnO_2}+\Phi_{DO}}\right)\Phi_{MnO_2}}_{Reduction}$$

where:
k_{MnO_2}=reduction rate in water column, sec^{-1}
$k_{Mn(II)0}$= oxidation rate in water column, $sec^{-1}(g\ m^{-3})^{-1}$
K_{MnO_2}=half saturation constant for oxygen for this reaction, $g\ m^{-3}$
$\quad\Phi_{DO}$ = dissolved oxygen concentration, $g\ m^{-3}$
$\Phi_{Mn(II)}$ = Mn(II) concentration, $g\ m^{-3}$
Φ_{MnO_2}= manganese dioxide concentration, $g\ m^{-3}$
pH=pH in water column

The rate equation for manganese dioxide in the aerobic sediment layer 1 is:

$$S_{MnO_21} = \underbrace{k_{Mn(II)1}\Phi_{DO}10^{2(pH1-7)}f_d\Phi_{Mn(II)1}}_{\text{Oxidation}}$$

where:
f_d = dissolved fraction of Mn(II)
$k_{Mn(II)1}$= Mn(II) oxidation rate in layer 1, $sec^{-1}(g\ m^{-3})^{-1}$
Φ_{DO} = dissolved oxygen concentration, $g\ m^{-3}$
$\Phi_{Mn(II)}$ = Mn(II) concentration, $g\ m^{-3}$
$pH1$ = pH in layer 1

The rate equation for manganese dioxide in the anaerobic sediment layer 2 is:

$$S_{MnO_22} = \underbrace{-k_{MnO_22}\Phi_{MnO_2}}_{Reduction}$$

k_{MnO_22}= manganese dioxide reduction rate in layer 2, sec^{-1}
Φ_{MnO_2} = manganese dioxide concentration, $g\ m^{-3}$

Mass balances for layer 1 and layer 2 are:

$$H_1\frac{d\Phi_{MnO_21}}{dt} = w_{12}\left(\Phi_{MnO_22}-\Phi_{MnO_21}\right) - w_2\Phi_{MnO_21} + w_1\Phi_{MnO_20} + H_1 S_{MnO_21}$$

$$H_2\frac{d\Phi_{MnO_22}}{dt} = -w_{12}\left(\Phi_{MnO_22}-\Phi_{MnO_21}\right) + w_2\left(\Phi_{MnO_21}-\Phi_{MnO_22}\right) + H_2 S_{MnO_22}$$

where:
Φ_{MnO_20} =manganese concentration in water column, $g\ m^{-3}$
$\quad H_1$ = height of layer 1, m
$\quad H_2$ = height of layer 2, m
$\quad w_1$ = particle settling velocity, $m\ s^{-1}$

KINETICS

w_{12} = particle mixing velocity between layer 1 and layer 2, $m\ s^{-1}$
w_2 = burial velocity, $m\ s^{-1}$

The implicit finite difference scheme for layer 1 is

$$H_1 \frac{\Phi_{MnO_21}^{t+\Delta t} - \Phi_{MnO_21}^{t}}{\Delta t}$$
$$= w_{12}\left(\Phi_{MnO_22}^{t+\Delta t} - \Phi_{MnO_21}^{t+\Delta t}\right) - w_2 \Phi_{MnO_21}^{t+\Delta t} + w_1 \Phi_{MnO_20}$$
$$+ H_1 k_{Mn(II)1} \Phi_{DO} 10^{2(pH1-7)} f_d \Phi_{Mn(II)1}^{t}$$

Rearranging

$$\left(-\frac{H_1}{\Delta t} - w_{12} - w_2\right)\Phi_{MnO_21}^{t+\Delta t} + w_{12}\Phi_{MnO_22}^{t+\Delta t}$$
$$= -\frac{H_1}{\Delta t} \Phi_{MnO_21}^{t} - w_1 \Phi_{MnO_20} - H_1 k_{Mn(II)1} \Phi_{DO} 10^{2(pH1-7)} f_d \Phi_{Mn(II)1}^{t}$$

And the finite difference scheme for layer 2

$$H_2 \frac{\Phi_{MnO_22}^{t+\Delta t} - \Phi_{MnO_22}^{t}}{\Delta t}$$
$$= -w_{12}\left(\Phi_{MnO_22}^{t+\Delta t} - \Phi_{MnO_21}^{t+\Delta t}\right) + w_2\left(\Phi_{MnO_21}^{t+\Delta t} - \Phi_{MnO_22}^{t+\Delta t}\right)$$
$$- H_2 k_{MnO_2} \Phi_{MnO_22}^{t+\Delta t}$$

Rearranging

$$(w_{12} + w_2)\Phi_{MnO_21}^{t+\Delta t} + \left(-\frac{H_2}{\Delta t} - w_{12} - w_2 - H_2 k_{MnO_2}\right)\Phi_{MnO_22}^{t+\Delta t} = -\frac{H_2}{\Delta t} \Phi_{MnO_22}^{t}$$

Total Inorganic Carbon

Carbon, hydrogen, and oxygen are the most abundant elements in living matter and form the essential backbone of organic material. Inorganic carbon directly influences pH.
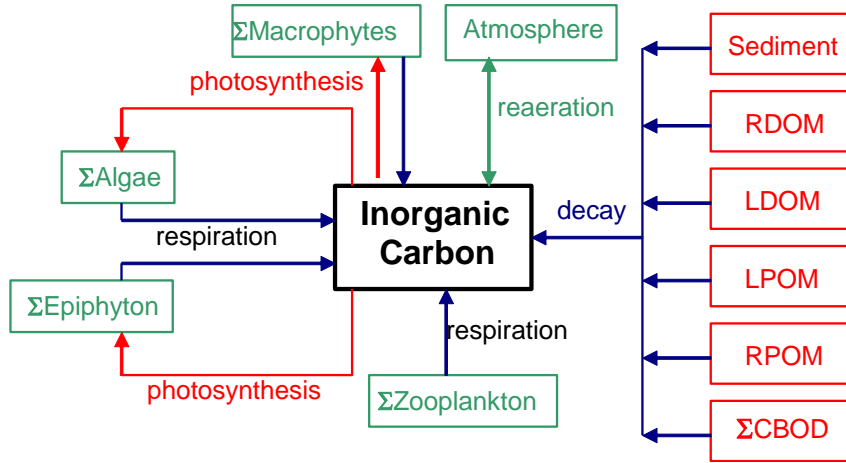
Figure 115. Internal flux between inorganic carbon and other compartments.

Referring to **Figure 115**, the rate equation for total inorganic carbon is:

$$S_{TIC} = \underbrace{\sum (K_{ar} - K_{ag})\,\delta_{Ca}\,\Phi_a}_{\text{net algal production}} + \underbrace{\sum (K_{er} - K_{eg})\,\delta_{Ce}\,\Phi_e}_{\text{net epiphyton production}} + \underbrace{K_{LPOM}\,\delta_{COM}\,\gamma_{OM}\,\Phi_{LPOM}}_{\text{labile POM decay}}$$

$$+ \underbrace{K_{LDOM}\,\gamma_{OM}\,\delta_{COM}\,\Phi_{LCOM}}_{\text{labile DOM decay}} + \underbrace{K_{RDOM}\,\gamma_{OM}\,\delta_{COM}\,\Phi_{RDOM}}_{\text{refractory DOM decay}} + \underbrace{K_{RPOM}\,\delta_{COM}\,\gamma_{OM}\,\Phi_{RPOM}}_{\text{refractory POM decay}}$$

$$+ \underbrace{K_{sed}\,\gamma_{OM}\,\delta_{COM}\,\Phi_{sed}}_{\text{1st-order sediment release}} + \underbrace{SOD\,\gamma_{OM}\,\delta_{COM}\,\frac{A_{sed}}{V}}_{\text{0-order sediment release}} + \underbrace{\frac{A_{sur}}{V_{sur}}K_{Lc}(\Phi_{sCO2} - \Phi_{CO2})}_{\text{reaeration}}$$

$$+ \underbrace{\sum K_{CBOD}R_{CBOD}\,\delta_{C-CBOD}\,\Theta^{T-20}\,\Phi_{CBOD}}_{\text{CBOD decay}} + \underbrace{\sum (K_{mr} - K_{mg})\,\delta_{Cm}\,\Phi_{macro}}_{\text{net macrophyte production}}$$

$$+ \underbrace{K_{zr}\,\delta_{Czoo}\,\gamma_{zoo}\,\Phi_{zoo}}_{\text{zooplankton respiration}}$$

$$(4\text{-}140)$$

where:

θ = temperature rate multiplier for BOD decay

γ_{OM} = organic matter temperature rate multiplier

δ_{Ce} = epiphyton stoichiometric coefficient for carbon

δ_{Ca} = algal stoichiometric coefficient for carbon

δ_{COM} = organic matter stoichiometric coefficient for carbon

$\delta_{C\text{-}CBOD}$ = CBOD stoichiometric coefficient for carbon

R_{BOD} = 5-day CBOD to ultimate CBOD ratio

A_{sed} = sediment surface area, m^2

A_{sur} = surface area of surface computational cell, m^2

SOD = sediment oxygen demand, $g\ m^{-2}\ sec^{-1}$

K_{Lc} = inorganic carbon interfacial exchange rate, $m\ sec^{-1}$

K_{ar} = algal dark respiration rate, sec^{-1}

K_{ag} = algal growth rate, sec^{-1}

KINETICS

K_{er} = epiphyton dark respiration rate, *sec^{-1}*
K_{eg} = epiphyton growth rate, *sec^{-1}*
K_{LDOM} = labile DOM decay rate, *sec^{-1}*
K_{RDOM} = refractory DOM decay rate, *sec^{-1}*
K_{LPOM} = labile POM decay rate, *sec^{-1}*
K_{RPOM} = refractory POM decay rate, *sec^{-1}*
K_{CBOD} = CBOD decay rate, *sec^{-1}*
K_{sed} = sediment decay rate, *sec^{-1}*
Φ_a = algal concentration, *g m^{-3}*
Φ_e = epiphyton concentration, *g m^{-3}*
Φ_{LDOM} = labile DOM concentration, *g m^{-3}*
Φ_{RDOM} = refractory DOM concentration, *g m^{-3}*
Φ_{LPOM} = labile POM concentration, *g m^{-3}*
Φ_{RPOM} = refractory POM concentration, *g m^{-3}*
Φ_{CBOD} = CBOD concentration, *g m^{-3}*
Φ_{sed} = organic sediment concentration, *g m^{-3}*
Φ_{TIC} = inorganic carbon concentration, *g m^{-3}*
Φ_{CO2} = carbon dioxide concentration, *g m^{-3}*
Φs_{CO2} = carbon dioxide saturation concentration, *g m^{-3}*

and the rate terms are evaluated in subroutine INORGANIC_CARBON.

The basic physics of gas transfer are the same for CO_2 and O_2. Using Higbie penetration theory, the gas transfer coefficient for CO_2 is related to that of oxygen by:

$$KL_{CO2} = KL_{O2}\sqrt{\frac{D_{CO2}}{D_{O2}}}$$

(4-141)

where:
KL_{CO2} = reaeration coefficient for CO_2
KL_{O2} = reaeration coefficient for oxygen
D_{CO2} = molecular diffusion coefficient for CO_2
D_{O2} = molecular diffusion coefficient for oxygen

Using the fact that the ratio of molecular diffusion coefficients of two gases A and B are related to their molecular weights, MW (Thibedoux, 1996)

$$\frac{D_A}{D_B} = \sqrt{\frac{MW_B}{MW_A}}$$

(4-142)

then

$$KL_{CO2} = KL_{O2}\left(\frac{MW_{O2}}{MW_{CO2}}\right)^{0.25} = 0.923 KL_{O2}$$

(4-143)

Hence, the reaeration rate equations presented for oxygen transfer are applicable to CO_2 transfer using a factor of 0.923.

Carbon dioxide concentration for the interfacial exchange rate is determined from Henry's Law. Prior to Version 4.2.2, the saturation concentration of carbon dioxide was determined from:

$$\Phi'_{CO2} = 0.286\exp{(-0.0314T_s)}P_a$$

(4-144)

where:

  Φ'_{CO2} = carbon dioxide saturation concentration as C, *g m^{-3}*
   P_a = altitude correction factor in atm
   T_s = surface cell water temperature, ^oC

This saturation concentration produces a CO2 saturation value that would be equivalent to the atmospheric CO2 from around 1960. Also, the FORTRAN coding had an error in application of the Pa term.

Since Version 4.2.2, the CO2 saturation was determined from

$$\Phi'_{CO2} = K_H P_{CO2} \tag{4-145}$$

where K_H is the temperature dependent Henry's Law constant in moles CO2/l/atm and P_{CO2} is the partial pressure of CO2 in atm. K_H in moles CO2/l/atm is determined from Edmond and Gieskes (1970):

$$K_H = 10^{\left(\frac{2385.73}{TK} + 0.0152642TK - 14.0184\right)} \tag{4-146}$$

where TK is the temperature of the water in ^oK. Converting to CO2 saturation as C rather than as CO2, the expression for CO2 saturation in mg C/l becomes

$$\Phi'_{CO2} = 12000 * 10^{\left(\frac{2385.73}{TK} + 0.0152642TK - 14.0184\right)} P_{CO2} \tag{4-147}$$

Computation of PCO2 in atm is based on

$$P_{CO2} = P_{CO2\_ppm} P_a \tag{4-148}$$

where PCO2_ppm is the ppm of CO2 in the atmosphere and Pa is the altitude correction or the atmospheric pressure in atm. This computation is based on Mortimer (1981):

$$P_a = \left(1 - \frac{H}{44.3}\right)^{5.25} \tag{4-149}$$

where:

  H = reservoir elevation from sea level, *km*

The model user can input a value of CO2 in the atmosphere in ppm or can use a regression equation based on the measured global average CO2 in the atmosphere. The global CO2 average data are from NOAA/ESRL (2020) and represent a spatial global average for each year. The best fit polynomial to that data is shown in Figure 116 between 1920 and 2019.

KINETICS
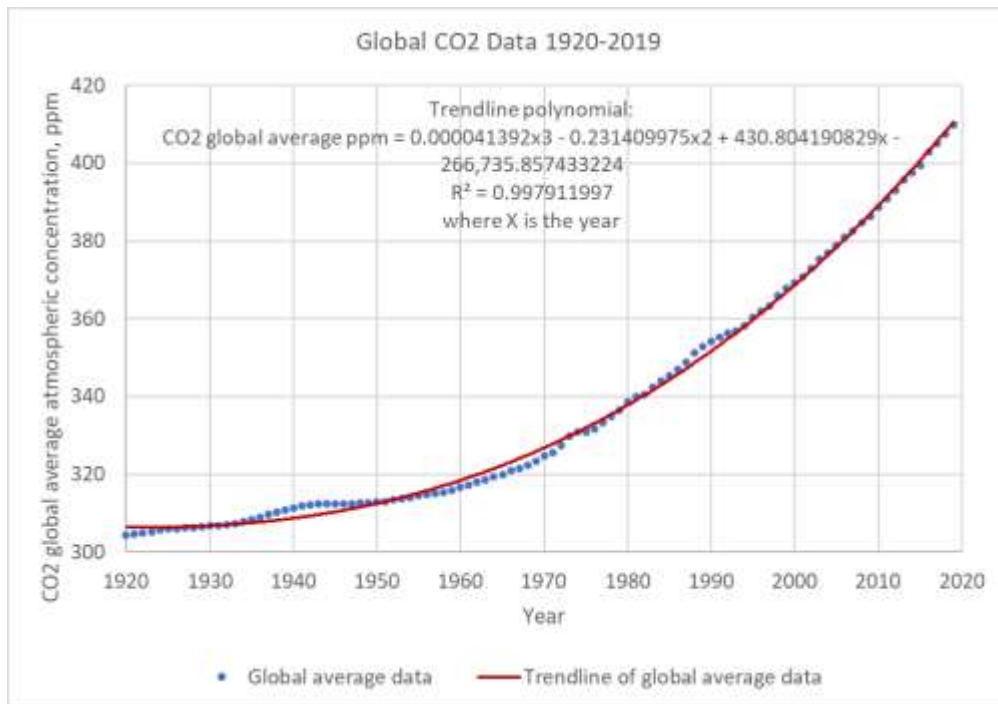
Figure 116. Global average CO2 gas concentration from 1920 to 2019 from NOAA/ESRL (2020) data.

The equation used in Figure 116 is CO2 global average concentration in ppm = (0.000041392*Year^3) − (0.231409975*Year^2) + (430.804190829*Year) - 266735.857433224, where the Year is the 4-digit year, such as 2015. A better curve fit is possible using more recent data. Using field data between 1980 and 2019, the best-fit curve is shown in Figure 117.
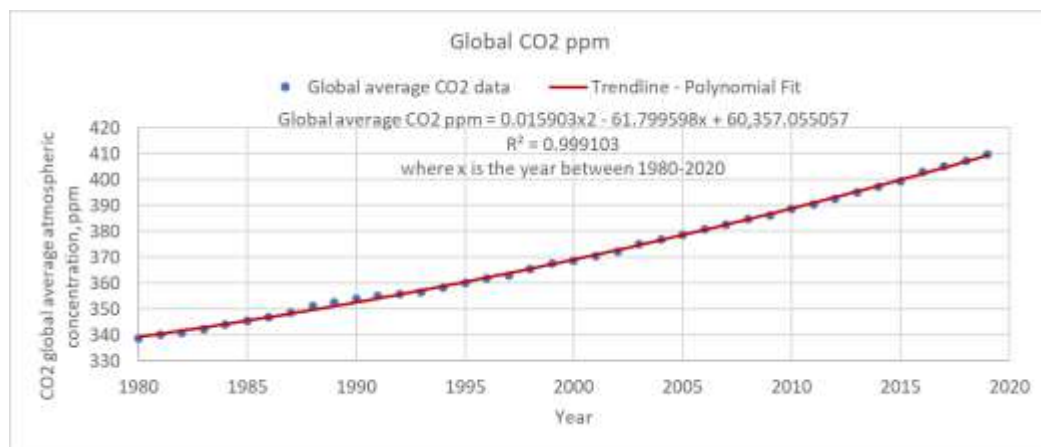
Figure 117. Global average CO2 gas concentration between 1980 and 2019 from NOAA/ESRL (2020) data.

If your model start year is after 1980, then this correlation is used. If you have a model year that starts before 1980, the broader correlation is used. The best fit equation for this correlation is shown above and is CO2 global average concentration in ppm = (0.015903*Year^2) - (61.799598*Year) + 60357.05507 where the Year is the 4-digit year, such as 1997.

TIC is in units of mg/l as C.

Alkalinity

Alkalinity is in units of mg/l as CaCO$_3$ and provides an indication of the buffering capacity of aquatic systems and their resistance to pH changes from acidic or alkaline loadings. Alkalinity, along with total inorganic carbon, is used to determine pH and concentrations of carbonate species in subroutine PH_CO2.

Alkalinity can be treated as conservative in the model and its internal rate term is set to zero. Alkalinity variations though are common in aquatic systems. Whiting, or large precipitations of carbonates, may occur. Sediment release of carbonates may increase alkalinity in the anoxic zones of many reservoirs. If these effects are important, a non-conservative model of alkalinity should be used.

An algorithm for non-conservative alkalinity was added to the CE-QUAL-W2 model based on work of Sullivan, et al. 2013 based on Stumm and Morgan (1996). This algorithm allows for determining alkalinity variations over time based on utilization of ammonia and nitrate during photosynthesis, production of ammonia during respiration, nitrification, and denitrification.

pH and Carbonate Species

The pH and carbonate species are computed using water temperature, TDS or salinity, alkalinity, and total inorganic carbon concentrations using basic carbonate relationships. Computed carbonate species are carbon dioxide, bicarbonates, and carbonates. The pH and carbonate species are computed in subroutine PH_CO2. These materials are not subject to transport and are computed at each water quality update interval.

Calculations performed by subroutine PH_CO2 are based on the carbonate-bicarbonate equilibrium reaction (Stumm and Morgan 1996):

$$HCO_3^- \leftrightarrow CO_3^= + H^+ \qquad \textbf{(4-150)}$$

$$H_2O \leftrightarrow H^+ + OH^- \qquad \textbf{(4-151)}$$

These equilibria express the source of bicarbonate and carbonate ions, alkaline constituents, and dissolution of atmospheric CO$_2$ in water. Contribution of calcium and magnesium carbonate to alkalinity is not included. The equilibrium state in terms of the equilibrium constants K$_i$ is:

$$K_1 = \frac{[H^+]\ [HCO_3^-]}{[H_2CO_3]} \qquad \textbf{(4-152)}$$

$$K_2 = \frac{[H^+]\ [CO_3^=]}{[HCO_3^-]} \qquad \textbf{(4-153)}$$

KINETICS

$$K_w = \frac{[H^+]\,[OH^-]}{[H_2O]}$$ (4-154)

where:
  $[X]$ = molar concentration, *moles liter^{-1}*
  $[H_2O]$ = unity (by definition)

Alkalinity is defined as:

$$[ALK] = [HCO_3^-] + 2[CO_3^=] + [OH^-] - [H^+]$$ (4-155)

The following condition prevails for the dissolution of carbonic acid:

$$[H_2CO_3] + [HCO_3^-] + [CO_3^=] = CONSTANT = C_T$$ (4-156)

By combining equations 53, 54, and 57, the quantities [HCO$_3$-] and [CO$_3$=] can be expressed in terms of [H+] and the constant CT. In addition, equation 55 allows for [OH-] to be expressed in terms of [H+]. When these expressions are included in equation 56, the result is:

$$[ALK] = \frac{C_T\,[H^+]\,K_1}{[H^+]\,K_1 + K_1\,K_2 + [H^+]^2} \frac{[H^+] + 2\,K_2}{[H^+]} + \frac{K_w}{[H^+]} - [H^+]$$ (4-157)

The model interprets the constant CT as moles per liter of total inorganic carbon and assumes [ALK] is known. Equation 58 is iteratively solved in subroutine PH_CO2 until the value of [H+] converges. The negative logarithm of [H+] is, by definition, pH.

Once equation 58 has been solved for [H+], then [H$_2$CO$_3$] is given by:

$$[H_2CO_3] = \frac{C_T}{1 + \dfrac{K_1}{[H^+]} + \dfrac{K_1\,K_2}{[H^+]^2}}$$ (4-158)

and is the same as [CO$_2$]. Bicarbonate concentration is computed from:

$$[HCO_3^-] = \frac{C_T}{1 + \dfrac{[H^+]}{K_1} + \dfrac{K_2}{[H^+]}}$$ (4-159)

and carbonate from:

$$[CO_3^=] = \frac{C_T}{1 + \dfrac{[H^+]^2}{K_1\,K_2} + \dfrac{[H^+]}{K_2}}$$ (4-160)

which are then converted to grams per cubic meter.

Equilibrium constants in the preceding equations are obtained by first expressing a thermodynamic temperature dependence for a related constant, K_i^*:

$$log \ K_i^* = a + \frac{b}{T} + cT + d \ log \ T \tag{4-161}$$

The constants a, b, c, and d are:

	a	b	c	d
K_w^*	35.3944	-5242.39	-0.00835	11.8261
K_1^*	14.8435	-3404.71	-0.03278	0
K_2^*	6.4980	-2902.39	-0.02379	0

The relation between K_i and K_i^* is obtained from the definition of the activity of a chemical species:

$$\{X\} \ = \ \gamma \ [\ X \ ] \tag{4-162}$$

where:
   {X} = activity of species X, *moles liter^{-1}*
    γ = dimensionless activity coefficient
   [X] = concentration, *moles liter^{-1}*

For the reaction:

$$A \ + \ B \ \Leftrightarrow \ C \ + \ D \tag{4-163}$$

the equilibrium constant K* is:

$$K^* = \frac{\{ C \} \ \{ D \}}{\{ A \} \ \{ B \}} \tag{4-164}$$

thus:

$$K^* = \frac{\gamma_C \ [C] \ \gamma_D \ [D]}{\gamma_A \ [A] \ \gamma_B \ [B]} = \frac{\gamma_C \gamma_D}{\gamma_A \gamma_B} \ K \tag{4-165}$$

$$K = \frac{\gamma_A \gamma_B}{\gamma_C \gamma_D} \ K^* \tag{4-166}$$

KINETICS

Activity coefficients are obtained from an extension of Debye-Huckel theory as:

$$Log\ \gamma = \frac{-AZ^2\sqrt{I}}{1 + 0.33a\sqrt{I}} + k_1 + k_2 I + k_3 I^2 \qquad \textbf{(4-167)}$$

where:

I = ionic strength
Z = ionic charge
A = approximately 0.5 for water at 25ºC
a = ionic size parameter
k_i = empirical coefficients

Ionic strength based on the concentration of Total Dissolved Solids in mg/l is approximated as (Sawyer and McCarty 1967):

$$I = 2.5X10^5 \Phi_{TDS} \qquad \textbf{(4-168)}$$

or for salinity in units of kg/m³:

$$I = 0.00147 + 0.019885\Phi_{salinity} + 0.000038\Phi_{salinity}{}^2 \qquad \textbf{(4-169)}$$

where:

Φ_{TDS} = total dissolved solids, $g\ m^{-3}$
$\Phi_{salinity}$ = salinity, $kg\ m^{-3}$

Values of the other parameters are:

	Z	a	k_1	k_2	k_3
HCO⁻₃	1	4	0.0047	0.042	-0.0093
CO⁼₃	2	4.5	0.0121	0.0972	-0.0207

Activity coefficients for [H+], [OH-], [H2CO3], and [H2O] are treated as special cases:

$$[H^+]\gamma = [H_2O]\gamma = 1 \qquad \textbf{(4-170)}$$

$$[H_2CO_3]\gamma = [OH^-]\gamma = 0.0755I \qquad \textbf{(4-171)}$$

Temperature Rate Multipliers

Most biological and chemical rates are temperature dependent. Subroutine RATE_MULTIPLIERS calculates the temperature dependence for all rates. It is called after the temperature solution so the temperature of the current computational interval is used.

A representative rate multiplier function is shown in **Figure 118** with its K and T parameters. The curve represents how biological process rates exhibit an optimum range and diminish asymmetrically at higher and lower temperatures (Thornton and Lessem, 1978).

$$\lambda_T = 0 \qquad where \ T \leq T_1$$

$$\lambda_T = \underbrace{\frac{K_1 e^{\gamma_1(T-T_1)}}{1 + K_1 e^{\gamma_1(T-T_1)} - K_1}}_{\gamma_{ar}} \underbrace{\frac{K_4 e^{\gamma_2(T_4 - T)}}{1 + K_4 e^{\gamma_2(T_4 - T)} - K_4}}_{\gamma_{af}} \quad where \ T_1 < T < T_4$$

$$\lambda_T = 0 \qquad where \ T \geq T_4$$

where:

$$\gamma_{ar} = \frac{1}{T_2 - T_1} \ ln \ \frac{K_2(1 - K_1)}{K_1(1 - K_2)}$$

$$\gamma_{af} = \frac{1}{T_4 - T_3} \ ln \ \frac{K_3(1 - K_4)}{K_4(1 - K_3)}$$

γ_{ar} and γ_{af} are the rising and falling limb temperature multipliers.

The user supplies temperatures T_1 to T_4 and multiplier factors K_1 to K_4. Temperatures T_1 and T_4 represent mortality limits, and T_2 and T_3 are used to define the optimum range. Maximum reaction rates supplied by the user are multiplied by λT to determine rates corresponding to the water temperature of a model cell. For non-algae temperature rate multipliers, only the K_1 and K_2 corresponding to T_1 and T_2 are used.

Note that for generic constituents and CBOD, the model user can choose Arrehnius temperature coefficients which are of the form

$$k_{T1} = k_{T2}\theta^{T1-T2}$$

where k_T is the kinetic first order rate constant in day^{-1} at a temperature T in °C and θ is an empirical coefficient dependent on the reaction.

KINETICS
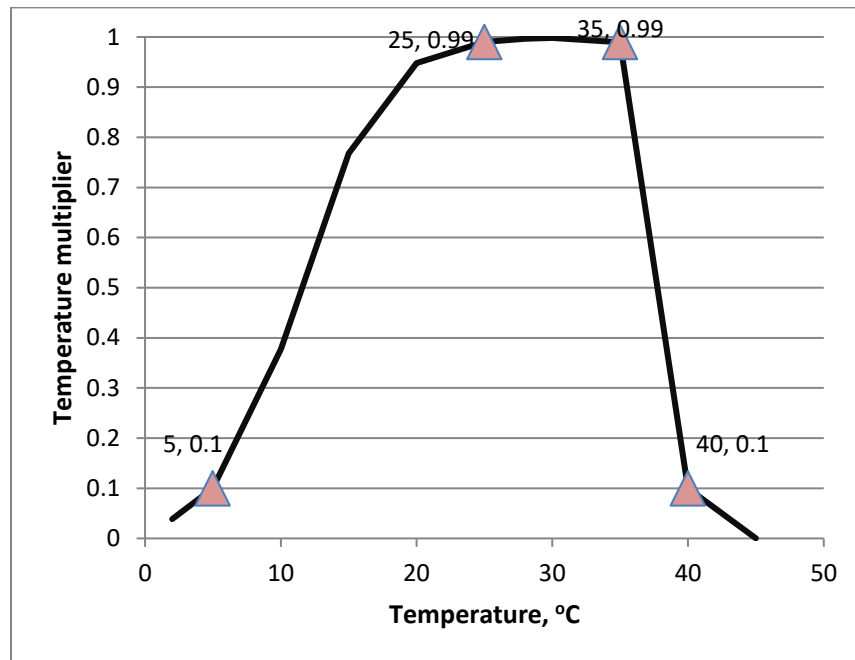
Figure 118. Temperature rate multiplier function.

5.   Numerical Solution

Characteristics of the Finite Difference Scheme

The solution of the governing equations in CE-QUAL-W2 is based on a finite difference numerical approach using variables defined in Figure 119 for no channel slope or Figure 120 for arbitrary channel slope. The finite difference solution has the following characteristics:

- space-staggered grid
- conservative formulation
- regular, structured, Cartesian grid with variable cell length Δx and cell thickness Δz
- Δt for stability requirement computed internally and is updated for each time step

This section outlines the numerical approach for the hydrodynamic equations (solution of U, W, and η) and advective-diffusion equations (T and C or Φ).
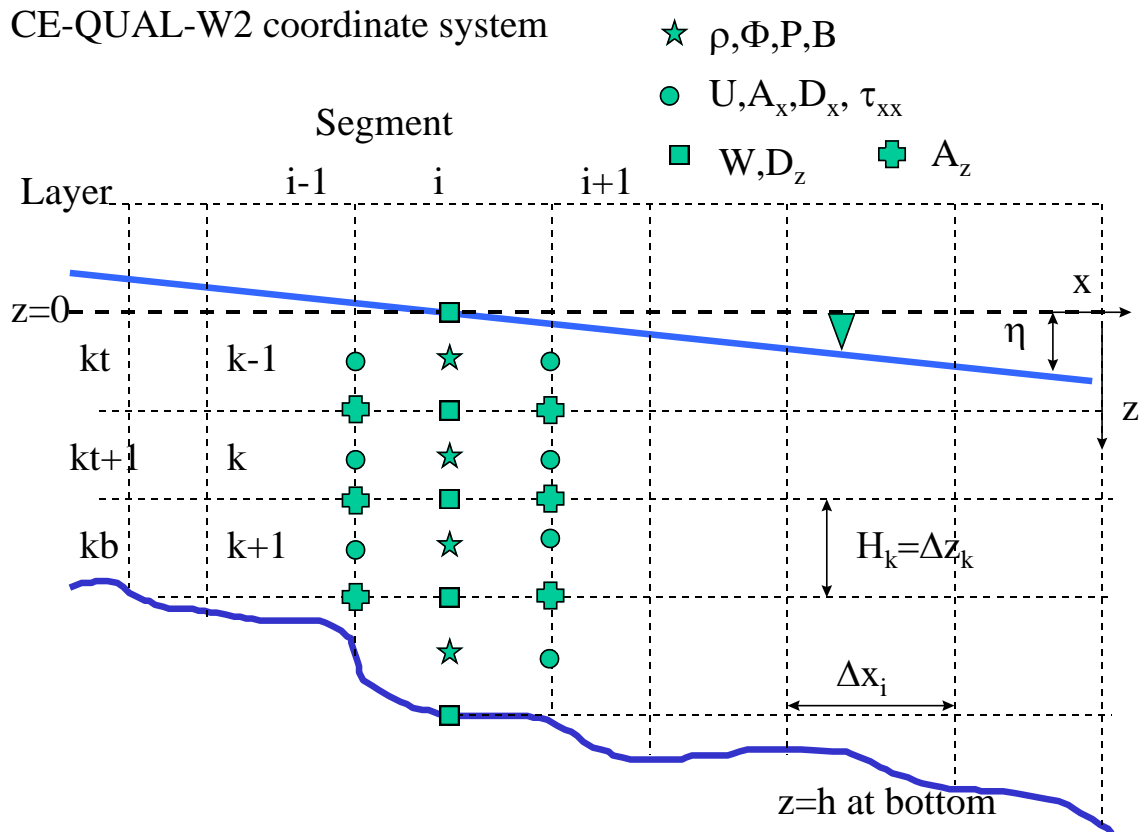
Figure 119. Computational grid variable definitions for no channel slope.

CE-QUAL-W2 coordinate system, $\alpha > 0$

Figure 120. Computational grid variable definitions for arbitrary channel slope.
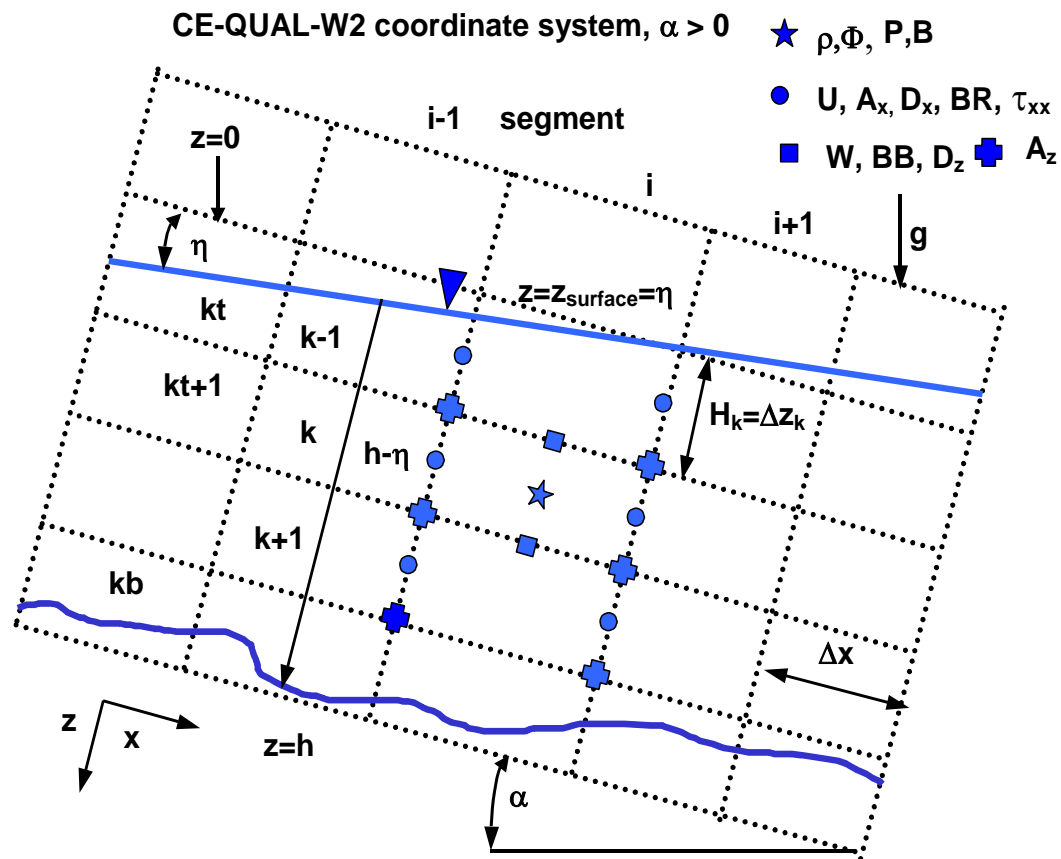
Hydrodynamic Equations Numerical Solution

Characteristics of the Hydrodynamics Numerical Solution

- Horizontal velocities and water levels are not solved simultaneously; water levels are solved first followed by velocities.
- Branch hydrodynamics are solved sequentially rather than simultaneously. This can cause instabilities if Δt is too large and hence the time step may have to be manually reduced.
- Water surface solution is solved implicitly using central spatial differences and the resulting simultaneous equations are solved using the Thomas algorithm.
- The horizontal momentum equation is solved explicitly using upwind (or backward) spatial differencing for the advection terms and central spatial differences for all other terms.
- The continuity equation is used to solve for vertical velocities using a central difference explicit solution.
- The order of the solution is as follows:

NUMERICAL SOLUTION

- Solve water surface equation for η at time level n+1 (n is the current time level).
- Compute U at n+1 using the momentum equation.
- Compute W at n+1 using the continuity equation.

Free-Water Surface Numerical Solution for η

The free surface equation:

$$B_\eta \frac{\partial \eta}{\partial t} = \frac{\partial}{\partial x}\int_\eta^h UBdz - \int_\eta^h qBdz \tag{5-1}$$

is solved by substituting the momentum equation:

$$\frac{\partial UB}{\partial t} + \frac{\partial UUB}{\partial x} + \frac{\partial WUB}{\partial z} = gB\sin\alpha + g\cos\alpha B\frac{\partial \eta}{\partial x} - \frac{g\cos\alpha B}{\rho}\int_\eta^z \frac{\partial \rho}{\partial x}dz$$
$$+ \frac{1}{\rho}\frac{\partial B\tau_{xx}}{\partial x} + \frac{1}{\rho}\frac{\partial B\tau_{xz}}{\partial z} + qBU_x \tag{5-2}$$

in finite difference form and then simplifying. The finite difference form of the momentum equation is:

$$UB_i^{n+1} = UB_i^n + \Delta t\left[-\frac{\partial UUB}{\partial x} - \frac{\partial WUB}{\partial z} + gB\sin\alpha + g\cos\alpha B\frac{\partial \eta}{\partial x}\right.$$
$$\left. - \frac{g\cos\alpha B}{\rho}\int_\eta^z \frac{\partial \rho}{\partial x}dz + \frac{1}{\rho}\frac{\partial B\tau_{xx}}{\partial x} + \frac{1}{\rho}\frac{\partial B\tau_{xz}}{\partial z} + qBU_x\right]_i^n \tag{5-3}$$

Defining for simplicity the term *F* as:

$$F = -\frac{\partial UUB}{\partial x} - \frac{\partial WUB}{\partial z} + \frac{1}{\rho}\frac{\partial B\tau_{xx}}{\partial x} \tag{5-4}$$

and substituting in for τ_{xx}, *F* becomes:

$$F = -\frac{\partial UUB}{\partial x} - \frac{\partial WUB}{\partial z} + \frac{\partial\left(BA_x\frac{\partial U}{\partial x}\right)}{\partial x} \tag{5-5}$$

Substituting in the term UB_i^{n+1} in the free surface equation for *UB*, the free surface equation becomes:

$$B_\eta \frac{\partial \eta}{\partial t} = \frac{\partial}{\partial x}\int_\eta^h UB_i^n dz + \Delta t\frac{\partial}{\partial x}\int_\eta^h F^n\, dz + \Delta t\frac{\partial}{\partial x}\int_\eta^h gB\sin\alpha dz$$
$$+ \Delta t\frac{\partial}{\partial x}\int_\eta^h g\cos\alpha B\frac{\partial \eta}{\partial x}\bigg|^n dz - \Delta t\frac{\partial}{\partial x}\int_\eta^h \frac{g\cos\alpha B}{\rho}\int_\eta^z \frac{\partial \rho}{\partial x}\bigg|^n dzdz$$
$$+ \Delta t\frac{\partial}{\partial x}\int_\eta^h \frac{1}{\rho}\frac{\partial B\tau_{xz}}{\partial z}\bigg|^n dz + \Delta t\frac{\partial}{\partial x}\int_\eta^h qBU_x^n dz$$
$$- \int_\eta^h q^n Bdz \tag{5-6}$$

Some of these terms can be simplified as follows:

NUMERICAL SOLUTION

$$\frac{\partial}{\partial x}\int_{\eta}^{h} gB \sin\alpha \, dz = g\sin\alpha \frac{\partial}{\partial x}\int_{\eta}^{h} B \, dz \tag{5-7}$$

$$\frac{\partial}{\partial x}\int_{\eta}^{h} g\cos\alpha \, B \frac{\partial\eta}{\partial x}dz = g\cos\alpha \frac{\partial}{\partial x}\left(\frac{\partial\eta}{\partial x}\int_{\eta}^{h} B \, dz\right) \tag{5-8}$$

$$\frac{\partial}{\partial x}\int_{\eta}^{h} \frac{g\cos\alpha B}{\rho}\int_{\eta}^{z}\frac{\partial\rho}{\partial x}dzdz = \frac{g\cos\alpha}{\rho}\frac{\partial}{\partial x}\int_{\eta}^{h} B \int_{\eta}^{z}\frac{\partial\rho}{\partial x}dzdz \tag{5-9}$$

$$\frac{\partial}{\partial x}\int_{\eta}^{h}\frac{1}{\rho}\frac{\partial B\tau_{xz}}{\partial z}dz = \frac{1}{\rho}\frac{\partial}{\partial x}\left(B\tau_{xz}|_h - B\tau_{xz}|_\eta\right) \tag{5-10}$$

Then substituting these into the above equation:

$$B_\eta \frac{\partial\eta}{\partial t} = \frac{\partial}{\partial x}\int_{\eta}^{h} UB_i^n dz + \Delta t \frac{\partial}{\partial x}\int_{\eta}^{h} F^n \, dz + \Delta t g\sin\alpha \frac{\partial}{\partial x}\int_{\eta}^{h} Bdz$$

$$+ \Delta t g\cos\alpha \frac{\partial}{\partial x}\left(\frac{\partial\eta}{\partial x}\Big|^n \int_{\eta}^{h} Bdz\right) - \Delta t \frac{g\cos\alpha}{\rho}\frac{\partial}{\partial x}\int_{\eta}^{h} B \int_{\eta}^{z}\frac{\partial\rho}{\partial x}\Big|^n dzdz \tag{5-11}$$

$$+ \Delta t \frac{\partial}{\partial x}\frac{1}{\rho}\left(B\tau_{xz}|_h - B\tau_{xz}|_\eta\right)^n + \Delta t \frac{\partial}{\partial x}\int_{\eta}^{h} qBU_x^n dz - \int_{\eta}^{h} q^n Bdz$$

All terms with η are grouped on the LHS such that:

$$B_\eta \frac{\partial\eta}{\partial t} - \Delta t g\cos\alpha \frac{\partial}{\partial x}\left(\frac{\partial\eta}{\partial x}\int_{\eta}^{h} Bdz\right) = \frac{\partial}{\partial x}\int_{\eta}^{h} UB_i^n dz + \Delta t \frac{\partial}{\partial x}\int_{\eta}^{h} F^n \, dz$$

$$+ \Delta t g\sin\alpha \frac{\partial}{\partial x}\int_{\eta}^{h} Bdz$$

$$- \Delta t \frac{g\cos\alpha}{\rho}\frac{\partial}{\partial x}\int_{\eta}^{h} B\int_{\eta}^{z}\frac{\partial\rho}{\partial x}\Big|^n dzdz$$

$$+ \Delta t \frac{\partial}{\partial x}\frac{1}{\rho}\left(B\tau_{xz}|_h - B\tau_{xz}|_\eta\right)^n \tag{5-12}$$

$$+ \Delta t \frac{\partial}{\partial x}\int_{\eta}^{h} qBU_x^n dz$$

$$- \int_{\eta}^{h} q^n Bdz$$

The first term on the LHS can be put into a backward finite difference form as:

$$B_\eta \frac{\partial\eta}{\partial t} \approx B_\eta \frac{\eta_i^n - \eta_i^{n-1}}{\Delta t} \tag{5-13}$$

The second term, $-\Delta t g\cos\alpha \frac{\partial}{\partial x}\left(\frac{\partial\eta}{\partial x}\int_{\eta}^{h} B \, dz\right)^n$, can be simplified using the chain rule for partial differential equations to:

$$-\Delta t g\cos\alpha \frac{\partial\eta}{\partial x}\Big|^n \frac{\partial}{\partial x}\int_{\eta}^{h} B \, dz - \Delta t g\cos\alpha \int_{\eta}^{h} B \, dz \frac{\partial^2\eta}{\partial x^2}\Big|^n \tag{5-14}$$

Then using a second-order central difference for the second derivative and a first order backward difference for the first derivative such that:

NUMERICAL SOLUTION

$$-\Delta tg\cos\alpha\left.\frac{\partial\eta}{\partial x}\right|^n\frac{\partial}{\partial x}\int_\eta^h Bdz-\Delta tg\cos\alpha\int_\eta^h Bdz\left.\frac{\partial^2\eta}{\partial x^2}\right|^n$$

$$\approx-\Delta tg\cos\alpha\frac{\eta_i^n-\eta_{i-1}^n}{\Delta x}\frac{\partial}{\partial x}\int_\eta^h B\,dz-\Delta tg\cos\alpha\int_\eta^h Bdz\frac{\eta_{i+1}^n-2\eta_i^n+\eta_{i-1}^n}{\Delta x^2} \qquad \textbf{(5-15)}$$

Also using a backward difference:

$$\frac{\partial}{\partial x}\int_\eta^h B\,dz=\frac{1}{\Delta x}\left(\left.\int_\eta^h Bdz\right|_i-\left.\int_\eta^h Bdz\right|_{i-1}\right)^n. \qquad \textbf{(5-16)}$$

Grouping and collecting terms and multiplying through by $\Delta t\Delta x$, the LHS becomes after simplification:

$$\eta_{i-1}^n\left[\frac{-g\cos\alpha\Delta t^2}{\Delta x}\left.\int_\eta^h Bdz\right|_{i-1}\right]+\eta_i^n\left[B_\eta\Delta x+\frac{g\cos\alpha\Delta t^2}{\Delta x}\left\{\left.\int_\eta^h Bdz\right|_i+\left.\int_\eta^h Bdz\right|_{i-1}\right\}\right]+$$

$$\eta_{i+1}^n\left[\frac{-g\cos\alpha\Delta t^2}{\Delta x}\left.\int_\eta^h Bdz\right|_i\right]=(RHS)_i^n\Delta x\Delta t+B_\eta\eta_i^{n-1}\Delta x \qquad \textbf{(5-17)}$$

where the RHS is defined as:

$$RHS=\frac{\partial}{\partial x}\int_\eta^h UB_i^n dz+\Delta t\frac{\partial}{\partial x}\int_\eta^h Fdz+\Delta tg\sin\alpha\frac{\partial}{\partial x}\int_\eta^h Bdz$$

$$-\Delta t\frac{g\cos\alpha}{\rho}\frac{\partial}{\partial x}\int_\eta^h B\int_\eta^z\frac{\partial\rho}{\partial x}dzdz+\Delta t\frac{\partial}{\partial x}\frac{1}{\rho}\left(B\tau_{xz}|_h-B\tau_{xz}|_\eta\right) \qquad \textbf{(5-18)}$$

$$+\Delta t\frac{\partial}{\partial x}\int_\eta^h qBU_x dz-\int_\eta^h qBdz$$

and is evaluated at time level n.

The integral of the cell widths can be put into a summation over the vertical layers as:

$$\left.\int_\eta^h Bdz\right|_i=\sum_{kb}^{kt}BH_{ri} \qquad \textbf{(5-19)}$$

$$\left.\int_\eta^h Bdz\right|_{i-1}=\sum_{kb}^{kt}BH_{ri-1} \qquad \textbf{(5-20)}$$

where BH_r is the value of the width times the layer depth for the right-hand side of a cell. In the code, this is the variable BR(I,K) times H(K), or the derived variable BHR(I,K).

Some of the right-hand side terms can be put into a format compatible with the model schematization such as:

$$\frac{\partial}{\partial x}\int_\eta^h(UB)_i^n\,dz\approx\frac{\partial}{\partial x}\sum_{kt}^{kb}UBH_r$$

$$\approx\frac{1}{\Delta x}\left(\left.\sum_{kt}^{kb}UBH_r\right|_i-\left.\sum_{kt}^{kb}UBH_r\right|_{i-1}\right)=\frac{1}{\Delta x}\sum_{kt}^{kb}(UBH_r|_i-UBH_r|_{i-1})^n \qquad \textbf{(5-21)}$$

$$\Delta t\frac{\partial}{\partial x}\int_\eta^h F^n\,dz\approx\Delta t\frac{\partial}{\partial x}\sum_{kt}^{kb}FH_r$$

NUMERICAL SOLUTION

$$\approx \frac{\Delta t}{\Delta x}\left(\sum_{kt}^{kb} FH_r\big|_i - \sum_{kt}^{kb} FH_r\big|_{i-1}\right) = \frac{\Delta t}{\Delta x}\sum_{kt}^{kb}(FH_r\big|_i - FH_r\big|_{i-1})^n \tag{5-22}$$

$$\Delta t g \sin\alpha \frac{\partial}{\partial x}\int_\eta^h Bdz \approx \Delta t g \sin\alpha \frac{\partial}{\partial x}\sum_{kt}^{kb} BH_r$$

$$\approx \frac{\Delta t g \sin\alpha}{\Delta x}\left(\sum_{kt}^{kb} BH_r\big|_i - \sum_{kt}^{kb} BH_r\big|_{i-1}\right) = \frac{\Delta t g \sin\alpha}{\Delta x}\sum_{kt}^{kb}(BH_r\big|_i - BH_r\big|_{i-1}) \tag{5-23}$$

$$\Delta t \frac{g\cos\alpha}{\rho}\frac{\partial}{\partial x}\int_\eta^h B\int_\eta^z \frac{\partial\rho}{\partial x}dzdz \approx \Delta t \frac{g\cos\alpha}{\rho}\frac{\partial}{\partial x}\int_\eta^h B\sum_{kt}^{kb}\frac{\partial\rho}{\partial x}H_r\,dz \approx$$

$$\Delta t \frac{g\cos\alpha}{\rho\Delta x}\sum_{kt}^{kb}\frac{\partial\rho}{\partial x}H_r\sum_{kt}^{kb}(BH_r\big|_i - BH_r\big|_{i-1}) \tag{5-24}$$

$$\Delta t \frac{\partial}{\partial x}\frac{1}{\rho}\left(B\tau_{xz}\big|_h - B\tau_{xz}\big|_\eta\right) \approx \frac{\Delta t}{\rho\Delta x}\left\{\left(B\tau_{xz}\big|_h - B\tau_{xz}\big|_\eta\right)_i - \left(B\tau_{xz}\big|_h - B\tau_{xz}\big|_\eta\right)_{i-1}\right\} \tag{5-25}$$

The lateral inflow of momentum term represents the gradient over *x* of the inflow momentum:

$$\Delta t \frac{\partial}{\partial x}\int_\eta^h q\,BU_x dz \approx \Delta t \frac{\partial}{\partial x}\sum_{kt}^{kb} qU_x BH_r \tag{5-26}$$

$$\int_\eta^h qBdz \approx \sum_{kt}^{kb} qBH_r \tag{5-27}$$

Combining these terms into one equation:

$$A\eta_{i-1}^n + X\eta_i^n + C\eta_{i+1}^n = D \tag{5-28}$$

where:

$$A = \left[\frac{-g\cos\alpha\,\Delta t^2}{\Delta x}\sum_{kt}^{kb} BH_r\big|\right]_{i-1}$$

$$X = \left[B_\eta\Delta x + \frac{g\cos\alpha\,\Delta t^2}{\Delta x}\left\{\sum_{kt}^{kb} BH_r\bigg|_i + \sum_{kt}^{kb} BH_r\bigg|_{i-1}\right\}\right]$$

$$C = \left[\frac{-g\cos\alpha\,\Delta t^2}{\Delta x}\sum_{kt}^{kb} BH_r\big|\right]_i$$

$$D = \Delta t\sum_{kt}^{kb}(UBH_r\big|_i - UBH_r\big|_{i-1}) + B_\eta\eta_i^{n-1}\Delta x + \Delta t^2\sum_{kt}^{kb}(FH_r\big|_i - FH_r\big|_{i-1})$$

$$+\Delta t^2 g\sin\alpha\sum_{kt}^{kb}(BH_r\big|_i - BH_r\big|_{i-1}) + \Delta t^2\frac{g\cos\alpha}{\rho}\sum_{kt}^{kb}(BH_r\big|_i - BH_r\big|_{i-1})\sum_{kt}^{kb}\frac{\partial\rho}{\partial x}H_r$$

$$+\Delta x\Delta t\sum_{kt}^{kb} qBH_r + \Delta x\Delta t^2\frac{\partial}{\partial x}\sum_{kt}^{kb} qU_x BH_r + \frac{\Delta t^2}{\rho}\left[\left(B\tau_{xz}\big|_h - B\tau_{xz}\big|_\eta\right)_i - \left(B\tau_{xz}\big|_h - B\tau_{xz}\big|_\eta\right)_{i-1}\right]$$

NUMERICAL SOLUTION

This equation is applied at all cells in the branch generating a system of equations that are solved for the water surface elevation at the n+1 time level using the Thomas algorithm. The resulting FDA is implicit in η because of the dependence of η in the momentum equation (see Figure 121).

The boundary conditions of either flow or head boundary are accounted for in applying the above equation to the boundary cells as shown in Figure 122 and Figure 123, respectively. The boundary condition implementation is the same as described in Cole and Buchak (1995).
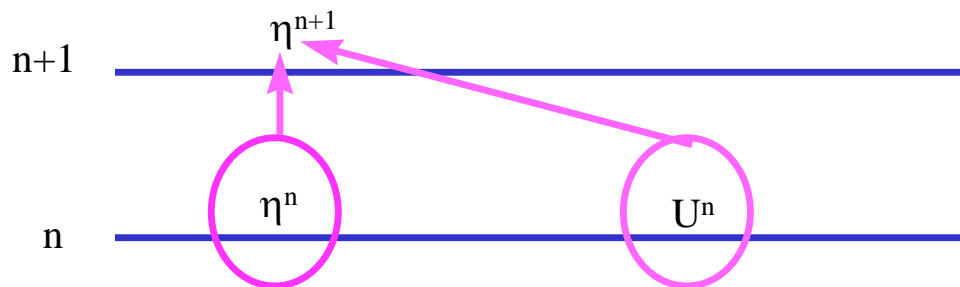
Figure 121. Solution of the water level, η.
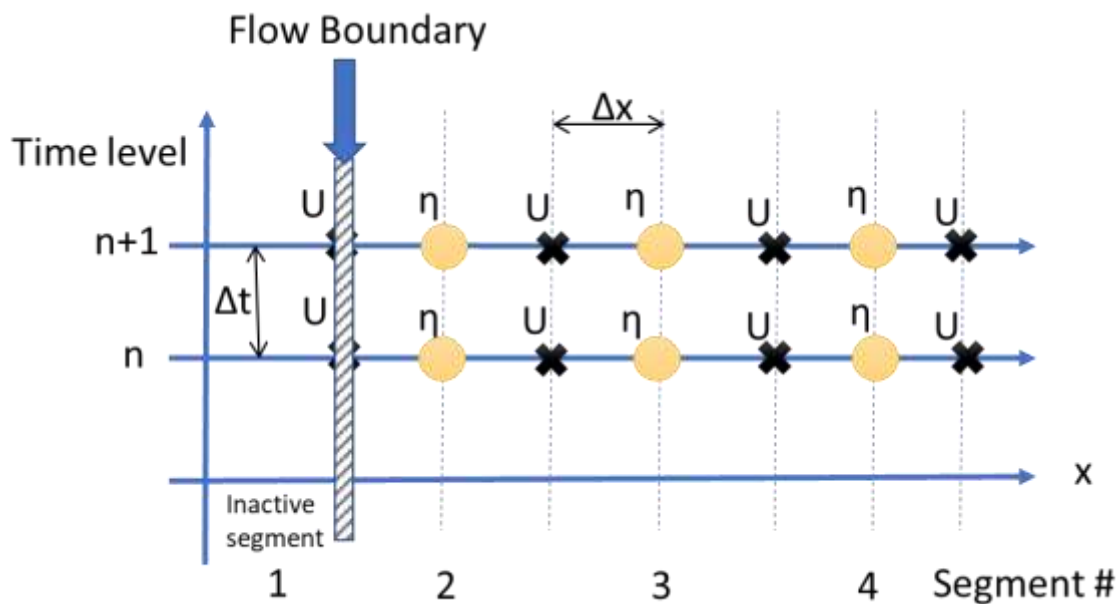
Figure 122. Grid for computation of a flow boundary in x. U, the longitudinal velocity, at the flow boundary or at the right-hand side of inactive segment 1 is computed from the flow rate.
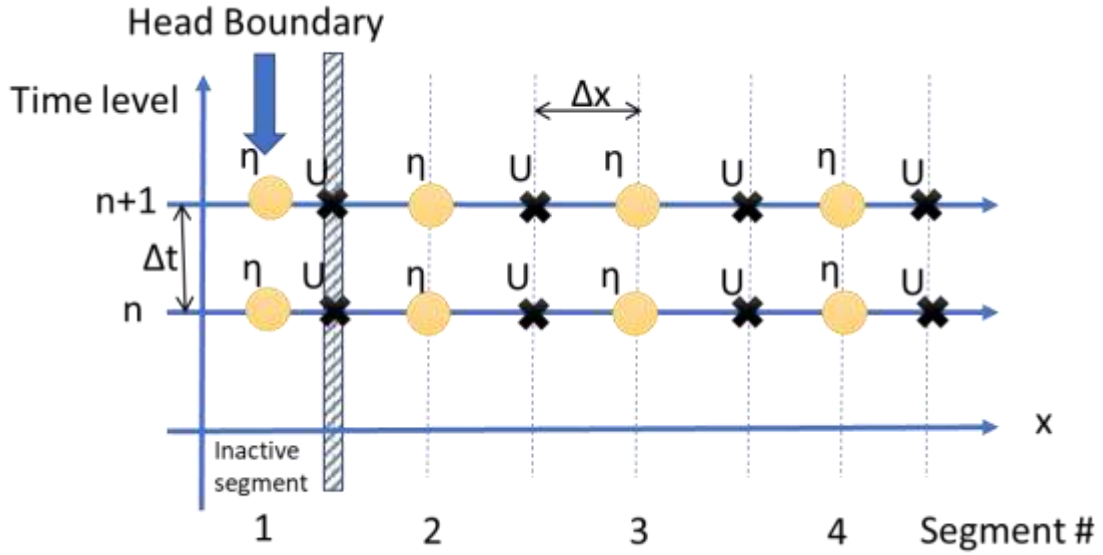
Figure 123. Grid for computation of a head boundary in x. U, the longitudinal velocity, at the flow boundary or at the right-hand side of inactive segment 1 is computed from the head difference between the boundary head (at center of inactive segment 1) and the head at the first grid cell (segment 2).

Horizontal Momentum Numerical Solution for Horizontal Velocity U

The x-momentum equation:

$$\frac{\partial UB}{\partial t} + \frac{\partial UUB}{\partial x} + \frac{\partial WUB}{\partial z} = gB\sin\alpha + g\cos\alpha B\frac{\partial \eta}{\partial x} - \frac{g\cos\alpha B}{\rho}\int_{\eta}^{z}\frac{\partial \rho}{\partial x}dz$$
$$+ \frac{1}{\rho}\frac{\partial B\tau_{xx}}{\partial x} + \frac{1}{\rho}\frac{\partial B\tau_{xz}}{\partial z} + qBU_x$$

(5-29)

is solved using either a fully explicit or an explicit/implicit finite difference solution technique specified by the user after the water surface equation is solved.

Explicit Solution

This scheme is based on solving the partial differential terms using an explicit finite difference technique where:

$$U_i^{n+1}B_i^{n+1} = U_i^n B_i^n + \Delta t\{-\frac{\partial UUB}{\partial x} - \frac{\partial WUB}{\partial z} + gB\sin\alpha + g\cos\alpha B\frac{\partial \eta}{\partial x}$$
$$- \frac{g\cos\alpha B}{\rho}\int_{\eta}^{z}\frac{\partial \rho}{\partial x}dz\frac{1}{\rho}\frac{\partial B\tau_{xx}}{\partial x} + \frac{1}{\rho}\frac{\partial B\tau_{xz}}{\partial z} + qBU_x\}_i^n$$

(5-30)

223

NUMERICAL SOLUTION

The various terms are put into finite difference form as follows. The longitudinal advection of momentum is an upwind difference scheme where the order of differencing is dependent on the sign of U, e.g., for $U > 0$

$$\frac{\partial UUB}{\partial x}\bigg|_{i,k} \cong \frac{1}{\Delta x_i}\left[B_{i,k}^n U_{i,k}^n U_{i,k}^n - B_{i-1,k}^n U_{i-1,k}^n U_{i-1,k}^n\right]\bigg| \tag{5-31}$$

The vertical advection of momentum is also an upwind scheme based on the velocity of W. For W > 0 or downward flow

$$\frac{\partial WUB}{\partial z}\bigg|_{i,k} \cong \frac{1}{\Delta z_k}\left[\left(W_{i,k}^n U_{i,k}^n B_{i,k}^n\right) - \left(W_{i,k-1}^n U_{i,k-1}^n B_{i,k-1}^n\right)\right]\bigg| \tag{5-32}$$

The gravity force is:

$$gB \sin \alpha = g \sin \alpha\, B_i^n \tag{5-33}$$

The pressure gradient is:

$$g \cos \alpha\, B \frac{\partial \eta}{\partial x} - \frac{g \cos \alpha B}{\rho} \int_\eta^z \frac{\partial \rho}{\partial x} dz = \frac{g \cos \alpha B_i^n}{\Delta x}(\eta_{i+1} - \eta_i)^n$$

$$-\frac{g \cos \alpha B_i^n}{\rho \Delta x}\sum \left(\rho_{i+1,k} - \rho_{i,k}\right)^n \Delta z_k \tag{5-34}$$

The horizontal advection of turbulent momentum is:

$$\frac{1}{\rho}\frac{\partial B \tau_{xx}}{\partial x} = \frac{\partial B A_x \frac{\partial U}{\partial x}}{\partial x} = \left(\frac{B_{i+1/2}^n A_x}{\Delta x_i \Delta x_{i+1/2}}\right)\left(U_{i+1,k}^n - U_{i,k}^n\right)$$

$$-\left(\frac{B_{i-1/2}^n A_x}{\Delta x_i \Delta x_{i-1/2}}\right)\left(U_{i,k}^n - U_{i-1,k}^n\right) \tag{5-35}$$

The contribution to longitudinal momentum by lateral branch inflows is:

$$qBU_x = qBU_x\big|_{i,k}^n \tag{5-36}$$

Using the definition of the shear stress:

$$\tau_{xz} = \left[\tau_w + \tau_b + \rho A_z \frac{\partial U}{\partial z}\right] \tag{5-37}$$

NUMERICAL SOLUTION

where A_z is the turbulent kinematic viscosity, the vertical transport of momentum is:

$$\frac{1}{\rho}\frac{\partial B\tau_{xz}}{\partial z} = \frac{\partial}{\partial z}\frac{B}{\rho}\left[\tau_w + \tau_b + \rho A_z \frac{\partial U}{\partial z}\right] = \left(\frac{B_{i,k+1/2}^n}{\Delta z_k \Delta z_{k+1/2}\rho}\right)$$

$$\left[\tau_w|_{i,k+1/2}^n + \tau_b|_{i,k+1/2}^n + \frac{\rho A_{z\ \ i,k+1/2}}{\Delta z_{k+1/2}}\left(U_{i,k+1}^n - U_{i,k}^n\right)\right] \qquad \textbf{(5-38)}$$

$$-\left(\frac{B_{i,k-1/2}^n}{\Delta z_k \Delta z_{k-1/2}\rho}\right)\left[\tau_w|_{i,k-1/2}^n + \tau_b|_{i,k-1/2}^n + \frac{\rho A_{z\ \ i,k-1/2}}{\Delta z_{k-1/2}}\left(U_{i,k}^n - U_{i,k-1}^n\right)\right]$$

Implicit Solution

The implicit technique was utilized to reduce the time step limitation for numerical stability when values of A_z were large, as for an estuary or a river system. This occurs because the time step limitation is a function of A_z. Only the vertical transport of momentum term was solved implicitly. All other terms for the solution of the horizontal momentum equation were the same as the explicit scheme.

The horizontal momentum equation can be separated into the following two equations:

$$\frac{\partial UB}{\partial t} + \frac{\partial UUB}{\partial x} + \frac{\partial WUB}{\partial z} = gB\sin\alpha + g\cos\alpha B\frac{\partial \eta}{\partial x} - \frac{g\cos\alpha B}{\rho}\int_\eta^z \frac{\partial \rho}{\partial x}dz$$

$$+ \frac{1}{\rho}\frac{\partial B\tau_{xx}}{\partial x} + \frac{1}{\rho}\frac{\partial B(\tau_b+\tau_w)}{\partial z} + qBU_x \qquad \textbf{(5-39)}$$

$$\frac{\partial UB}{\partial t} = \frac{1}{\rho}\frac{\partial}{\partial z}\left(BA_z \frac{\partial U}{\partial z}\right) \qquad \textbf{(5-40)}$$

Equation 93 is written as:

$$U_i^* B_i^{n+1} = U_i^n B_i^n + \Delta t\{-\frac{\partial UUB}{\partial x} - \frac{\partial WUB}{\partial z} + gB\sin\alpha + g\cos\alpha B\frac{\partial \eta}{\partial x}$$

$$- \frac{g\cos\alpha B}{\rho}\int_\eta^z \frac{\partial \rho}{\partial x}dz + \frac{1}{\rho}\frac{\partial B\tau_{xx}}{\partial x} + \frac{1}{\rho}\frac{\partial B(\tau_b+\tau_w)}{\partial z} + qBU_x\}_i^n \qquad \textbf{(5-41)}$$

where U^* is the velocity at the new time level before the application of equation 94. Equation 92 is solved similarly to the solution of the fully explicit technique outlined above.

Equation 94 is then solved using a fully implicit technique as:

$$\frac{\partial UB}{\partial t} = \frac{(U_i^{n+1}B_i^{n+1} - U_i^* B_i^{n+1})}{\Delta t} = \frac{1}{\rho}\frac{\partial}{\partial z}\left(\rho B^{n+1}A_z \frac{\partial U^{n+1}}{\partial z}\right) \qquad \textbf{(5-42)}$$

This can be rewritten as:

$$U_i^{n+1}B_i^{n+1} = U_i^* B_i^{n+1} + \left(\frac{\Delta t B_{i,k+1/2}^{n+1}}{\Delta z_k}\right)\left[\frac{A_{z\ \ i,k+1/2}}{\Delta z_{k+1/2}}\left(U_{i,k+1}^{n+1} - U_{i,k}^{n+1}\right)\right]$$

$$- \left(\frac{\Delta t B_{i,k-1/2}^{n+1}}{\Delta z_k}\right)\left[\frac{A_{z\ \ i,k-1/2}}{\Delta z_{k-1/2}}\left(U_{i,k}^{n+1} - U_{i,k-1}^{n+1}\right)\right] \qquad \textbf{(5-43)}$$

Regrouping terms at n+1 time level on the LHS, the equation can be written as

NUMERICAL SOLUTION

$$AU_{i,k-1}^{n+1} + VU_{i,k}^{n+1} + CU_{i,k+1}^{n+1} = DU_{i,k}^* \qquad\qquad \textbf{(5-44)}$$

where:

$$A = \left(\frac{-\Delta t B_{i,k-1/2}^{n+1}}{B_{i,k}^{n+1}\Delta z_k}\right)\left[\frac{A_{z\ \ i,k-1/2}}{\Delta z_{k-1/2}}\right]$$

$$V = 1 + \left(\frac{\Delta t B_{i,k+1/2}^{n+1}}{B_{i,k}^{n+1}\Delta z_k}\right)\left[\frac{A_{z\ \ i,k+1/2}}{\Delta z_{k+1/2}}\right] + \left(\frac{\Delta t B_{i,k-1/2}^{n+1}}{B_{i,k}^{n+1}\Delta z_k}\right)\left[\frac{A_{z\ \ i,k-1/2}}{\Delta z_{k-1/2}}\right]$$

$$C = \left(\frac{-\Delta t B_{i,k+1/2}^{n+1}}{B_{i,k}^{n+1}\Delta z_k}\right)\left[\frac{A_{z\ \ i,k+1/2}}{\Delta z_{k+1/2}}\right]$$

D=1

The resulting simultaneous equations are solved for U^{n+1} using the Thomas algorithm.

The resulting horizontal velocities are then corrected to preserve branch continuity (or more correctly to "force" continuity). The lack of a continuity balance is a result of numerical errors in the solution of the FDAs for η^n and U^{n+1}. Cole and Buchak (1995) discuss the algorithm to correct horizontal velocities from continuity. The correction is calculated segment by segment: the change in the water layers over time should equal the net flow into the segment by horizontal velocities. The change or correction in velocity is apportioned equally to the horizontal velocity of all vertical layers. Other numerical models iterate by re-solving the water surface equation after updated horizontal and vertical velocities are computed. This results in significant computational time but a more correct solution.

Boundary Conditions

The solution of the horizontal momentum equation can either accept a flow boundary condition (as shown in Figure 124) or a head or water level condition (as shown in Figure 125). For the flow boundary condition, the velocities at the flow boundary are specified based on the flow rates provided by the user. For the head condition, the model user sets the head or water level as a function of time.

NUMERICAL SOLUTION
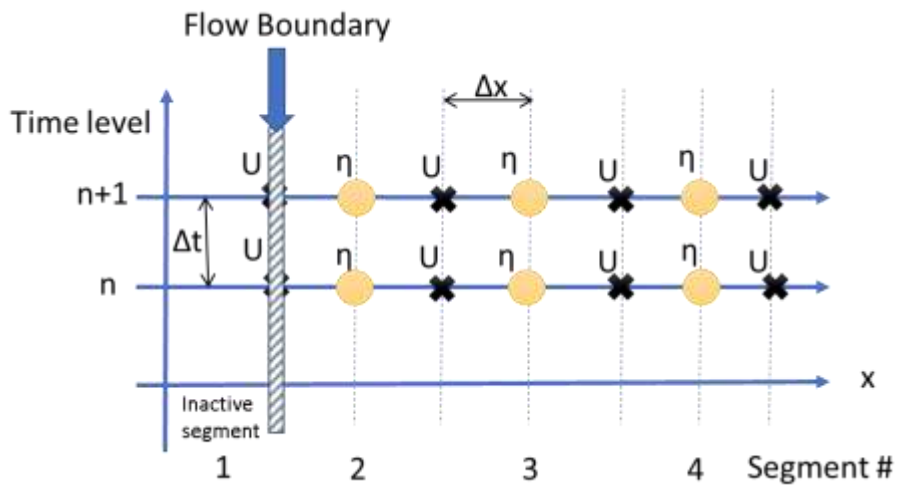
Figure 124. Flow boundary condition where velocities are specified on a boundary.
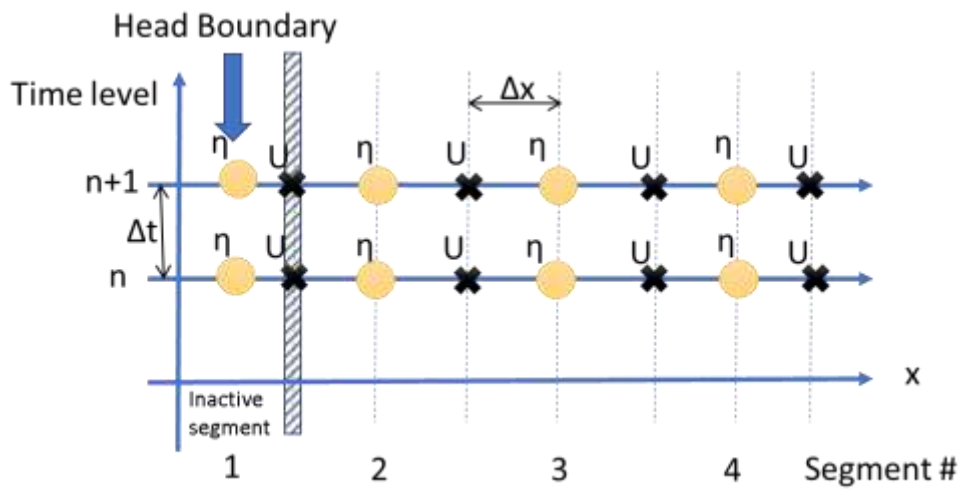
Figure 125. Head boundary condition for solution of momentum equation.

Solution of Vertical Velocity W

The continuity equation

$$\frac{\partial UB}{\partial x} + \frac{\partial WB}{\partial z} = qB$$

is used to solve for W after discretizing into finite differences as

$$\frac{WB_{i,k} - WB_{i,k-1}}{\Delta z_k} = -\left(\frac{UB_{i,k} - UB_{i-1,k}}{\Delta x_i}\right) + q_{i,k}B_{i,k}$$

These variables are illustrated in Figure 126.
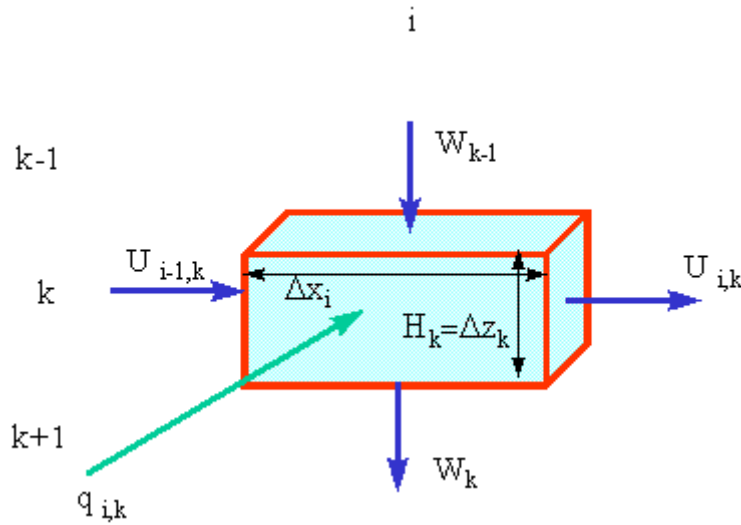
Figure 126. Solution of vertical velocity, w, from continuity equation.

The algorithm starts at the bottom cell using corrected horizontal velocities and where $WB_{k=0}$ such that:

$$WB_{i,k-1} = -WB_{i,k} + \Delta z_k \left(\frac{UB_{i,k} - UB_{i-1,k}}{\Delta x_i}\right) - \Delta z_k q_{i,k} B_{i,k}$$

Numerical Stability

The numerical stability criterion is based on the following equation that only considers momentum equation stability

$$\Delta t \leq \frac{1}{2\left(\frac{A_x}{\Delta x^2} + \frac{A_z}{\Delta z^2}\right) + \frac{Q}{V} + \frac{\sqrt{\frac{\Delta \rho}{\rho} \frac{gH}{2}}}{\Delta x}}$$

Δt = timestep, *sec*
A_x = longitudinal eddy viscosity, *m² sec⁻¹*
A_z = vertical eddy viscosity, *m² sec⁻¹*

NUMERICAL SOLUTION

    Q = total flow into or out of a cell, $m^3\ sec^{-1}$

    V = cell volume, m^3

    g = gravitational acceleration, $m\ sec^{-2}$

    H = maximum waterbody depth, m

    ρ = water density, $kg\ m^{-3}$

    $\Delta\rho$ = surface to bottom water density difference, $kg\ m^{-3}$

This criterion does NOT guarantee numerical stability since it is based on a linearized form of the PDEs. There is no check on stability for the advective-diffusion equation since it is usually not limiting. But the advective-diffusion equation can become unstable also.

Advective-Diffusion Equation Numerical Solution

Characteristics of the Constituent Numerical Solution

- the advective diffusion equation is solved by splitting the solution between horizontal and vertical transport
- the horizontal transport is solved explicitly where QUICKEST (a third order numerical scheme, Leonard, 1979) numerical scheme is used for horizontal explicit transport, central differences are used for diffusion
- vertical transport is solved using an implicit/explicit general time weighted scheme for advection and a fully implicit scheme for diffusion, simultaneous equations are solved using the Thomas algorithm

Solution of Advective-Diffusion Equation

The advective-diffusion transport equation

$$\frac{\partial B\Phi}{\partial t} + \frac{\partial UB\Phi}{\partial x} + \frac{\partial WB\Phi}{\partial z} - \frac{\partial \left(BD_x \frac{\partial \Phi}{\partial x} \right)}{\partial x} - \frac{\partial \left(BD_z \frac{\partial \Phi}{\partial z} \right)}{\partial z} = q_\Phi B + S_\Phi B$$

is solved by splitting the two-dimensional FDA into 2 one-dimensional parts: (1) horizontal transport and sources/sinks and lateral inflows/outflows and (2) vertical transport. The horizontal part of the solution is
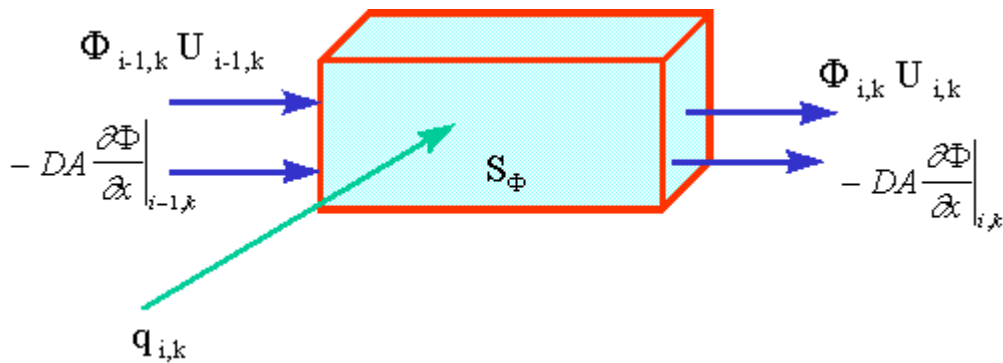
Figure 127. Horizontal advective and diffusive transport.

NUMERICAL SOLUTION

$$\frac{\partial B\Phi}{\partial t} \cong \frac{B\Phi_{i,k}^* - B\Phi_{i,k}^n}{\Delta t} \cong \left[-\frac{\partial UB\Phi}{\partial x} + \frac{\partial \left(BD_x \frac{\partial \Phi}{\partial x} \right)}{\partial x} + q_\Phi B + S_\Phi B \right]_{i,k}^n$$

and the variables are illustrated in Figure 127. The time level * is the intermediate concentration (or temperature) only considering horizontal fluxes, sources/sinks, and lateral inflows. In this step the diffusion term is a central spatial difference and the advection term uses the ULTIMATE/QUICKEST differencing technique (see discussion below). In Version 2, the QUICKEST scheme was introduced which uses quadratic upstream differencing rather than linear upstream differencing. Cole and Buchak (1995) discuss this differencing algorithm which eliminates much of the numerical diffusion associated with upstream differencing.

The result from this explicit computation is then used to compute the vertical transport (see Figure 128). The resulting FDA is put in a general time weighted scheme:
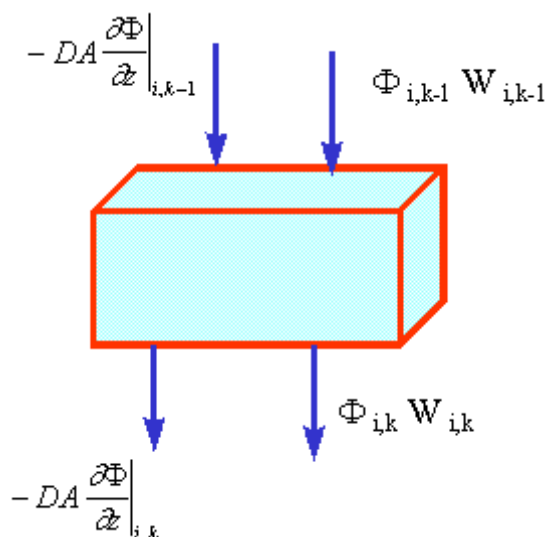
Figure 128. Vertical advective and diffusive transport.

$$\frac{\partial B\Phi}{\partial t} \cong \frac{B\Phi_{i,k}^{n+1} - B\Phi_{i,k}^*}{\Delta t} \cong \left(-\Theta \frac{\partial WB\Phi}{\partial z} \right)_{i,k}^n + \left(-(1-\Theta) \frac{\partial WB\Phi}{\partial z} \right)_{i,k}^{n+1} + \left(\frac{\partial \left(BD_z \frac{\partial \Phi}{\partial z} \right)}{\partial z} \right)_{i,k}^{n+1}$$

where Θ is the degree of implicitness (=0 explicit; =0.5 Crank-Nicholson; =1 fully implicit). Central differences are used for the spatial derivatives for both the vertical diffusion and vertical advection terms. This equation is applied to all vertical layers and solved using the Thomas algorithm. The model user can choose the degree of implicitness for this equation.

Advective Transport in x and z

The first step in the numerical solution is to define the computational grid (**Figure 129**). The grid is space-staggered since some state variables are defined at the segment centers and some at segment interfaces, displaced by Δx/2 or Δz/2 from the segment center. The grid discretizes a waterbody into computational cells whose locations are defined by their segment [I] and layer number [K], i.e., cell (K,I). Variables defined

NUMERICAL SOLUTION

at the boundary include the horizontal and vertical velocities, U and W, longitudinal eddy viscosity and diffusivity, A_x and D_x, vertical eddy viscosity and diffusivity, A_z and D_z, and internal shear stress τ_x. The density, ρ, temperature, T, constituent concentration, Φ, pressure, P, and average cell width, B are defined at the cell center.

Since the constituent concentration is defined at the center and velocities are defined at the boundaries, spatial averaging of velocities is not required to determine fluxes into or out of the control volume at a fixed time level. In addition, the horizontal velocity is surrounded by a cell with water surface elevations and densities defined on either side. Thus, the horizontal velocity is computed from horizontal gradients of the surface slope and densities without requiring spatial averaging of these variables.

The geometry is specified by a cell width, B, thickness or vertical grid spacing, H or Δz, and length, Δx. Several additional geometric variables are used in the calculations. These additional variables include the average cross-sectional area between two cells (k,i) and (k,i+1):

$$BH_{r_{k,i}} = \frac{B_{k,i}H_{k,i} + B_{k,i}H_{k,i+1}}{2} \qquad \textbf{(5-45)}$$

the average widths between two cells (k,i) and (k+1,i):

$$B_{b_{k,i}} = \frac{B_{k,i} + B_{k+1,i}}{2} \qquad \textbf{(5-46)}$$

and the average layer thickness between layers k and k+1:

$$\overline{H}_{k,i} = \frac{H_k + H_{k+1}}{2} \qquad \textbf{(5-47)}$$

The numerical procedure for solving the six unknowns at each timestep is to first compute water surface elevations. With the new surface elevations, new horizontal velocities can be computed. With new horizontal velocities, the vertical velocities can be found from continuity. Using new horizontal and vertical velocities, the water surface elevation equation can be solved for η simultaneously for a model branch. The solution for η is thus spatially implicit at the same time level and eliminates the surface gravity wave speed criterion:

$$\Delta t < \frac{\Delta x}{\sqrt{gH_{max}}} \qquad \textbf{(5-48)}$$

that can seriously limit timesteps in deep waterbodies. Then the temperature and constituent concentrations are computed from the energy and constituent mass balance equations.

NUMERICAL SOLUTION
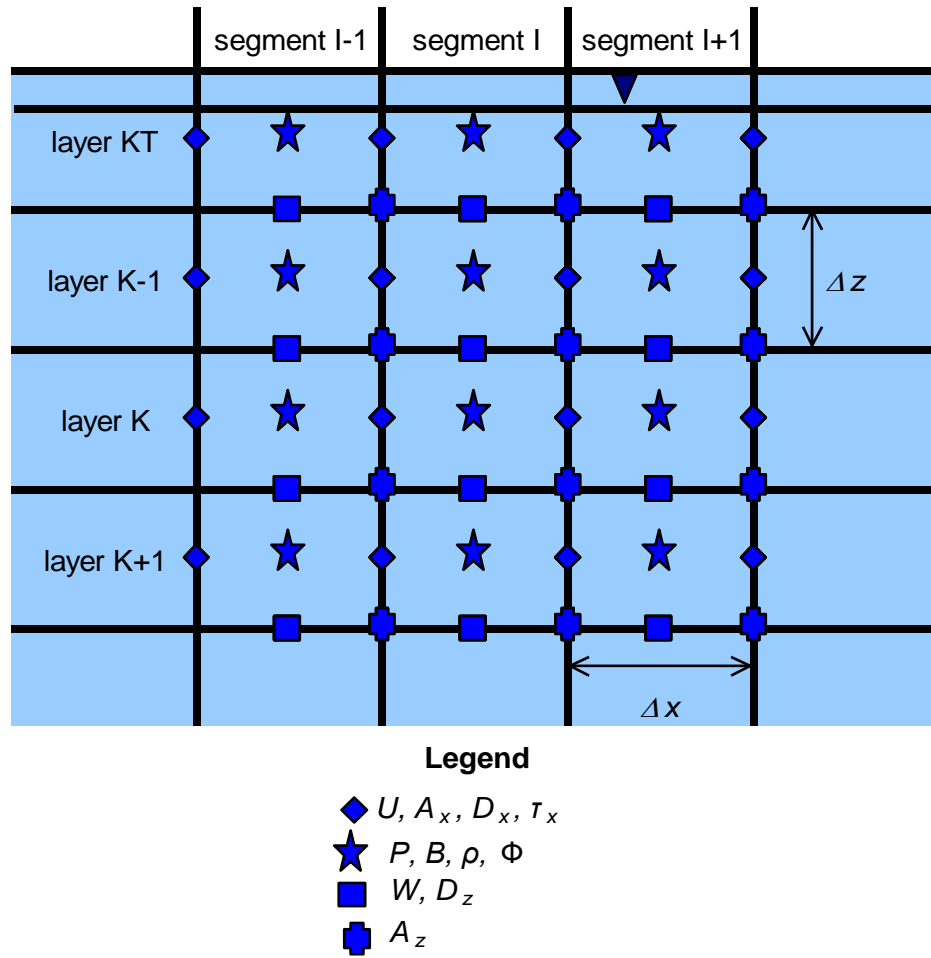
Figure 129. Variable locations in computational grid.

Version 1.0 used upwind differencing in the constituent transport advective terms in which the cell concentration immediately upstream of the velocity was used to calculate mass fluxes. A major problem with upwind differencing is the introduction of numerical diffusion, which acts like diffusion but is an artifact of the numerical scheme. The false longitudinal diffusion coefficient (m^2/s) added to the model can be computed from

$$\alpha_e = \frac{u\Delta x}{2}(1 - C) \tag{5-49}$$

where:

α_e = numerical diffusion coefficient, m^2/s

u = velocity, m/s

Δx = longitudinal grid spacing, m

C = Courant number = $\frac{u\Delta t}{\Delta x}$

NUMERICAL SOLUTION

A similar condition holds for vertical advection. In many cases, numerical diffusion can overwhelm physical diffusion producing inaccurate results when strong gradients are present. The problem is particularly pronounced for stratified reservoirs and estuaries.

Numerical diffusion has been reduced by implementing an explicit, third-order accurate QUICKEST horizontal/vertical transport scheme (Leonard, 1979), and time-weighted, implicit vertical advection. Tests of this scheme are reported in Chapman and Cole (1992).

QUICKEST uses an additional spatial term to estimate concentrations used in computing horizontal and vertical fluxes. A nonuniform grid QUICKEST scheme was developed using a three-point Lagrangian interpolation function to estimate constituent values at grid cell interfaces. Specifically, advective multipliers for each of three upstream weighted grid cells are derived in terms of cell lengths and the local cell interface velocity. Time invariant parts of the interpolation functions are calculated once thus minimizing computations for additional constituents.

Implicit vertical transport including variable layer heights has also been implemented. Vertical diffusion is fully implicit and advection employs a time-weighted, central difference, implicit scheme. A unique feature of vertical advection, in the explicit part of the time-weighted scheme, is QUICKEST which increases overall accuracy.

As implemented in the code, the new transport scheme is a two-part solution for constituent concentrations at the new timestep. First, horizontal advection is computed using QUICKEST and diffusion is computed using central differencing. This part also includes the explicit vertical advection contribution (which utilizes QUICKEST) and all sources and sinks.

Next, the implicit part of vertical advection and diffusion are included. Diffusion is always fully implicit. The user can time-weight advection by specifying a value for **[THETA]** which varies from 0 to 1. For **[THETA]** equal to 0, the solution is explicit in time and vertical advection is accounted for in the first part of the algorithm. For **[THETA]** equal to 1, the solution is fully implicit in time and vertical advection is accounted for in this part of the algorithm. A Crank-Nicholson scheme where vertical advection is time-weighted between the explicit (using QUICKEST) and implicit parts results if **[THETA]** is set to 0.5 or greater. The following is a description of QUICKEST, the preferred transport scheme.

Non-Uniform Grid QUICKEST Formulation

In one dimension, the conservative control volume advective transport of a constituent Φ integrated over a timestep is:

$$\Phi_i^{n+1} = \Phi_i^n - \frac{\Delta t}{\Delta x}(U_r \Phi_r^n - U_l \Phi_l^n) \tag{5-50}$$

where:

Φ_i = constituent concentration at a grid point, $g\ m^{-3}$
$\Phi_{r,l}$ = right and left cell face constituent concentrations, $g\ m^{-3}$
$U_{r,l}$ = right and left cell face velocity, $m\ s^{-1}$
t = time, s

The QUICKEST algorithm was originally derived using an upstream weighted quadratic interpolation function defined over three uniformly spaced grid points. This interpolation function estimates cell face concentrations required by the conservative control volume transport scheme. For example, the right cell face concentration estimate for a flow positive to the right is:

NUMERICAL SOLUTION

$$\Phi_r = T_{i-1}\Phi_{i-1} + T_i\Phi_i + T_{i+1}\Phi_{i+1} \tag{5-51}$$

where T are advective multipliers which weight the contribution of three adjacent grid point concentrations.

The advective multipliers are obtained by collecting terms associated with each constituent defined by the QUICKEST advection operator. For a non-uniform grid, a combination of two and three-point Lagrangian interpolation functions (Henrici, 1964) are used to compute the QUICKEST estimate for the right cell face concentration centered about cells i and i+1:

$$\Phi_r = P_1(x) - \frac{U\Delta t}{2}P_2(x) + \left[D_x\Delta t - \frac{1}{6}[\Delta x^2 - (U\Delta t)^2]\right]P_2''(x) \tag{5-52}$$

where:

x = the local right cell face position
D_x = diffusion coefficient

Defining a local coordinate system of three non-uniformly spaced grid cells denoted by x_{i-1}, x_i, and x_{i+1} with corresponding constituent values, the interpolation functions required in Equation 118 are:

$$P_1(x) = \frac{(x-x_i)}{(x_{i+1}-x_i)}\Phi_{i+1} + \frac{(x_{i+1}-x)}{(x_{i+1}-x_i)}\Phi_i \tag{5-53}$$

$$P_2(x) = \frac{(x-x_i)(x-x_{i-1})}{(x_{i+1}-x_i)(x_{i+1}-x_{i-1})}\Phi_{i+1} + \frac{(x-x_{i+1})(x-x_{i-1})}{(x_i-x_{i+1})(x_i-x_{i-1})}\Phi_i$$
$$+ \frac{(x-x_{i+1})(x-x_i)}{(x_{i-1}-x_{i+1})(x_{x-1}-x_i)}\Phi_{i-1} \tag{5-54}$$

Taking the first derivative of $P_1(x)$ and the second derivative of $P_2(x)$ and substituting into Equation 118, it is then possible to group terms and obtain the advective multipliers. For example, the T_{i+1} multiplier is:

$$T_{i+1} = \frac{(x-x_i)}{(x_{i+1}-x_i)} - \frac{U\Delta t}{2}\frac{[(x-x_i)+(x-x_{i-1})]}{(x_{i+1}-x_i)(x_{i+1}-x_{i-1})}$$
$$+ \frac{2\left(D_x\Delta t - \frac{1}{6}[\Delta x_i^2 - (U\Delta t)^2]\right)}{(x_{i+1}-x_i)(x_{i+1}-x_{i-1})} \tag{5-55}$$

Similar functions are obtained for T_i and T_{i-1} multipliers that complete the formulation for the QUICKEST algorithm.

From a computational standpoint, most geometric components of the multipliers are time-invariant and are computed once and stored in arrays. The time-varying part of the multipliers (U, Δt, D_x) are updated each timestep during computation of the T arrays. However, when the QUICKEST scheme is applied vertically, the spatial part of the multipliers for layers [KT] and [KT]+1 are updated each timestep to accommodate the surface elevation fluctuation.

ULTIMATE/QUICKEST Numerical Transport Solution Scheme

In Version 2, the QUICKEST numerical scheme replaced the upwind numerical scheme used in Version 1 for solving the advective terms in the advection-diffusion equation. Compared to the upwind scheme,

QUICKEST resulted in improved numerical accuracy in simulating sharp fronts since the upwind transport scheme adds excessive numerical diffusion.

A problem with the QUICKEST scheme is that it can give rise to spurious oscillations at the leading and trailing edge of a sharp front or gradient. This can occur where there are fresh/salt water interfaces, point source discharges, or cases of strong temperature stratification. Even though the upwind scheme always gives physically realistic solutions, it introduces numerical diffusion that artificially reduces sharp gradients.

An improvement was introduced by Leonard (1991) that eliminated spurious oscillations but preserved the higher-order solution scheme of QUICKEST. This technique is a universal (in the sense that it can be applied to numerical schemes other than QUICKEST) limiter for maintaining monotonic profiles near a gradient and is called the ULTIMATE solution scheme.

In order to illustrate the scheme, consider the solution of the unsteady advective equation:

$$\frac{\partial B\Phi}{\partial t} + \frac{\partial BU\Phi}{\partial x} = 0 \qquad \textbf{(5-56)}$$

where:
Φ = concentration, $g\ m^{-3}$
B = width, m
U = velocity, $m\ s^{-1}$
x = longitudinal coordinate, m
t = time, s

The finite difference scheme for this based on a positive flow ($U > 0$) is:

$$\Phi_i^{n+1} = \frac{1}{B_i^{n+1}}\left(B_i^n\Phi_i^n - \left\{\left[\frac{UB\Delta t}{\Delta x}\right]_R\Phi_R - \left[\frac{UB\Delta t}{\Delta x}\right]_L\Phi_L\right\}\right) \qquad \textbf{(5-57)}$$

The value i refers to the center grid point, R is the right-hand face value, and L is the left hand face value (**Figure 130**).
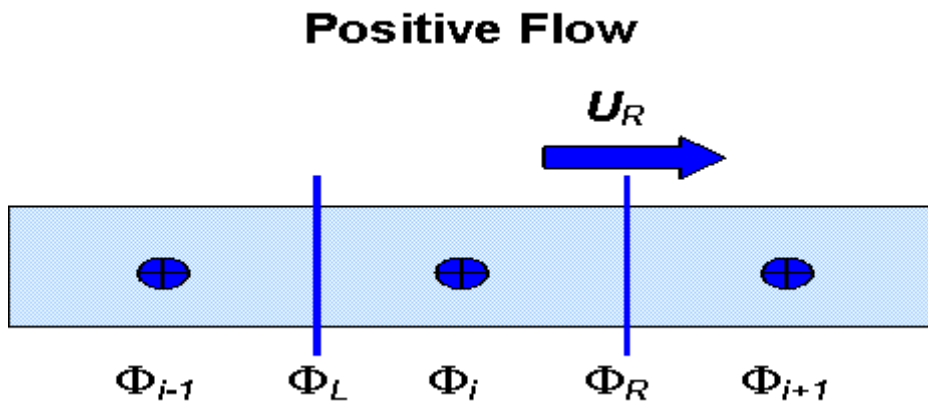
Figure 130. ULTIMATE schematization for positive flow.

Numerical Solution

Where (in **Figure 130**):

Φ_{i-1} = upstream concentration, $g\ m^{-3}$

Φ_i = center concentration, $g\ m^{-3}$

Φ_{i+1} = downstream concentration, $g\ m^{-3}$

Φ_L = left face concentration, $g\ m^{-3}$

Φ_R = right face concentration, $g\ m^{-3}$

U_r = right face horizontal velocity, $m\ s^{-1}$

Figure 131 shows a sketch of variables used for a negative flow. The term $U\Delta t/\Delta x$ is called the Courant number. The problem to resolve is how to choose the concentrations at the "face" values since concentrations are defined at the center of a cell. An upwinding scheme would say that the concentration at the left face is Φ_{i-1} and the concentration at the right face is Φ_i for positive flow. In order to improve numerical accuracy, there are other higher-order numerical techniques, such as QUICKEST (Leonard, 1979), to estimate these face values. In CE-QUAL-W2, Φ_R and Φ_L are initially computed based on the QUICKEST method. However, if the criteria for a monotonic solution are violated, the values for Φ_R and Φ_L are revised to assure a monotonic solution. This is the essence of the ULTIMATE algorithm that eliminates over/undershoots in the numerical transport scheme.
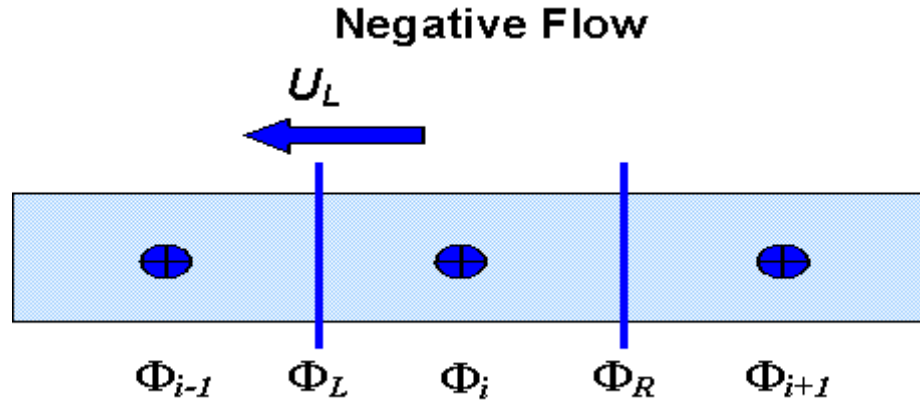
Figure 131. ULTIMATE schematization for negative flow.

Where (in **Figure 131**):

Φ_{i-1} = downstream concentration, $g\ m^{-3}$

Φ_i = center concentration, $g\ m^{-3}$

Φ_{i+1} = upstream concentration, $g\ m^{-3}$

Φ_L = left face concentration, $g\ m^{-3}$

Φ_R = right face concentration, $g\ m^{-3}$

U_L = left face horizontal velocity, $m\ s^{-1}$

To outline the procedure for simple conditions, the velocity, segment spacing and segment widths are assumed constant, so that Equation 123 can be written as:

$$\Phi_i^{n+1} = \left(\Phi_i^n - \left\{ \left[\frac{U\Delta t}{\Delta x} \right]\ \Phi_R - \left[\frac{U\Delta t}{\Delta x} \right]\ \Phi_L \right\} \right) \tag{5-58}$$

Defining normalized variables based on:

$$\widetilde{\Phi} = \frac{\Phi - \Phi_{i-1}^n}{\Phi_{i+1}^n - \Phi_{i-1}^n},$$ (5-59)

for location i (the center location) and the right face value for positive flow as in **Figure 130**, we have the following:

$$\widetilde{\Phi}_i^n = \frac{\Phi_i^n - \Phi_{i-1}^n}{\Phi_{i+1}^n - \Phi_{i-1}^n}$$ (5-60)

$$\widetilde{\Phi}_R = \frac{\Phi_R - \Phi_{i-1}^n}{\Phi_{i+1}^n - \Phi_{i-1}^n}$$ (5-61)

If $\widetilde{\Phi}_R \leq \dfrac{\widetilde{\Phi}_i^n}{\left[U\Delta t / \Delta x \right]_R}$ for $0 < \widetilde{\Phi}_i^n \leq 1$ (5-62)

$$\widetilde{\Phi}_i^n \leq \widetilde{\Phi}_R \leq 1 \text{ for } 0 < \widetilde{\Phi}_i^n \leq 1$$ (5-63)

$$\widetilde{\Phi}_i^n = \widetilde{\Phi}_R \text{ for } \widetilde{\Phi}_i^n < 0 \text{ or } \widetilde{\Phi}_i^n > 1$$ (5-64)

The face value is unadjusted from that computed by the numerical scheme and the QUICKEST value of Φ_R is used without alteration. These conditions are shown as the shaded region in **Figure 132**.

If these conditions are not met, then Φ_R is adjusted to force a monotonic solution. The value of the face is replaced with the nearest allowable value of $\widetilde{\Phi}_R$ based on the above criteria that will ensure these criteria are met. The face value is determined by using:

$$\Phi_R = \Phi_{i-1}^n + \widetilde{\Phi}_R(\Phi_{i+1}^n - \Phi_{i-1}^n)$$ (5-65)

Numerical Solution

This procedure is applied to all the faces and then Equation 124 is solved to update the concentration at the next time level. This means that the right face concentration will be the left face concentration for the next segment thus ensuring mass conservation.
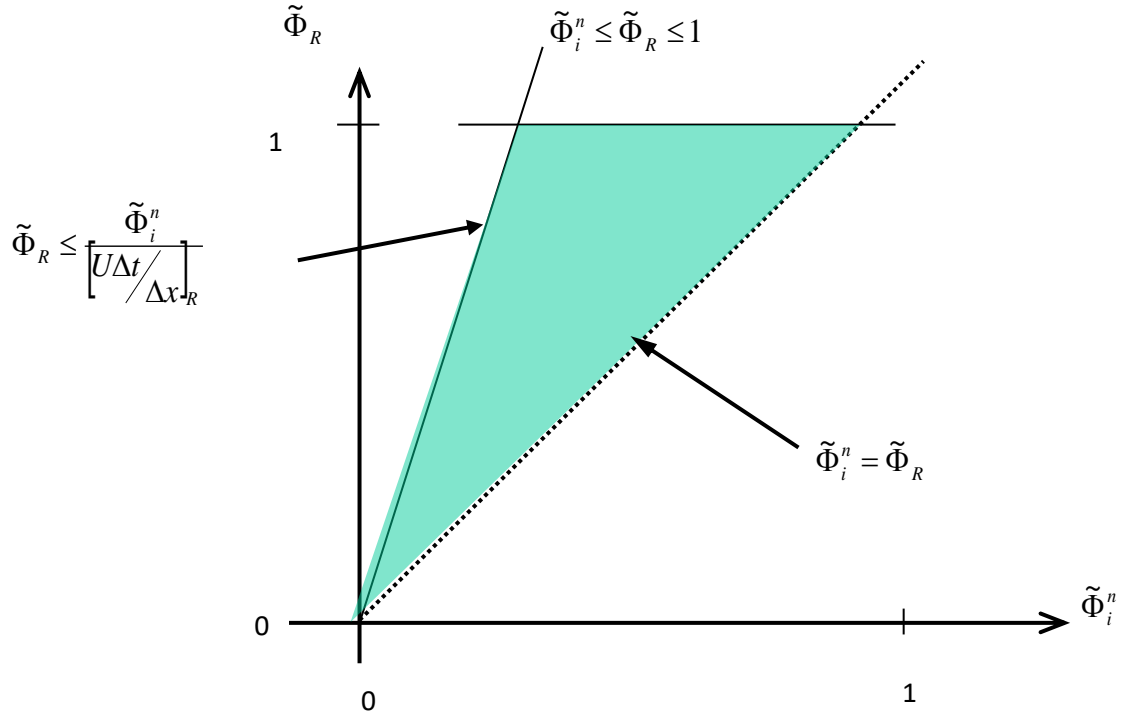
Figure 132. Definition sketch for monotonic solution domain.

According to tests performed by Lin and Falconer (1997), the QUICKEST-ULTIMATE scheme with splitting of the diffusion and source/sink terms conserved mass and eliminated numerical oscillations. Leonard (1991) also indicated that the QUICKEST scheme coupled with the ULTIMATE scheme was numerically accurate and cost-effective in terms of computational time.

Figure 133 shows the results of a square pulse of 100 $g\ m^{-3}$ moving downstream using the UPWIND, QUICKEST, and ULTIMATE/QUICKEST numerical transport schemes. The UPWIND scheme has a large amount of numerical diffusion whereas the QUICKEST scheme has non-physical oscillations about the leading and trailing edge of the solution. The ULTIMATE/QUICKEST numerical solution greatly reduces numerical diffusion and eliminates the over and undershoots.

For any case of unequal grid spacing, the order of accuracy diminishes. Leonard (1991) recommends that if used with non-uniform grid spacing, the formal accuracy of the method is only preserved if the grid does not expand or contract more than about 125%.

Even though the ULTIMATE scheme can be used with any suitable numerical technique, Leonard (1991) indicates that when coupled with the 3rd order QUICKEST scheme and a 2nd order central difference diffusion operator, the results are virtually indistinguishable from other higher-order advection solvers.
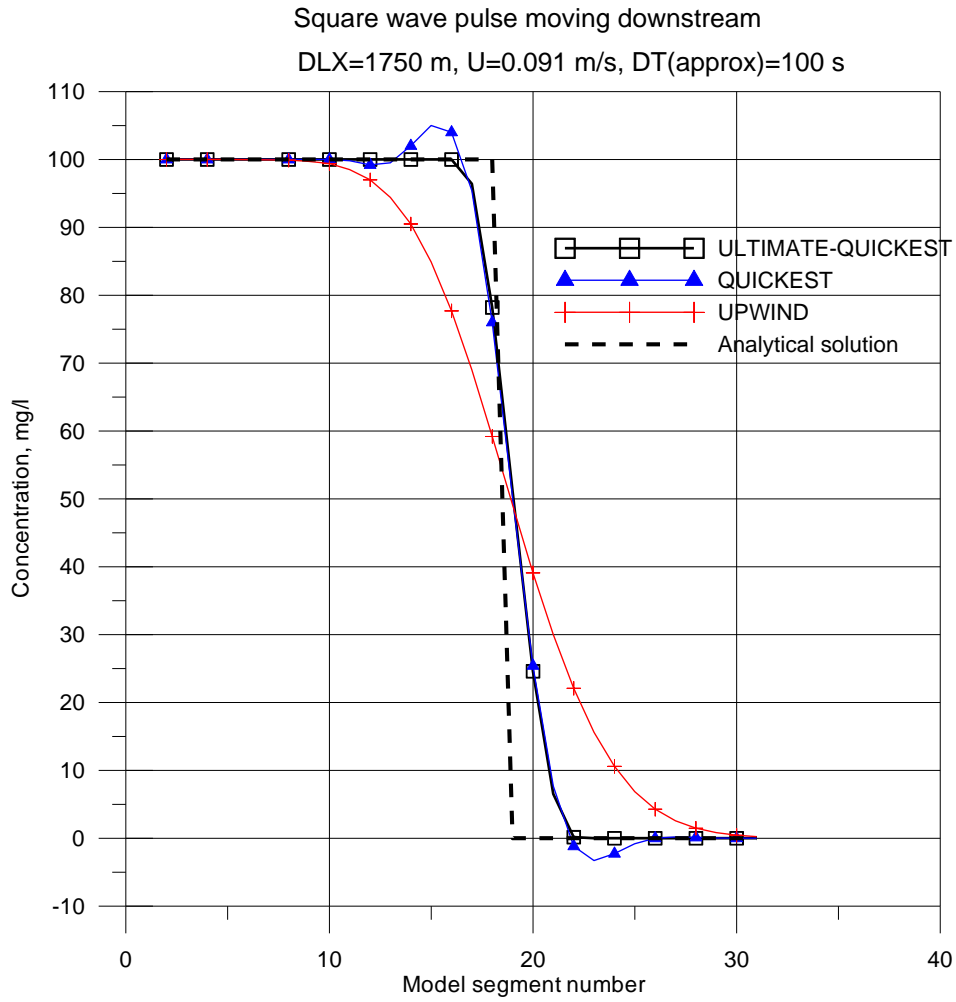
Figure 133. Comparison of UPWIND, QUICKEST, and ULTIMATE/QUICKEST schemes for conservative tracer transport.

The following shows a straightforward procedure by Leonard to compute the right and left face values if they do not meet the monotonic criteria, as well as a procedure for variable velocities.

Based on the sign of the velocity for each face, compute DEL:

$$DEL = \Phi_{i+1}^n - \Phi_{i-1}^n \qquad \textbf{(5-66)}$$

If $|DEL| < 10^{-5}$ set $\Phi_{face} = \Phi_i^n$ and proceed to the next face (the face value is the L or R face). Otherwise, compute:

$$\widetilde{\Phi}_i^n = \frac{\Phi_i^n - \Phi_{i-1}^n}{\Phi_{i+1}^n - \Phi_i^n} = \frac{\Phi_i^n - \Phi_{i-1}^n}{DEL} \qquad \textbf{(5-67)}$$

If $\widetilde{\Phi}_i^n < 0$ or $\widetilde{\Phi}_i^n > 1$, set $\Phi_{face} = \Phi_i^n$ and proceed to the next face. If not, compute:

$$\widetilde{\Phi}_{face} = \frac{\Phi_{face} - \Phi_{i-1}^n}{\Phi_{i+1}^n - \Phi_{i-1}^n} = \frac{\Phi_{face} - \Phi_{i-1}^n}{DEL} \qquad \textbf{(5-68)}$$

Numerical Solution

where Φ_{face} is computed based on the user's chosen numerical scheme (such as QUICKEST or another scheme).

1. If $\widetilde{\Phi}_{face} < \widetilde{\Phi}_i^n$, $\widetilde{\Phi}_{face} = \widetilde{\Phi}_i^n$
2. if $\widetilde{\Phi}_{face} > \dfrac{\widetilde{\Phi}_i^n}{\left(\frac{U\Delta t}{\Delta x}\right)}$, $\widetilde{\Phi}_{face} = \dfrac{\widetilde{\Phi}_i^n}{\left(\frac{U\Delta t}{\Delta x}\right)}$
3. if $\widetilde{\Phi}_{face} > 1$, $\widetilde{\Phi}_{face} = 1$

Then recompute the face value according to $\Phi_{face} = \widetilde{\Phi}_{face} DEL + \Phi_i^n$.

Once all the face values are determined, use the finite difference form of the solution to determine the solution (Equation 123). Leonard (1991) also showed a numerical technique that minimized the computational burden when using ULTIMATE with the QUICKEST scheme. This technique is described as follows.

Based on the sign of the velocity for each face, define C, D, and U nodes (center, downstream, and upstream) corresponding for positive flow to i, i+1, and i-1, respectively.

Compute DEL and CURV, where $DEL = \Phi_{i+1}^n - \Phi_i^n$ and $CURV = \Phi_{i+1}^n - 2\Phi_i^n + \Phi_{i-1}^n$

1. If $|CURV| \le 0.6|DEL|$, then use the QUICKEST computed value for the face value, Φ_{face} (the face value is the R or L face as shown in Figure 134).
2. If not, and if $|CURV| \ge |DEL|$, then set $\Phi_{face} = \Phi_i^n$
3. If not, and DEL>0, limit Φ_{face} by Φ_i^n below, or the smaller of

$\Phi_{reference} = \Phi_{i-1}^n + \dfrac{(\Phi_i^n - \Phi_{i-1}^n)}{\left(\frac{U\Delta t}{\Delta x}\right)}$ and Φ_{i+1}^n

4. If not, and DEL<0, limit Φ_{face} by Φ_i^n, or the larger of $\Phi_{reference} = \Phi_{i-1}^n + \dfrac{(\Phi_i^n - \Phi_{i-1}^n)}{\left(\frac{U\Delta t}{\Delta x}\right)}$ and

Φ_{i+1}^n

5. Once all the face values are determined, use Equation 123 to obtain the solution.

The procedure outlined above is based on unidirectional and uniform magnitude velocity and segment widths. If the velocity regime and widths are variable, then the following procedure is followed in order to maintain a monotonic solution. Consider the following limitations based on definitions shown in **Figure 134**.
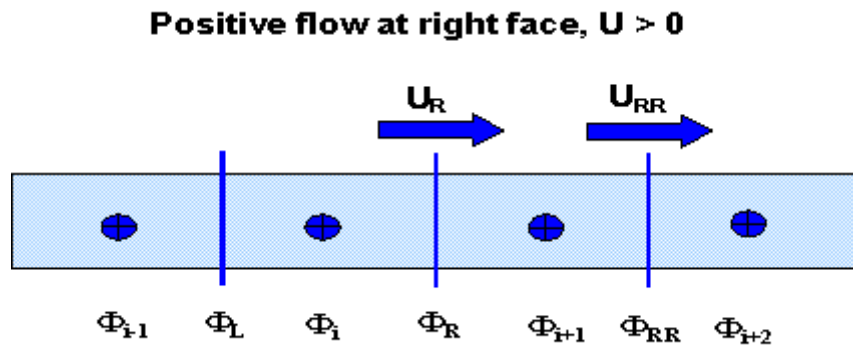

Figure 134. Definition sketch for variable velocity.

Where (in **Figure 134**):

Φ_{i-1} = upstream concentration
Φ_i = center concentration
Φ_{i+1} = center concentration
Φ_L = left face concentration at i
Φ_R = right face concentration at i
Φ_{RR} = right face concentration at I+1

Assuming that U_R is positive and the concentration times width (ΦB) increases monotonically, i.e., $(B\Phi)_{i-1}^n < (B\Phi)_i^n < (B\Phi)_{i+1}^n < (B\Phi)_{i+2}^n$, between segment i-1 and i+2, then the goal of the technique is to estimate Φ_R, or really $B_R\Phi_R$, and to update the concentration using Equation 123. Equation 123 can be written as a condition for Φ_R as:

$$\left[\frac{UB\Delta t}{\Delta x}\right]_R \Phi_R = B_i^n \Phi_i^n - \Phi_i^{n+1} B_i^{n+1} + \left[\frac{UB\Delta t}{\Delta x}\right]_L \Phi_L \tag{5-69}$$

If it is assumed that $B_i^n \Phi_i^n \leq B_R \Phi_R \leq B_{i+1}^n \Phi_{i+1}^n$, then this is equivalent to saying that $B_i^n U_i^n \Phi_i^n \leq B_R^n U_R^n \Phi_R \leq B_{i+1}^n U_{i+1}^n \Phi_{i+1}^n$ or that the net flux into a segment is increasing.

Using the monotonic limitation that $B_i^{n+1}\Phi_i^{n+1} \geq B_{i-1}^n \Phi_{i-1}^n$ then Equation 135 becomes:

$$\left[\frac{UB\Delta t}{\Delta x}\right]_R \Phi_R \leq B_i^n \Phi_i^n - \Phi_{i-1}^n B_{i-1}^n + \left[\frac{UB\Delta t}{\Delta x}\right]_L \Phi_L \tag{5-70}$$

Then making a conservative assumption that $B_L\Phi_L \geq B_{i-1}^n \Phi_{i-1}^n$, Equation 136 becomes:

$$\left[\frac{UB\Delta t}{\Delta x}\right]_R \Phi_R \leq B_i^n \Phi_i^n - \Phi_{i-1}^n B_{i-1}^n + \left[\frac{UB\Delta t}{\Delta x}\right]_{i-1}^n \Phi_{i-1}^n \tag{5-71}$$

Another condition is also imposed on $B_R\Phi_R$ by looking at the control volume segment centered at i+1. Using similar reasoning as above and assuming that $U_{RR} > 0$, the other criterion for $B_R\Phi_R$ is

$$\left[\frac{UB\Delta t}{\Delta x}\right]_R \Phi_R \leq B_{i+2}^n \Phi_{i+2}^n - \Phi_{i+1}^n B_{i+1}^n + \left[\frac{UB\Delta t}{\Delta x}\right]_{RR} \Phi_{i+1}^n \tag{5-72}$$

These criteria would be altered appropriately if the function were monotonically decreasing rather than increasing.

Vertical Implicit Transport

Focusing on vertical advective and diffusive transport, constituent transport can be written as:

$$\frac{\partial B\Phi}{\partial t} + \frac{\partial WB\Phi}{\partial z} - \frac{\partial}{\partial z}\left(BD_z \frac{\partial \Phi}{\partial z}\right) = RHS \tag{5-73}$$

where RHS represents horizontal transport and all sources/sinks. Integrating the transport equation vertically and over time gives:

$$BH\Phi^{n+1} + \theta H\Delta t \delta_z(WB\Phi^{n+1}) - H\Delta t \delta_z\left(BD_z \frac{\partial \Phi^{n+1}}{\partial z}\right) = BH\Phi^* \tag{5-74}$$

where:
Φ^* = all n-time level horizontal and explicit vertical transport and sources/sinks

θ = time-weighting for vertical advection; 0 for fully explicit, 0.55 for Crank-Nicholson, and 1 for fully implicit

Expanding the differential operators in terms of central differences and collecting terms, the above equation can be recast as:

$$A_{t_i} \Phi_{i-1}^{n+1} + V_{t_i} \Phi_i^{n+1} + C_{t_i} \Phi_{i+1}^{n+1} = D_{t_i} \qquad \text{(5-75)}$$

where:

$$V_{t_i} = 1 + \frac{\Delta t}{BH_{k,i}} \left[\theta \left(\frac{W_{k,i} B_{b_{k,i}} - W_{k-1,i} B_{b_{k-1,i}}}{2} \right) + \frac{B_{b_{k,i}} D_{z_{k,i}}}{\bar{H}_k} + \frac{B_{b_{k-1}} D_{z_{k-1,i}}}{\bar{H}_{k-1}} \right]$$

$$A_{t_i} = \frac{\Delta t B_{b_{k,i}}}{BH_{k,i}} \left(\theta \frac{W_{k,i}}{2} - \frac{D_{z_{k,i}}}{\bar{H}_k} \right)$$

$$C_{t_i} = -\frac{\Delta t B_{b_{k-1,i}}}{BH_{k,i}} \left(\theta \frac{W_{k-1,i}}{2} + \frac{D_{z_{k-1,i}}}{\bar{H}_{k-1}} \right)$$

The coefficients are computed once, stored in arrays, and used to update each constituent. This is accomplished by loading the explicit part of the solution, Φ*, with each successive constituent and inverting the resulting matrix via a Thomas tridiagonal solver.

6.   References

Abbot, M. B. 1982. "A model system for design and operation of storm-sewer networks," *Engineering application of computational hydraulics*, M. B. Abbot and J. A. Cunge, eds., Vol. 1, Homage to Alexandra Preissmann, Pitman Advanced Publishing Program, Boston, 11-36.

Adams, E. E., Harleman, D.R.F., Jirka, G., and Stolzenback, K. D. 1981. "Heat Disposal in the Water Environment", Ralph M. Parsons Laboratory for Water Resources and Hydrodynamics, Department of Civil Engineering, MIT, Cambridge, MA.

Ambrose, R. B.; Wool, T.; Connolly, J. P.; and Schanz, R. W. 1988. "WASP4, A Hydrodynamic and Water Quality Model: Model Theory, User's Manual, and Programmer's Guide," Environmental Research Laboratory, Environmental Protection Agency, EPA 600/3-87/039, Athens, Ga.

Anderson, D. A., Tannehill, J. C., Pletcher, R. H. 1984. Computational Fluid Mechanics and Heat Transfer, Hemisphere, New York.

Annear, R. and Wells, S. A. 2007. A comparison of five models for estimating clear-sky solar radiation, *Water Resources Research*, 43, W10415, doi:10.1029/2006WR005055.

APHA 1985. *Standard Methods for the Examination of Water and Wastewater*, APHA, Washington, DC.

Ashton, G.D. 1979. "Suppression of River Ice by Thermal Effluents", *CRREL Rpt. 79-30*, US Army Engineer Cold Regions Research and Engineering Laboratory, Hanover, NH.

Banks, R.B. 1975. "Some Features of Wind Action on Shallow Lakes," *ASCE, J. Env. Engr. Div.*, 101(EE3), pp. 489-504.

Banks, R. B. and Herrera, F. F. 1977. Effect of Wind and Rain on Surface Reaeration. *J. Envir. Engr. Div. ASCE*, 101(EE5):813-827.

Barkau, R. 1997. "UNET One-Dimensional Unsteady Flow Through a Full Network of Open Channels, User's Manual, US Army Corps of Engineers, Hydrologic Engineering Center, Davis, Ca.

Barrett, M.J.; Gameson, A.L.; and Ogden, C.G. 1960. Aeration Studies of Four Weir Systems, *Water and Water Engineering*, London.

Batchelor, G. K. 1967. *An Introduction to Fluid Dynamics*, Cambridge University Press, NY.

Belov, A. P., and Giles, J. D. 1997. "Dynamical model of buoyant cyanobacteria." Hydrobiologia, (349), 11.

Berger, C. J. 2000. "Modeling Macrophytes of the Columbia Slough," Ph.D. Dissertation, Environmental Sciences and Resources, Portland State University, Portland, OR.

References

Berger, C. J. and Wells, S. A. 1999. "Hydraulic and Water Quality Modeling of the Columbia Slough, Volume 1: Model Description, Geometry, and Forcing Data", Technical Report EWR-2-99, Department of Civil Engineering, Portland State University, 109 pp.

Berger, C. and Wells, S. A. 2008. "A Macrophyte Water Quality and Hydrodynamic Model," ASCE, Journal of Environmental Engineering, Volume 134, Issue 9, pp. 778-788.

Berger, C. and Wells, S. A. 2014. "Updating the CEMA Oil Sands Pit Lake Model," Report to Cumulative Environmental Management Association, Alberta, Canada, August 2014.

Brady, D.K., Graves, W.L., and Geyer, J.C. 1969. "Surface Heat Exchange at Power Plant Cooling Lakes", *Cooling Water 2, Discharge Project No. 5, Publication No. 69-901,* Edison Electric Institute, New York, NY.

Broecker, H. C., Petermann, J., and Siems, W. 1978. The Influence of Wind on CO2 Exchange in a Wind-Wave Tunnel, *J. Marine Res.*, 36(4):595-610.

Brookes, J. D., and Ganf, G. G. 2001. "Variations in the buoyancy response of Microcystis aeruginosa to nitrogen, phosphorus and light." Journal of Plankton Research, 23(12), 1399–1411.

Brooks, N. H. and Koh, R. C. 1969. Selective withdrawal from density-stratified reservoirs. J. Hydraul. Div. A.S.C.E. 95 (HY4), 1369–1397.

Butts, T.A. and Evans, R.L. 1983. "Small Stream Channel Dam Aeration Characteristics," ASCE J. Env. Engr., Vol 109, No 3, pp. 555-573, June 1983.

Cao, Z., Pender, G., and Meng, J. 2006. Explicit Formulation of the Shields Diagram for Incipient Motion of Sediment, ASCE, *Journal of Hydraulic Engineering*, October, 1097-1099, 10.1061/(ASCE)07339429(2006)132:10(1097).

Carr, G. M., H. C. Duthie and W. D. Taylor (1997). "Models of aquatic plant productivity: a review of the factors that influence growth," *Aquatic Botany*, 59, 195-215.

Celik I., Rodi W. 1984. "Simulation of Free-Surface Effects in Turbulent Channel Flow", PhysicoChemical Hydrodynamics, Vol. 5, No 3 / 4, 1984, pp 217-227.

Celik I., Rodi W. 1988. "Modeling Suspended Sediment Transport in Nonequilibrium Situations", Journal of Hydraulic Engineering, Vol. 114, No. 10, October, 1988, pp 1157-1191.

Cervarich, A., Overman, C., Wells, S. A., Berger, C. 2020. Dexter Reservoir Model Calibration Updates and Management Scenarios. Prepared for ERDC Contracting Office U.S. Army Corps of Engineers Engineer Research and Development Center, Water Quality Research Group, Department of Civil and Environmental Engineering, Portland State University, 109 pp.

Chapman, R.S. and T.M. Cole. 1992. "Improved Thermal Predictions in CE-QUAL-W2", in *Hydraulic Engineering Saving a Threatened Resource - In Search of Solutions Proceedings of the Hydraulic Engineering sessions at Water Forum '92*, M. Jennings and N. G. Bhowmik, eds., August 2-6, 1992, Baltimore, MD. American Society of Civil Engineers. New York, NY.

References

Chapman, R. S., Gerald, T. K., and Dortch, M. S. 1994. "New York Bight Study. Report 3, Three-Dimensional Particle Tracking Model for Floatables and Dissolved and Suspended Materials." Technical Report CERC-94-4, U.S. Army Engineer Waterways Experiment Station, Vicksburg, MS.

Chapra, S. 1997. *Surface Water Quality Modeling*, McGraw-Hill, NY.

Chapra, S. C. 2008. Surface water quality modeling. Waveland Press.

Chapra, S.C., and Reckhow, K.W. 1983. *Engineering Approaches for Lake Management, Vol 12: Mechanistic Modeling*, Butterworth Publishers, Boston, MA.

Chu, C. and Jirka, G. (2003) "Wind and Stream Flow Induced Reaeration," Journal of Environmental Engineering, ASCE, Vol 129, No 12, 1129-1136.

Churchill, M.A., Elmore, H. L., and Buckingham, R.A. 1962. "Prediction of Stream Reaeration Rates," *J. San. Engr. Div., ASCE*, SA4:1, Proc. Paper 3199.

Clay, C.H. 1995. *Design of Fishway and Other Fish Facilities*, Lewis Publishers, Ann Arbor.

Cole, T. and Buchak, E. 1995. CE-QUAL-W2: A Two-Dimensional, Laterally Averaged, Hydrodynamic and Water Quality Model, Version 2.0, Technical Report El-95-1, U.S. Army Engineer Waterways Experiment Station, Vicksburg, MS.

Columbia Basin Research. 2000. "Columbia River Salmon Passage Model, CRISP 1.6, Theory and Calibration", Technical Report, School of Aquatic and Fisheries Sciences, University of Washington, 238 pp.

Cotton, M., Reedha, D., Stansby, P. 2005. "Low-Reynolds Number two-equation turbulence modeling for open channel flow: development and evaluation of free surface boundary conditions on the dissipation rate equation", Journal of Hydraulic Research, Vol 43, No 6, pp. 632-643.

Covar, A. P. 1976. "Selecting the Proper Reaeration Coefficient for Use in Water Quality Models," presented at the US EPA Conference on Environmental Simulation and Modeling, April 19-22, Cincinnati, OH.

Cui, Y. J., Liu, D. F., Zhang, J., Yang, Z. J., Khu, S. T., Ji, D. B., Song, L. X., and Long, L. H. 2016. "Diel migration of Microcystis during an algal bloom event in the Three Gorges Reservoir, China." Environmental Earth Sciences, 75(7).

Cushman-Roisin, B. 1994. *Introduction to Geophysical Fluid Dynamics*, Prentice-Hall, Englewood Cliffs, NJ.

Davis, J.E., Holland, J.P., Schneider, M.L., and Wilhelms, S.C. 1987. "SELECT: A Numerical, One-Dimensional Model for Selective Withdrawal," Instruction Report E-87-2, Corps of Engineers, Waterways Experiment Station, Hydraulics Laboratory, Vicksburg, MS.

DiLaura, D.L. 1984. "IES Calculation Procedures Committee Recommended practice for the calculation of daylight availability." *Journal of the Illuminating Engineering Society of North America*, 13 (4) p. 381-392.

DiToro, D.M. 2001. *Sediment Flux Modeling*. Wiley-Interscience. New York. 656pp.

Downing, A.L., and G.A. Truesdale. 1955. Some factors affecting the rates of solution of oxygen in water. *J. Applied Chemistry*, Vol. 5, pp.570-581.

References

Dunsbergen, D. W. and Stalling, G. S. 1993. The combination of a random walk method and a hydrodynamic model for the simulation of dispersion of dissolved matter in water, *Transactions on Ecology and the Environment* Vol 2, WIT Press, ISSN 1743-3541.

Edinger, J.E., Brady, D.K., and Geyer, J.C. 1974. "Heat Exchange and Transport in the Environment", *Rpt. No. 14, EPRI Publication No. 74-049-00-34*, prepared for Electric Power Research Institute, Cooling Water Discharge Research Project RP-49), Palo Alto, CA.

Edinger, J. E. 2002. *Waterbody Hydrodynamic and Water Quality Modeling*, ASCE Press, Reston, Virginia.

Edmund, J. M. and Gieskes, J. A. T. M. 1970, "On the Calculation of the Degree of Saturation of Sea Water with Respect to Calcium Carbonate Under In Situ Conditions," Geochim. Cosmochim. Acta 34:1261-1291.

Elliot, W. P. 1958. "The growth of the atmospheric internal boundary layer", EOS, *Transactions of the American Geophysical Union*, Vol 39, Issue 6, 1048-1054.

Engelund, F. 1978. Effect of Lateral Wind on Uniform Channel Flow. *Progress Report 45*, Inst. of Hydrodynamic and Hydraulic Engr., Tech. Univ. of Denmark.

Environmental Laboratory. 1985. "CE-QUAL-R1: A Numerical One-Dimensional Model of Reservoir Water Quality; User's Manual", *Instruction Rpt. E-82-1*, US Army Corps of Engineers, Waterways Experiment Station, Vicksburg, MS.

Environmental Laboratory. 1995. "CE-QUAL-RIV1: A Dynamic, One-Dimensional Longitudinal. Water Quality Model for Streams: User's Manual," *Instruction Report EL-95-2*, USACE Waterways Experiments Station, Vicksburg, MS.

EPA. 1971. "Effect of Geographical Location on Cooling Pond Requirements and Performance," in Water Pollution Control Research Series, Report No. 16130 FDQ, Environmental Protection Agency, Water Quality Office, Washington, District of Columbia, 160 pp.

EPA 1985. Rates, Constants and Kinetics in Surface Water Quality Modeling, Environmental Research Laboratory, EPA/600/3-85/040, Athens, Ga.

ERM and Golder. 2011. CEMA Oil Sands Pit Lake Model. Technical Report 09-1336-1008, submitted to CEMA, Canada, May 2011, 86 pp.

Fang, X. and Stefan, H. G. 1994. "Modeling Dissolved Oxygen Stratification Dynamics in Minnesota Lakes under Different Climate Scenarios," *Project Report 339*, St. Anthony Falls Hydraulic Laboratory, University of Minnesota, Minneapolis. [update]

Ferziger J., Peric, M. 2002. Computational Methods for Fluid Dynamics, Springer Verlag.

French, R. H. 1985. *Open-Channel Hydraulics*, McGraw-Hill, New York.

Ford, D.E., and Johnson, M.C. 1983. "An Assessment of Reservoir Density Currents and Inflow Processes", *Technical Rpt. E-83-7*, US Army Engineer Waterways Experiment Station, Vicksburg, MS.

Ford, D. E. and Stefan, H. G. 1980. "Thermal predictions using integral energy model", *J. Hydraul. Div.*, Am. Soc. Civ. Eng. 106: 39–55.

References

Gameson, A.L.H. and Gould, D.J., 1975. In Proc. Int. Symp. On Discharge of Sewage from Sea Outfalls, Pergamon Press, London.

Garstecki, B. 2021. Modeling Cyanobacteria Production, Fate and Transport in Surface Waterbodies, M. S. thesis, Department of Civil and Environmental Engineering, Portland State University, 175 pp.

Gelda, R. K., Auer, M. T., Effler, S. W., Chapra, S. C., and Storey, M. L. 1996. "Determination of Reaeration Coefficients: A Whole Lake Approach", *ASCE J. Envir. Engr.*, Vol 122, Issue 4, 269.

Gill, A.E. 1982. "Appendix 3, Properties of Seawater", *Atmosphere-Ocean Dynamics*, Academic Press, New York, NY, pp 599-600.

Giese, A.C. 1968. *Cell Physiology*, 3d ed., W.B. Saunders Co., Philadelphia, PA.

Gould, S. 2006. "k-ε Turbulence Model in CE-QUAL-W2", Research Project Report, Department of Civil and Environmental Engineering, Portland State University, Portland, OR, 53 pp.

==Hamblin and Salmon (1975), "the vertical diffusion of momentum is probably the most important internal parameter" f==

Hargrave, B.T. 1972. "Oxidation-Reduction Potentials, Oxygen Concentration and Oxygen Uptake of Profundal Sediments in a Eutrophic Lake", *Oikos*, Vol 23, pp 167-177.

Hathhorn, W. E. 1997. "Simplified Approach to Particle Tracking Methods for Contaminant Transport", ASCE, J. Hydraul. Eng., 123(12):1157-1160.

HEC 1997a. "UNET One-Dimensional Unsteady-Flow Through a Full Network of Open Channels, User's Manual," US Army Corps of Engineers, Hydrologic Engineering Center, Davis, CA.

HEC 1997b. "HEC-RAS River Analysis System Hydraulic Reference Manual Version 2.0," US Army Corps of Engineers, Hydrologic Engineering Center, Davis, CA.

Henderson, H. 1966. *Open Channel Flow*, The MacMillan Company, NY.

Henrici, P. 1964. *Elements of Numerical Analysis*, John Wiley & Sons, Inc., New York.

Henry, Michelle. 2008. "Wind-Wave Effects and an Improved Fetch Algorithm For CE-QUAL-W2." Honors thesis submitted in partial fulfillment of the requirements for the degree of Bachelor's of Science, Civil Engineering, Portland State University, Portland, OR.

Hoerner, S. F. (1965). *Fluid-Dynamic Drag*. Hoerner Fluid Dynamics.

Hsi, G. and J. H. Nath (1968). "Wind drag within simulated forest canopy field." Technical Report prepared for U. S. Army Materials Command, Grant No. DA-AMC-28-043-65-G-20.

Ibelings, B. W., Mur, L. R., and Walsby, A. E. (1991). "Diurnal changes in buoyancy and vertical distribution in populations of Microcystis in two shallow lakes." Journal of Plankton Research, 13(2), 419–436.

Kang, S. W., Sheng, Y. P., and Lick, W. 1982. "Wave Action and Bottom Shear Stresses in Lake Erie", *Journal Great Lakes Research*, 8(3):482-494.

References

Kanwisher, J. 1963. "On the Exchange of Gases Between the Atmosphere and the Sea", *Deep Sea Research with Oceanography*, Vol 10, pp 195-207.

Kraus, E., 1972. *Atmosphere-Ocean interaction,* Oxford University Press, London, 275 pp, 275 pp.

Krishnappan, B., Lau, Y. 1986. "Turbulence Modeling of Flood Plain Flow", *Journal of Hydraulic Engineering*, Vol. 112, No. 4, April, pp 251-266.

Kromkamp, J. C., and Mur, L. R. (1984). "Buoyant density changes in the cyanobacterium Microcystis aeruginosa due to changes in the cellular carbohydrate content." FEMS Microbiology Letters, 25(1), 105–109.

Kromkamp, J., Konopka, A., and Mur, L. R. (1988). "Buoyancy regulation in light limited continuous cultures of Microcystis aeruginosa." Journal of Plankton Research, 10(2), 171–183.

Kromkamp, J., and Walsby, A. E. (1990). "A computer model of buoyancy and vertical migration in cyanobacteria." Journal of Plankton Research, 12(1), 161–183.

Lai (1986) correction to the x-momentum equation

Langbien, W. B. and Durum, W. H. 1967. "The Aeration Capacity of Streams," USGS, Washington, D.C. Circ. 542.

Leonard, B. P. 1979. "A Stable and Accurate Convective Modelling Procedure Based on Upstream Interpolation", *Computer Methods in Applied Mechanics and Engineering*, Vol 19, pp. 59-98.

Leonard, B. P. 1991. "The ULTIMATE conservative difference scheme applied to unsteady one-dimensional advection," *Computer Methods in Applied Mechanics and Engr*, 88, 1991), 17-74.

Limerinos, J.T. 1970. "Determination of the Manning coefficient from measured bed roughness in natural channels", U.S. Geological Survey Water-Supply Paper 1898-B, 47 pp.

Lin, B., and Falconer, R. A. 1997. "Tidal Flow and Transport Modeling Using ULTIMATE QUICKEST Scheme", *J. of Hydraulic Engineering*, *ASCE*, 123(4), 303-314.

Liss, P.S.   1973. "Processes of gas exchange across an air-water interface," Deep Sea Research, Vol. 20, pp 221-238.

Long, B. M., Jones, G. J., and Orr, P. T. (2001). "Cellular microcystin content in N-limited Microcystis aeruginosa can be predicted from growth rate." Applied and Environmental Microbiology, 67(1), 278–283.

Jarrett, R. D., 1984. "Hydraulics of high-gradient streams", American Society of Civil Engineers, *Journal of Hydraulic Engineering*, HY11, v. 110, p. 1519-1539.

Jarrett, R. D. 1985. "Determination of Roughness Coefficients for Streams in Colorado", USGS Water Resources Investigations Report 85-4004, Lakewood, CO, 60 pp.

Martin, J. L., and McCutcheon, S. C. 1999. Hydrodynamics and Transport for Water Quality Modeling, CRC Press, Lewis Publishers.

References

Mastropietro, M. A. 1968. "Effects of Dam Reaeration on Waste Assimilation Capacities of the Mohawk River," *Proceedings of the 23rd Industrial Waste Conference, Purdue University*.

Maykut, G. N. and N. Untersteiner. 1971. "Some results from a time dependent, thermodynamic model of sea ice", *J. Geophys. Res.*, 83: 1550-1575.

Melching, C. and Flores, H. 1999. "Reaeration Equations Derived from USGS Database," *J. Envir. Engr*., *ASCE*, 125(5), 407-414.

Mills, W.B.; Porcella, D.; Ungs, M; Gherini, S.; Summers, K.; Lingfung, M.; Rupp, G.; Bowie, G. Haith, D. 1985. "A Screening Procedure for Toxic and Conventional Pollutants in Surface and Ground Water," *EPA/600/6-85/002a*, Environmental Research Laboratory, Athens, GA.

Mitchell, R., and Chamberlain, C. 1978. "Factors affecting the survival of indicator organisms", *Indicators of Enteric Contamination in Natural Waters*, G. Berg (ed.), Ann Arbor Science Publ., Inc., Ann Arbor, MI, pp 15-38.

Moog, D.B. and Jirka, G.H. 1998. "Analysis of reaeration equations using multiplicative error," *J. Envin Engr, ASCE*, 124(2), 104-110.

Mortimer, C.H. 1981. "The Oxygen Content of Air Saturated Fresh Waters over Ranges of Temperature and Atmospheric Pressure of Limnological Interest", *International Vereinigung Theoretische and Angewandte Limnologie*, Vol 22, pp 2-23.

Munk, W.H., Anderson, E.R. 1948. "Notes on a theory of the thermocline", *J. Mar. Res*., 7, 276–295.

Nakagawa H., Nezu I., Ueda H. 1975. "Turbulence of Open Channel Flow Over Smooth and Rough Beds", Proceedings of the Japan Society of Civil Engineers, No 241 September, pp. 155-168.

Nakamura, T., Adachi, Y., and Suzuki, M. (1993). "Flotation and sedimentation of a single Microcystis floc collected from surface bloom." Water Research, 27(6), 979–983.

Nautical Almanac. 2001. *The Nautical Almanac 2001*. TheNatuticalAlmanac.com.

Nielson, P. 1992. Coastal bottom boundary layers and sediment transport, Volume 4, Advanced Series on Ocean Engineering, World Scientific Publishing Co. Ltd., River Edge, NJ.

NOAA/ESRL (Earth Systems Research Laboratories). 2020. Atmospheric Carbon Dioxide Dry Air Mole Fractions from quasi-continuous measurements at Mauna Loa, Hawaii, Barrow, Alaska, American Samoa and South Pole. Compiled by K.W. Thoning, A. Crotwell, and D.R. Kitzis. National Oceanic and Atmospheric Administration (NOAA), Earth System Research Laboratories (ESRL), Global Monitoring Laboratory (GML): Boulder, Colorado, USA. Version 2019-07 at https://doi.org/10.15138/yaf1-bk21

O'Connor, D. J. and Dobbins, W.E. 1958. "Mechanism of Reaeration in Natural Streams," *ASCE Trans*., 86(SA3):35-55.

O'Conno*r, D.J. 1983. "*Wind Effects on Gas-Liquid Transfer Coefficients*" J. Envir Engr ASCE*, Vol. 109, pp. 731-752.

References

Oregon Health Authority.2020a. Oregon Health Authority: Cyanobacteria Advisory Archive : Cyanobacteria Blooms : State of Oregon. Available at: https://www.oregon.gov/oha/ph/healthyenvironments/recreation/harmfulalgaeblooms/pages/archive.aspx (Accessed: 24 February 2020).

Oregon Health Authority.2020b. Oregon Health Authority: Recreational use advisory issued for Upper Klamath Lake July 19 : External Relations Division : State of Oregon. Available at: https://www.oregon.gov/oha/ERD/Pages/Recreational-use-advisory-issued-Upper-Klamath-Lake-July-19-2019.aspx (Accessed: 24 February 2020).

Overman, C. 2019. Modeling Vertical Migration of Cyanobacteria and Zooplankton. M.S. Thesis Department of Civil and Environmental Engineering, Portland State University, 233 pp.

Overman, C. and Wells, S. A. 2021. Modeling Cyanobacteria Vertical Migration, *J. Environmental Modeling*, in-print.

Owens, M., Edwards, R., and Gibbs, J. 1964. "Some Reaeration Studies in Streams," *Int. J. Air Water Pol*l., 8:469-486.

Patterson, J.C. and Hamblin, P.F., "Thermal Simulation of a Lake with Winter Ice Cover", *Limnology and Oceanography*, 33(3), 1988, P. 323-338.

Pauer, James J. and Martin T. Auer. 2000. "Nitrification in the water column and sediment of a hyper-eutrophic lake and adjoining river system," *Water Resources*, Volume 34, No. 4, pp. 1247-1254.

Petryk, S. (1969), "Drag on Cylinders in Open Channel Flow," PhD. Thesis, Colorado State University, Fort Collins, Colorado.

Petryk, S. and G. Bosmajian III. 1975. "Analysis of flow through vegetation," *Journal of the Hydraulics Division*, Proceedings of the ASCE, 101(HY7), 871-884.

Prakash, S., Vandenberg, J. A., E. M. Buchak. 2015. Sediment Diagenesis Module for CE-QUAL-W2. Part 2: Numerical Formulation. Environmental Modeling & Assessment. Print ISSN 1420-2026. Online ISSN 1573-2967. http://dx.doi.org/10.1007/s10666-015-9459-1. Springer International Publishing. April.

Press W., Teukolsky S., Vetterling W., Flannery B. 1996. Numerical Recipes in Fortran: The Art of Scientific Computing, Cambridge University Press.

Reynolds, C. S. 1984. The ecology of freshwater phytoplankton. Cambridge University Press, Cambridge.

Reynolds, C. S., Oliver, R. L., and Walsby, A. E. 1987. "Cyanobacterial dominance: The role of buoyancy regulation in dynamic lake environments." New Zealand Journal of Marine and Freshwater Research, 21(3), 379–390.

Rodi, W. 1993. *Turbulence Models and Their Application in Hydraulics, 3rd edition, IAHR*, A.A. Balkema, Rotterdam.

Roesner, L. A., J. A. Aldrich, and R. E. Dickinson. 1988. "Storm water management model user's manual version 4: EXTRAN addendum 1 EXTRAN," *Cooperative Agreement CR-811607*, U.S. Environmental Protection Agency, Cincinnati, Ohio.

References

Rowe, M. D., Anderson, E. J., Wynne, T. T., Stumpf, R. P., Fanslow, D. L., Kijanka, K., Vanderploeg, H. A., Strickler, J. R., and Davis, T. W. (2016). "Vertical distribution of buoyant Microcystis blooms in a Lagrangian particle tracking model for short-term forecasts in Lake Erie." *Journal of Geophysical Research*: *Oceans*, 121(7), 5296–5314.

Ryan, Patrick J. and Keith D. Stolzenbach. 1972. Chapter 1: "Environmental Heat Transfer" in *Engineering Aspects of Heat Disposal from Power Generation*, D. R. F. Harleman, ed., R. M. Parson Laboratory for Water Resources and Hydrodynamics, Department of Civil Engineering, Massachusetts Institute of Technology, Cambridge, MA.

Ryan, P.J. and D.R.F. Harleman. 1974. "Surface Heat Losses from Cooling Ponds," *Water Resources Research*, Vol 10, No 5, Oct 1974, pp. 930-938.

Sabersky, R.; A. Acosta, E. Haupmann. 1989. *Fluid Flow A First Course in Fluid Mechanics*, Macmillan Publishing Co., NY.

Sand-Jensen, K. and J. Borum. 1991. "Interactions among phytoplankton, periphyton, and macrophytes in temperate freshwaters and estuaries." *Aquatic Botany*, 41, 137-175.

Sawyer, C.N., and McCarty, P.L. 1967. *Chemistry for Sanitary Engineers*, 2d ed., McGraw-Hill, St. Louis, MO.

Schindler, D.W. 1971. "Food Quality and Zooplankton Nutrition", *J. of Animal Ecology*, Vol 40, pp 598-595.

Schindler, D.W., Kling, H.J., Schmidt, R.V., Prokopowich, J., Frost, V.E., Reid, R. A., Capel, M. 1973. "Eutrophication of Lake 227 by Addition of Phosphate and Nitrate: The Second, Third and Fourth Years of Enrichment, 1970, 1971, 1972", *J. of the Fisheries Research Board of Canada*, Vol 30, pp 1415-1428.

Schneider, M. and L. Hamilton. 2015a. SYSTDG Developer's Manual. U.S. Army Corps of Engineers, Northwestern Division, Reservoir Control Center.

Schneider, M. and L. Hamilton. 2015b. SYSTDG User's Manual. U.S. Army Corps of Engineers, Northwestern Division, Reservoir Control Center.

Shanahan, P. 1980. "XXXXXXXXXx" *Technical Report 268*, R. M. Parson Laboratory, MIT, Cambridge, MA. – setting vertical eddy viscosity critical

Shanahan, P. and Harleman, D. 1982. "Linked Hydrodynamic and Biogeochemical Models of Water Quality in Shallow Lakes," *Technical Report 268*, R. M. Parson Laboratory, MIT, Cambridge, MA.

Simoes, F. 1998. "An Eddy Viscosity Model for Shallow-Water Flows," *Water Resources Engineering 98, ASCE*, NY, 1858-1863.

Sher-Kaul, S., Oertli, B., Castella, E. and J. Lachavanne. 1995. "Relationship between biomass and surface area of six submerged aquatic plant species." *Aquatic Botany*, 51, 147-154.

Shubel, J. R., Wilson R. E., and Okubo, A. 1978. Vertical transport of suspended sediment in Upper Chesapeake Bay. Estuarine transport processes. Edited by B. Kjerfve, University of South Carolina Press, Columbia, S.C., pp. 161-176.

References

Smith, D.J. 1978. "WQRRS, Generalized computer program for River-Reservoir systems," *USACE Hydrologic Engineering Center HEC*, Davis, California, User's Manual 401-100, 100A, 210 pp.

Soong, T. W., DePue, M., Anderson, D. 1995. "The Changes of Manning's Roughness Coefficient with River Stages," *Water Resources Engineering*, ed. by W. H. Epsey and P. Combs, ASCE, pp.1759-1763.

Spencer, J. W. 1971. "Fourier series representation of the position of the sun." *Search* 2(5), 172.

St. John, J. P, T. W, Gallagher, and P. R. Paquin, 1984. "The Sensitivity of the Dissolved Oxygen Balance to Predictive Reaeration Equations", in *Gas Transfer at Water Surfaces*, W, Brutsaert and G. H. Jirka (Eds)., D. Reidel Publishing Co., Boston, 577-589.

Stumm, W., and Morgan, J.J. 1996. *Aquatic Chemistry*, Wiley Interscience, New York, NY.

Sullivan, A. B., Rounds, S. A., Asbill-Case, J. R., and Deas, M. L. 2013. Marcrophyte and pH Buffering Updates to the Klamath River Water Quality Model Upstream of Keno Dam, Oregon. U. S. Geological Survey Scientific Investigations Report 2013-5016, 52 p.

Swean, T., Leighton, R., Handler, R., Swearingen J. 1991. "Turbulence Modeling Near the Free Surface in an Open Channel Flow", AIAA 91-0613, 29th Aerospace Sciences Meeting, Reno, Nevada, January 7-10.

Tchobanoglous, G. and Schroeder, E. 1987. *Water Quality: Characteristics, Modeling, and Modification*, Addison-Wesley, Reading, MA.

Tennessee Valley Authority (TVA). 1972. Heat and Mass Transfer between a water surface and the atmosphere, Water Resources Report 0 6803, Lab Report #14, Norris, TN.

Thackston, E. L. and Krenkel, P. A. 1966. "Reaeration Predictions in Natural Streams," *J. San. Engr. Div., ASCE*, 89(SA5):1-30.

Thackston, E., L. and Dawson, J. W. 2001. "Recalibration of a Reaeration Equation," J. Envir. Engr., ASCE, 127(4), 317-321.

Thibodeaux, L. 1996. *Environmental Chemodynamics*, Wiley-Interscience, NY.

Thomann, R. V. and Fitzpartrick, J. F. 1982. "Calibration and Verification of a Mathematical Model of the Eutrophication of the Potomac Estuary," report by HydroQual, Inc. Mahwah, NJ, to DES, District of Columbia.

Thomann, R. V. and Mueller, J. A. 1987. *Principles of Surface Water Quality Modeling and Control*, Harper and Row, NY.

Thornton, K.W., and Lessem, A.S. 1978. "A Temperature Algorithm for Modifying Biological Rates", *Transactions of the American Fisheries Society*, Vol 107, No. 2, pp 284-287.

Tsivoglou, E. C. and Wallace, S. R. 1972. "Characterization of Stream Reaeration Capacity," *USEPA, Report No. EPA-R3-72-012*.

References

Ugarte, A. and Madrid, M. 1994. "Roughness Coefficient in Mountain Rivers," *Proceedings National Conference on Hydraulic Engineering, ASCE*, pp. 652-656.

USBR. 2001. Water Measurement Manual, US Department of the Interior, Bureau of Reclamation, Washington, D.C., 317 pp.

Visser, P. M., Ibelings, B. W., Bormans, M., and Huisman, J. 2016. "Artificial mixing to control cyanobacterial blooms: A review." Aquatic Ecology, 50(3), 423–441.

Visser, P. M., Passarge, J., and Mur, L. R. 1997. "Modelling vertical migration of the cyanobacterium Microcystis." Hydrobiologia, 349, 99–109

Vollenweider, R.A. 1968. "Scientific Fundamentals of the Eutrophication of Lakes and Flowing Waters, with Particular Reference to Nitrogen and Phosphorus as Factors in Eutrophication", *Tech. Rept. OECD, DAS/CSI/68.27*, Paris, France.

_____. 1976. "Advances in Defining Critical Loading Levels for Phosphorus in Lake Eutrophication", *Mem. Inst. Ital. Idrobiol.*, Vol 33, pp 53-83.

Wake, A. 1977. "Development of a Thermodynamic Simulation Model for the Ice Regime of Lake Erie", Ph.D. thesis, SUNY at Buffalo, Buffalo, NY.

Wallace, B. B., and Hamilton, D. P. 1999. "The effect of variations in irradiance on buoyancy regulation in Microcystis aeruginosa." Limnology and Oceanography, 44(2), 273–281.

Wanninkhof, R., J. R. Ledwell, and J. Crucius. 1991. "Gas transfer velocities on lakes measured with sulfur hexafluoride", in Proceedings of the Second International Symposium on Gas Transfer at Water Surfaces, edited by S.C. Wilhelms and J. S. Gulliver, pp. 441-455, American Society of Civil Engineers, New York.

Weiler, R.R.   1974. "Carbon dioxide exchange between water and atmosphere, "*Journal of Fisheries Research, Board Committee*, Vol. 31, pp. 329-332.

Wells, S. A. 1997. "Theoretical Basis for the CE-QUAL-W2 River Basin Model, " Department of Civil Engineering, *Technical Report EWR-6-97*, Portland State University, Portland, OR.

Wells, S. 2001. "Turbulence Closure Modeling in CE-QUAL-W2", Research Report, Department of Civil and Environmental Engineering, Portland State University, 37 pp.

Wells, S. A. 2009. "Hydrodynamic Compressible and Incompressible Modeling of the Density Structure and Hydrodynamics of Hypersaline Systems," Proceedings, IAHR Conference, Vancouver, BC, August 9-14.

WES. 1996. Evaluation and Analysis of Historical Dissolved Gas Data from the Snake and Columbia Rivers, Waterways Experiments Station, *ACOE Dissolved Gas Abatement Study Phase 1 Technical Report*, Vicksburg, MS.

WES. 1997. "Total Dissolved Gas Production at Spillways on the Snake and Columbia Rivers, Memorandum for Record," Waterways Experiments Station, *ACOE Dissolved Gas Abatement Study Phase 1 Technical Report*, Vicksburg, MS.

References

Wu, Z., Shi, J., and Li, R. 2009. "Comparative studies on photosynthesis and phosphate metabolism of Cylindrospermopsis raciborskii with Microcystis aeruginosa and Aphanizomenon flos-aquae." Harmful Algae, 8(6), 910–915.

Wu, Z., and Song, L. 2008. "Physiological comparison between colonial and unicellular forms of Microcystis aeruginosa Kütz. (cyanobacteria)." Phycologia, 47(1), 98–104.

Wuest, A. and Lorke, A. 2003. Small-Scale Hydrodynamics In Lakes. Annu. Rev. Fluid Mech. 2003. 35:373–412, doi: 10.1146/annurev.fluid.35.101101.161220.

Wunderlich, W. 1972. "Heat and Mass Transfer between a Water Surface and the Atmosphere", *Rpt. No. 14, Rpt. Publication No. 0-6803*, Water Resources Research Laboratory, Tennessee Valley Authority, Division of Water Control Planning, Engineering Laboratory, Norris, TN.

Yakhot, V. and Orszag, S. 1986. "Renormalization Group Analysis of Turbulence 1: Basic Theory," *J. Sci. Comput*. 1(1), 3-51.

Yu, S.L., T.J. Tuffy, and D.S. Lee. 1977. "Atmosphere Reaeration in a lake," *Office of Water Resources and Technology*, U.S. Department of the Interior.

Zhang, Z. and Treadhill, T. 2019. "CE-QUAL-W2 Version 4.2 for Predicting Total Dissolved Gas," Technical Note, ERDC/TL, Corps of Engineers.

Zhang, M., Shi, X., Yu, Y., and Kong, F. (2011). "The acclimative changes in photochemistry after colony formation of the cyanobacteria Microcystis aeruginosa 1: Photoadaptive changes of M. Aeruginosa." Journal of Phycology, 47(3), 524–532.

Zhu, W., Feng, G., Chen, H., Wang, R., Tan, Y., and Zhao, H. (2018). "Modelling the vertical migration of different-sized Microcystis colonies: coupling turbulent mixing and buoyancy regulation." Environmental Science and Pollution Research, 25(30), 30339–30347.

Zhu, W., Li, M., Luo, Y., Dai, X., Guo, L., Xiao, M., Huang, J., and Tan, X. (2014). "Vertical distribution of Microcystis colony size in Lake Taihu: Its role in algal blooms." Journal of Great Lakes Research, 40(4), 949–955.

Zison, S.W., Mills, W.B., Deimer, B., and Chen, C.W. 1978. "Rates, Constants, and Kinetics Formulations in Surface Water Quality Modeling", *EPA-600/3-68-105*, US Environmental Protection Agency, Washington, DC.